BRITISH GEOLOGICAL SURVEY
Natural Environment Research Council

Fluid Processes Group Series
Technical Report WE/98/11C
Issue 2 (May 1998)

A THREE TASK PROJECT

TASK 1. Laboratory work to examine microbial effects on redox and quantification of the effects of microbiological perturbations on the geological disposal of HLW (TRU)

TASK 2. Geochemical Profile through Tsukiyoshi Fault Zone

TASK 3. Presentation of Year One Results at two international conferences

J M West (Editor)

British Geological Survey,
Sir Kingsley Dunham Centre
Keyworth,
Nottingham, U.K., NG12 5GG

CONTENTS

PREFACE

In April 1997 the Power Reactor and Nuclear Fuel Development Corporation (PNC) of Japan commissioned a Three Task project from the British Geological Survey (BGS). Task 1 was a continuation of work started in 1996 to examine microbial effects on redox and to quantify the effects of microbiological perturbations on the geological disposal of HLW (TRU). Task 2 was commissioned to provide information on the Tsukiyoshi Fault for use in ongoing work at the Tono Geoscience Centre. Task 3 was to publish the results of work undertaken in 1996/97 by attending two conferences.

This report details the results of all the Tasks undertaken in 1997/98.

TASK 1. LABORATORY WORK TO EXAMINE MICROBIAL EFFECTS ON REDOX AND QUANTIFICATION OF THE EFFECTS OF MICROBIOLOGICAL PERTURBATIONS ON THE GEOLOGICAL DISPOSAL OF HLW (TRU)

PNC Representatives: H. Yoshida, K. Hama, K. Aoki
Project Manager: J. M. West
Mineralogical Characterisation and Field work:
A. E Milodowski, P. D. Wetton,
M. R. Gillespie, P. J. Henney, V. L. Hards
Laboratory studies: K. Bateman, S. J. Baker, P. Coombs,
J. M.West
Chemical Analyses: M. Cave, S. Reeder, P. Blackwell,
S. Chenery, M. Ingham, J. Trick, J. Wragg
Microbiological Analyses: S. J. Baker, P. Coombs
Adminstration, QA Procedures and Report Preparation:
C. Cole, R. U. Leader, J. Mackrill
Financial administration: L. Riley

1. INTRODUCTION

The Power Reactor and Nuclear Fuel Development Corporation (PNC) of Japan is currently undertaking a joint research programme with the Swedish Nuclear Fuel and Waste Management Company (SKB). This programme will investigate the capability of the near-repository host rock to consume dissolved oxygen in groundwater remaining in the backfill and near-field rock following the operational phase of a repository. These investigations will be carried out *in situ* in a single hydraulically-conductive fracture within SKBs underground research facility at the Äspö Hard Rock Laboratory, Äspö Island, southeastern Sweden (Figure 1).

The British Geological Survey (BGS) was contracted by PNC to participate in this study using laboratory studies to evaluate the microbiological effects influencing redox, particularly in a situation where oxygen ingress occurs. The results from Year 1 are given in West et al (1997). The results from Year 2 are described in this report.

2. BACKGROUND

During the construction and operation of a deep repository for high level waste (HLW), the subsurface environment will be open to oxidising surface conditions and surface water inflow. The Äspö Redox investigations in Block scale, reported in Banwart (1995), investigated the possibility of oxygen ingress into vertical fracture zones which may occur during repository construction due to increased surface inflow. In this study a hydraulically vertical fracture zone, which had been intersected at 70m depth during tunnel construction, had shown that oxidising surface waters rapidly mixed with the original saline waters. However, intensive anaerobic respiration by microorganisms resulted from the increased recharge. There appeared to be an inflow of reducing capacity in the form of 'young' surface organic carbon rather than oxygen at 70m, presumably because oxygen and other oxidants had been scavenged by microbes at shallower depths. Thus, after an initial oxic period, the fracture zone remained persistently anoxic. It was proposed that the microbial processes involved included anaerobic respiration coupled to reduction of iron hydroxide, methanogenesis, precipitation of calcite and secondary ferrous minerals. Thus, fracture performance was affected by groundwater dilution and by microbial processes. These will have implications for radionuclide solubility and sorption, stability and mobility of colloids and speciation. The Redox Experiment in detailed Scale (REX) study was set up as a result of this work to further study redox experiments but in a more controlled manner.

3. THE REX PROJECT AND COMPLEMENTARY LABORATORY STUDIES AT BGS

The objective of the REX Project is to investigate oxygen consumption in a simulated repository by creating a controlled oxidising perturbation to the deep rock environment at Äspö. The specific objectives of the programme are:

1. Assess the capacity of the host rock to buffer against oxidising disturbance.
2. Determine the kinetics (half life) of oxygen consumption.
3. Apply quantitative descriptions of these processes, that can be used in performance assessment of the repository redox stability for the post-closure phase.
4. Demonstrate the capacity of oxidised rock surfaces to retard uranium migration after oxidation of the rock.

The work carried out and described in this report is a complementary laboratory study to the REX programme. It examines the interaction of microbes with mineralogical surfaces involved with groundwater flow. As has been recognised, fracture flow will dominate groundwater movement at Äspö. The mineralogical nature of the fracture surfaces and subsequent changes to those surfaces will be important with regard to radionuclide sorption and retardation, and also with respect to buffering groundwater redox through rock-water interaction. The mineralogy of the surfaces will also be important with respect to microbial interaction in terms of redox reactions mediated by microbial activity, and in providing substrates for microbes. Thus, the study required a multi-disciplinary approach involving collection of fracture material and construction of experiments designed to simulate bacterial interactions in the Äspö fracture groundwater system. The experiments were started in Year 1 using batch systems and a complete interpretation of the results is given in this report. During this reporting year (Year 2) a series of flow through columns have been set up under anaerobic conditions which will be run for a minimum of 6 months. After this time period some of the columns will be removed for analysis with the remaining being run under aerobic conditions.

4. GEOLOGICAL BACKGROUND

4.1. Bedrock geology of the Äspö site

For a detailed account of the geology, structure and fracturing characteristics of the Äspö site, the reader is referred to the previous detailed and summary SKB reports (Kornfält & Wickman, 1988; Wickman et al., 1988; Talbot & Munier, 1989; Tullborg et al., 1991; Wickman & Kornfält, 1995; Tullborg, 1995), and references therein. A brief summary of the geology of the Äspö site is presented below (taken largely from the recent summary in Tullborg, 1995). A summary of the geology is given in West et al (1997) and full details of the lithology are repeated in Appendix 1.

4.2. The REX Experimental Block

The location of the area designated for the REX Experimental Block is described in the SELECT Report (Winberg et al., 1996). Two fully-cored low-angle/sub-horizontal boreholes, KA2858A and KA2862A, have been drilled at this site (Figure 2) in order to evaluate the geology, hydrogeology and fracture characteristics. These two boreholes have been the subject of the detailed fracture mineral logging reported in West et al (1997) and are partially repeated in Appendix 2.
The geology of the block has been described by Winberg et al. (1996). It consists of Småland Granite west of L=2/850m and Äspö Diorite east of L=2/850m (refer to

long-tunnel (upper level) measurements shown in Figure 2). The main structural elements in the REX Experimental Block area are shown in Figure 2. Two 20m wide zones of ductile fracturing cross the tunnel at L=2/760 and 2/830m (not shown in Figure 2). No groundwater discharge is seen where these two fracture zones intersect the Äspö tunnel. Two 0.5m wide NE-trending ductile fracture zones cross the tunnel at L=2/740 and 2/865 m. A thrust, trending NE and dipping 50%SE, intersects the tunnel at L=2/760. A second NE-trending thrust dips 25%SE and intersects the tunnel leg at the overlying tunnel, Z=250 m, at L=1/830 m.

The main hydrogeological features are shown, in simplified form, in Figure 2. To the northwest, the block is bounded by a large NE-trending ductile fracture zone (estimated transmissivity (Winberg et al., 1995) = $4x10^{-7}$-$1x10^{-4}$ m^2s^{-1}) referred to as EW-1. This consists of two main branches associated with intense fracturing, mylonitisation and hydrothermal alteration. The eastern edge of the block is delineated by a NNW-trending fracture zone (NNW-4) which intersects the tunnel at L=2/930 m. NNW-4 is considered to be highly conductive (Winberg et al., 1995), with an estimated transmissivity of up to $1x10^{-4}$ m^2s^{-1}, where it intersects the higher levels of the Äspö tunnel. The south side of the block is hydrologically bounded by a NW-trending fault zone (NW-3) which intersects the tunnel at L=2/910 m, and intersects Zone NNW-4 immediately south of the tunnel at L=2/930 m.

The lithology of Borehole KA2858A is dominated by Äspö Diorite (62.3% of sequence), but sections of Småland Granite (12.1% of sequence) and fine-grained granite (25.6% of sequence) are encountered between 5-20m distance, and towards the end of the borehole between 43-60m distance (Winberg et al., 1995). The borehole intersects a set of fractures with a trend of N20E. In this region the core is locally strongly foliated, chloritised and reddened. Core "disking" occurs at L=12.6 m, associated with bodies of fine grained granite, separating Småland Granite from Äspö Diorite. Groundwater flow was detected during drilling at 44.66m (0.3 l/m), and subsequent hydrogeological testing indicated that the bulk of groundwater flow in the borehole is attributable to a flow-zone between 40.0-40.7 m. The borehole terminates at 59.70 m.

Borehole KA2862A lies entirely within the Äspö Diorite, and also intersects a zones of N20E-trending fractures (Winberg et al., 1995). The core, in part, is strongly foliated, chloritised and reddened. During drilling, the borehole remained dry until a depth of 10.37m when groundwater inflow was intersected (0.15 l/m). From 11.20m the core is foliated and altered along N20E-trending epidote-chlorite-mineralised fractures. The end of the borehole intersects a zone of N60-70W-trending calcite- and chlorite-mineralised fractures (one at L=15.5m dips 85%SE; four parallel fractures between L=15.65-15.80 dip 85%NE). These fractures are considered to be the margins of the major fracture zone, NW-3. The water flow into the borehole increases to about 2.0 l/m from about 15m depth. The borehole terminates at 15.98 m.

5. THE BATCH EXPERIMENTS

A series of batch experiments were conducted to study rock-water interactions. These experiments were designed to study simple systems and were aimed at identifying relevant reactions both chemical and biological. They were essentially pilot studies to aid in the development of microbial and analytical geochemical procedures, as well as gathering basic data on rock-water interactions relevant to the Äspö site. Materials used in the experiments included rock and groundwater material from Äspö plus microorganisms native to the site.

5.1. Mineralogical characterisation of geological materials from the REX block

5.1.2 Introduction

The laboratory experiments and microbiological modelling were aimed at simulating the conditions within the REX Experimental Block at Äspö. Consequently, background data for the mineralogical characteristics of the host rock, and the groundwater fracture-flow system in the REX Block were required. In particular, it is important to understand the nature of the natural surfaces in contact with, and interacting with, the groundwater (and hence its associated microbiological components) in order to design laboratory experiments that represent a realistic simulation of the in situ conditions in the field-scale REX experiment. To this end, BGS and PNC undertook a brief field visit to the Äspö Laboratory to undertake detailed visual examination of cored boreholes from the REX Block - to identify and describe fractures which could be considered to represent *"Potential Flowing Features"* (PFFs) (West et al 1997), and to undertake collection of appropriate geological materials for use in the BGS laboratory simulation experiments. The details of the visual examination and mineralogical logging of the drillcores from the two boreholes in the REX block (boreholes KA2858A and KA2862A) are described in Appendix 2 and in more detail in West et al (1997).

Twelve core samples, each containing examples of one or more PFFs or other fracture mineralisation, were selected on-site at Äspö from boreholes KA2858A and KA2862A. Seven rock samples (including a large block of granodiorite for use in the BGS laboratory experiments) Åspö Hard Rock Laboratory. In addition to containing PFFs, some of these samples contain mineralised fractures that are generally typical of those described in Tullborg (1989, 1995) and Tullborg et al. (1991). These samples were subsequently shipped to BGS for detailed mineralogical and petrographical analysis. Summary sample information is given in Table 1. This table provides an approximate position for the polished thin sections prepared for petrographic analysis from the borehole samples. For more precise location of the PFFs in the two studied boreholes, the reader should refer to the borehole logs presented in Appendix 2 and in West et al (1997). In addition, water samples for detailed chemical characterisation and large-volume water samples (2x10 litres), for use in the BGS laboratory experiments were also collected from the same two boreholes (KA2858A and KA2862A) in the REX experiment gallelry region 40. Summary field and laboratory

data for groundwater geochemistry and bulk groundwater samples are given in Appendix 3. Details of the material used in the experiments are given in Section 5.2.

The following discussion is concerned with the mineralogical and geochemical characterisation of the geological samples collected from the REX site. Data were obtained in order to:

(i) define mineralogical and geochemical boundary conditions and input data for the microbiological model;
(ii) provide background information for setting up the laboratory experiments;
(iii) provide data on the mineralogy of a representative sample of Äspö Diorite from the REX experiment gallery region which was used as starting material in the laboratory experiments.

It should be noted that the mineralogical analyses undertaken to date are primarily for the provision of background data for setting up the laboratory and modelling studies. It is not the purpose of this study to provide a systematic characterisation of the mineralogy and geochemistry of either the Äspö diorite and/or its associated fracture mineralisation, within either the REX block or the Äspö Hard Rock Laboratory.

5.1.2. Preparation of Granodiorite Experimental Starting Material

A large (10-15 kg) block of granodiorite (sample C853) was collected, from the walls of the REX alcove in the Äspö tunnel, to be used as starting material in experimental charges at BGS. The sample was taken from the right-hand wall (down-tunnel side) of the REX alcove, located at the level of, and approximately 3m from, the position of borehole KA2862A. The sample is bounded on one surface by a fracture feature referred to on the REX Block area Fracture Map (unpublished SKB documentation from the Äspö Hard Rock Laboratory), as *Fracture 11*.

In order to prepare material suitable for use in the experiments, the "apparently-weathered" surfaces - contaminated by aerosols and dust deposited on the Äspö tunnel walls since its construction - were removed. The mineralised fracture surface and accompanying wallrock alteration zone of *Fracture 11*, were also trimmed off. The aim was to produce a block representative of the background unaltered granodiorite from which crushed material for experimental use would subsequently be prepared and characterised.

The experiments required crushed material within a limited grain size range of 125 to 250 μm. For this purpose, the "cleaned and trimmed" granodiorite block was jaw-split by a manual rock-splitter equipped with hardened chromium steeljaws. The fragmented material was then passed twice through a laboratory jaw-crusher equipped with hardened chromium steel jaws. The resulting crushed rock was passed through a riffle-splitter and two sub-samples were obtained.

One split from the riffle-split jaw-crushed material was milled in an agate vibrating-cup (Tema) mill before being riffle split again and milled for 30 minutes to a fine powder in a P5 agate ball mill. This material was then used in the preparation of a

fused glass bead and pressed powder pellets for whole-rock XRF analysis, and for sulphur analysis. The second split of jaw-crushed material was further prepared by dry-sieving through 250 μm and 125 μm mesh sieves, to produce a restricted 125-250 μm grain size fraction for use as starting material in the experiments. Dry-sieving was used rather than wet-sieving (which would have been more efficient in removing fines) because it was considered essential that the mineral surfaces were not pre-conditioned by reaction with water, prior to the experiments.
Prior to use in the experiments, the 125-250 μm fraction material was examined under the scanning electron microscope (SEM) to check the grain surfaces for the presence of fines (see also Section 5.3.2.2 for analytical methodology). SEM observation revealed that the material initially sieved between 125-250 μm still contained a very high proportion of fines "adhering" to the surfaces of the coarser sand-sized crushed grains. Much of this fine material was less than 5 μm and completely occluded the grain surfaces. It was considered that the presence of this material, which would have a relatively high surface area, would confuse the interpretation of data from the experiments and, furthermore, would obscure the observation and recognition of any reacting mineral surfaces if experimental residues were subsequently to be examined. Consequently, the initially-prepared 125-250 μm fraction was re-sieved to remove further fines. SEM examination of this refined material revealed that most fines were eventually removed.

In producing this limited grain size fraction from the granodiorite, there was a risk that the mineralogy may have been altered or modified by mechanical separation of minerals with different physical properties (i.e. different original grain size, hardness differences etc.) during sieving. The mineralogy of the 125-250 μm fraction was therefore checked by X-ray diffraction (XRD) analysis and compared with the XRD data obtained from "total" (i.e. unsieved) bulk rock (see Section 5.1.3.3) .

5.1.3. Analytical Methodology

5.1.3.1. Optical petrographic analysis

Polished thin sections (PTS) were prepared from all samples and examined with an optical petrographic microscope. PTSs were prepared normal to PFF planes to provide cross-sections through mineralisation in PFFs (if any) and through adjacent wallrock. In addition, PTSs were prepared from the bulk granodiorite sample selected for use in the laboratory experiments. Prior to PTS preparation, the open fracture surfaces of the PFF samples were embedded in epoxy-resin, in order that any delicate surface coating phases were preserved in position during subsequent section preparation. The samples were then vacuum-impregnated with epoxy-resin to stabilise the sample during cutting and sectioning. A blue dye was added to the epoxy-resin to enable porosity to be readily distinguished within the polished thin section. Cutting and section polishing were carried out using paraffin-based rather than water-based lubricants in order to preserve water soluble minerals such as gypsum or anhydrite, which were suspected to be present. It was considered that, if present, evaluation of the distribution of these soluble sulphate minerals may have important implications for interpreting geomicrobiological interactions in the system.

Optical petrographic observations were made using a high-quality Zeiss optical petrographic microscope.

5.1.3.2. Scanning electron microscopy

Backscattered scanning electron microscopy

After optical examination, the polished thin sections were studied by backscattered scanning electron microscopy (BSEM). BSEM observations were made using a Cambridge Instruments Stereoscan S250 Mark I SEM instrument equipped with a KE Developments 4-element solid-state backscattered electron detector. Mineral identification was made by qualitative examination of the characteristic energy-dispersive X-ray spectra (EDXA) recorded during observation of a given phase, with a Link Systems 860 Mark I energy-dispersive X-ray spectrometer fitted to the electron microscope. Observations were made at 20 kV electron beam excitation. The EDXA system has a detection limit of approximately 0.2% (weight) for most common elements but this is probably of the order of 0.5% (weight) for for heavier elements such as uranium, thorium and lanthanides. The polished sections were coated with a thin layer of carbon (c.250 Å thick) prior to examination in the SEM in order to make the surface electrically conductive.

Images obtained by BSEM are related to the composition of the material being examined. Image brightness is proportional to the average atomic number of the material, thus allowing the distribution of different minerals, or phases, to be determined on the basis of their chemical composition (Goldstein et al., 1981).

Secondary electron scanning electron microscopy

The surface mineralogy and morphology of the PFF samples, and of crushed granodiorite material prepared for use in the laboratory experiments, were examined by SEM in secondary electron image mode.

Samples of the PFF surfaces were prepared as small stub-mounted rock fragments (typically 1-2 cm across). These were taken from the original sample either by carefully fracturing a fragment from the PFF fracture surface using a very fine hardened steel chisel, or by cutting small blocks from the sample using a small diamond-impregnated jewellers saw. These fragments were mounted onto an aluminium pin-type SEM stub using Leit-CCC conducting carbon cement.

The surfaces of particles of crushed granodiorite were also prepared as stub-mounted samples by carefully sprinkling crushed granodiorite material onto double-sided adhesive tabs which were affixed to aluminium pin-type SEM stubs. Any loose material was gently removed by shaking and very lightly blowing clean with an aerosol duster.

All stub-mounted samples were coated with a thin film of carbon (c. 200Å thick), using an Emitech high-vacuum carbon-arc evaporation coater, to ensure that all surfaces for examination in the SEM were electrically conductive.

SEM analysis was undertaken using a Leo 435VP digital variable-pressure SEM fitted with an Oxford Instruments Ltd ISIS 300 digital X-ray microanalysis (EDXA) system. The samples were examined, under a 20 kV electron beam excitation, with the instrument operating under the normal "high vacuum" SEM mode. Images were digitally recorded as "tif" image files which were then written to an optical disk. Images were subsequently printed as required using a Hewlet Packard laser printer or Codonics photographic-quality dye-sublimation printer.

General comments regarding the use of scanning electron microscopy

BSEM and SEM in conjunction with EDXA proved extremely useful, allowing phases to be identified by a combination of high-resolution textural information and semi-quantitative assessment of the proportions of elements in crystal structures. In this way the majority of phases, even trace amounts of very fine-grained or cryptogranular crystals, have been identified unequivocally. Phase identities over which there is still some doubt are listed below.

(i) **Carbonates**: - because of the range of solid-solutions possible in carbonate minerals, the identity of a carbonate is sometimes not obvious from the qualitative peak array obtained by EDXA. For example, ferroan dolomite ($Ca[MgFe][CO_3]_2$) can be difficult to distinguish from ankerite ($Ca[MgFe Mn][CO_3]_2$) on the basis of qualitative peak size and distribution. Most carbonates, however, display distinctive, unequivocal peak patterns, and in the few cases where this has not been the case other criteria, such as comparing grey levels generated by backscattered electron images, have been used to facilitate identification. In the petrographic descriptions here, the terms are used qualitatively and subjectively but do reflect the relative Fe^{2+} content.

(ii) **Clay minerals:** - are generally very difficult to identify from their qualitative (EDXA) chemistry alone. Occasionally, where characteristic form is observed under BSEM or SEM and matched with distinctive chemistry (e.g. kaolinite) reliable identification can be made. However, clay minerals commonly occur in fine admixture with other phases (e.g. carbonates and iron oxides). In cases where the material has a grain size less than 1-2μm, it is impossible to resolve the chemistry of individual particles/phases because the excitation volume from which the X-ray signal is generated under the electron beam is larger than the volume of the phase of interest. In these cases, the EDXA spectrum may represent the overall composition of a mixture of particles or phases, or be largely derived from the substrate on which the fine particle resides within the X-ray excitation volume. Where a clay-like texture is not observed and the chemistry is inconclusive (e.g. K, Al, Si and minor Fe peaks obtained by EDXA, which could be an Fe-containing illite or a white mica-like celadonite, or glauconite) broad terms (e.g. *'illitic'* clay etc.) are used rather than the more definitive mineral names (e.g. *'illite'*).

(iii) **Iron and titanium oxides**: - a wide variety of different iron and titanium oxides and hydroxides exist in nature (e.g. hematite (Fe_2O_3), magnetite-titanomagnetite (Fe_3O_4), ilmenite ($FeTiO_3$), anatase (TiO_2), brookite (TiO_2) and rutile (TiO_2) as well as complex mixed Ti-Fe oxides and oxyhydroxides). It is impossible, from the EDXA spectra alone, to definitively distinguish between the different oxide or oxyhydroxide species. Definitive identifications normally rely on supporting observations from other analytical techniques such as X-ray diffraction or reflected-light optical petrographic observation. However, BSEM image brightness and contrast can provide some indications of relative differences in hydration state between oxides and oxyhydroxides - i.e. the presence of water (either as water of hydration or structural water) reduces the backscatter coefficient (as a result of lowered average atomic number and/or density) and gives rise to a duller image in more hydrous materials.

The high spatial resolution (compared to that of optical petrography) of the BSEM/SEM technique has made it a very effective tool in the study of mineral paragenesis, especially for fine grained materials. In addition, because the technique images phases according to their atomic mass, it is particularly useful for the location of dense, or high atomic mass, trace minerals, such as U-rich and Th-rich minerals.

5.1.3.3. X-ray diffraction analysis

X-ray diffraction (XRD) analysis was undertaken on the bulk diorite sample (sample C853) intended for preparation and use as feedstock starting material in the BGS laboratory experiments. The sand fraction was produced simply by sieving the crushed whole rock, and the aim of this work was to see if any mineral fractionation had occurred during this procedure (see Section 5.1.2), as well as to provide background mineralogical data for the diorite sample.

The XRD analysis for the bulk granodiorite sample was undertaken using the tema-milled powder, while the sand fraction (125-250 μm) was analysed as produced. A sub-sample of each (~3g) was taken and micronised under acetone for fifteen minutes and dried in an oven at 55°C. The resultant powder was then back loaded into standard aluminium sample holders for analysis. XRD analysis was carried out using a Phillips PW1700 series diffractometer using Co-K_α radiation and operating at 45kV and 40mA. The micronised powder mounts were scanned over the range 3-50 °2θ on analysis program 7 (slow bulk rock analysis routine). Diffraction data were analysed using Phillips APD1700 software coupled to a JCPDS database running on a DEC Micro Vax 200 micro-computer system.

5.1.3.4. Electron microprobe analysis

Mineral chemistry was determined by electron microprobe analysis (EMPA) of minerals in polished thin section. Analysis was undertaken at the BGS using a CAMECA SX50 wavelength-dispersive electron microprobe fitted with three wavelength-dispersive spectrometers. The analyses were performed with an

accelerating voltage of 15 kV, a beam current of 20 nA and with a spot size (i.e. beam diameter) of 1 to 5 μm for the silicate minerals. Carbonate minerals were analysed using a lower accelerating voltage of 10 kV, a beam current of 10 nA and with a spot size of 5 to 15 μm, depending on the state of the sample in thin section. The spot size was increased to further reduce the possible effects of beam damage on the carbonate samples. The instrument was calibrated using a range of appropriate synthetic and natural standard materials. Accuracy and precision of these analyses are estimated to be better than 3% RSD. The raw X-ray counts were collected and processed using the CAMECA proprietary QUANTIVIEW 3.0 software package. The data were then exported from the microprobe via the ethernet network onto a PC and imported to Excel 5.0 spreadsheet for further data manipulation and processing.

5.1.3.5. Laser-ablation microprobe - inductively-coupled plasma - mass spectrometry

Limited trace element analysis for selected minerals was determined by laser-ablation microprobe - inductively-coupled plasma - mass spectrometry (LAMP-ICP-MS). Analyses were primarily focussed on obtaining data for U and Th in major mineral phases, as this information was indicated to be of potential interest to PNC. LAMP-ICP-MS can determine trace element compositions in minerals at lower detection levels than is possible by conventional EMPA techniques. The method works on the principle that the test material is placed in an ablation cell and a small amount of sample is removed by ablation with a laser. The ablated material is introduced into the ICP-MS and element ratios are determined.

LAMP-ICP-MS analysis was undertaken using a laser ablation microprobe system designed and purpose-built for the BGS by the Department of Chemistry, Birkbeck College, University of London. The system is based on a Spectron Nd:YAG ultraviolet laser system connecting to a high-quality Leitz optical microscope. The laser-microscope system utilises a custom-designed laser ablation chamber, with an optical quartz window, which is flushed by an argon carrier gas stream. The argon stream transfers ablated material to an ICP-MS instrument, via a polythene tube that connects the ablation cell to the ICP torch, using a modified dual-flow sample introduction system described in Chenery & Cook (1993). The LAMP-ICP-MS used by BGS achieves both very small beam diameters (down to 4 micron craters) and very good detection limits (sub-ppm levels are detectable using 40 micron craters). The design and basic operation of the LAMP are described in UK Patent No. 91066337.0, Serial 2254444, and in Chenery & Cook (1993).

The elements are determined using a VG Plasmaquad 2 Plus ICP-MS (serial no.732). Inductively coupled plasma is used to ionise the samples and a quadrupole mass spectrometer to scan for, or peak jump to, ions with a mass to charge ratio in the range 6-250. All the system parameters are monitored continuously to provide safe operation. The system is controlled by computer through dedicated ICP-MS software, with analytical results being stored automatically on the hard disc and reported on the NR-10 printer.

The dedicated ICP-MS software is used to convert the raw intensity data into relative concentration data using aqueous calibration standards. This corrects the raw intensity data for isotopic abundance and instrument sensitivity for isotopes of different mass. These data are imported into an Excel spreadsheet. Using the spreadsheet the relative concentrations are:

(1) blank subtracted
(2) corrected for any changes in sensitivity during the analytical run
(3) any values below detection limit identified and marked in a small font and italics in the tables.
(4) LAMP-ICP-MS data are determined in terms of relative concentrations (in effect elemental ratios). Data for a common major element determined from EMPA from the same areas of the sample were used to convert these values to absolute concentrations. Alternatively, compositions can calculated by scaling the LAMP-ICP-MS elemental ratios to a common element by assuming "ideal" major element compositions for known mineral phases. This internal standard calculation method is described in Querol & Chenery (1995).

After checking QC standards, the concentration data are ready for reporting, unless requested otherwise, as Excel spreadsheets. During the project all processed files are held on the Analytical Geochemistry Group server computer. For archiving at the end of the project, the master ICP-MS data files, the ASCII relative concentration files and the final Excel spreadsheets are stored on floppy disks.

5.1.3.6. Whole rock geochemistry

Major and trace element analyses (with the exception of Fe(II) and S) were determined by X-ray fluorescence analysis (XRF). XRF was undertaken using two sequential, fully-automated, wavelength-dispersive XRF spectrometers (Philips PW2400 and Philips PW1480/10 XRF spectrometers) fitted with a 60 kV generator and 3 kW rhodium ("Super Sharp") end-window X-ray tube, and a 100 kV generator and 3 kW tungsten side-window X-ray tube, respectively.

Major element analysis of whole-rock samples by XRF was carried out to determine SiO_2, TiO_2, Al_2O_3, Fe_2O_3, MnO, MgO, CaO, Na_2O, K_2O and P_2O_5 contents. Samples were Tema-milled and finely powdered, then prepared as fused glass beads with di-lithium tetraborate flux at approximately 1200%C. Loss on ignition (LOI) was also determined by heating the samples to 1050%C prior to glass bead preparation. Analyte angles were calibrated from international and in-house standard reference materials. All standards and unknowns were prepared as fused glass beads. Drift correction was catered for by an external ratio monitor, and background corrections applied where necessary. It should be noted that Fe_2O_3 determined represents the total Fe in the samples.

Trace elements were determined by XRF using pressed powder pellets. Pellets were prepared by grinding powdered samples with Elvacite 2013 binder (Dupont *n*-butyl methacrylate copolymer) in an agate planetary ball mill, followed by pressing at 25 tons load into 40 mm diameter pellets.

Total sulphur was determined by a combustion method after Rundle (1974) with sulphur as sulphide determined by difference after ignition at 650%C. Fe (II) was determined by titration using the method of French & Adams (1972).

Whole-rock geochemical analyses of diorite represented by sample C853 are presented in Table 2. The data are broadly similar to previously-reported compositional data for the Äspö Diorite summarised in Appendices 1 and 2.

5.1.4. Mineralogical and Petrographic Observations

5.1.4.1. Petrographic and mineralogical characteristics of the host rocks

Background host rock to PFFs in the REX Block

The dioritic host rocks to all the PFF samples examined have broadly similar mineralogical and textural characteristics, though there are minor variations from sample to sample in modal primary mineralogy and alteration characteristics. The most common rock type is comprised dominantly of plagioclase feldspar (Table 3) with subordinate K-feldspar (orthoclase) or mixed Na-K alkali feldspar, minor quartz and chloritised biotite. Textural and mineralogical alteration have removed any evidence for the original presence (if any) of other primary ferromagnesian minerals (such as pyroxene or amphibole). Primary accessory minerals are magnetite, ilmenite and apatite, with traces of pyrite, chalcopyrite and galena. In one sample, a primary pyrite crystal was seen to enclose several very fine-grained crystals of thorite (Th-REE-silicate). The rocks originally would have been medium- to coarse-grained, however alteration and local recrystallisation have created a large proportion of fine-grained crystals. K-feldspar and Na-K alkali feldspar occurs in the 'groundmass' and as megacrysts up to c.30 mm in diameter.

All the rocks have undergone substantial mineralogical alteration and varying degrees of physical alteration. Plagioclase feldspar is generally highly turbid and partially replaced by epidote, sericite and calcite. Biotite, though occasionally fresh-looking, has in most samples been altered to chlorite. Clusters of chlorite-epidote-titanite-(apatite) crystals may represent altered amphibole. All the samples now contain varying proportions of secondary epidote, sericite (phengitic mica), Mg-Fe chlorite, titanite and calcite. Between them, these minerals can constitute up to c. 25% of the rock volume, though 15-20% is more common.

Physical alteration manifested in several textural features, including kinked and strained crystals of biotite, chlorite and feldspar, quartz which has recrystallised strongly to form mosaics of sub-equigranular crystals, often with sutured boundaries, and thin shear and granulation seams, along which substantial alteration has masked much of the original texture.

The degree of mineralogical alteration made modal analysis difficult, however there was some variation in modal proportions of the key primary minerals. Samples C860, C861, C862, C863, C864 and C867 were essentially similar and of quartz-

monzodiorite composition (classification and terminology after Le Maitre et al., 1989). In contrast, samples C865, C866 and C868 had no K-feldspar megacrysts, a higher proportion of quartz, practically no bioitite (or altered biotite), more sericitic alteration and less epidote. These samples had modal compositions more typical of granodiorite. Sample C870 had a higher proportion of quartz and K-feldspar, less plagioclase and virtually no primary ferromagnesian minerals. Its modal composition was typical of a granite.

Crushed diorite material prepared for laboratory experiments

XRD revealed that the whole-rock "diorite" (bulk sample, unsieved) in sample C853 is composed of major quartz, with minor albite, mica, orthoclase, calcite and trace amounts of chlorite and possibly titanite and magnetite. Augite was also identified as a minor constituent but its identification from the very complex XRD pattern is ambiguous, and is not supported petrographic observations.

The XRD trace of the bulk rock was compared with that obtained from the sieved 125-250 μm material prepared from the same crushed C853 material, in order to check whether physical fractionation of minerals had occured during sample preparation. However, the analysis showed it to be virtually identical to the bulk C853 sample. Minor differences were observed in some peak intensities; the mineral phases these correspond to are listed in Table 10. From this it can be seen that the125-250 μm size fraction contained a slightly greater percentage of quartz and chlorite, while other mineral phases showed little or no detectable change in abundance, other than a slight drop to compensate for the increase in quartz.

5.1.4.2. Physical characteristics of PFFs

PFFs in the two REX boreholes and in the walls of the REX alcove virtually never occur singly. In the wallrock adjacent to the main PFFs (which are usually represented by core breaks), is a zone containing other, usually smaller, fissures. This can range from one feature to a network of connected fissures. In most cases the 'damage zone' does not extend more than 1 mm from a PFF surface, however some sections of core up to c. 5 cm wide contain several closely-spaced fissures. The presence of the 'damage zone ' means that a much larger surface area of rock is exposed to groundwater than is apparent from the main PFFs.

All the fissures were very narrow; apertures rarely exceeded 200 μm, and the vast majority were considerably narrower. In the plane of the thin sections the fissures tended to be continuous (i.e. they do not pinch-out, as tensional gashes might do), thus they probably represent laterally extensive, sheet-like pore spaces through the rock, at least over the scale of several centimetres to tens of centimetres.

Most fissures have formed by relatively simple parting of the rock. They have generally clean surfaces with very little relief. Locally however, some fragmentation of the wallrock minerals has occurred during fissure development, as illustrated in Plates 1 & 2. In most cases the fragmentation has occurred where a fissure passes through quartz crystals (e.g. Plate 3 & 4). Similarly, quartz in the damage zone very

often has a greater development of fissures within it than adjacent minerals such as feldspars (e.g. Plate 5), reflecting the relatively brittle nature of quartz compared to these other minerals.

Some fissures have developed by reactivating older veins. These are generally extremely thin features, usually <200 μm, and most commonly are K-feldspar +/- epidote +/-chlorite veins (Plates 6). Most, however, appeared to have developed as new tectonic structures in previously unfractured rock.

5.1.4.3. Alteration associated with PFFs

Most fissure surfaces were lined by wallrock minerals that are not obviously altered beyond the level of pervasive background alteration. However, K-feldspar occasionally formed a thin lining on PFF surfaces and may have formed by wallrock alteration soon after PFF development (Plate 7). Some PFF surfaces were coated in assemblages of alteration minerals - Fe-chlorite, phengite/muscovite, titanite. These may represent reactivated and altered K-feldspar +/-epidote veins.

The degree of dissolution porosity in host rock minerals was usually greatest in proximity to fissures, thus it is likely that dissolution of these minerals is, or has been, caused by reaction with recent groundwaters. Plagioclase feldspar (albite-andesine compositions) was by far the most susceptible mineral to dissolution, as evidenced by the development of dissolution pits in this mineral (see Plates 8-10). The pits ranged up to c.200 μm in diameter, the largest were generally immediately adjacent to fissures (Plate 10), while smaller but more numerous pits can develop up to c. 300μm from fissures. Dissolution pits do occur at greater distances from fissures, but they were generally very small and relatively uncommon. Locally, magnetite crystals within 200 μm of fissure surfaces have corroded slightly, and may be dissolving in groundwaters, however this was rare.

5.1.4.4. Authigenic mineralisation in PFFs

Less than 10% of all fissure space was occupied by authigenic minerals, and in most PFFs the wallrock minerals will represent a major part of the fracture surface mineralogy exposed to porewater. A relatively simple assemblage of authigenic minerals has been identified, one or more of which occurs in major fissures in all of the PTS' examined. Textural relationships suggested the paragenetic sequence of mineralisation was:

chlorite -> fluorite	->	calcite, pyrite, smectite	->	barite
[early hydrothermal]		[young/contemporary]		

However, in the samples examined in this study, it was relatively rare for two or more of these minerals to occur together in fissures and the actual paragenesis may not be this simple.

Fe-Mg chlorite locally formed a thin coating on fissure surfaces (Plate 11), however in the majority of cases it appeared to be an alteration product of an earlier vein

mineralisation rather than an authigenic mineral. Fluorite was very rare, and very fine-grained, but locally formsed a partial fill in fissures. Calcite was more common, occurring as a discontinuous cement in fissure networks (Plates 2, 6), and as isolated, very fine-grained, generally euhedral crystals sitting on fissure surfaces (Plate 12). In some cases the calcite formed more continuous patches, locally filling fissures, however it was generally not particularly extensive. Some of these may represent an earlier generation of sealed calcite veins. Euhedral calcite crystals had equant to c-axis elongate morphology (Plates 12 & 13). Some calcite, particularly in C860AP1, had surfaces that look corroded, suggesting that some dissolution has occurred. However, most late-calcite surfaces were pristine. Some dilute acid solution was used occasionally during the core logging exercise to test for the presence of calcite on some core surfaces, and it is possible that the presence of corroded-looking calcite, only in this sample, is a result of acid having been applied to the PFF surface.

Calcite often nucleated preferentially on the surfaces of older wallrock-hosted calcite exposed on fissure surfaces or on pore surfaces, or on the exposed surfaces of late-reactivated old calcite veins (Plate 14). It also seemed to have nucleated more successfully in areas where there was a lot of wallrock surface available, such as where the wallrock fragmented and in dissolution pits in feldspars (Plates 9 & 10). Authigenic pyrite was relatively common, always fresh (Plate 15) and often contained a small proportion of Zn. It was rarely euhedral, and tended to occur in isolated patches. Occasionally, it was associated intimately with calcite and/or barite (Plate 16).

Both the late-stage pyrite and late-stage calcite may also be associated with late-stage clay alteration developing from the underlying silicate mineral substrate (Plate 15). SEM-EDXA studies revealed that the clay mineral contains major Mg, Al, Si and Fe with subordinate to minor Ca and K. The qualitative compositional data obtained to date suggested that this is a mixed-layer chlorite-smectite mineral. The development of this late-stage clay was very closely associated with the alteration of the underlying silicate host rock minerals and results in the development of major microporosity in the immediate surface of exposed wallrock (Plates 15 & 17).

Authigenic barite was relatively common, fresh and contains variable proportions of Sr. A complex rare earth element-Ca-Si-F mineral, with fibrous morphology, has developed as a very rare, late-stage alteration product on surfaces where older fluorite mineralisation has been re-fractured and exposed to recent groundwater (Plate 18).

There was some evidence for local brecciation of authigenic minerals, perhaps indicating some minor tectonic activity following mineralisation. However, in the majority of fissures authigenic crystals were undamaged and it is possible the apparent brecciation locally is the result of blasting or coring or core handling.

Other minerals lining open fracture surfaces included chlorite, sericite, K-feldspar and wallrock minerals.

5.1.4.5. Mineral compositions

Mineral composition data were obtained from phases comprising the bulk rock sample being used for experimental studies (sample C853) and a sample containing the dominant autigenic minerals lining PFFs (sample C851). Full details of the mineral-chemical data from the EPMA and LAMPS-ICP-MS analyses are listed in the spreadsheets included in Appendix 4.

Host rock-forming minerals

Points were selected from the main rock forming mineral phases: plagioclase, K-feldspar, green mica and opaques. Representative analysis are listed in Table 3.

All the phases in the sample showed evidence of hydrothermal alteration with the chloritisation of biotite, which was also associated with the development of granular opaques, and the sericitisation of the feldspars, in particular plagioclase. Analytical points were selected to avoid heavily altered areas. The results showed that the bulk of the plagioclases was almost pure albites (Ab95-97), with a few rare cores showing An30 with the K-feldspars dominantly being almost pure orthoclase (Or90; up to 2% BaO) and a few Ab50-Or50 mixed compositions. This suggests that most of the feldspars have equilibrated at low temperatures, possibly associated with hydrothermal alteration. The green "micas" were chloritised biotites with minor K loss and slightly elevated MgO abundances. The opaque grains were magnetite.

LAMPS-ICP-MS analyses were carried out principally to determine Th and U concentrations within the major rock forming phases (plagioclase, K-feldspar and chloritised mica), and representative analyses are listed in Table 5. U and Th abundances were below detection limits in all cases apart from a single "chlorite" with 6 ppm U present.

Authigenic minerals in PFFs

EPMA data were obtained from late-stage calcite and pyrite, and from hydrothermal vein K-feldspar, these phases being the main constituents of the PFF mineral assemblage. Representative analyses are listed in Table 6.

Qualitative EDXA observations suggested that calcite in the PFFs contained little or no Fe^{2+} or Mn^{2+} in solid-solution. In this respect, however, it should be noted that EDXA has only limited sensitivity and is unlikely to detect the presence of less than c.0.3 weight percent of these elements. Nevertheless, quantitative wavelength-dispersive EMPA data (Table 6) tended to support this observation. Pyrite quantitative EMPA and qualitative EDXA data similarly indicated a very simple chemistry. With the exception of minor Zn (which was observed in some qualitative EDXA observations), there was little evidence for significant incorporation of other redox-sensitive chalcophyllic elements such as As, Pb, Co, Ni or Cu into pyrite.

The main emphasis in the LAMPS-ICP-MS study was again placed on likely hosts for Th and U amongst the main mineral phases in the PFFs, including rather poorly

formed, fibrous mats and aggregates of a pale yellow/green "chlorite" which forms part of the substrate for the late-authigenic PFF phases in many fractures. This "chlorite" includes irregular patches of epidote, granular opaques and irregular, apparently corroded, titanites. Th and U contents of the calcite and the majority of the chlorite were below detection limits except for U which is present up to 6 ppm in some chlorites. The "epidote", which includes true epidote as well as possible corroded and altered titanite contained the highest Th and U concentrations recorded, up to 2.4% Th and 600 ppm U.

The low Th and U abundances within the majority of the mineral phases within the PFF, in particular the calcite and "chlorite", suggested that no significant Th and U remobilisation has occurred.

5.1.5. Implications for Microbiology and Redox

Detailed mineralogical observations on PFFs from the two REX boreholes (KA2858A and KA2862A) and from the walls of the REX alcove area have identified that, within the REX block, only a limited number of mineral species are likely to be significant with respect to either redox reactions or the provision of energy and nutrients for microbiological interaction. With respect to these processes, the principal mineral-hosted elements are the redox-sensitive elements Fe (present as Fe^{2+} and Fe^{3+}), Mn (present Mn^{2+}, Mn^{3+}, Mn^{4+}), and S (present as sulphates and sulphides), and C (present as carbonates).

The principal mineral source for C will be calcite. Calcite is readily accessible to the groundwater in most PFFs. Examination of the PFFs from the REX block shows that this mineral is a very late-stage deposit. There is little evidence to indicate that calcite is dissolving in the PFFs. Any corrosion observed in the samples studied is most probably an artifact resulting from the use of dilute acids in testing the core samples for the presence of carbonate minerals. The close correspondence between calcite distribution, open fractures and active groundwater flow suggests that calcite may be actively precipitating in the modern groundwater system. Calcite commonly contains significant amounts of Fe^{2+} and Mn^{2+} in solid-solution (up to several weight percent). Indeed, even within the Äspö area, ferroan and manganoan calcites have been described from fracture mineralisation (Tullborg et al., 1991). However, the results from this study suggest that the calcites within the REX block region do not contain significant amounts of these elements and, therefore, are unlikely to participate in redox reactions in the groundwater system. Nevertheless, calcite may have a significant influence on the buffering of pH and bicarbonate in the system.

Pyrite is present as late-stage fracture mineralisation in PFFs in the REX block. This mineral therefore represents a potential source of reduced Fe and S species in the system. Although often present in only small quantities, it is known to be a highly reactive mineral with respect to redox reactions involving Fe and S, and in microbiological interactions. Its surfaces are exposed to open porosity and consequently it will be readily accessible to groundwater moving through PFFs. Despite the relatively small volume of pyrite (marcasite) present as fracture

mineralisation, nevertheless it is extremely common in PFFs. This, together with its accessibility to the open porosity, will mean that it is likely to have a significant influence on redox reactions and oxygen consumption during the *in situ* REX experiments, at least in the early stages of evolution, or until the pyrite is consumed. In addition to the late-stage fracture mineralisation, pyrite and other sulphides (galena and chalcopyrite) are as primary igneous trace components in the host rock. These too are exposed on PFF surfaces and will contribute, to a small degree, to the "pyrite budget" in the groundwater system. Petrographic analysis of the pyrite from the REX block shows it to be fresh with no evidence for oxidation, dissolution or alteration. Again, as with calcite, its distribution is closely associated with the distribution of open fractures and active groundwater flow. Consequently, it is considered that pyrite could be actively precipitating from groundwaters in the REX block region. Co-precipitation of pyrite and calcite in the PFFs could account for the lack of Fe in the calcite since Fe would be preferentially precipitated as sulphide rather than carbonate, in the presence of sulphide ions (due to the very low solubility of pyrite relative to Fe carbonate).

Apart from pyrite, the only other source of S identified in PFFs during the study was barite. Potentially, barite can provide a source of SO_4^{2-} species. However, this mineral has an extremely low solubility and it is considered that this is unlikely to influence S budgets in the system.

Petrographic analysis reveals that, far from being obscured by hydrothermal vein mineralisation, the host rock is well-exposed in the surfaces of PFFs. The host quartz monzodiorite rocks contain a number of Fe-bearing minerals, present in significant proportions. Since these are exposed in the surface of PFFs, they represent potentially important buffers for Fe and redox that must be taken into account in any modelling considerations. Important phases in the host rock include biotite, chlorite and magnetite - which can be sources of both Fe^{2+} and Fe^{3+}, and ilmenite - which may provide a source of Fe^{3+} and Mn. Much smaller amounts of Fe^{2+} and Fe^{3+} may also be present in sericite and phengitic mica. These are unlikely to represent significant sources in comparison to biotite and chlorite. In some altered lithologies, epidote is also a major component of the host rock. Epidote may represent an important localised source of Fe^{3+} in the system.

In addition to the host rock lithologies, epidote and chlorite are also present as vein minerals. Locally these may be exposed to the groundwater in PFFs developed by reactivation of these early hydrothermal veins.

Detailed petrographic analysis of the PFFs from the REX block revealed that a zone of significantly enhanced microporosity may extend for a few millimetres into the host rock. This is present as fine networks of open microcracks, often partly mineralised by the same late-stage calcite and pyrite that is present in the main fissures - indicating connectivity with the major fractures. In addition, there is often a significant amount of secondary porosity produced as a result of the dissolution of feldspar minerals immediately adjacent to the PFF surface. This may have an important influence on redox buffering since it exposes a much higher surface area of

the host rock (and hence Fe and S bearing minerals) to the groundwater system, than would be expected for a simple planar fracture. Therefore, rock-matrix diffusion may have a significant influence on redox.

SEM observations of the surface of PFFs reveals a significant degree of roughness and microporosity at the scale of 5-20 μm. Consequently, these surfaces furnish a very favourable environment in which sessile bacteria can readily attach themselves to fracture surfaces. This will tend to favour the development of bacterial colonies, and therefore influence the development of redox conditions within the REX block.

5.2. Laboratory studies

5.2.1. Methodologies

5.2.1.1. Selection of materials to be used in experiments

Solid phase material

As stated in Appendix 2 and West et al (1997), close examination of the PFFs in the REX boreholes indicates that flow is probably strongly channelled along asperities or irregularities in the fracture surface. Although the host rock minerals, or reactivated surface of old chlorite veins, dominate the mineralogy of the 'total' fracture surface, the distribution of late-stage mineralisation (on fracture surfaces) suggests that pyrite and calcite are very important phases lining the "hydraulically active" channels within the potential flowing features. During logging, it was also noticed that pyrite (or other sulphides) was also present in fine grained disseminations in the matrix of the host rocks in the REX block. Pyrite is important in certain microbial processes and may significantly affect redox buffering. As a result of these findings, it was decided to use crushed Åspö Diorite in the experiments. Details of the collection and preparation of the material are given in Sections 5.2 and 5.3. Groundwater collected from Åspö borehole KA285 A was selected for the experiments, details of chemical analysis are given in Appendices 3 and 6.

Selection and preparation of microbes to be used in experiments

Microbial activity is of significance in the geochemical processes as it can influence mineral dissolution and precipitation, pH, alkalinity and redox status. Detailed studies into the subsurface microbiology of Åspö (Pedersen and Karlsson, 1995) had revealed the presence of many different bacteria in the granitic groundwater. Iron and sulphate reducing bacteria were highlighted as being of particular significance in Åspö geochemistry. The implications of iron reduction and sulphate reduction are discussed in detail in an earlier study (Banwart, 1995).

Studies previously undertaken by Goteborg University (Pedersen et al. 1996) had characterized an iron reducing isolate from the Åspö environment and had found it closely related to *Shewanella putrefaciens*. As pyrite was present in the fracture material *S. putrefaciens* (Åspö 5) was therefore selected as the most representative

iron reducing bacteria (IRB) for the study. *S. putrefaciens* uses ferric iron as an electron acceptor, in the process of iron reduction. It is a facultative anaerobe, able to use dissolved oxygen if available and to convert to anaerobic processes when it is absent. *S. putrefaciens* (Åspö 5) was obtained as a freeze dried culture from Goteborg University.

The second microbe selected was a sulphate reducing bacteria (SRB), tentatively called *Desulfovibrio asponium* (Åspö 2). Previous activity studies (Pedersen et al 1995) of bacterial samples from the Äspö environment, which looked at lactate utilization and sulphide production, had indicated an SRB presence. DNA sequencing results had shown a close identity to Desulfovibrio spp. *D. asponium* (Åspö 2) was obtained from the German Collection of Microorganisms.

The bacteria were to be added to the reactors in numbers calculated using BGSE (section 5.2.2.2). The number of SRB added to the SRB containing reactors was $1.57x10^5$ per ml of groundwater and the number of IRB added to the IRB containing reactors was, $3.161x10^5$ - $1.28x10^6$ per ml of groundwater. These numbers were less than the amounts calculated by BGSE to be added as some loss occurred from centrifuging the original cultures. A mixed culture of the two was added in the experiments using both bacteria, the number of IRB added was $5.3x10^5$ per ml of groundwater and the number of SRB, $5.45x10^5$ per ml of groundwater. As these reactions were set-up at different times there is a slight variation in the starting numbers of bacteria (see table 'Results' for actual numbers).

S. putrefaciens was received in a freeze dried state , it was rehydrated and enriched using an iron citrate medium (Pedersen et al, 1995, and Appendix 5). The medium was gassed with nitrogen/carbon dioxide mixture and adjusted to pH 7 prior to adding the culture. The enrichment was incubated in an anaerobic atmosphere ($H_2/CO_2/N_2$) at 35 °C. Samples were taken at intervals to determine bacterial numbers using the total count method of epifluorescence microscopy (see Section 5.2.2.3)

D. asponium was similarly rehydrated this time using Postgates B medium (Appendix 5) and incubated at 30 °C in an anaerobic atmosphere. The numbers of bacteria were determined as for *S. putrefaciens*.

The bacteria were isolated from the medium by centrifuging at 4000 rpm, resuspended in Åspö groundwater and the process repeated until traces of the enrichment media were removed. The bacteria were then resuspended in groundwater before being added to the reaction vessels in the predetermined numbers.

5.2.2.2. Preliminary modelling

Before the experiments could be implemented preliminary modelling was necessary to determine the numbers of bacteria that could be supported by the mixing groundwater and rock. The microbiology code BGSE was used for these calculations (Noy et al, 1996; Baker et al, 1996). BGSE enables an assessment of maximum microbial growth rates to be made based on availability of nutrients and energy in existing

mineralogical and groundwater analyses. Emphasis is placed on elements which are major microbial nutrient sources (namely carbon, nitrogen, sulphur and phosphorus); and on species which can act as electron donors and acceptors for energy generation (principally organic carbon, oxygen, nitrate, FeOOH and sulphate). Reactions and growth are assumed to take place within a mixing cell. Microbial energy requirements are taken to be 45 $KJ.g^{-1}$ microbe (dry weight) as growth energy, a maintenance energy of 45 $KJ.g^{-1}$ microbe (dry weight) and a minimum utilisable energy of 15 $KJ.g^{-1}$ microbe (dry weight) (Thauer & Morris, 1984; Thauer et al., 1977). Calculations were based on data from groundwater analyses from KA 2858A (Appendix 6) and from the analyses of Åspö Diorite (Appendix 1 and Appendix 4). Nutrient and energy inventories were calculated for both the groundwater and rock (Table 7) and maximum microbial numbers calculated for a 1:1 (*v/w*) ratio of groundwater and rock in a sealed system. Using these inventories, BGSE gives a maximum yield of $6.631x10^{-2}g$ (dry weight).m^{-3} biomass for sulphate reducing bacteria; and $5.959x10^{-4}$ g (dry weight).m^{-3} for iron reducing bacteria. This dry weight can be converted to microbial numbers. Using conversion values from Stroes-Gascoyne (1989), the dry weight of one bacterium is about $1.5x10^{-15}g$.cell. Thus the maximum number of sulphate reducing bacteria that could be supported is $4.42x10^{7}$ bacteria.ml^{-1} (assuming 100% porosity in the mixing cell); and the maximum number of iron reducing bacteria that could be supported would be $3.97x10^{5}$ bacteria.ml^{-1}. The numbers calculated were then divided in half and resulting number of organisms were inoculated into the experiments. The lower figure allowed the possibility of nutrients and energy sources being available for microbial growth and maintenance.

5.2.2.3. Experimental set-up and procedure

A series of batch experiments were conducted to study rock-water interactions. These experiments were designed to study simple systems and were aimed at identifying relevant reactions both chemical and biological. They were essentially pilot studies to aid in the development of microbial and analytical geochemical procedures, as well as gathering basic data on rock-water interactions relevant to the Äspö site.

The experiments were conducted in BGS designed batch reactors (Figure 3), constructed of PEEK (PolyEtherEtherKetone) which is a metal free, chemically inert plastic. All reaction vessels were sterilized by autoclaving prior to assembly, and contained 20g of crushed Åspö Diorite (125-250 &m) (Section 5.1) and 20 ml of Åspö groundwater collected from Åspö borehole KA285 A (Appendix 6) giving a fluid:rock of 1:1, this being the optimum conditions for the bacterial growth, as determined by the BGSE modelling (Section 5.2.2.2). Experiments were conducted with either SRB, IRB or a mixture of both SRB and IRB, together with control experiments without any bacteria. Details of the experiments are given in Table 8.

Fluids used in the experiments were characterised both chemically and microbially before and after the experimental runs.

Assembly of Reaction Vessels

Reaction vessels were assembled in an anaerobic chamber in a series of rock/water/bacteria combinations. The procedure used is given below:-

1 Sterilise crushed Äspö Diorite by autoclaving, and place in sterilized reaction vessel.

2 Sterilise Äspö groundwater by filtration through 0.2 μm filters

3 Working in a glove box under anaerobic conditions (80% N_2 10% CO_2, 10% H_2) add 20ml of sterile Äspö groundwater + appropriate bacteria, and 20g sterile crushed Äspö Diorite to the reaction vessel

4 Seal and incubate. In order to increase reaction rates the experiments were conducted at 30 %C. This was to enable results to be obtained in a reasonable time.

5 After a set duration, working in a glove box under anaerobic conditions (80% N_2, 10% CO_2, 10% H_2), open the batch reactor. Prepare/preserve reactants for chemical, microbiological and mineralogical analysis. Rock samples were transferred to moisture tight containers and preserved for future studies. The samples for future investigation by SEM were freeze dried and those for epifluorescence microscopy were preserved in gluteraldehyde fixative.

Chemical analyses

Chemical analyses included major anions and cations; trace elements; redox sensitive species including FeII/FeIII, $NH_4/NO_3/NO_2$, $SO_4/S_2O_3/H_2S$, As^{III}/As^{V}, Se^{IV}/Se^{VI} and selected microbial nutrients (e.g. C, O, N, P). Each of the sampled fluids was split into several subsamples. A subsample of 1 ml was taken for immediate analysis of pH using an Orion 520 pH meter, fitted with a Whatman glass combination electrode calibrated at room temperature with NBS traceable buffers at pH 7 and 10. Cations were determined by inductively coupled plasma-optical emission spectrometry (ICP-OES). Anions were determined by Ion Chromatography (IC). A further subsample was complexed to 0.1% with respect to 2,2-bipyridyl, this was used for the determination of reduced iron by colorimetry using a Phillips PU 8740 scanning UV/visible spectrophotometer. Another subsample was taken and preserved with respect to NaOH solution and used for the determination of reduced sulphur by Hydride Generation Inductively Coupled Plasma-Optical Emission Spectrometry (HGICP-OES). Ammonia was determined by flow injection analysis (FIA) using a Tecator FIAstar analyser. Table 15 gives details of the sample preservations used for the various analytical methods.

Microbiological analyses

A subsample of 1 ml was taken for microbiological analyses to which was added a fixative solution in order to prevent any deteriation of the bacteria prior to staining. Glutaraldehyde is a commonly used fixative for bacterial samples - whilst respiration ceases, the cells retain their original morphology . 1ml of sample was added to a 10ml solution of 0.5% gluteraldehyde in cacodylate buffer and stored in the dark at 4%C (Jass & Lappin-Scott, 1992).

The numbers of bacteria present in the groundwater was assessed using a total count method of epifluoresence microscopy (Hobbie et al., 1977). This method is based upon a light source transmitting short wavelength radiation onto a specimen that has been filtered and retained on a membrane. The specimen is first stained with a fluorochrome solution, acridine orange, which interacts with the nuclear material of the bacteria and emits longwave radiation. When the membranes are viewed under the microscope the bacteria appear as bright green and red fluorescing cells against a dark background which enables them to be counted. By examining 20 randomly selected fields of view individual numbers can be counted and the number of bacteria per ml of sample determined. The staining procedure involves the following steps:

1. Preparation
Polycarbonate membrane filters (Millipore 0.2 μm pore size, 25 mm diameter) were stained before use in a solution of Irgalan Black (2g in 1 litre of 2 % acetic acid). This technique (Jass and Lappin-Scott, 1992) of staining membrane filters with Irgalan Black produces a high contrast between bacteria and background when viewed under an epifluorescent microscope, and therefore enhances identification of the bacterial cells.

2. Staining
To prepare the stain, 5 mg acridine orange powder was added to 50 ml of phosphate buffer (Appendix 5). This was filter sterilised using a 0.45 μm Acrodisc filter (Gelman). The sample and fixative solution was shaken and 5ml drawn through a vacuum filter system (Millipore) resulting in any bacteria present collecting on the filter surface. 1 ml of acridine orange stain was dispensed onto the filter and after 6 minutes this was drawn through, followed immediately by rinsing with filtered deionized water to remove excess stain. The vacuum was left running for a short time to begin drying the filter, before switching off and allowing it to air dry completely. The filter was then transferred to a microscope slide, a drop of immersion oil placed onto the edge of the filter, and covered with a glass coverslip.

3. Counting
The slides were examined using a Zeiss Microscope with a Zeiss III RS epifluorescent unit attached. A x10 magnification Zeiss eyepiece equipped with a graticule to aid counting was used in conjunction with a Zeiss 'Neofluar' epifluorescent x100 magnification objective. For each sample, 20 fields of view were randomly selected and the bacteria contained on them counted. From this information the average number of bacteria per ml of sample were calculated in accordance with the method given in Jass & Lappin-Scott (1992).

5.2.2. Results and Discussion

5.2.2.1. Chemistry

A full listing of the chemical analysis data for all the experimental fluids can be found in Appendix 6, the data has an associated analytical error of 5%. All the experiments used the same starting fluid (Äspö groundwater collected from borehole KA285 A (also used in 5.2.2.2) the composition of which is given in Appendix 6. The following discussion of the chemistry of the experimental fluids is concerned with differences between the starting fluid composition and the experimental fluid chemistries.

In all the experiments with rock in the reactors, pH of the fluids is seen to progressively drop (Figure 4) from a starting value of pH = 6.96 to pH 6.3 after 3 weeks reaction. In all the experiments without rock in the reactors (ie fluid only), the pH of the fluids is seen to drop pH 5.5 after 4 weeks reaction. This drop in pH is probably a result of a slow equilibrium of the experimental fluids with the anaerobic atmosphere ($H_2/CO_2/N_2$) present in the reactors (i.e. CO_2 going into solution). The drop in pH observed in the experiments with rock in the reactors, is probably buffered by rock-water interactions.

Evidence for rock-water interactions is supported by the gain of Mg, K, Si and Al in all experiments (Figures 5 and 6) containing rock in the reactors. This suggests that there has been some dissolution of some primary minerals present in the rock, although it is not possible to confirm this without detailed mineralogical analysis of the reacted materials.

Gain of carbonate to all experiments with fluid and rock (Figure 7), is probably as result of solution CO_2 from the anaerobic atmosphere. This may be partially augmented by dissolution of carbonate phase(s) present in the rock, since HCO_3 concentrations are greatest in the experiments with rock present. Detailed mineralogical analysis of the reacted materials would help to determine what is the source(s) of the increase in HCO_3 levels.

Many of the redox sensitive species ($NH_4/NO_3/NO_2$, As^{III}/As^{V}, Se^{IV}/Se^{VI}) were found to be below the detection limits of analytical methods used. However data was successfully obtained for S species (SO_4/H_2S) and Iron (FeII/FeIII), this data is presented in Figures 8 and 9. From Figure 8 it can be seen that the concentration of Total sulphur remains fairly constant (within experimental and analytical errors) in all the experiments. In the experiments involving SRB there is a small amount of reduced sulphur observed which suggests that the SRB were 'active' in these experiments, although the concentrations of HS^- detected were small. No reduced sulphur was observed in the other experiments.

Figure 9 shows the concentrations of iron in the experiments. It should be noted that the reduced iron concentrations are apparently greater than the total Fe concentrations. This is due to the different analytical techniques used to determine these species. Assuming that all iron is as reduced Fe, the data effectively represent total Fe

determined by independent techniques. The analytical errors in the methods must be taken into consideration when comparing the data. Most of the samples have reduced Fe and total Fe that are in agreement within these analytical error ranges. A few of the data have reduced Fe values that are higher than total Fe, even after taking into account potential analytical errors. These discrepancies may be explained by systematic errors that may arise because of matrix effects caused by the fluid chemistry. These effects may possibly cause suppression of the total Fe as determined by ICP and/or interferences in the reduced Fe as determined by colorimetry. Further work would be required to study such effects in detail.

In the case of the experiments without any bacteria present the concentrations of iron and manganese remain very low. Similar concentrations are seen in the experiments with IRB present. This suggests that is little dissolution of any iron phases present in the rock used in the experiments. However, in the experiments with SRB present the concentrations of iron (both total iron and reduced iron) is seen to increase from that of the starting fluid. The source of this iron is not clear, there are two possible explanations for the increased iron concentrations. The first is that the iron derives from the enrichment media used to prepare the bacteria, which was either not fully washed out during the preparation process, or was sorbed on to the bacteria. Alternatively it may be due to microbial enhanced dissolution of an iron bearing phase present in the rock. Without detailed mineralogical analysis of the reacted materials it is not possible to determine what is the source of the iron. However the enhanced Mn concentrations (Figure 10) in the experiments containing rock compared to those with no rock would support microbial enhanced dissolution of the rock.

5.2.2.2. Microbiology

A table of the results of bacterial enumeration by epifluorescence microscopy given in Appendix 7 and shown as graphs in Figure 11.

The numbers of SRB (Figure 11) present in Run numbers 531 - 533 decreased over the incubation period, most noticeably after the first week of incubation, decreasing from 1.57×10^5 to 4.55×10^4 per ml of fluid. This steady decline in numbers suggests they are able to survive for a limited period but that there is a limiting factor influencing their growth. An examination of the groundwater chemistry (Appendix 6) would suggest that carbon may be the limited factor. The chemical analysis shows sulphide is present and that SRB appear to be influencing the fluid chemistry. Microbial analysis of Run 534 (no rock) failed to detect a bacterial presence.

The number of IRB (Figure 11), in contrast, showed an initial increase at week two of incubation (Run 541) from 3.161×10^5 to 3.962×10^5 per ml. An assessment of numbers after the first week was unable to be made due to the large amount of precipitation on the membrane surface. By week three of the incubation period, numbers of IRB had decreased to 1.335×10^5 per ml. Run 543 (no rock) had a decrease in number from 1.06×10^6 to 6.283×10^5 per ml of fluid. Although IRB are increasing they appear to exert less of an influence on the fluid chemistry. An iron source may be available to them from the rock and further characterization of the residual solid material should provide more information.

The results from the mixed cultures of SRB and IRB (Figure 11) showed a small increase after the first week after which numbers decreased with none detected at week three (Run 540). Run 546 (no rock) had only a slight decrease in number over the period, from 2.04 $x10^6$ to 1.742 $x10^6$ per ml. The large number present in Run 546 appears to be as a result of possible contamination of the fluid by the iron media from the original culture, chemical analysis of the fluid seems to confirm this with large amounts of iron detected. Examination of the bacteria by epifluorescence microscopy showed that the IRB (by morphology) appeared to predominate. Previous studies (Ekendahl, 1996) had noted that iron reducers will alter the levels of electron donors in such a way that SRB are unable to metabolize. In other words, the iron reducers appear to out-compete the SRB. The SRB numbers in the mixed cultures appear to have decreased whilst there is an increase in the number of IRB detected.

5.3. Mineralogical investigation of batch experiment residues

5.3.1. Analytical methods

5.3.1.1. Scanning electron microscopy sample preparation

Experimental residues from the REX Year 1 batch experiments (West et al., 1997) were recovered and stored in sealed containers filled with an inert (oxygen-free) nitrogen-hydrogen atmosphere prior to petrographic analysis and mineralogical characterisation. The characterisation of the residues was not included within the remit of the Year 1 REX programme (West et al. 1997). Therefore, the preserved residues were stored under refrigeration at 5 °C for 6 months until they could be analysed during the present (Year 2) REX programme.

Each residue was subsampled and any remaining material was resealed under a nitrogen gas atmosphere to prevent alteration due to oxidation. The storage containers were then sealed within individual polypropylene bags also filled with nitrogen gas. These were then placed in refrigerated storage.

Two preparation routes were followed to prepare specimens from the subsampled residues for examination in the scanning electron microscope (SEM):

(i) in an 'as received' condition;
(ii) after washing the residues to remove residual saline pore fluid.

It was found necessary to wash the samples (ii) since preliminary SEM observations of the 'as received' material showed that mineral surfaces were encrusted by salts (mainly NaCl crystals) precipitated from the residual experimental fluid. These obscured the observation of any fine surface detail, making assessment of the effects of dissolution or precipitation on grain surfaces impossible.

(I) Preparation of material in 'as received' state
The subsampled residues were rapidly frozen by immersion of about 1 cm^3 of material in liquid nitrogen, fixing the solid materials in an ice glass. The frozen samples were then placed in an Edwards Modulyo freeze dryer and dried under vacuum for a period of 24 hours. When dried, the residues were placed in sealed containers topped with an oxygen-free nitrogen atmosphere and stored in a desiccator. Portions of the dried material were mounted on 12 mm diameter aluminium pin-type SEM stubs using LEIT-C carbon-based electrically-conducting adhesive. The prepared stubs were coated with carbon by evaporation using an Edwards E306A coater to give a coating thickness of approximately 25 nm

(ii) Preparation of material washed free of residual saline pore fluid
The solid residues were resampled, and the subsampled material was washed to remove the saline experimental pore fluid. Each subsampled residue was subjected to gentle washing in sterile, filtered, deionised water. Three washes were performed with 60 seconds settling time between washes to minimise loss of fine material from the samples. Washed material was then flushed twice with acetone to displace the residual water from the washing process. The subsamples were then placed under vacuum for 2 hours in the Edwards Modulyo freeze dryer to remove the acetone. Portions of the dried material were then mounted on 12 mm diameter aluminium pin-type SEM stubs using carbon based double-sided adhesive tabs. Duplicate samples were also prepared using LEIT-C conductive carbon conductive adhesive as an alternative SEM stub mount, but it was found to be unnecessary to examine these during this study. The prepared stubs were coated with carbon by evaporation using an Edwards E306A coater to give a coating thickness of approximately 25 nm.

5.3.1.2. Cryogenic scanning electron microscopy preparation

Preparation of the solid residues for examination in wet-state under cryogenic conditions in the SEM (CryoSEM analysis) was performed using an Oxford CT1500 cryogenic SEM preparation and cryogenic transfer system fitted to a LEO 435VP variable pressure SEM. Initially samples were prepared in an 'as received' condition; however salt contamination precipitated from the experimental fluid on freezing prevented observation of the grain surfaces. Therefore a washing procedure was instigated to minimise salt formation on the samples during sample freezing.

Subsamples were taken from each experimental residue in 'as received' condition. The material was flushed with 25 ml of sterile filtered, deionised water and allowed to settle. Excess water was then decanted off and flushing repeated for a total of three flushes. An aliquot of the flushed subsample was then loaded into a two-part brass specimen cup fitted to the cryogenic sample preparation and transfer device.

The specimen was then inserted into the cryogenic pre-freezing chamber and rapidly frozen in a melting solid nitrogen/liquid nitrogen slush at ²196 °C. After freezing had occurred the slushing chamber was evacuated and the specimen withdrawn in to the vacuum enclosure of the cryogenic transfer device to prevent deposition on the sample, of ice from atmospheric water vapour. Once a suitable vacuum had been established the cryogenic transfer device was sealed and connected to the cryogenic

preparation unit fitted to the side of the SEM sample chamber. The specimen was transferred to the preparation chamber when working vacuum had been established. The upper section of the specimen cup was then sheared away from its base to produce a freshly exposed fracture surface through the frozen specimen.

The fractured specimen was then installed directly onto the cold stage within the SEM and the specimen surface examined. Excess ice present on the sample surface was etched from the sample by heating the cold stage to -80 °C. When etching was completed the specimen was taken back into the cryogenic preparation chamber and cooled to approximately -170 °C. The specimen was then sputter-coated with gold to allow high resolution imaging of the specimen surface. Typical coating conditions were 2 x 10^{-1} mbar argon atmosphere and 10 mA sputter current for periods of 2 to 6 minutes until a satisfactory coating had been achieved.

5.3.1.3. X-ray diffraction studies

X-ray diffraction (XRD) analysis was undertaken on both the starting material (sample C853), initially used as a feedstock in BGS laboratory experiments (cf. West et al., 1997), and the residues (MPG codes D248-259; Table 10) from the experiments, the aim being to assess any mineralogical changes that may have occurred during the batch experiments. Both the bulk samples and fine (< 63 μm) fractions of the starting material and experimental residues were analysed.

Representative subsamples (≈ 3g), of the materials supplied were micronised under acetone for five minutes. For fine-fraction analysis, the remaining material was dispersed in 100 ml distilled water by treatment with ultrasound for approximately 3 minutes. The resulting suspension was then sieved on a 63 μm sieve, and the < 63 μm fraction collected. The micronised powders and fine fractions were then dried in an oven at 55 °C and back-loaded into standard aluminium XRD sample holders.

XRD analysis was carried out using a Phillips PW1700 series diffractometer using Co-Ka radiation and operating at 45 kV and 40 mA. The mounts were scanned over the range 3-50 _2q at a scanning speed of 0.5 _2q/minute. Diffraction data were analysed using Phillips APD1700 software coupled to a ICDD database running on a DEC Micro Vax 2000 micro-computer system.

5.3.1.4. Conventional SEM analysis

The stub mounted samples were examined using a LEO 435VP variable pressure SEM operating under both high vacuum and variable pressure conditions. Variable pressure operation was necessary for a limited number of specimens in order to eliminate sample charging, where the carbon coating of loose sample material did not provide satisfactory earthing of accumulated electron charge. The SEM instrument was operated at 20 kV accelerating voltage and probe currents of 75 to 150 pA. Mineral identifications were aided by qualitative X-ray microanalysis, using an Oxford Instruments ISIS 300 energy-dispersive X-ray (EDXA) microanalysis system fitted to the SEM.

5.3.1.5. Cryogenic SEM analysis

Solid residues from each experimental run were examined by cryogenic scanning electron microscopy (CryoSEM). Analysis was performed using a LEO 435VP variable pressure SEM fitted with an Oxford Instruments SEM cold-stage. Identification of mineral surfaces under observation was aided by qualitative observation of X-ray spectra using an Oxford Instruments ISIS 300 energy-dispersive X-ray (EDXA) microanalysis system.

Specimens were examined in the SEM under high vacuum conditions. Standard instrument conditions were 20 kV accelerating voltage and 75 pA probe current, appropriate to allow EDXA identification of minerals. Preliminary searches of the specimens were performed prior to gold coating using backscattered imaging (BSEM) mode. This allowed location of rare phases, e.g. pyrite, magnetite, sphene, etc., due to their high BSEM responses relative to the bulk of the specimen. Stage positions were stored in the computer memory of the SEM for each grain found. This allowed their precise relocation after removal of the sample from the SEM for gold coating and subsequent re-insertion for observation. When coated the specimens were examined in secondary electron imaging (SEI) mode to allow best resolution of surface features.

5.3.2. Results and discussion

5.3.2.1. Conventional SEM observations

Crushed diorite starting material (sample C853)

The Äspö Diorite used in the experiments was crushed and prepared as sand-grade material in the grain size range 125 to 250 μm (West et al., 1997). SEM observations on the starting material (West et al., 1997) showed that, although most of the fines formed during crushing of the rock were removed by subsequent sample preparation, a small amount of fine-grained (<1 μm) mineral particulate still adhered to the grain surfaces (Plate 1). Higher concentrations of fine particulate material occur embedded in pits and irregularities in many grain surfaces. This is particularly true of the feldspar grains (Plate 19) which tend to have very rough or well-developed 'stepped' cleavage surfaces. The fine grained particulate material has a similar mineralogy to the bulk diorite material and is composed largely of quartz, albite, orthoclase, biotite and chlorite (or chloritised biotite).

Quartz grains typically have smooth surfaces or finely-ribbed conchoidal fracture surfaces. There is little evidence of pitting and the fractured edges of the grains are sharp. The majority of biotite, chlorite and chloritised biotite grains have a characteristic flaky morphology which has developed by fracturing along the minerals prominent basal [001] cleavage (Plate 20). Basal cleavage surfaces are characteristically smooth and generally absent of any corrosion or etch-pitting. The fractured edges of the grains are much more irregular and stepped, and may be distorted and bent as a result of mechanical damage during crushing. However, in general, little or no exfoliation of the mica sheets along their basal [001] cleavage is evident (Plate 20). In contrast, the surfaces grains of albite or orthoclase are much

more irregular. These minerals typically have stepped surfaces (Plate 21) developed as a result of fracturing along the three intersecting strong cleavage directions of these minerals. Many of the feldspar grain surfaces also appear to be etched or pitted in the starting material. This most probably represents the fine-scale natural, in situ, dissolution and microporosity development of the feldspars which was also observed in detail in thin section (cf. West et al., 1997). However, the fractured edges of the feldspar grains are characteristically sharp.

Other minor components observed in the starting material include, minor to trace amounts of hornblende, sphene and magnetite, and trace amounts of pyrite, chalcopyrite and epidote. The hornblende and epidote grains are morphologically similar to the feldspar grains. Trace amounts of calcite were also observed. These grains are also characterised by sharp, stepped cleavage surfaces. In contrast, magnetite and pyrite grains have largely been liberated during crushing as intact euhedral crystals (e.g. Plate 22). The pyrite crystals characteristically display clean, smooth crystal faces with no evidence for dissolution or alteration. Magnetite crystals can be similarly fresh-looking but many grains also display evidence of surface etch-pitting or corrosion (Plate 23). The etching often takes the form of irregular or worm-like interconnected 'channels' that most probably represents intracrystalline grain-boundary dissolution in the in situ rock.

Batch experiment residues

Residues from all the batch experiments containing Äspö Diorite (Table 10) were examined by SEM. No significant difference could be discerned between the residues from each of the different types of batch experiments: i.e. those experiments 'with SRB', 'with IRB', 'with both IRB and SRB' or 'without bacteria'. Consequently, any of the qualitative mineralogical changes that were observed in the experiments could not be specifically correlated with microbial activity. The principal variations observed in the alteration of the Äspö Diorite residues appear to be related to the duration of the experiments: i.e. the three week experimental runs showed greater evidence of rock-water reaction than the two week experiments, which in turn, displayed more alteration than one week duration experiments.

In general, very little difference was observed, for most minerals present in the sand-grade fraction material, between the initial starting material (sample C853) and the experimental residues. No conclusive evidence for the dissolution of the major minerals; quartz, K-feldspar (orthoclase) and plagioclase (albite) was observed in the sand-grade material. The grain surface features observed in the experimental residues was indistinguishable from those observed in the starting material. Although the feldspar grains commonly display etched and pitted surfaces, this could not be attributed to dissolution during the course of the experiments since, similar etched surfaces can be observed in feldspars in the starting material. No conclusive evidence for the dissolution or alteration of pyrite, magnetite, epidote, calcite or sphene was observed.

Only biotite or chloritised biotite displayed any evidence of reaction within the sand-grade grain-size material. In the starting material (Section 3.2.1.1.) the biotite or

chlorite-biotite grains typically displayed tight packing of the cleavage sheets (Plate 20). However, minor alteration of the biotite appears to have occurred during the batch experiments. This has resulted in exfoliation along the basal [001] cleavage at the edges of the mica grains (Plate 24). In contrast, the platy basal [001] cleavage surfaces of the biotite and chlorite show no evidence of corrosion and dissolution. This implies preferential attack and dissolution along the [001] cleavage at the mica flake edges. Dissolution of biotite and chlorite is most evident in the three week experiments but is apparent in the residues from the two week experiments. However, dissolution of biotite can only just be perceived in the residues from one week experiments, but often the biotite grains are indistinguishable from those in the starting material. No difference in dissolution behaviour of the biotite was observed between the experiments with SRB, IRB and SRB + IRB inoculations, or between these experiments and the experiments without bacteria present.

Another subtle alteration effect observed was the loss of the fine-grained (^{2} 1 μm) particulate mineral matter from the surfaces of the sand-size fraction material. The extent of removal of fines increased progressively from the one week experiments (which showed little difference to the starting material), through the two week experiments, to the three week experiments (which showed the most significant loss of fine material). In part, the loss of fines from the surfaces of the sand-grade grains might be attributable to 'washing' in the experimental fluid. However, after three weeks the fine-grained particulate material typically displays rounding and the development of corrosion embayments of the particle edges (Plate 25), in contrast to the sharply angular particulate seen on the grain surfaces in the starting material. Fine particles of quartz, albite, orthoclase, biotite and chlorite all appear to be affected. This strongly suggests that at least some dissolution of all the major minerals has occurred during the batch experiments. No difference in dissolution behaviour of the fine particulate material could be determined between the experiments with SRB, IRB and SRB + IRB inoculations, or between these experiments and the experiments without bacteria present.

No microbiological structures were observed or preserved in the batch experiment residues prepared for conventional SEM observation.

5.3.2.2. CryoSEM observations

Experiments without bacteria inoculation (Runs 535, 536 and 537)

Residues for the experiments containing only Äspö groundwater and the crushed diorite showed no evidence of biological structures. Grains from sample D251 (Run 535, 1 week reaction) showed little evidence of reaction with the experimental fluid. Mineral fines present on the crushed grain surfaces show no evidence of dissolution and retain their original sharp angular morphology. Biotite grains showed minor opening or exfoliation along basal plane surfaces but no evidence of actual etching on plate edges. Minor etching was observed on calcite grains within the sample however these may be pre-experimental dissolution fabrics inherited from the calcite in the original diorite. Smooth fracture faces seen mainly on quartz grains showed a fine

coating of amorphous material. This may be an organic biofilm and EDXA analysis shows it contains trace quantities of Fe, Na, K and Al.

Samples from the two and three week experiments showed no evidence of reaction except for biotite grains. These showed increased opening or exfoliation along basal planes and minor rounding of grain edges (see similar observations reported in Section 5.3.2.1 Mineral fines showed evidence of minor dissolution having occurred, with more rounded and embayed forms evident than for the one week experiment. The later experiments showed reduced levels of the fine coating material seen on quartz surfaces than was seen in the one week experiment. Where present, the coatings exhibited similar morphology and mineralogy as observed in the one week experiment, and to that observed previously in Section 5.3.2.1.

Experiments inoculated with cultured iron reducing bacteria, (Runs 542, 541 and 539)

The one week experiment inoculated with IRB showed little evidence of biological or chemical reaction. All mineral phases observed appeared unaltered in comparison to the starting material. A single filament possibly of biological origin was observed on the surface of a quartz grain but no discrete associated bacteria cells could be identified or differentiated.

Residues from the two week experiments showed organic spherical cell forms very tentatively identified as 'bacteria'. The forms observed were coccoid in nature but of smaller size than normally expected for bacteria, all being less than 1 μm in diameter. EDXA analysis of the forms showed no additional detectable elements present that could be differentiated from those detectable from the underlying mineral grain substrate. Coccoids were observed on grain surfaces and also trapped within the ice formed during cryo-fixation (Plates 26 and 27). Strings of coccoid cells tend to be concentrated in the 'lee' of irregularities in grain surfaces - e.g. along the 'valleys' of ribbed conchoidal fractures in quartz grains or cleavage steps in feldspar grains.

Residue from the three week experiments showed no evidence of coccoids seen in the two week experiments. No obvious mineralogical alteration or mineral dissolution was observed.

Experiments inoculated with cultured sulphur reducing bacteria (Runs 531, 532 and 533)

Examination of the residue from the one week experiment revealed structures present within the coatings of some grain surfaces. EDXA showed the coatings to be composed of ice with traces of Fe, Na, K and Si. These traces may be due to the presence of salts within the ice matrix or fine clays or oxides entrapped within the ice. Examples of these are shown in Plates 28 and 29. These structures form a 2-dimensional framework on the grain surfaces. The typical width of the cross-members within the structures is 0.5-1 μm. identification of the mineral species on which the structures lay was not possible. EDXA showed only Au (from the gold coating) and O (from ice) to be present when analysing areas outside the structures themselves. This

was revealed to be due to poor etching of ice from the grain surfaces, during cryoSEM, leaving a considerable thickness of ice remaining on grain surfaces. No obvious bacterial structures were observed in the sample.

The two week duration experiment showed no evidence of the structures as observed in the one week experiment. Grain surfaces in this sample showed no evidence of either organic biofilms or of biological etching effects on mineral surfaces. However, organic rod-like cellular forms, approximately 10 μm in length and 0.3 μm thick, with an organic composition were observed on the surface of a single albite grain. These were clustered together within a depression in the grain surface. An example is shown in Plate 30.

The three week duration experiments showed the development of significant volumes of organic filamentous biofilm structures on grain surfaces and binding grains together within the sample. These filaments lay upon the surfaces of, and were suspended between grains of feldspar and quartz. Filaments observed fell into two groups. The first group had significant volumes of ice and fine-grained minerals attached to their surfaces. This group is similar to structures seen in the one week experiment (Plates 31 and 32). These were mainly observed lying directly across grain surfaces. The second group consisted of filaments suspended between grains. These have generally clean surfaces but locally trap occasional accretions of fine mineral matter where filaments intersect. Typical filament thickness observed was 20-30 nm with lengths of up to 200 μm. Examples of these filaments are shown in Plates 33-34.

Experiments inoculated with combined cultures of iron reducing and sulphate reducing bacteria (Runs 545, 544 and 540)

Biologically-derived structures were observed in residues from one week reaction with the mixed bacterial culture. Rafts of biofilm were observed on the surfaces of quartz grains. The material contains many bacterial structures with elongate or rod-like morphology, thought to represent IRB. These are similar to the morphology of IRB reported from the Äspö groundwaters by Pedersen et al. (1996). These bacterial cells occur within an organic gel-like mucilage (Plates 35 and 36). A single example of what is thought to be a possible IRB structure is shown in Plate 37 'bonding' or attached to a quartz grain surface. Fine spherical particles seen on many quartz surface are residual ice remaining from the cryoSEM sublimation process. No structures with obvious SRB morphologies (cf. Pedersen et al., 1996) were observed in the sample.

No evidence of biological structures or of bacteria were observed in the residue from the two week experiment. The three week experiment residue showed the development of filament organic structures (Plate 21 and 22) similar to those observed in the three week experiments inoculated with SRB only. These were observed only upon the ice surfaces and not actually on mineral grain surfaces. They are therefore interpreted to be present within the interstitial pore fluid, rather than attached to mineral surfaces.

5.3.2.3. X-ray diffraction analysis

XRD analysis of both the bulk and separated fine (< 63 mm) fraction of the starting crushed diorite material (sample C853) revealed that both were mineralogically similar. Both the bulk crushed rock and the fine particulate material (observed on grain surfaces by SEM) are composed of major quartz, along with minor amounts of albite, orthoclase, mica and chlorite, and a trace of hematite.

No significant differences could be discerned by XRD analysis between the original bulk crushed diorite (sample C853) and the residues from the batch experiments. All the batch experiment residues were found to contain halite as a minor or trace phase. This has been shown by SEM observation (Section 3.2.2) to be derived by crystallisation, during drying of samples of the residue, from the interstitial experimental groundwater solution used in the experiments. In the bulk XRD analyses, variations in peak intensities for the main diffraction lines (or lines free of significant interference) have been recorded (Table 4) for each of the main mineral phases present in both the starting material and the reacted residue samples. From this it can be seen that all diffraction peak intensities vary, sometimes showing a uniform increase when compared to the starting material. This indicates that the variation is probably due simply to analytical error. Nevertheless, the data appear to show a relative increase in abundance of clay/mica minerals in the reaction residues. However, the SEM observations (see above) indicate that this is unlikely, and any variations observed are considered to be due to subsampling errors.

Similar variation were observed in the XRD analyses of the fine fraction extracted from the reaction residues (Table 12a). The most pronounced changes in diffraction peak intensity are within the analytical error, and/or are most probably due to variations during subsampling of material. This evaluation is reinforced by normalising all diffraction peak intensities to that of the quartz, assuming its variation to be entirely analytical (Table 12b).

5.4. Discussion

The field work at the Hard Rock Laboratory examined Potential Flowing Features (PFF) in two boreholes (KA2858A and KA2862A). Close examination of the PFFs in the REX boreholes indicates that flow is probably strongly channelled along asperities or irregularities in the fracture surface. The distribution of mineralisation on these surfaces suggests that although the total fracture surface area may be dominated by host rock minerals, or reactivated surfaces of old chlorite mineralisation, much of the actual ("wetted") surface in contact with groundwater may be dominated or strongly influenced by calcite coated with minor to trace amounts of pyrite. Pyrite (or other sulphides) is also present in fine grained disseminations in the matrix of the host rocks in the REX block. This may be significant for the evaluation of microbial interactions in the REX programme, as it will be very susceptible to reaction.

Detailed mineralogical characterisation of geological materials from the REX block showed that only a limited number of mineral species are likely to be significant with respect to either redox reactions or the provision of energy and nutrients for

microbiological use. With respect to these processes, the principal mineral-hosted elements are the redox-sensitive elements Fe (present as Fe^{2+} and Fe^{3+} in pyrite, biotite, chlorite, epidote, magnetite and ilmenite), Mn (present Mn^{2+}, Mn^{3+}, Mn^{4+} present in ilmenite), and S (present as barite and sulphides - largely pyrite marcasite, galena and chalcopyrite), and C (present as calcite).

The results of the chemical and mineralogical analyses showed evidence for dissolution of primary minerals particularly the fine particles of quartz, albite, orthoclase, biotite and chlorite but no conclusive evidence for the dissolution or alteration of pyrite, magnetitie, epidote, calcite or sphene was observed in the mineralogical analysis. Many of the redox sensitive species ($NH_4/NO_3/NO_2$, AsIII/AsV, SeIV/SeVI) were found to be below the detection limits of analytical methods used. Total sulphur remains fairly constant (within experimental and analytical errors) in all the experiments. In the experiments involving SRB there is a small amount of reduced sulphur observed which suggests that the SRB were 'active' in these experiments, although the concentrations of HS- detected were small. No reduced sulphur was observed in the other experiments. When SRB are present the concentrations of iron (both total iron and reduced iron) increases from that of the starting fluid. The source of this iron is not clear, but may be derived from microbially enhanced dissolution of an iron bearing phase present in the rock. No conclusive mineralogical evidence could be found for this. No evidence was found for the precipitation of new (secondary) reaction products. Given the very short timescales (three weeks maximum) and low-temperature (30 °C) of the experiments, the lack of any observed alteration is not suprising. Previous rock-water interaction experiments involving seawater and granitic rocks (e.g. Milodowski et al., 1989) show that even at higher temperatures (up to 200 °C) only a small amount of mineral dissolution and secondary mineral formation may be formed over a comparable timescale (four weeks). Therefore, significantly less alteration would be expected from experiments conducted for only one to two weeks duration and at only 30 °C.

In addition to the minor dissolution of sand-grade biotite, the removal of fine grained particulate mineral matter from grain surfaces was observed. These fines were produced during rock crushing, and were originally present in the starting material, and have a similar mineralogy to the bulk crushed diorite. The abundance of fine mineral particulate decreases with increasing experiment duration. In part, the fines may have been washed (i.e. rinsed) from the coarser grain surfaces by the fluid component used in the experiments. However, the fine mineral particles appear to change from original sharply angular morphologies seen in the starting material, to progressively more rounded and embayed particles in the one week, two week and three week duration experiments. This appears to indicate that preferential dissolution of fine mineral particles has occurred in the batch experiments. In all experiment 'types', quartz, biotite, chlorite, albite and orthoclase 'fines' show evidence of dissolution.

Both SRB and IRB appeared to be able to grow in the batch systems albeit for a limited period due to exhausation of nutrient and energy supplies. SRB seem to have a greater effect on groundwater chemistry than IRB with sulphide being produced. IRB appear to have no effect on groundwater chemistry in these experiments.

However, when the two types of bacteria are mixed together the IRB appear to dominate the system but no conclusive evidence was obtained from the mineralogical analyses.

Only tentative identification of bacterial structures could be made from observations even in experiments where high populations were reported. Development or preservation of biofilms and biologically-derived structures is very limited. In part this may be partly caused by the loss of biofilm material during sample preparation, which required the saline pore fluid to be rinsed from the residues before any observations could be made (due to salt contamination). Biofilaments were observed in experiments with SRB, SRB + IRB and in the 'without bacteria' residues. Their presence in the 'without bacteria' experiment residues raises the possibility that the filamentous structures may be a post-reaction artefact formed during long term storage of samples. Alternatively, the materials used in the 'without bacteria' experiments may not have been totally sterile or abiotic. Possibly bacteria may have been present in the Äspö groundwaters used for the experiments. Biofilaments, biofilms and cellular microbial structures observed in the samples closely resemble those present in Pedersen et. al. (1996). These features are clearly visible under cryoSEM observation but were not preserved in samples prepared for conventional SEM analysis. Filamentous structures are associated with bacteria having both rod and coccoid morphology.

In the experiments with IRB, bacteria we found to be preferentially concentrated on grains with rough surfaces. Cells or strings of cells were found to be more densely aggregated within hollows and other irregularities such as 'valleys' between the ribs of conchoidal fracture surfaces of quartz or the cleavage steps in feldspar grain surfaces. This would suggest that these bacteria are encouraged by sites which enable them to attach themselves (or their biofilms) to the mineral surfaces. Therefore it seems feasible that rough surfaced fractures are more likely to be favourable for bacterial activity than smooth surfaced fractures (at least with respect to IRB). This may have important implications with respect to potential microbial activity in groundwaters flowing through the different potential flowing features (PFFs) in the REX block at Äspö. Hydraulically-conductive fractures or PFFs which have opened by reactivation and dilation along sheared clay-mineralised rich fault gouge or sheared chlorite veins will tend to have smooth or polished microsurfaces, due to the inherent well-developed basal cleavage properties of the phyllosilicate minerals. In contrast, fractures which in effect are developed as 'new' fractures in the diorite, rather than reactivation of pre-existing chlorite veins will tend to have rougher surfaces. Furthermore, the latter type of PFFs often developed significant microporosity in the adjacent wallrock due to the dissolution of feldspar and/or to microfissuring. This will further increase the effective 'roughness' of the porosity in the PFFs. Consequently, substrate conditions might be expected to be more favourable for biological activity (at least with respect to IRB) in these PFFs than in PFFs developed within reactivated fault gouge or chlorite veins.

Poor observation or preservation of biological structures are probably due to the prolonged storage of the residues. Unfortunately, because of budgetary limitations, detailed analysis of the residues from the Year 1 experiments was not contracted until

Year 2 of the REX programme. It is therefore recommended that future work should be performed as promptly as is practical after completion of the experiments. Also sub-samples for cryoSEM analysis should be stored cryogenically (under liquid nitrogen) immediately upon removal from the reaction vessels.

5.5. Conclusions

1. The anaerobic batch experiments have shown that bacteria from the Äspö site have an effect on groundwater chemistry and that there appears to be a link between their presence and primary mineral dissolution. The sulphate reducing bacteria appeared to have a greater effect on groundwater chemistry than the iron reducers with sulphide being produced.

2. Both sulphate reducing bacteria and iron reducing bacteria grew in the low nutrient environment albeit for a limited period because of the sealed nature of the systems.

3. Biofilaments, biofilms and cellular microbial structures were clearly visible in the samples under cryoSEM observation and appear to be concentrated on rough surfaces. This may have important implications with respect to potential microbial activity in groundwaters flowing through potential flowing features (PFFs) with rough surfaces in the REX block at Äspö or, indeed, at other similar sites. In such PFFs substrate conditions might be expected to be more favourable for biological activity and thus effects on geochemistry and mineralogy could be localised.

4. These findings have shown there is a need to continue the experiments to explore further the effects of microbes on fluid/rock interactions in both anaerobic and aerobic conditions. These limited experiments have indicated that microbes can change groundwater chemistry and, possibly, enhance mineral dissolution. The concentration of biofilms on 'rough' surfaces also needs to be examined. If microbial activity is concentrated on 'new' fractures which could be caused by repository excavations then their effects would be particularly evident in the near-field. However, it is too early to speculate further on the implications of such activity.

6. COLUMN EXPERIMENTS

6.1. Introduction

6.2. Field Sampling and Characterisation of Starting materials for year two Flow-through Experiments

6.2.1. Field Sampling

A brief field visit was made to the Äspö Hard Rock Laboratory, Äspö Island, Figholm, Sweden during 16-17 September 1997 in order to collect further samples of groundwater and Äspö Diorite for use in the Year 2 Laboratory Experimental Programme. As in Year 1, the samples were all collected from the REX alcove in the underground laboratory. A full description of the sampling site is provided by Milodowski et al. (1996) and West et al. (1997).

6.2.1.1. Groundwater sampling

Groundwater samples were taken from a gently inclined, sub-horizontal borehole - borehole KA2858A - which had previously been sampled for the Year 1 laboratory experiments (West et al., 1997). This borehole has been completed with three packered intervals: Section 1 samples water entering the borehole between 6.02 and 38.77 m; Section 2 samples the borehole between 39.77 and 40.77 m; and Section 3 samples the borehole between 41.77 and 59.77m from the tunnel wall. Section 2 was sampled for use in the BGS experiments.

Two 20 litre samples were collected anaerobically using special stainless steel flasks. These were fitted with an inlet tube that reached to the base of the flask and an outlet tube at the top. Both the inlet and outlet had spring-loaded needle-valves that opened when the clip-fit connecting pressure hoses were fitted, and these also sealed the vessel automatically once the hoses were removed. The vessels were rinsed three times with water from borehole KA2858A prior to sample collection and then flushed for 20 minutes with oxygen-free nitrogen before filling with the groundwater. Subsequently, the flasks were connected to the discharge line from Section 2 of the borehole and filled from the bottom-upwards, (displacing the nitrogen-top atmosphere as they were filled with water). The two vessels were connected in series during filling, and a bubble trap was fitted at the outlet to the second flask to prevent any back-diffusion of atmospheric oxygen during the sampling operation.

The borehole was opened and allowed to discharge three borehole-volumes of groundwater before any sampling started. This was done in order to flush out any 'stagnant' groundwater residing within the borehole. During this process the flow was measured by timing the collection of a measured volume of groundwater in a large measuring cylinder. The groundwater discharge from Section 2 of borehole KA2858A was estimated to be 0.22 litres/minute.

The groundwater was also sub-sampled for chemical analysis. Samples for analysis were collected immediately before filling, and immediately after filling, the large

stainless steel sampling flasks. Eh (±0.1 mV), pH (±0.01 pH unit), temperature (±0.1 °C) and conductivity were determined during sampling using portable meters (Orion Research Model SA250) fitted with specific ion electrodes. The Eh was measured with a standard Pt-Ag/AgCl electrode verified with Zobell's Solution (standard solution Eh = 200-250 mV). Eh readings were corrected for temperature (corrected Eh = uncorrected Eh + (244-T), where T is the temperature in degrees Celsius). The pH electrode was calibrated using standard pH4 and pH7 buffer solutions. The conductivity electrode was calibrated using a standard KCl solution.

Dissolved O_2 was determined in the field using a commercially-available small portable colorimetric test kit (CHEMetrics). This contained pre-prepared vials of colorimetric reagent, sealed under vacuum, into which a fixed volume of groundwater was taken up when the tip of the vial was broken whilst immersed in the groundwater sample. The colour developed was assessed visually by comparison with a set of vials of standard concentrations for a range of dissolved oxygen contents from 1 to 12 ppm.

Bicarbonate was determined in the field by titration using a portable mechanical autotitrator kit. The water sample (25 ml) was titrated with standard sulphuric acid using Bromocresol Green indicator solution. Titrations were checked in the field against a 200 ppm bicarbonate standard solution which had been pre-prepared at BGS.

Water samples for subsequent chemical analysis at BGS were collected, filtered and preserved in the field. A 30 ml sample for major and trace cation analysis was collected directly into a plastic syringe. This was then filtered "on-line" through a 0.45 μm pore diameter Acrodisc nylon filter, directly into Nalgene bottles. Samples were preserved by acidification to 1% with respect to AristaR nitric acid. Acid used in sample preservation was measured and dispensed using a hand-held autopipette. A 30 ml sample was similarly collected and filtered for ammonium analysis. However, this was preserved by acidification with 2 mls of AristaR sulphuric acid. A 30 ml sample for major and trace anions, total inorganic carbon (TIC) and total organic carbon (TOC) was collected in a similar manner as for major and trace cations, except the water samples remained unacidified. Samples for determination of reduced Fe were taken and preserved by collecting and filtering "on-line" through a 0.45 μm pore diameter Acrodisc nylon filter directly into Sterylin plastic tubes to which 1 ml of 1% 2,2-bipyridyl solution (HCl acidified) had be added. The volume was made up to 10 ml total with the sample. The 2,2-bipyridyl forms a stable red-coloured complex with ferrous iron in solution. A 30 ml sample of unfiltered water was collected and for subsequent analysis of reduced sulphur. This was preserved by the addition of two pellets of sodium hydroxide. Blank samples for each of these preservations, using double-distilled water, were also prepared on-site.

6.2.1.2. Rock sampling

A large (c.15-20 kg) block of diorite was collected from the tunnel wall within the REX alcove in the Äspö Hard Rock Laboratory, from the same location as that previously sampled during Year 1 (Milodowski et al., 1996; West et al., 1997). The sample was taken from the right-hand wall (down-tunnel side) of the REX alcove,

located at the level of, and approximately 3m from, the position of borehole KA2862A (refer to Milodowski et al., 1996 for further locational information).

Both rock and water samples were couriered to BGS by SKB upon completion of the sampling visit. On receipt of the samples by BGS in the United Kingdom, the large-volume water samples (in the stainless steel flasks) were placed in cold storage at 5 °C until required for use in the Year 2 laboratory experiments.

6.2.2. Preparation of diorite experimental starting material

The experimental work requires crushed material within a limited grain-size range of 125-250 μm (hereafter referred to as the "sand fraction"). The sample itself was composed of a solid block, ≈ 50 cm in length, bounded by fracture planes. It was first scrubbed to remove surface contamination, then jaw crushed. A representative sub-sample of the jaw crushed material was retained for analysis while the remainder was further prepared by wet-sieving to pass a 250 μm sieve. The <250 μm material was then sieved on 125 μm. Sub-samples of the retained jaw crushed material, the sand fraction and fines (<125 μm) were then tema-milled for subsequent analytical work to assess any fractionation that had resulted from the particle-size splitting of the sample.

6.2.3. Analytical methodology

6.2.3.1. Groundwater analyses

The samples of groundwater collected from the Äspö Hard Rock Laboratory were chemically analysed at the BGS. HCO_3^- was determined by automatic titration with 0.01 M sulphuric acid. Ca, Mg, Na, K, Total P, Total S, Si, Ba, Sr, Mn, Total Fe, Al, Co, Ni, Cu, Zn, Cr, Mo, Cd, Pb, V, Li and B were analysed by inductively-coupled plasma - atomic emission spectrometry (ICP-AES). Cl, Br, SO_4^{2-}, NO_3^-, NO_2^- and HPO_4^{2-} were determined by ion chromatography. F was analysed by ion-selective electrode. The analysis of TIC and TOC was performed using an automated total carbon analyser with a non-dispersive infrared detector. Reduced S was determined by hydride generation ICP-AES. Flow-injection analysis coupled with colorimetric analysis was used for the determination of NH_4. Reduced Fe was determined by ultraviolet/visible spectrophotometry. The field measurement of pH, Eh, temperature, conductivity, HCO_3^- and dissolved O_2 have been described above.

6.2.3.2. Petrographic analysis of Äspö Diorite sample

Two standard thin sections were prepared from the Äspö Diorite starting material (sample D337), one from the outer edge (section P1) and one from the centre (section P2) to give a measure of heterogeneity in the material. Optical petrographic observations were made using a high-quality Zeiss optical petrographic microscope. Photomicrographs were taken using a Zeiss Ultraphot photomicroscope fitted with a Zeiss M35 camera on 200 ASA Kodak Gold film.

6.2.3.3 X-ray diffraction analysis of Äspö Diorite sample

X-ray diffraction (XRD) analysis was undertaken on both the bulk diorite sample (D337), the sand fraction prepared for use in further BGS laboratory experiments and the removed fines (which were to be discarded). The aim of this was to assess any mineralogical fractionation that may have occurred in the preparation and cleaning-up of the sand-grade fraction material intended for use in the BGS column experiments. A representative subsample (≈ 3 g), of each of the tema-milled materials was micronised under acetone for five minutes. The resulting powders were then dried in an oven at 55 °C and backloaded into standard aluminium sample holders. XRD analysis was carried out as described in Section 5.3.1.3.

6.2.3.4. Geochemistry of Äspö Diorite sample

Major and trace elements were determined by X-ray fluorescence analysis (XRF). XRF was undertaken using two sequential, fully automated, wavelength dispersive XRF spectrometers (Philips PW2400 and Philips PW1480/10 XRF spectrometers) fitted with a 60 kV generator and 3 kW rhodium ("Super Sharp") end-window X-ray tube, and a 100 kW and 3 kW tungsten side-window X-ray tube respectively.

Major element analysis of the bulk-rock and sand fraction was carried out to determine SiO_2, TiO_2, Al_2O_3, Fe_2O_3 (total), MnO, MgO, CaO, Na_2O, K_2O, P_2O_5, BaO and SrO contents. Samples were tema milled and finely powdered, then loss on ignition (LOI) determined by heating samples to 1050 °C. Analyte angles were calibrated from international and in-house standard reference materials. All standards and unknowns were prepared as fused glass discs using di-lithium tetraborate flux at approximately 1200 °C. Drift correction was catered for by an external ratio monitor, and background corrections applied where necessary. It should be noted that Fe_2O_3 (total) determined represents the total Fe content of the samples.

Trace elements were determined by XRF using pressed powder pellets. Pellets were prepared by grinding representative splits of the powdered samples with Elvacite 2013 binder (Dupont n-butyl methacrylate copolymer) in an agate planetary ball mill, followed by pressing at 25 tons load into 40 mm diameter pellets.

6.2.4. Results and discussion

6.2.4.1. Groundwater analyses

Groundwater chemical analyses are presented in Table 13. Although the data are not discussed in detail here, since this is outwith the remit of the study, a number of features were noted. These are briefly described below.

It is apparent from the data that the composition of the groundwater changed during collection of the large-volume (40 litres) samples. The concentration of most species (with the exception of Field HCO_3^-, F, TIC, reduced S, Si, Al, and B, which show a decrease in concentration) increased from the start of sampling to the completion of sampling. The changes are significantly large for Eh, pH, Ca, Na, K, Cl, SO_4, Br,

Total S, reduced S, Ba and Sr. Dissolved O_2, Total P, NH_4^-,Co, Ni, Cu, Zn, Cr, Cd, Pb and V were all below analytical detection limit. These changes during groundwater production most probably reflect differences in chemistry between the groundwater in the "disturbed zone" in the host rock immediately adjacent to the borehole wall - which would have been sampled initially, and more distant "background" water which would have been sampled in the later stages of production. Because of this variation, it is recommended that an average of the two analyses is used in the setting up of the laboratory experiments and in subsequent use of the large volume water samples.

There are also significant differences between the field and subsequent laboratory pH analyses. Field pH is 0.99 to 1.3 pH units higher than measurements performed subsequently in the laboratory at BGS. It was noted during sampling that the groundwater effervesced strongly as it discharged from the borehole (see also previous sampling for Year 1, in West et al., 1997). Thus it is likely that outgassing contnued to occur in the subsamples collected for laboratory analysis of anion species. Outgassing of CO_2 will strongly influence the pH and this may be responsible for the observed discrepancy between the field and laboratory analyses.

6.2.4.2 Petrographic analysis of Äspo Diorite sample

Hand specimen description

The Äspo Diorite sample collected from the walls of the REX alcove in September 1997 (sample D337) is coarse-grained igneous rock. It is composed of approximately 50 % rounded, pink alkali feldspar (up to 4 mm) and approximately 10 % colourless/white quartz surrounded by a finer-grained mafic mineral assemblage dominated by biotite mica.

Thin section petrography

Petrographic analysis showed that sample D337 is a hydrothermally altered, partially recrystallised diorite (Plate 40a & b). Two thin sections were cut, one from the edge of the sample and a second from the centre; comparison of the two confirmed the sample to be relatively homogeneous.

Examination of the thin sections, using a petrographic microscope, showed that diorite sample is composed of major primary alkali feldspars, quartz and equant opaques, accompanied by secondary interstitial phases including: abundant green/brown biotite, epidote, carbonate, and accessory muscovite and sphene - possibly replacing ilmenite as the Ti-host. The feldspar crystals reach 2.5 mm in length, are heavily sericitised, are generally untwinned, and include a few string perthites exsolution lamellae. The quartz has been partially recrystallised and shows lobate, sutured margins, strain extinction and the development of subgrains. The biotite forms irregular, randomly oriented flakes and is often intergrown with anhedral epidote.

6.2.4.3. XRD analysis of Äspö Diorite

XRD analysis of the bulk crushed diorite sample (whole rock, pre- removal of fines) was found to comprise major quartz and albite along with minor amounts of orthoclase, mica and chlorite, and traces of hematite, calcite and possibly cristobalite. Changes in mineralogy between the whole rock (pre-removal of fines) and the sand (with fine fraction removed) and fine fraction were minimal. Only very slight variations in the relative proportions of the major minerals present in each of these three fractions were indicated from XRD peak intensities. The most notable difference was observed between the sand fraction and whole rock; where it appears that the mica-phase and calcite decrease, while chlorite and albite increase. The differences in the XRD peak observations are summarised in Table 14. Figure 12 shows the XRD profiles for both the bulk diorite and the sand fractions, illustrating the magnitude of the differences.

Analysis of the fines reinforces the above conclusions, showing a complimentary relationship to the sand fraction (Table 15).

6.2.4.4. Geochemistry

Major and trace element analyses of the diorite starting material (D337), both in terms of bulk rock and the sand fraction to be used in subsequent experiments, are presented in Table 15. Also given is the previously reported geochemical data for sample C853 (West et al., 1997), the diorite sample used in the Year 1 batch experiments.

Some fractionation has occurred with removal of the "fines" from D337. Specifically, SiO_2, Al_2O_3 and Na_2O increase, while Fe_2O_3 (total), MgO and K_2O decrease, suggesting that the mafic mineral phases (biotite etc.) are concentrated into the fine fraction while felsic minerals (quartz and feldspars) are more resistant to crushing, and are concentrated into the sand fraction.

The whole rock geochemistry of the two samples (C853 & D337) is broadly similar. The most significant differences are in the oxides CaO and K_2O, LOI and the trace elements Rb and Ba. The greater LOI obtained for D337 might suggest it was more altered, and it is noteworthy that all of the elements concerned are considered mobile during hydrothermal alteration and weathering (e.g. Wood et al. 1976).

The major element data were subsequently used to calculate CIPW normative mineralogies for both samples C853 (West et al., 1997), D337 whole rock, and the prepared sand fraction from D337. CIPW norms were calculated using the computer programme Igpet III (Carr 1990), and these are reported in Table 16. Since Fe had only been determined in terms of Fe_2O_3 (total) for sample D337, the Fe^{2+}:Fe^{3+} ratio was set arbitrarily to that determined by wet chemical methods for sample C853 (West et al., 1997).

6.3. Laboratory Experiments

Eight column experiments are being conducted under anaerobic conditions. Four of the columns contain only Äspö diorite reacting with Äspö groundwater. The remaining four columns contain Äspö diorite and mixed SRB and IRB cultures again reacting with the Äspö groundwater.

6.3.1. Design of equipment

The equipment (Figs.13 and 14) consists of a fluid reservoir containing the Äspö groundwater connected via a peristaltic pump to the PEEK columns (30cm long, 0.7cm ID) which are connected in turn to the collection vessels (one per column). The whole apparatus is contained within an anaerobic chamber with a controlled nitrogen/hydrogen/carbon dioxide atmosphere.

The columns are packed with crushed Äspö diorite and a mixture of IRB and SRB. Fluid flow through the column is controlled by the peristaltic pump. The fluid was filter sterilised before use and the inlet end of the column contained a 0.2μm filter in order to ensure that no other bacteria other than the SRB and IRB were present in the column. The outlet end of the column contained a 10μm filter which is large enough for bacteria to pass through therefore enabling monitoring of bacteria that may be washed out of the column.

The collection vessels are periodically changed and whilst still in the anaerobic chamber are sub-sampled for chemical and microbiological analyses. Techniques are as described in Section 5.2.2.3.

7. RECOMMENDATIONS

The column experiments to investigate the effects of microbial activity under realistic flow-through conditions are underway. These have been started under anaerobic conditions to compare results with the anaerobic batch experiments. Subsequently it is intended that they will be run aerobically to evaluate the effects of oxygen ingress on the systems.

8. ACKNOWLEDGEMENTS

We gratefully acknowledge the funding from PNC for this work. SKB are acknowledged for providing access and facilities during this work. In particular, we are very grateful to Katinka Klingberg and Dr Mansueto Morosini (SKB, Äspö Hard Rock Laboratory) for their invaluable help and assistance, both during logging and sampling, and subsequently in shipping samples and equipment from Sweden to England. Grateful thanks to the Department of General and Marine Microbiology, Goteborg University for their help in selecting and obtaining the bacterial isolates; and to Dr Peter Wikberg (SKB), Dr Ignasi Puigdomenech (The Royal Institute of Technology) and Dr Steven Banwart (University of Sheffield) for their support and technical advice. Dr Eva-Lena Tullborg (Terralogica AB) is also thanked for useful discussions on the mineralisation at Äspö. Colleagues in Analytical Geochemistry Group (BGS) are acknowledged for collating the necessary equipment for groundwater sampling and field analysis. UK Nirex Ltd are also acknowledged for giving permission for reference to be made to observations from their flow-zone characterisation studies at Sellafield.

9. REFERENCES

Baker, S. J., West, J. M. And Noy, D. J. 1996 Complementary Laboratory work to examine Microbial effects on redox and Quantification of the effects of microbiological perturbations on the geological perturbations on the geological disposal of HLW (TRU). Task 2. A Biogeochemical Assessment of the Tono Mine geology. *Report of the British Geological Survey.* **WE/96/32C.**

Banwart, S. (Ed) 1995 The Äspö redox investigations in block scale. Project summary and implications for repository performance assessment. *SKB Technical Report* **95-26.**

Banwart, S., Laaksoharju, M., Nilsson, A-C, Tullborg, E-L. & Wallin, B. 1992. The Large Scale Redox Experiment: initial characterisation of the fracture zone. *SKB Swedish Hard Rock Laboratory Progress Report*, **25-92-04.**

Carr, M J. 1990. *Igpet III*.

Chenery, S.& Cook, J.M. 1993. Determination of rare earth elements in single mineral grains by laser ablation microprobe-inductively coupled plasma mass spectrometry. *Journal of Analytical Atomic Spectrometry*, **8**, 299-303.

Deer, W.A., Howie, R.A. & Zussman, J. 1962. *Rock-Forming Minerals: Volume 1; Ortho- and Ring Silicates.* Longman Group Ltd, London.

Dickson, J.A.D. 1966. Carbonate identification and genesis as revealed by staining. *Journal of Sedimentary Petrology*, **36**, 491-505.

Ekendahl, S. Deep Subsurface Ecosystems. Numbers, Activity and Diversity of Groundwater bacteria in Swedish Granitic Rock. Dept. Of General and Marine Microbiology, Goteborg University, Sweden. 1996.

French, W.J. & Adams ,S.J. 1972. A rapid method for the extraction and determination of Iron (II) in silicate rocks and minerals . *Analyst.* **92**, pp. 828-831

Goldstein, J.L., Newbury, D.E., Echlin, P., Joy, D.C., Fiori, C. & Lifshin, E. 1981. *Scanning electron microscopy and X-ray microanalysis.* Plenum Press, New York.

Hobbie, J.E., Daley, R.J. & Jasper, S. 1977. Use of Nucleopore Filters for Counting Bacteria by Fluorescence Microscopy. *Applied and Environmental Microbiology*, **33**, (5), 1225-1228.

Jass, J., & Lappin-Scott, H.M. 1992. B Practical Course on Biofilm Formation Using The Modified Robbins Device. Biofilm Technologies Research Group, University of Exeter, England. pp. 1-34

Kornfält, K-A. & Wickman, H. 1988. The rocks of the Äspö Island. *SKB Swedish Hard Rock Laboratory Progress Report*, **25-88-12.**

Landström, O. & Tullborg, E-L. 1995. Interactions of trace elements with fracture filling minerals from Äspö Hard Rock Laboratory. *SKB Technical Report*, **95-13**.

Le Maitre, R.W., et al. (editors). 1989. *A Classification of Igneous Rocks and Glossary of Terms. Recommendations of the International Union of Geological Sciences Subcommission on the Systematics of Igneous Rocks.* Blackwell Scientific Publications, Oxford, United Kingdom.

Mazurek, M., Bossart, P. & Eliasson, T. 1995. Classification and characterization of water-conducting features at Äspö: results of Phase I investigations. *SKB Swedish Hard Rock Laboratory Progress Report*, **25-95-03**.

Milodowski, A.E., Savage, D., Bateman, K. & Hughes, C.R. 1989. The precipitation of solids from potential heat exchange fluids for use in a HDR system in granite. *Geothermics*, **1/2**, 233-240.

Milodowski, A.E., Gillespie, M.R., Shaw, R.P. & Bailey, D.E. 1995. Flow-zone characterisation: Mineralogical and fracture orientation characteristics in the PRZ and Fleming Hall Fault Zone area boreholes, Sellafield. *UK Nirex Ltd Report*, **SA/95/001**.

Milodowski, A.E., Gillespie, M.R. & Yoshida, H. 1996. Mineralogical logging and characterisation of flowing features in the two REX boreholes KA2858A and KA2862A, Äspö Hard Rock Laboratory, southeastern Sweden. *British Geological Survey, Technical Report*, **WE/96/15C**.

Nirex. 1995. Flow zone characterisation of the RCF area: summary report. *UK Nirex Ltd Report*, **S/95/006**.

Noy D.J., Williams L.A., Rochelle C.A., and West J.M., 1996. Computer modelling of microbial processes using MGSE - an Overview (Microbial Growth in Subsurface Environments*). Report of the British Geological Survey* **WE/96/26**.

Pedersen, K., & Karlsson. Investigations of Subterrean Microorganisms. Their importance for performance assessment of radioactive waste disposal. *SKB Technical Report* **95-10**. Stockholm. 1995

Pedersen, K., Arlinger, J., Ekendahl, S., and Hallbeck, L. 1996. 16S ribosomal-RNA gene diversity of attached and unattached bacteria in boreholes along the access tunnels to the Äspo hard rock laboratory, Sweden. *Fems Microbiology Ecology*, **19**, No. 4, 249-262.

Querol X. & Chenery, S. 1995. The determination of trace element affinities in coal by laser ablation microprobe - inductively coupled plasma - mass spectrometry. Whateley, M.K.G. & Spears, D.A. (editors). European Coal Geology. *Special Publication of the Geological Society of London*, **82**, 147-155.

Rundle, L.M. 1974. A combustion method for the determination of total sulpher in limestones. *Analyst*. **99**, pp. 163-165.

Stroes-Gascoyne, S. 1989 The potential for microbial life in a Canadian high-level nuclear fuel waste disposal vault: A nutrient and energy source analysis. *AECL Report.* **AECL-9574.**

Talbot, C. & Munier, R. 1989. Faults and fracture zones in Äspö. *SKB Swedish Hard Rock Laboratory Progress Report*, **25-89-11.**

Thauer, R. K., Kungermann, K., Decker, K. 1977. Energy conservation in chemotrophic anaerobic bacteria. *Biological Reviews*, **41**, 100-180.

Thauer, R. K., Morris, I. G. 1984. Metabolism of chemolithotrophic anaerobes_ Old views and new aspects. In: The microbe Part II Prokaryotes and Eukaryotes (Eds D. P. Kelly, N. G. Carr) Cambridge University Press. pp. 123-168.

Tullborg, E-L. 1989. Fracture fillings in the drillcores KAS05-KAS 08 from Äspö, southeastern Sweden. *SKB Swedish Hard Rock Laboratory Progress Report*, **25-89-16.**

Tullborg, E-L. 1995. Mineralogical and chemical data on rocks and fracture minerals from Äspö. *SKB Swedish Hard Rock Laboratory Progress Report*, **25-90-01.**

Tullborg, E-L., Wallin, B. & Landström, O. 1991. Hydrochemical studies of fracture minerals from water conducting fractures and deep groundwaters at Äspö. *SKB Äspö Hard Rock Laboratory Technical Note*, **25-95-07g.**

Van Straaten, L.M.J.U. 1978. Dendrites. *Journal of the Geological Society, London*, **135**, 137-151.

West, J. M. Aoki, K., Baker, S. J., Bateman, K., Coombs, P., Gillespie, M. R., Henney, P. J., Reeder, S., Milodowski, A. E. and Yoshida, H. 1997 Complementary laboratory work to examine microbial effects on redox and quantification of the effects of microbiological perturbations on the geological disposal of HLW (TRU). Task 1. Äspö Hard Rock Laboratory - Redox Experiment in detailed scale (REX).). *Report of the British Geological Survey* **WE/97/3C.**

Wickman, H. & Kornfält, K-A. 1995. Updating of the geological model at Äspö. *SKB Swedish Hard Rock Laboratory Progress Report*, **25-95-04.**

Wikman, H., Kornfält, K-A., Riad, L., Munier, R. & Tullborg, E-L. 1988. Detailed investigation of the drillcores KAS 02, KAS 03 and KAS 04 on Äspö Island and KLX 01 at Laxemar. *SKB Swedish Hard Rock Laboratory Progress Report*, **25-88-11.**

Winberg, A., Andersson, P., Hermanson, J. & Stenberg, L. 1996. Results of the Select Project: investigation programme for the selection sites for the operational phase. *SKB Swedish Hard Rock Laboratory Progress Report*, **HRL-96-01.**

Wood, D A, Gibson, I L & Thompson, R N. 1976. Elemental mobility during zeolite facies metamorphism of the Tertiary basalts of Eastern Iceland. *Contributions to Mineralogy and Petrology*, **55**, 241-254

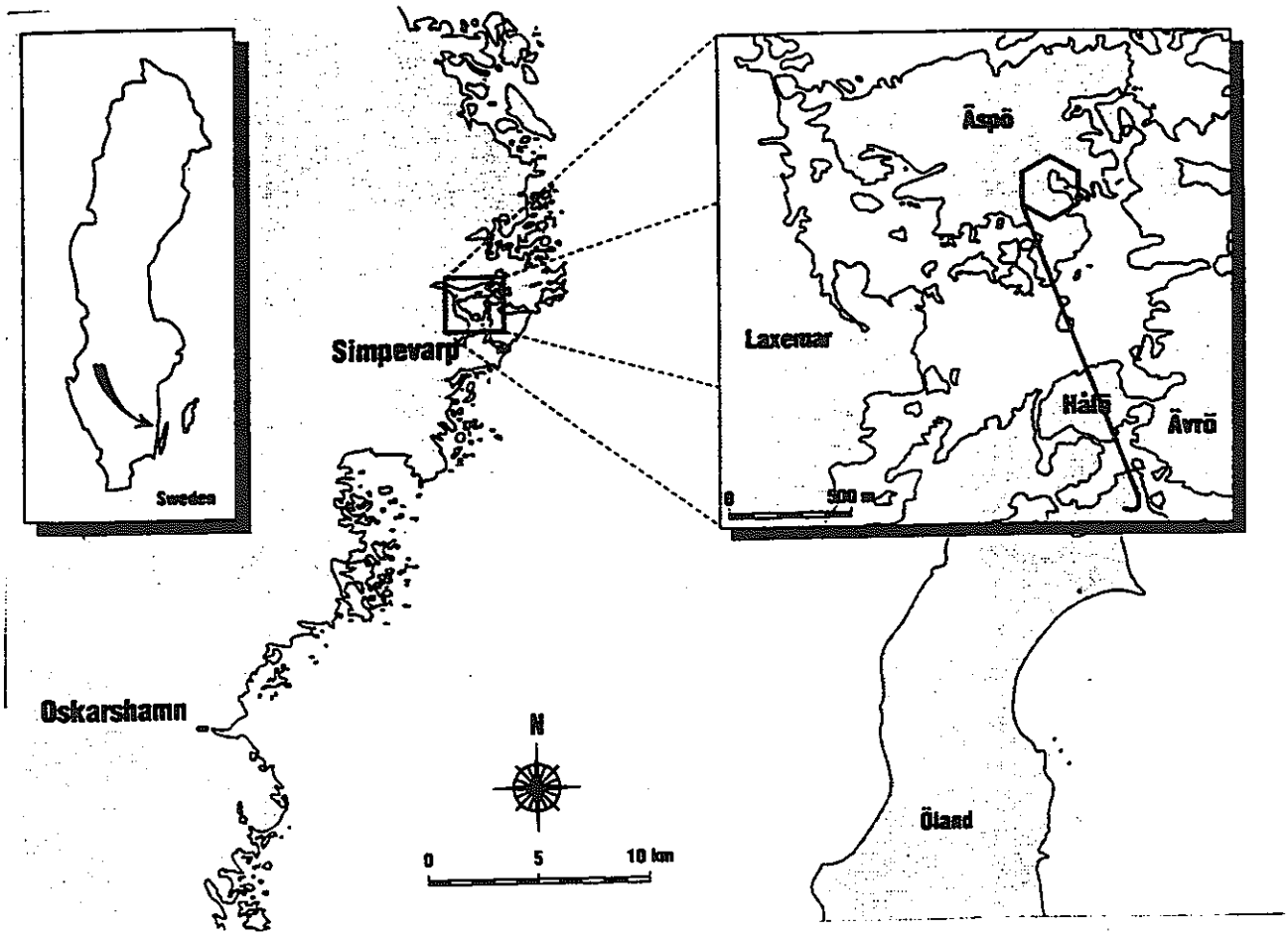

Figure 1. Location of the Äspö Hard Rock Laboratory (from Landström & Tullborg, 1995)

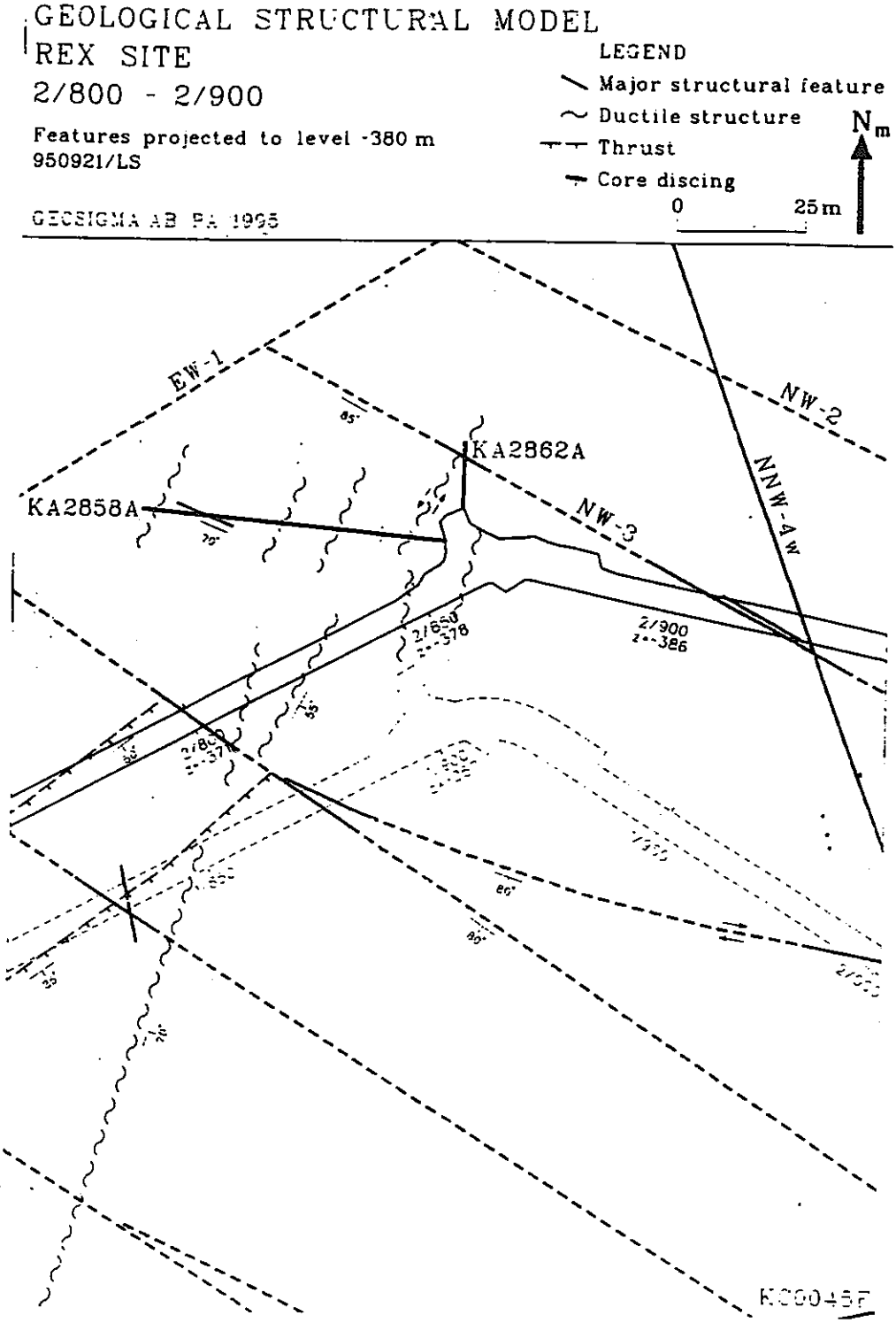

Figure 2. Summary of structural elements of the REX block (from Winberg et al 1996)

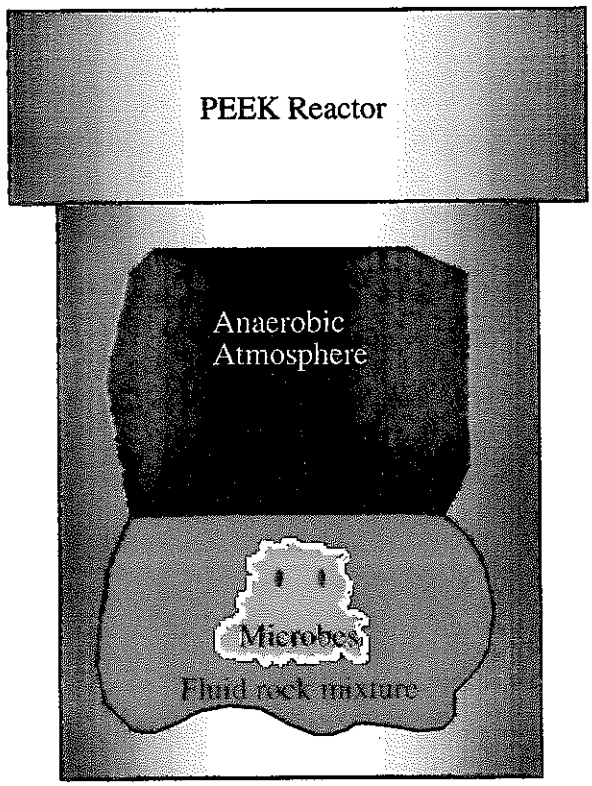

Figure 3. PEEK reactor vessel

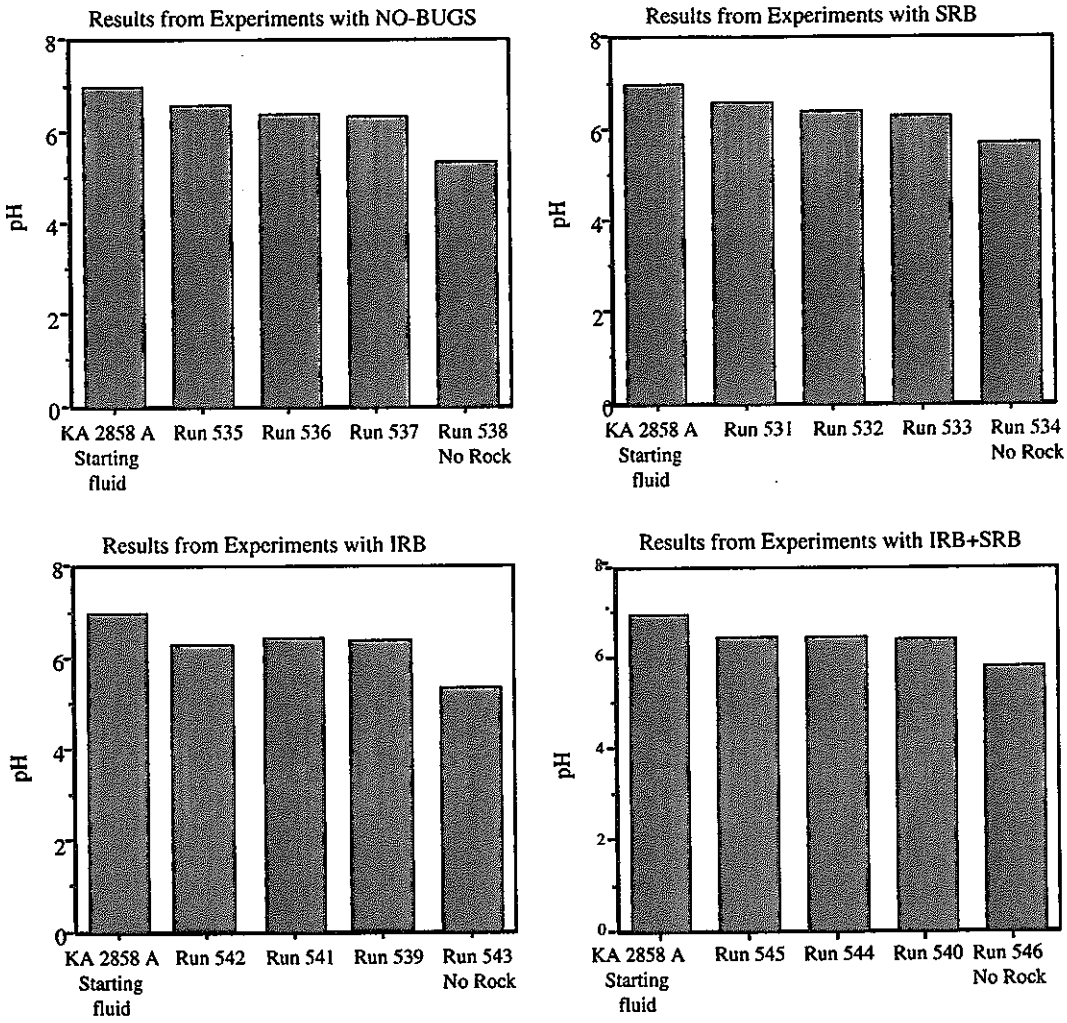

Figure 4 Graphs showing changes in pH for all experiments.

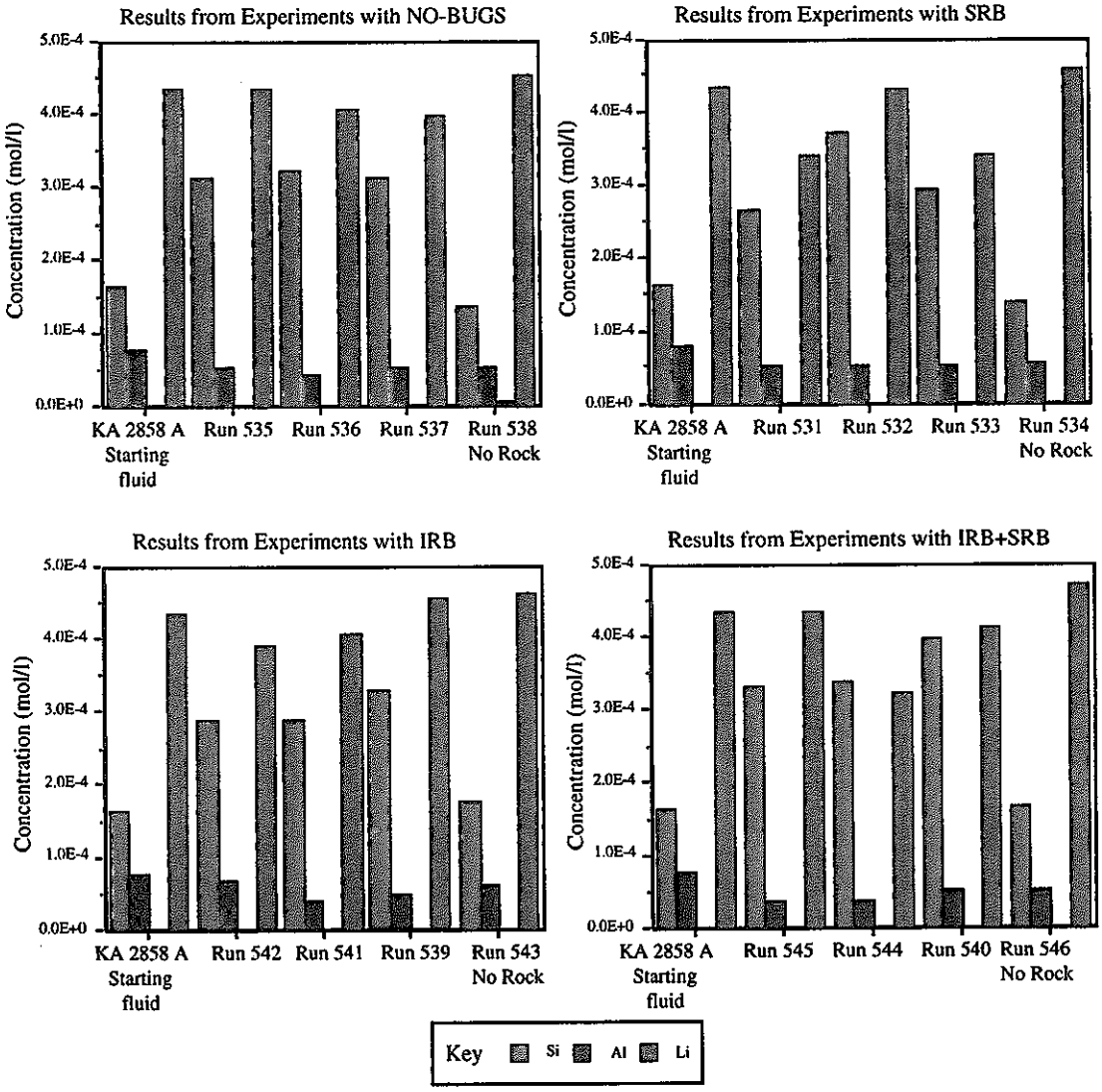

Figure 6. Graphs showing changes in Si, Al and Li concentrations (mol/l) for all experiments.

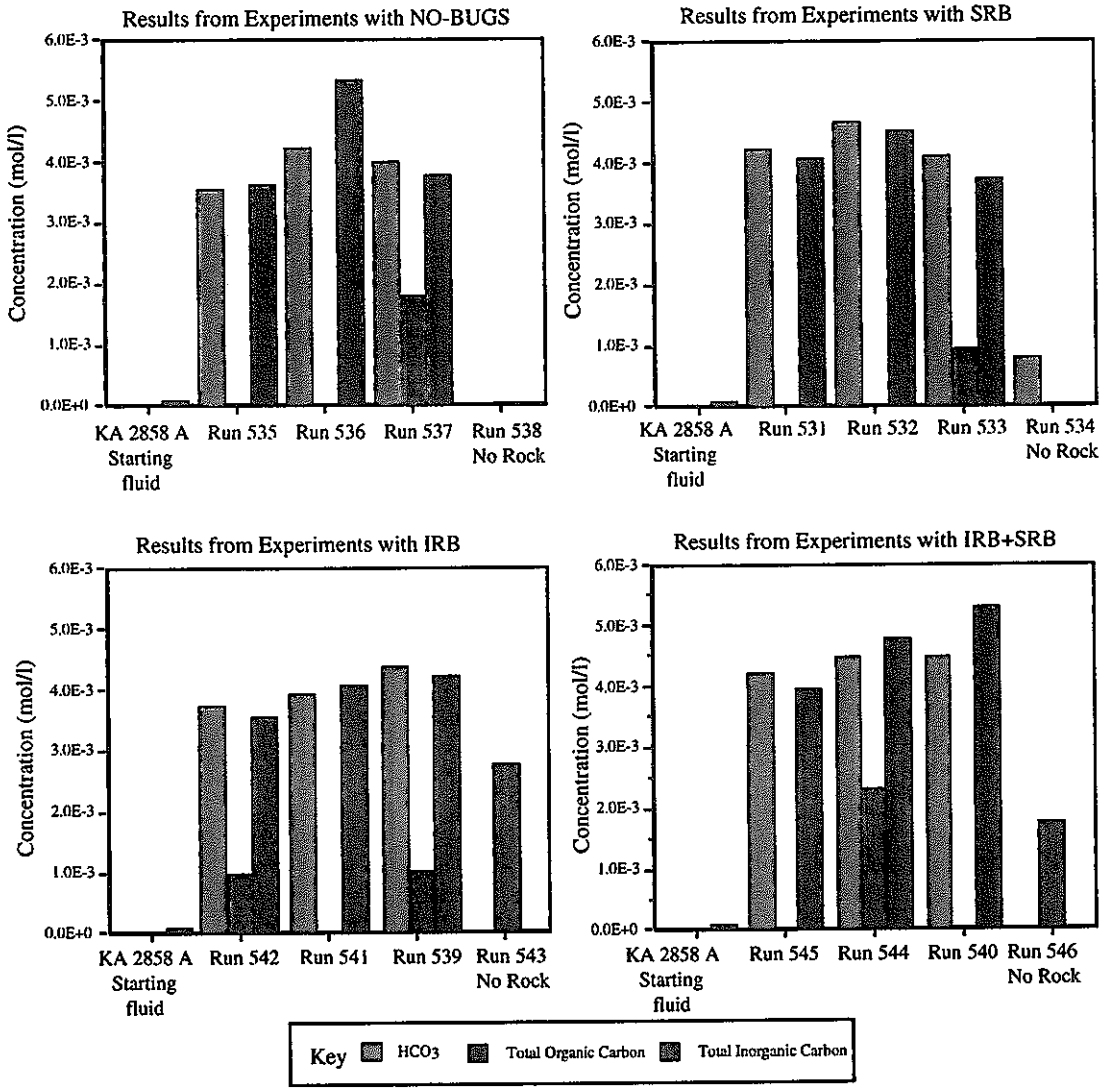

Figure 7. Graphs showing changes in carbon concentrations (mol/l) for all experiments.

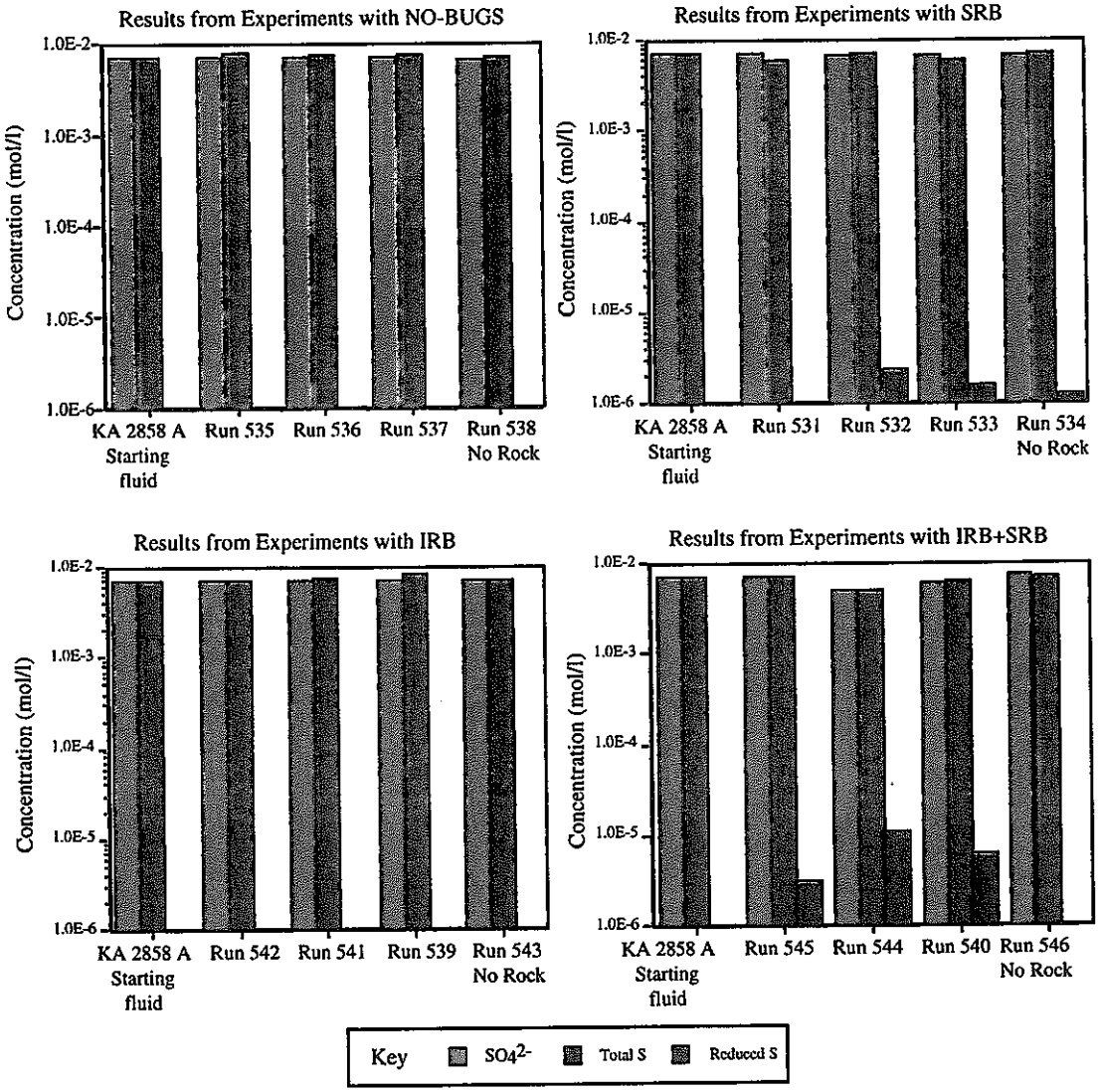

Figure 8. Graphs showing changes in S species concentrations (mol/l) for all experiments

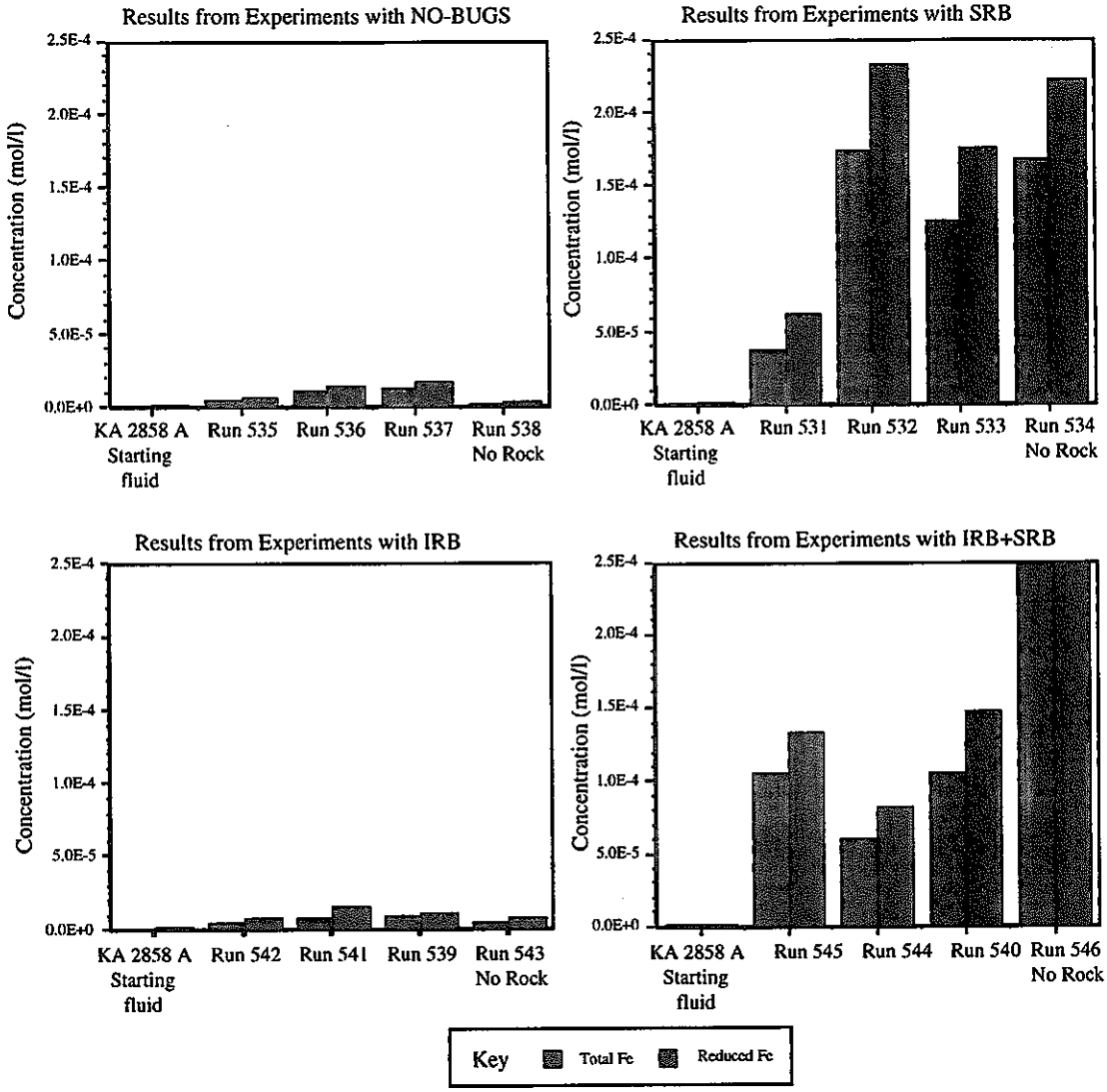

Figure 9. Graphs showing changes in Fe concentrations (mol/l) for all experiments

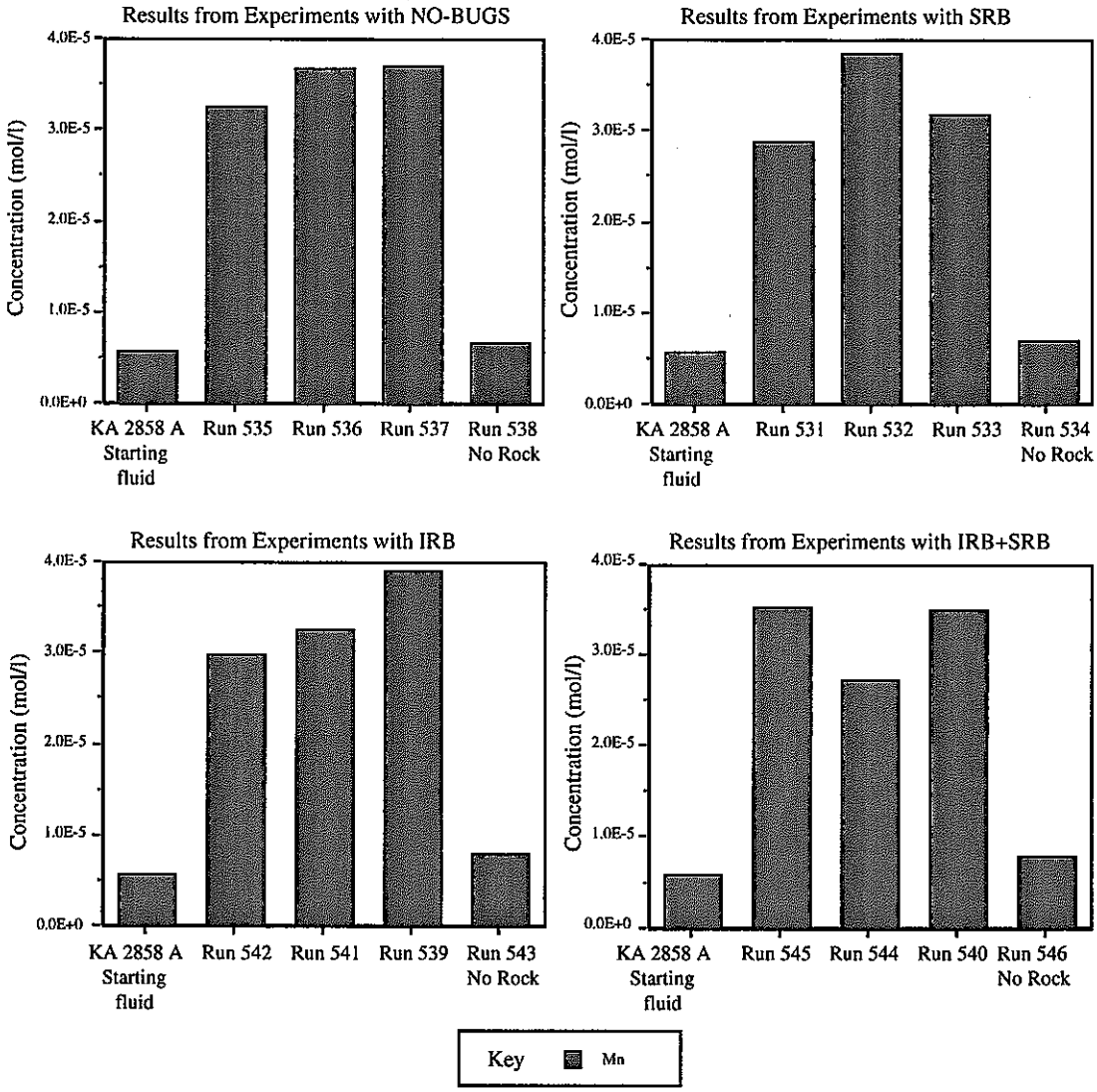

Figure 10. Graphs showing Mn concentrations (mol/l) for all experiments.

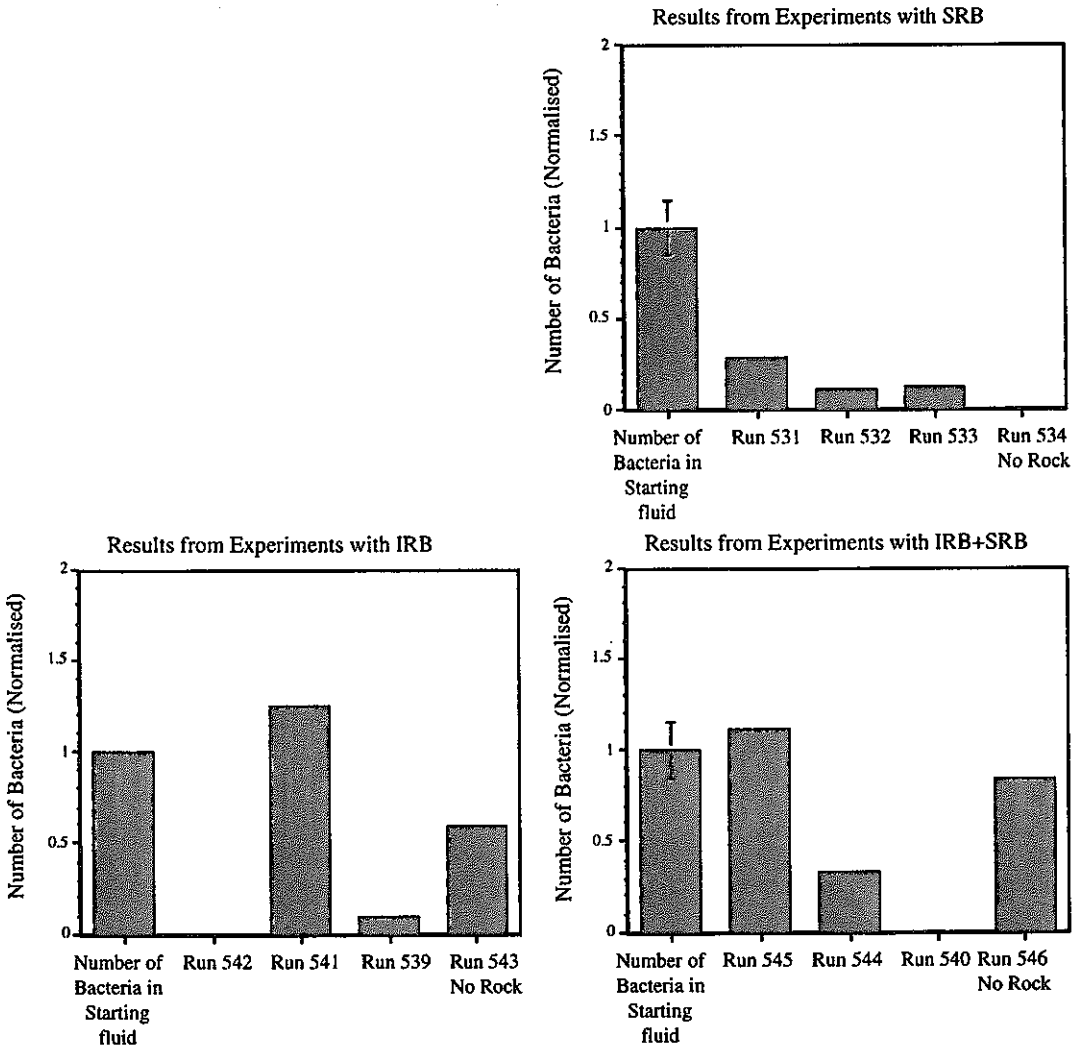

Figure 11. Graphs showing changes in microbial numbers (numbers/ml) for all experiments.

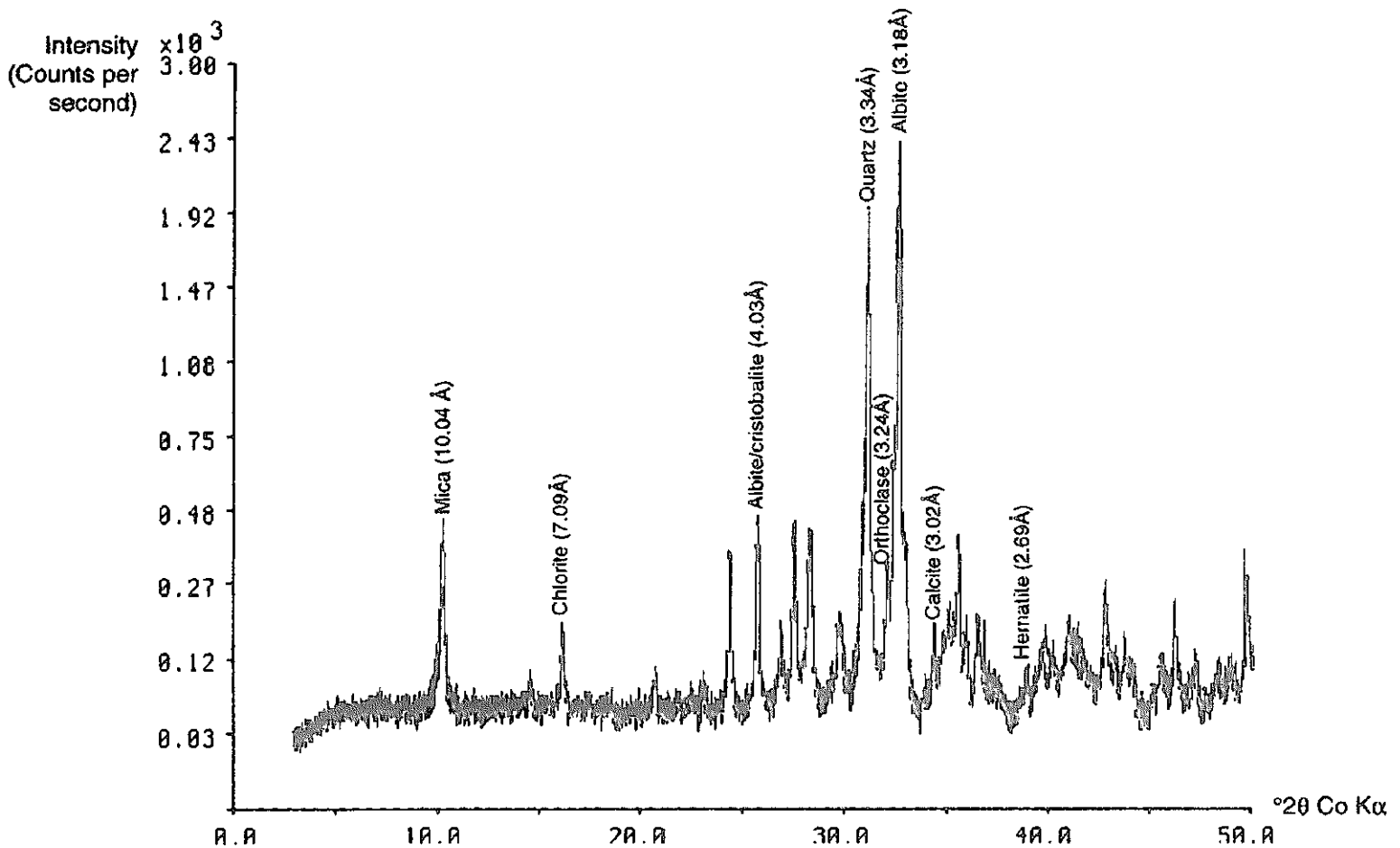

Figure 12. Diorite starting material (sample D337); overlain X-ray diffraction (XRD) profiles for comparison of mineralogical differences between prepared sand fraction (black) and original bulk diorite (red)

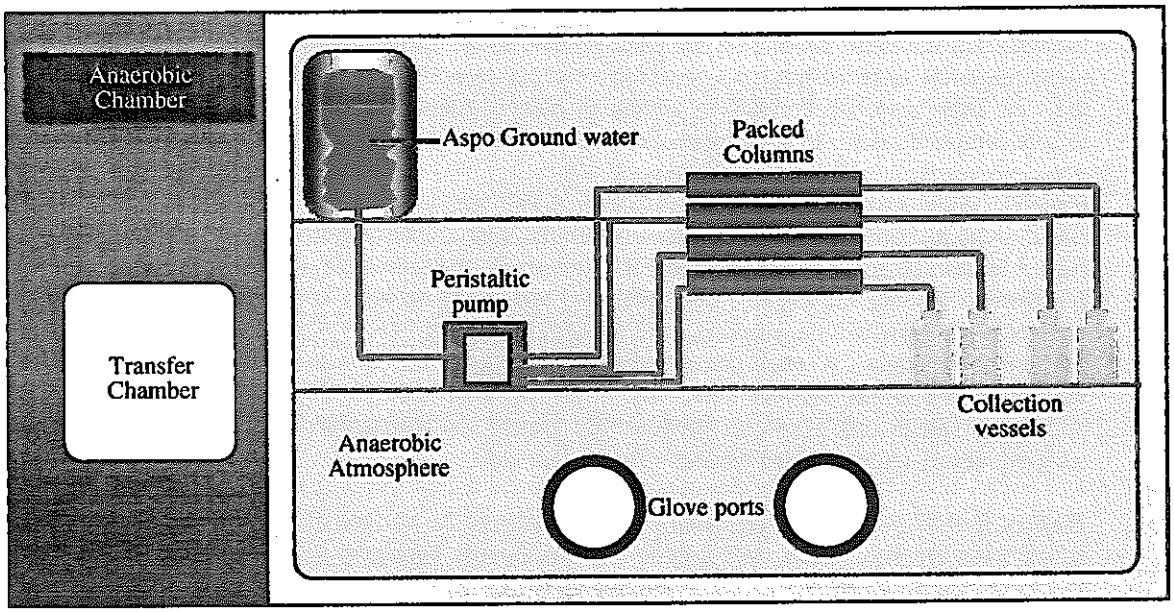

Figure 13. Schematic of column set-up

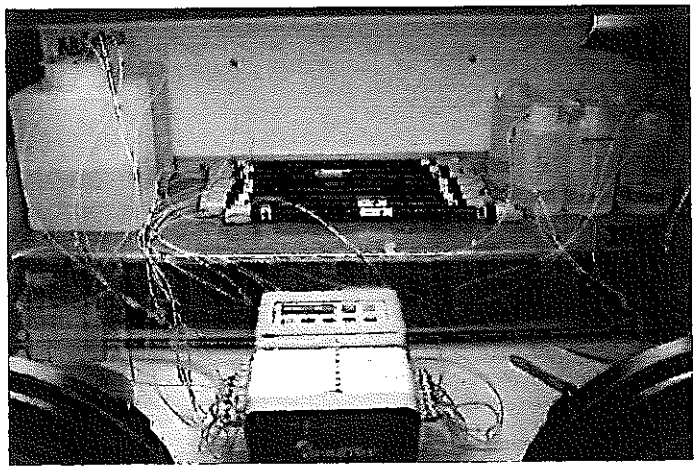

Figure 14. Picture of column set-up

Plate 1. BSEM image through one surface of a PFF and adjacent wallrock, Feature 38, sample C863. Black areas are pore space. Wallrock minerals are quartz (clean dark grey areas), Ca-Na feldspar (pitted dark grey areas), K-feldspar (mid-grey) and phengitic mica (platy, mid grey crystals). Authigenic minerals are calcite (light grey) and pyrite (white spots). The main PFF surface runs along the minerals in the top of the view, with a well-developed damage zone of fractured/brecciated rock extending 50-100 &m back into the wallrock.Wallrock dissolution has been greatest in the Ca-Na feldspar (as evidenced by the pitting). Some relatively large wallrock dissolution cavities (up to c. 100 &m diameter) in the bottom centre part of the view have been largely filled by authigenic calcite. Authigenic calcite and traces of authigenic pyrite locally cement the damage zone breccia fragments but have not formed on the main surface of the PFF.

Plate 2. BSEM image through one surface of a PFF and adjacent wallrock, Feature 30, sample C862. Black areas are pore space. Wallrock minerals are quartz (rare, clean dark grey areas), Ca-Na feldspar (pitted dark-mid grey areas), K-feldspar (mid-grey) and phengitic mica (platy, mid grey crystals). Authigenic minerals are calcite (very light grey) and pyrite (white). The main PFF surface runs along the bottom of the view, with a subsidiary and sub-parallel fissure PFF 100-200 &m into the wallrock (running mid-left to top right). A small amount of pyrite has grown on the main PFF surface, which is otherwise largely unmineralised, whereas nearly half of the subsidiary PFF (in this view at least) has been filled by authigenic calcite and pyrite. In between and around the two larger PFFs is a network of connected, smaller, largely unmineralised fissures - the damage zone.

Plate 3. BSEM image showing detail of a small part of the surface of PFF Feature 13 in sample C860. Black areas are pore space, dark grey is wallrock quartz, light grey is mainly authigenic calcite, though there are also traces of Fe-Mg chlorite lining quartz fragment surfaces. The main PFF surface runs along the top margin of the minerals. A damage zone of very small, irregular, connected fissures has developed in the quartz, probably at the same time as the main PFF formed. The damage zone is locally cemented by authigenic chlorite and calcite.

Plate 4. BSEM image showing fractures developed in the damage zone to feature 27 in sample C861. The 'main' PFF in this sample runs parallel to the fissures in this view, two hundred microns beyond the top left corner.Black areas are pore space, dark grey is quartz (part of a large crystal in the wallrock), the patchy grey area in the bottom right is Ca-Na-feldspar-K-feldspar-epidote-calcite and the grey mineral in the fissures is authigenic calcite. This image illiustrates how quartz has fractured far more than other minerals in the wallrock and often contains localised networks of very small, connected fissures with a very large surface area which have (so far) been mineralised only weakly by authigenic minerals such as calcite.

Plate 5. BSEM image of diorite/granodiorite wallrock and the surface of PFF feature 5 in sample C867. Black areas are pore space, dark grey areas are quartz, mid- and light-grey areas are feldspars and platy phengitic mica. A damage zone of very thin, connected and largely unmineralised fissures has developed in the wallrock adjacent to the main PFF, but not that it has developed to a much greater extent in the quartz grain than in adjacent areas of feldspar and mica. The main PFF surface in this view has no authigenic mineralisation developed along it, however pore spaces up to c.100 &m diameter developed by dissolution of Ca-Na-feldspar (which are best developed to the right of centre, in the bottom half of this view) have been largely occupied by authigenic calcite with euhedral terminations into remaining open space.

Plate 6. BSEM image of an unlogged PFF fissure which is parallel to Feature 55 in sample C869. The image shows a thin vein of K-feldspar and calcite running left to right through the granodiorite wallrock (which, in this view, consists of quartz, feldspars, epidote, phengitic mica and magnetite). The vein has re-opened along its lower margin to create a fissure PFF approximately 80 &m wide now partly filled by authigenic calcite crystals with euhedral terminations into open spaces. Note that much of the 'new' calcite appears to have nucleated originally on 'old' calcite in the older vein. A further very thin (c.20 &m wide) fissure has opened along the bottom of the mineralised parts of the PFF fissure, however this new opening may be an artefact caused by drilling and/or core handling.

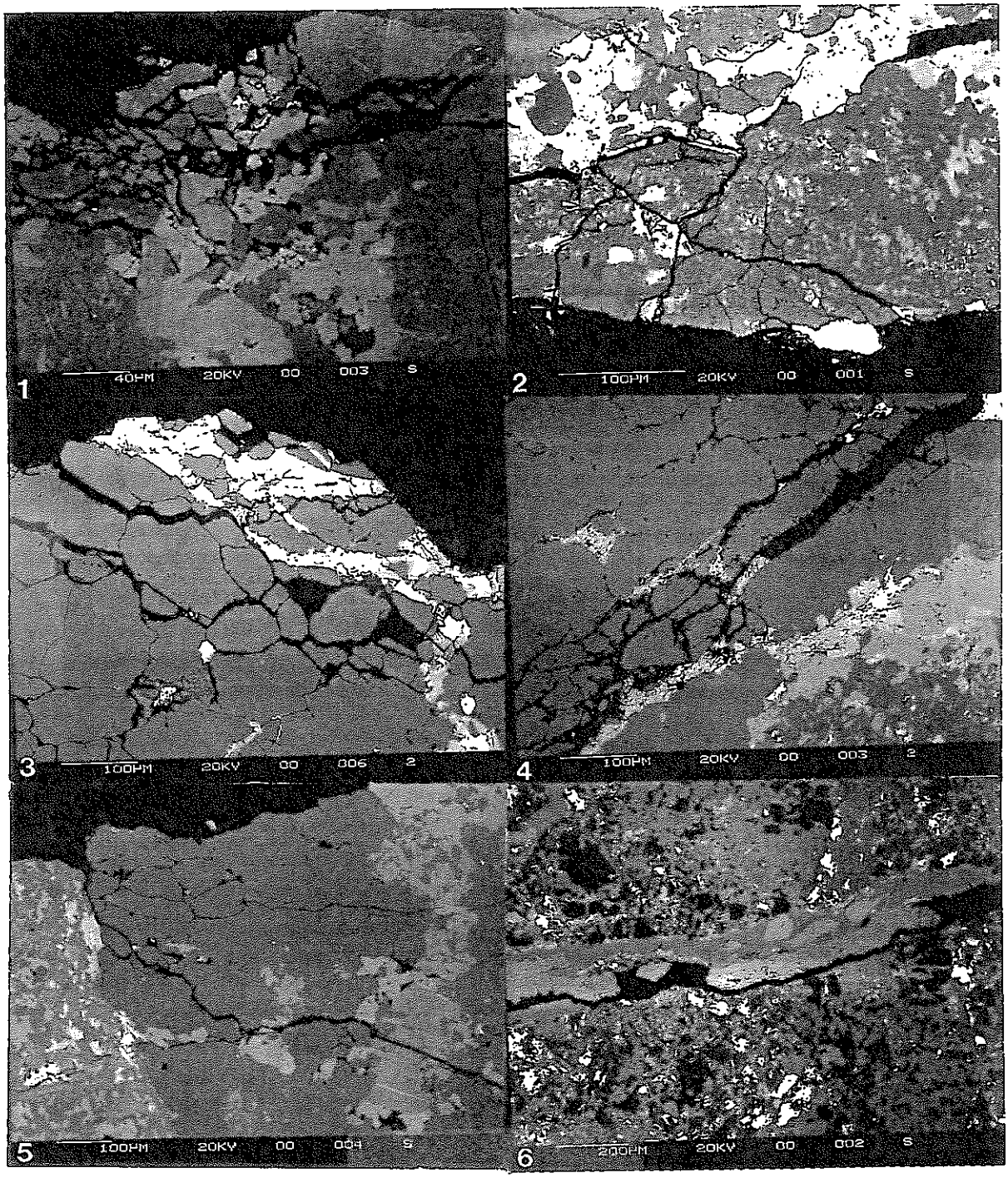
1
40µM 20kV 00 003 S
2
100µM 20kV 00 001 S
3
100µM 20kV 00 006 2
4
100µM 20kV 00 003 2
5
100µM 20kV 00 004 S
6
200µM 20kV 00 002 S

Plate 7. BSEM image showing Feature 38, a c.100 &m wide vein of calcite and adjacent wallrock in sample C863. The wallrock is comprised of rare quartz (dark grey), Ca-Na-feldspar (dark grey with dissolution pits), K-feldspar (mid-grey) and phengitic mica (platy, mid-grey). Pore spaces (black areas) in the wallrock have developed mainly from the dissolution of Ca-Na-feldspar. Authigenic calcite (probably an older generation than is found on present-day PFF surfaces) has sealed the thin vein, however it has re-activated along its upper surface to create a new, thin, largely unmineralised PFF (black area along the top edge of the image). Along the boundary between the wallrock and the older calcite vein is a thin seam of K-feldspar, which probably formed as an alteration product when the original fracture opened.

Plate 8. BSEM image showing part of PFF Feature 5 and adjacent wallrock in sample C867. The wallrock consists of quartz (dark grey), Ca-Na-feldspar (mid-dark grey), K-feldspar (mid-grey), biotite (platy, light-grey) and a single crystal of magnetite (white). Pore spaces are black. The main PFF surface runs along the top part of the image, and a thin, subsidiary PFF fissure is sub-parallel to it and 300-400 &m from it in the bottom part of the image. There is no authigenic mineralisation on the surfaces of either of these features in the field of view. Dissolution porosity (pore spaces generally 20 &m diameter) is developed extensively in the wallrock around these fissures. The pore spaces are largely unmineralised, though authigenic calcite has developed in them locally.

Plate 9. BSEM image showing the surface of PFF Feature 5 and adjacent wallrock in sample C867. The wallrock consists of quartz (dark grey), Ca-Na-feldspar (mid-dark grey), K-feldspar (mid-grey) and phengite (platy, mid-grey). Pore spaces are black. The main PFF surface runs along the top part of the image, with no authigenic mineralisation on the surface in the field of view. Substantial dissolution porosity (pore spaces generally 120 &m diameter) is developed extensively in the wallrock adjacent to the PFF. The pore spaces have locally been filled to a considerable degree by authigenic calcite. Note that a quartz crystal in the top left part of the view has been recrystallised into a number of sub-grains separated by hairline fissures, probably at the time the PFF formed.

Plate 10. BSEM image showing the surface of PFF Feature 5 and adjacent wallrock in sample C867. A single, relatively large (150 &m) and several smaller dissolution pits have developeed in the wallrock adjacent to the essentially unmineralised surface of the PFF. Authigenic calcite has now occupied much of the large pit.

Plate 11. BSEM image showing Fe-chlorite platelets growing from the surface of PFF Feature 73 into pore space (black) in sample C865. The chlorite platelets are growing from the surface of an older epidote-phengite-feldspar vein. The wallrock, forming the bottom half of the image, is comprised of phengitic mica, feldspar and traces of magnetite.

Plate 12. BSEM image of an unlogged PFF developed parallel to, and within several millimetres of, Feature 55 in sample C869. A hairline vein of K-feldspar which runs from lower left to upper right of this field of view has been partly exploited by a fissure PFF with euhedral, sub-equant crystals of authigenic calcite (light grey) growing into pore space (black). The wallrock consists of quartz, Ca-Na-feldspar, K-feldspar, epidote, mica and magnetite.

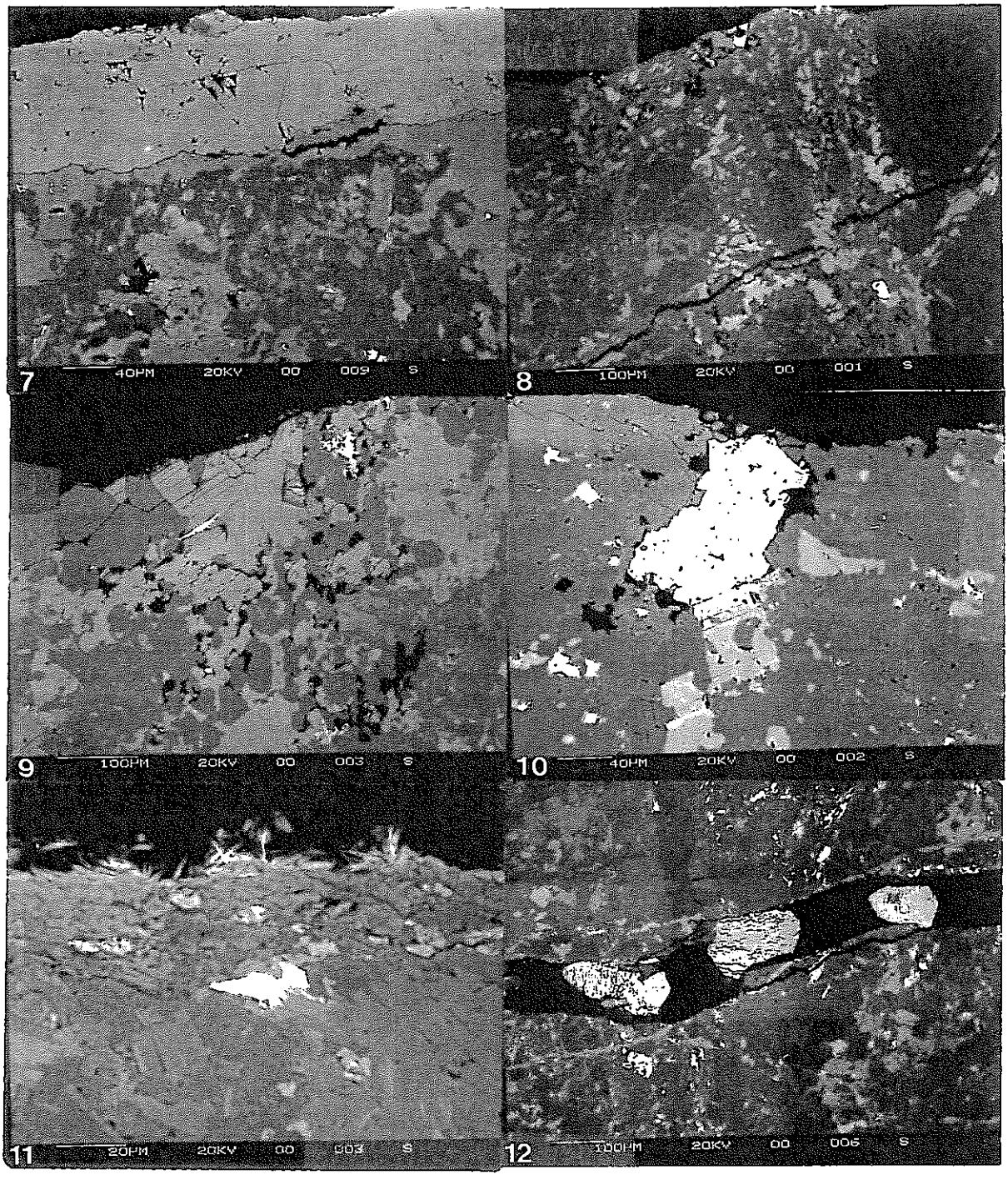
7
40μm 20kV 00 009 S
8
100μm 20kV 00 001 S
9
100μm 20kV 00 003 S
10
40μm 20kV 00 002 S
11
20μm 20kV 00 002 S
12
100μm 20kV 00 006 S

Plate 13. SEM image showing fresh, euhedral crystals of authigenic calcite with stubby scalenohedral morphology sitting on the surface of the PFF in sample C849.

Plate 14. BSEM image showing authigenic mineralisation lining the surface of PFF Feature 38 in sample C863. The dark area in the bottom third of the image is granodioritic wallrock comprised principally of quartz and feldspars. The grey strip across the centre of the image is a vein of K-feldspar with a single crystal of calcite. The calcite is just right of centre, slightly lighter grey than the feldspar and has filled a dissolution cavity in the adjacent wallrock. The top surface of this vein has reactivated to create a new fissure PFF along the top third of the image. A crystal of late-stage, euhedral, authigenic calcite with sub-equant form has crystallised on the surface of the PFF and appears to have nucleated from the point where a very small area of calcite in the older vein is exposed on the surface of the new PFF.

Plate 15. SEM image showing authigenic pyrite with pristine (i.e. uncorroded) faces and euhedral form growing on the surface of the PFF in sample C849. Altered and very fine-grained wallrock, which forms much of the surface of the PFF, occupies the top and right parts of the image. K-feldspar in the wallrock has altered to smectite locally. Some smectite appears to be growing over pyrite at the bottom right corner of the image, and may therefore post-date it.

Plate 16. BSEM image showing authigenic pyrite (white) and authigenic calcite (mid-dark grey) developed in a PFF in sample C849. The PFF at this point has been largely sealed by authigenic minerals, however much of the PFF surface in this sample is unmineralised. The wallrock, to the left of the PFF, is comprised mainly of quartz and feldspars. The black area at the right side of this image is unmineralised in the thin section, but would originally have been occupied by wallrock forming the other margin to the PFF.

Plate 17. SEM image showing part of the surface of a PFF in sample C849. Very fine flakes of authigenic smectite are particularly well-developed in the top right part of this image developing by alteration of wallrock silicate minerals (principally feldspar) exposed on the surface of the PFF. Also included in this image are very fine-grained epidote and chlorite crystals. This image illustrates the typical very fine grainsize and high surface area of minerals forming the surfaces of PFFs.

Plate 18. BSEM image of a part of the surface of PFF Feature 214 in sample C871. The grey mineral along the bottom of the image is authigenic K-feldspar forming part of a vein. The feldspar (and other vein minerals outside this field of view, including epidote and fluorite) has corroded locally and been replaced by grey fibrous chlorite. Chlorite forms the surface of much of this PFF, but traces of a very fine-grained, fibrous mineral (white in this view) comprised of rare earth elements, Ca, Si and F were observed locally, growing into the PFF. Fluorite is a minor component in the K-feldspar-epidote-fluorite vein and has been fractured and altered locally, probably in relation to development of the present-day PFF. The breakdown of fluorite presumably provides a local source of F for this mineral.

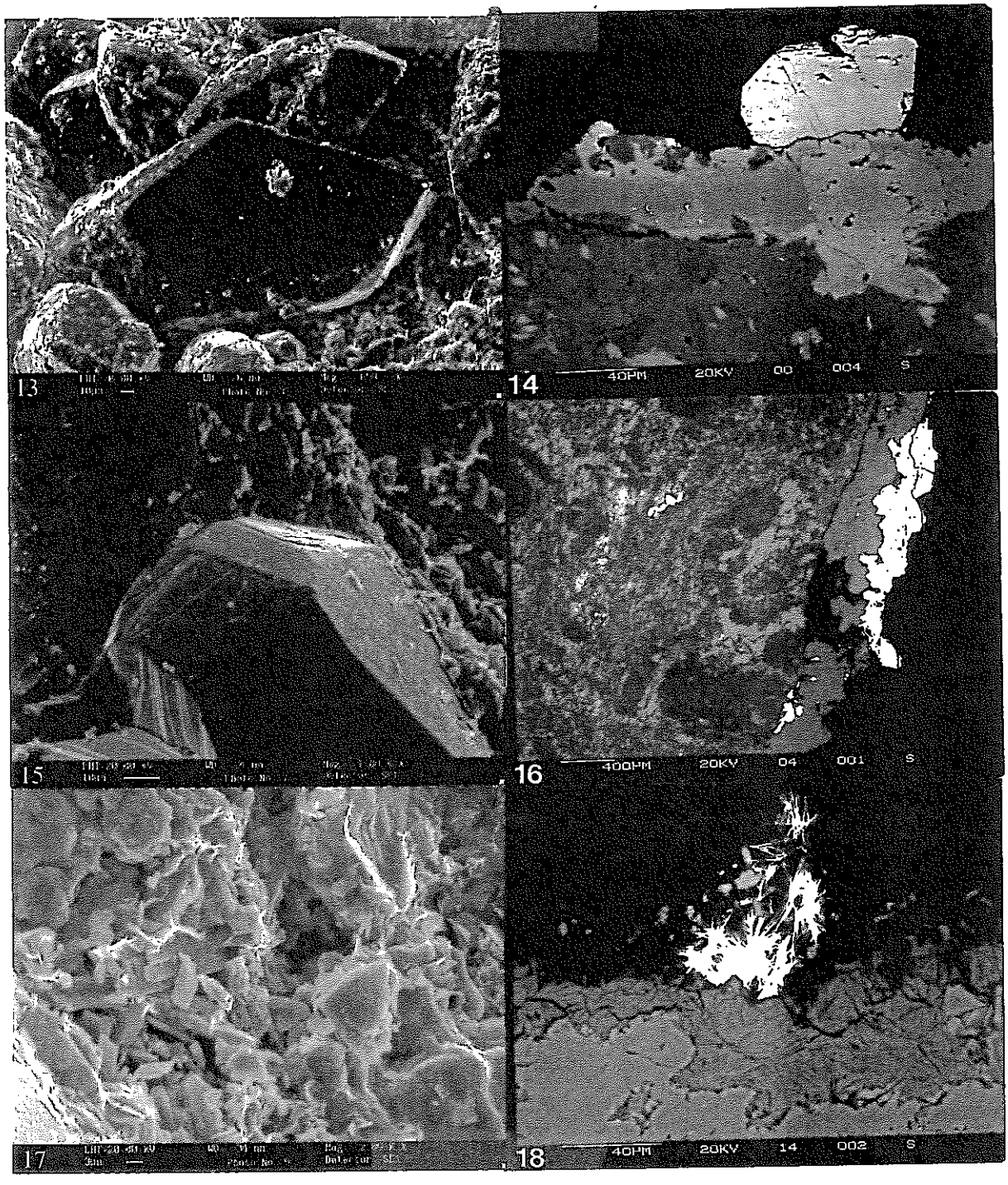
13
14
40PM 20KV 00 004 S
15
16
400PM 20KV 04 001 S
17
18
40PM 20KV 14 002 S

Plate 19: SEM photomicrograph showing fine-grained mineral particulate scattered on the surface of an orthoclase grain. Fine particulate material is also concentrated in pits and irregularities in the grain surface. Granodiorite starting material (sample C853)

Plate 20: SEM photomicrograph of typical biotite grain showing smooth basal [001] cleavage surfaces and irriegular but 'tight' cleavage at grain edge. Granodiorite starting material (sample C853)

Plate 21: SEM photomicrograph showing rough 'stepped' cleavage surfaces of a typical orthoclase grain. Etching is also apparent on the cleavage surfaces. Granodiorite starting material (sample C853)

Plate 22: SEM photomicrograph of pyrite showing euhedral crystal form with no evidence of alteration. Granodiorite starting material (sample C853)

Plate 23: SEM photomicrograph of the surface of a magnetite grain surface showing corrosion pitting forming interconnection. . Granodiorite starting material (sample C853)

Plate 24: SEM photomicrograph showing alteration at the edge of a biotite grain associated with exfloliation along the basal [001] cleavage. Run 537; 'without bacteria, 3 weeks' (sample D252).

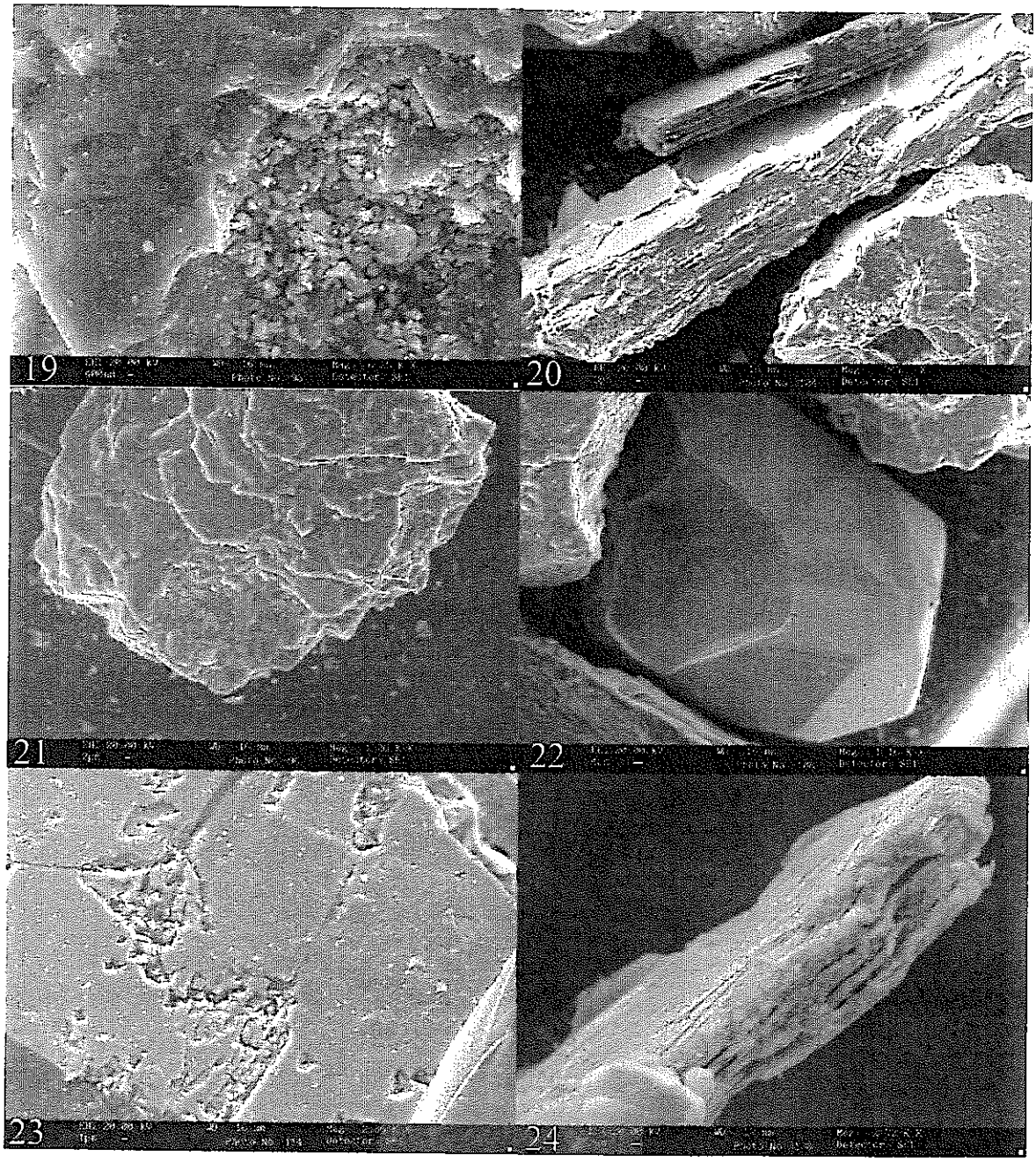
19
20
21
22
23
24

Plate 25: SEM Photomicrograph of fine mineral particulate material resting on the surface of a quartz grain. The fines display rounding of particle edges as a reult of dissolution. Run 537; 'without bacteria, 3 weeks' (sample D252).

Plate 26: CryoSEM photomicrograph of coccoid forms on 'lee' side of ribbed conchoidal fracture surface on quartz. Run 541:'iron reducing bacteria, 2 weeks' (sample D256).

Plate 27: CryoSEM photomicrograph showing spread of coccoid forms across a typical quartz grain surface. Run 541; 'iron reducing bacteria innoculated, 2 weeks' (sample D256).

Plate 28: CryoSEM photomicrograph of structures buried with the icw layer upon a grain surface. Run 531; 'sulphate reducing bacteria innoculated, 1 week' (sample D248).

Plate 29: High magnification cryoSEM photomicrograph of stuctures present on grain surfaces. Run 531; 'sulphate reducing bacteria innoculated, 1 week' (sample D248).

Plate 30: CryoSEM photomicrograph of rod-like form with organic composition lying in a depression in the surfaceof an albite grain. Run 532; 'sulphate reducing bacteria innoculated, 2 weeks' (sample D249).

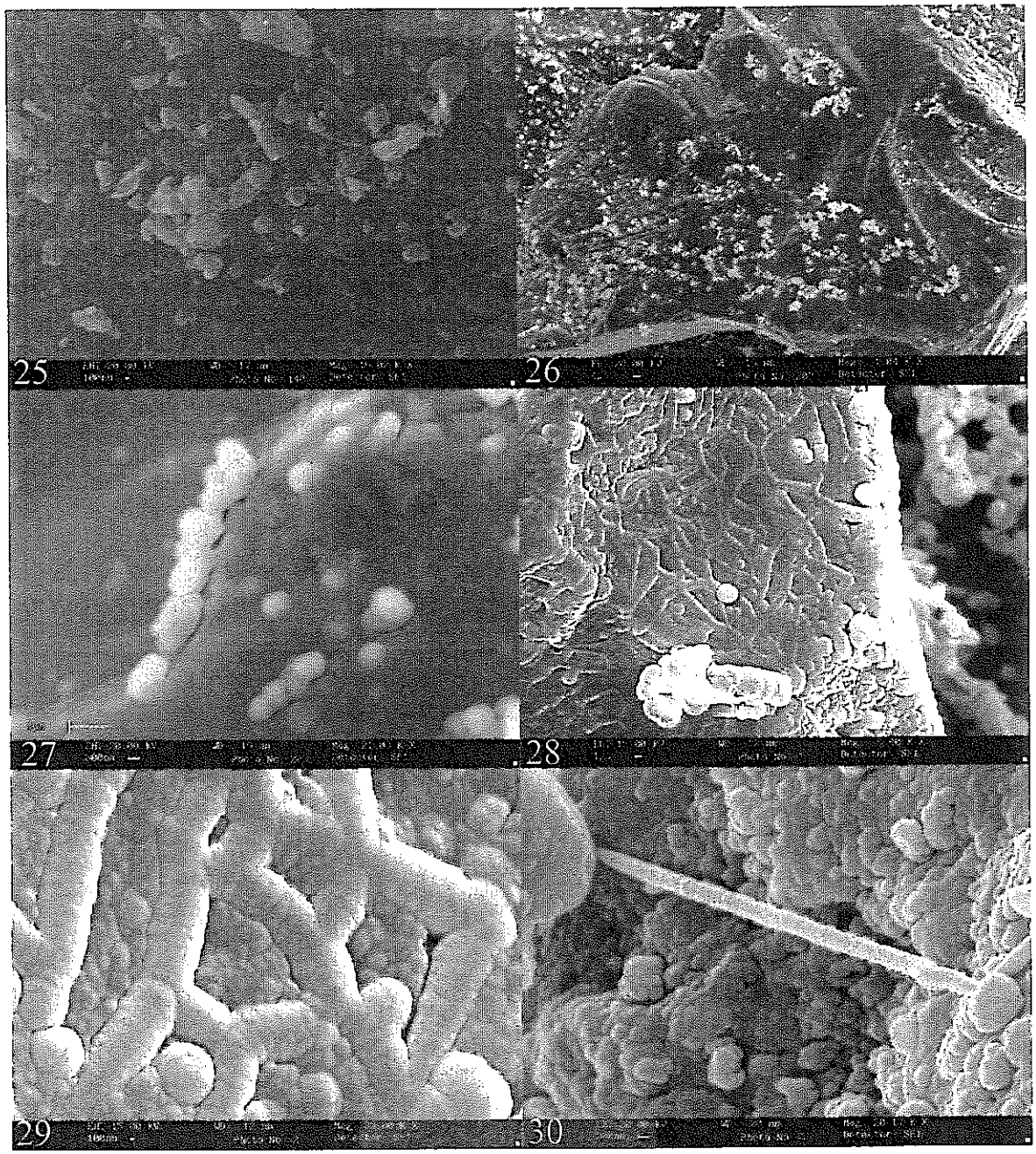
25
26
27
28
29
30

Plate 31: CryoSEM photomicrograph of filaments on quartz coated by residual amorphous ice and mineral fragments. Run 533; 'sulphate reducing bacteria inoculated, 3 weeks' (sample D250).

Plate 32: High magnification cryoSEM photomicrograph showing detail of filament structures on grain surface. Run 533; 'sulphate reducing bacteria inoculated, 3 weeks' (sample D250).

Plate 33: CryoSEM photomicrograph of biofilament linking two K-feldspar grains. Run 533; 'sulphate reducing bacteria inoculated, 3 weeks' (sample D250).

Plate 34: CryoSEM photomicrograph of complex biofilament strucure suspended between grains showing attached clay/iron oxide particles where filaments intersect. Run 533; 'sulphate reducing bacteria inoculated, 3 weeks' (sample D250).

Plate 35: High magnification cryoSEM photomicrograph of filament intersections and attached mineral matter. Run 533; 'sulphate reducing bacteria inoculated, 3 weeks' (sample D250).

Plate 36: CryoSEM photomicrograph of biofilament on grain surface containing many rod-like forms identified as iron-reducing bacteria. Run 545; 'sulphate reducing and iron reducing bacteria inoculated, 1 week' (sample D259).

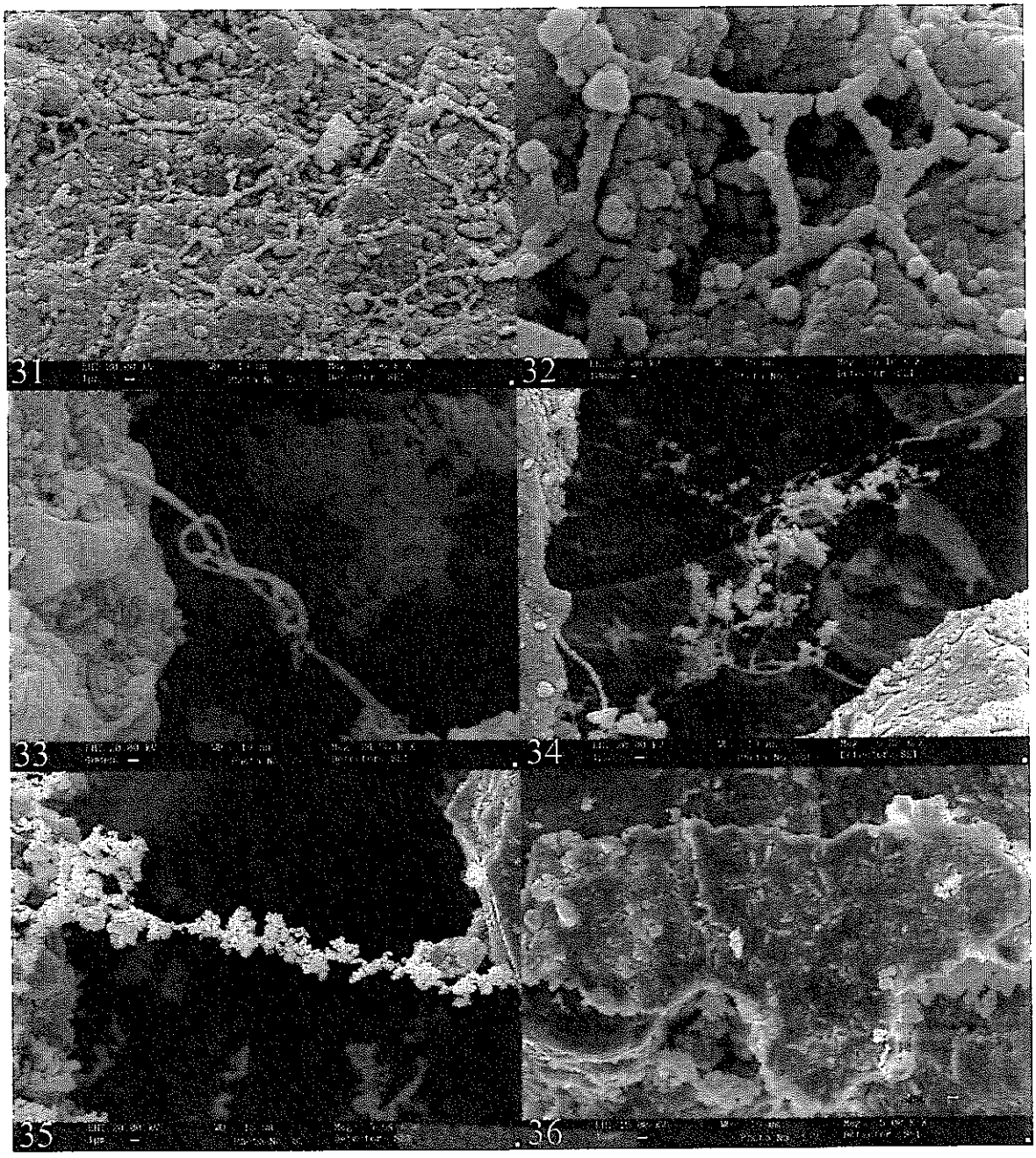
31
32
33
34
35
36

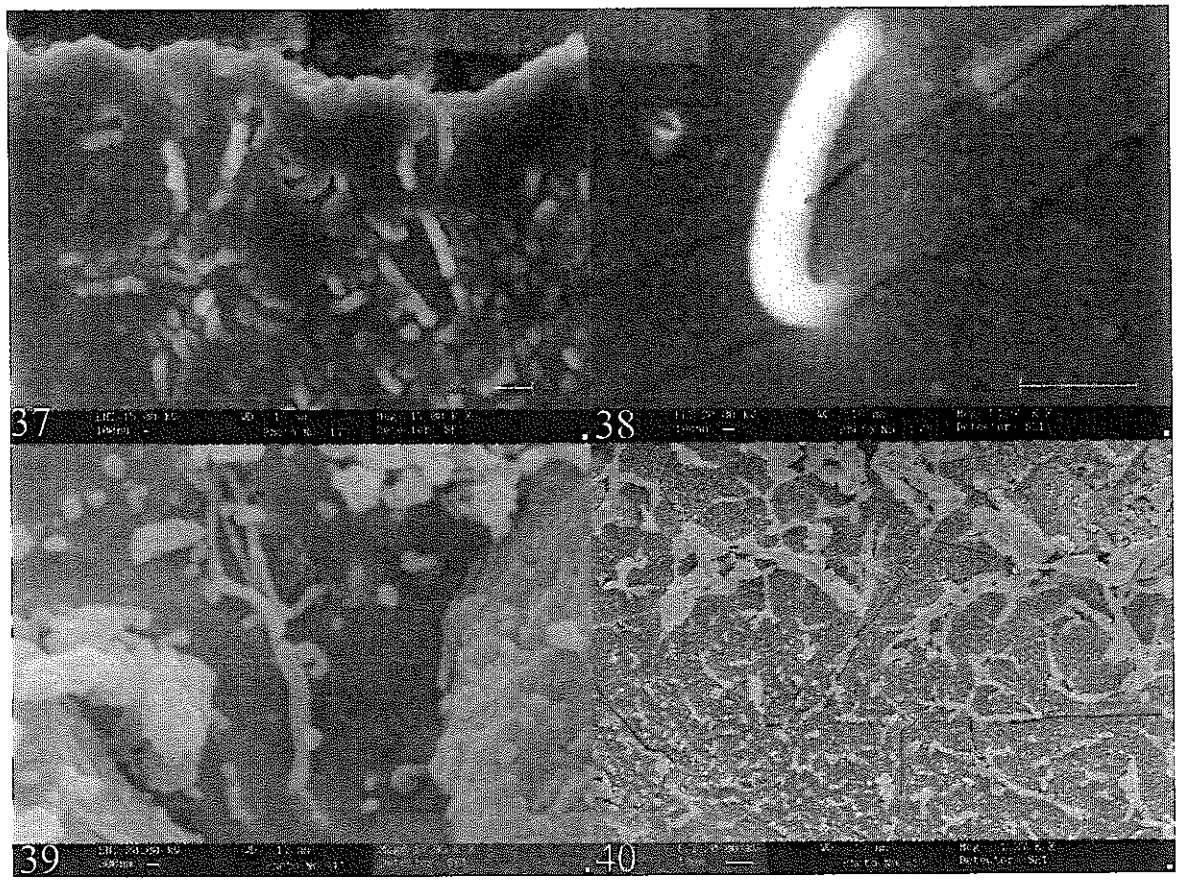

Plate 37: High magnification cryoSEM photomicrograph showing rod-like forms within the biofilm gel. Run 545; ' sulphate reducing and iron reducing bacteria inoculated, 1 week' (sample D250).

Plate 38: CryoSEM photomicrograph showing a single iron reducing bacteria bonding to a quartz grain surface. Fine surface coating on quartz is residual ice from etching process. Run 545; ' sulphate reducing and iron reducing bacteria inoculated, 1 week' (sample D250).

Plate 39: CryoSEM photomicrograph of biofilaments on ice surfaces between grains. Run 540; ' sulphate reducing and iron reducing bacteria inoculated, 3 weeks' (sample D255).

Plate 40: CryoSEM photomicrograph of biofilaments and attached biofilm on ice surface between grains. Run 540; ' sulphate reducing and iron reducing bacteria inoculated, 3 weeks' (sample D255).

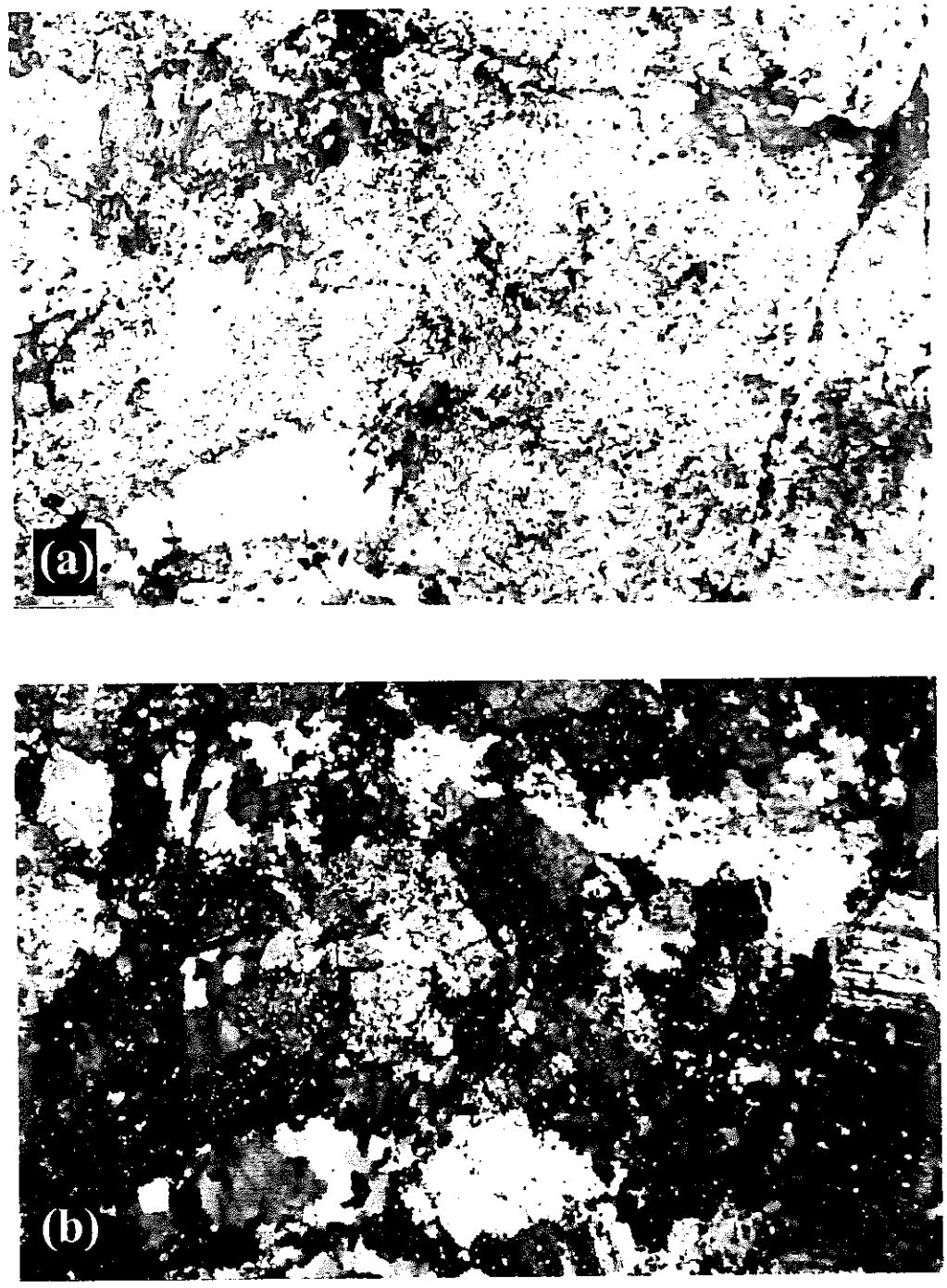

Plate 41: Optical micrographs of diorite starting material, D337

(a) Field of view dominated by dusty/speckled alkali feldspar along with colourless quartz, green biotote (top left), opaque oxides and brown epidote. (Plane polarised light, field of view 8.3mm).

(b) Identical view, crossed polars. Note lobate grain boundaries and subgrain development in quartz (bottom left) and presence of albite lamellae in feldspar (right)

Table 1. Summary information for samples examined.

Typical mineral compositions in the host rock from Aspo boreholes KA2862A and KA 2858A

Sample code	Location	Summary description
C849	REX alcove, *Fracture 01*	Sub-vertical PFF seeping groundwater but locally sealed, formed at right angles to *Fracture 01.*
C850	REX alcove, *Fracture 01*	Another surface from same PFF as C849
C851	REX alcove, *Fracture 01*	Chloritic surface from REX *Fracture 1*
C852	REX alcove, *Fracture 11*	Sub-horizontal epidote, calcite and ?fluorite vein with reddened alteration halo from REX *Fracture 11*
C853	REX alcove, *Fracture 11*	Large bulk rock sample of Aspo diorite cut by a segment of REX *Fracture 11*
C854	Tunnel wall opposite REX alcove	?PFF surface of calcite and fresh sulphide exposed on tunnel wall
C855	Tunnel wall opposite REX alcove	?PFF surface of calcite and fresh sulphide exposed on tunnel wall
C860	Borehole KA2862A, c.3.93 m	Feature 13. Refer to borehole log for detail
C861	Borehole KA2862A, c.6.87 m	Feature 27 Refer to borehole log for detail
C862	Borehole KA2862A, c.7.25 m	Features 30 and 31. Refer to borehole log for detail
C863	Borehole KA2862A, c.8.80 m	Feature 38. Refer to borehole log for detail
C864	Borehole KA2862A, c.10.0 m	Feature 48. Refer to borehole log for detail
C865	Borehole KA2862A, c.13.86 m	Feature 73, 74 & 75. PTS prepared from Feature 73. Refer to borehole log for detail
C866	Borehole KA2862A, c.15.73 m	Feature 81. Refer to borehole log for detail
C867	Borehole KA2858A, c.0.63 m	Features 5 & 9. Refer to borehole log for detail
C868	Borehole KA2858A, c.5.5 m	Features 39 & 40. PTS prepared from Feature 40. Refer to borehole log for detail
C869	Borehole KA2858A, c.6.75 m	Features 54 and 55. Refer to borehole log for detail
C870	Borehole KA2858A, c.10.44 m	Feature 85. Refer to borehole log for detail
C871	Borehole KA2858A, c.40.17 m	Feature 214. Refer to borehole log for detail

Table 2. Whole rock chemical analysis of diorite sample

Bulk chemical composition of the host rock in the REX experiment site, Aspo (BGS sample C853)

oxide	wt %	element	ppm	element	wt %
Sio2	59.72	Ni	17	s	0.018
TiO2	0.77	Cu	15		
Al2O3	2.265	As	<1		
FeO	2.705	Se	<1		
MnO	0.11	Rb	169		
MgO	2.01	Sr	934		
CaO	3.81	Y	20		
Na2O	4.35	Zr	253		
K2O	3.76	Nb	15		
P2O5	0.30	Pb	18		
LOI	1.54	Sc	10		
		V	69		
Total	98.95	Cr	26		
		Co	14		
		Ba	1786		

Table 3. Typical compositions of major mineral types determined from EMPA (data from sample C853)

Magnetite	%	Mica	%	Alkali feldspar	%	Plagioclase	%
SiO2	0	SiO2	39.05	SiO2	66.547	SiO2	65.09
TiO2	0.077	TiO2	1.811				
Al2O3	0	Al2O3	17.152	Al2O3	19.044	Al2O3	22.2
Cr2O3	0.1	Cr2O3	0				
MgO	0	MgO	12.377				
		CaO	0.066	CaO	0.738	CaO	3.812
MnO	0.048	MnO	0.587				
FeO	31.084	FeO	19.258	FeO	0.111	FeO	0.119
Fe2O3	68.786	F	0.708				
		Na2O	0.05	Na2O	5.665	Na2O	8.582
		K2O	5.223	K2O	7.328	K2O	0.064
		H2O	3.743				
				BaO	0.597	BaO	0.03
				Rb2O	0	Rb2O	0
				SrO	0.109	SrO	0.243
Total	100.095	Total	100.03	Total	100.14	Total	100.1
Magnetite	**cations**	**Mica**	**cations**	**Alkali feldspar**	**cations**	**Plagioclase**	**cations**
Si	0	Si	5.741	Si	2.989	Si	2.859
Ti	0.018	Ti	0.2	Al	1.008	Al	1.149
Al	0	Al	2.972				
Cr	0.024	Cr	0				
Mg	0	Mg	2.712				
		Ca	0.01	Ca	0.036	Ca	0.179
		Fe2+	2.368	Fe2+	0.004	Fe2+	0.004
Fe3+	15.94						
				Sr	0.003	Sr	0.006
				Ba	0.011	Ba	0.001
		Na	0.014	Na	0.493	Na	0.731
		K	0.979	K	0.42	K	0.004
Mn	0.012	Mn	0.073				
		H2O	0				
Total cations	23.999	Total cations	14.771	Total cations	4.964	Total Cations	4.933

Typical mineral compositions in the host rock from Aspo boreholes KA2862A and KA2858A

Table 4. Variations in x-ray peak intensity between bulk and 'sand-sized' fractions of C853.

	Bulk Rock	**Crushed Rock 125-250 μm Fraction**	
2θ(d)	Mineral phase	Peak intensity (counts)	Peak intensity (counts)
24.28 (4.25)	Quartz	350	520
31.06 (3.34)	Quartz	2302	3306
29.27 (3.54)	Orthoclase and chlorite	172	214
46.18 (2.28)	Quartz	238	302
47.17 (2.24)	Quartz	104	144
40.17 (2.60)	Augite	172	121
14.48 (7.08)	Chlorite	146	184
21.82 (4.73)	Chlorite	94	105

Typical mineral compositions in the host rock from Aspo boreholes KA2862A and KA2858

Table 5. Representative LAMP-ICP-MS data for major minerals in bulk rock and PFFs
(All values in mg/kg. Concentrations in italics are below that detection limit value (ppm))

	Sample Name	Phase	Magnesium	Aluminium	Calcium	Iron	Strontium	Barium	Thorium	Uranium
			Mg 24	Al 27	Ca 44	Fe 57	Sr 88	Ba 138	Th 232	U 238
Bulk	C853AP1C	Plagioclase	3659	150000	*31496*	*27469*	637	1205	*17*	*4*
	C853AP1H	K-feldspar	18492	150000	*24826*	*27369*	1493	2906	*14*	*3*
	C853AP1O	Chlorite	204138	150000	*8697*	358629	*1*	*5*	*5*	6
PFF	C851AP1F	Calcite	720	410	400000	2670	79	27	*0.8*	*0.2*
	C851AP1I	Chlorite	208224	150000	9568	271720	141	15	*5*	3
	C851AP1O	Epidote	13408	150000	57017	45321	1566	1056	31	9
	C851AP1U	Epidote	11344	150000	167258	231271	16604	1864	24557	559

Table 6. Representative compositions for major authigenic minerals in PFFs determined by EMPA

Barite	%	K-Feldspar	%	Pyrite	%	Calcite	%
		SiO2	63.8145			Mg(CO3)	0
		Al2O3	17.3976			Ca(CO3)	101.0389
		CaO	0.3299			Mn(CO3)	0
SO3	28.9588	FeO	0.065	As	0.024	Fe(CO3)	0
FeO	0.0622	SrO	0.0557	S	53.111	Zn(CO3)	0.2756
CuO	0.0033	BaO	0	Fe	47.052	Sr(CO3)	0
SrO	1.2837	Na2O	0.0925	Cu	0	Ba(CO3)	0
BaO	69.8642	K2O	17.3228	Co	0.039	Pb(CO3)	0.0748
PbO	0	Rb2O	0	Ni	0.02	K2(CO3)	0.0213
Total oxide	100.1722	Total oxide	99.0781	Total	100.247	Total	101.41
		Si	2.8435			Mg	0
		Al	0.9346			Ca	1.9945
		Ca	0.0293			Mn	0
S	0.931	Fe2+	0.3917			Fe	0
Fe	0.0022	Sr	0.0007			Zn	0.0043
Cu	0.0001	Ba	0.0041			Sr	0
Sr	0.0319	Na	0.0037			Ba	0
Ba	1.1727	K	0.9636			Pb	0.0006
Pb	0	Rb	0.0003			K	0.0006
Total cations	2.138	Total cations	5.1745			Total cations	2

Table 7. Nutrient and Energy Inventories used in preliminary modelling of microbial numbers to be used in batch studies

	Nutrients (mol.m^{-3})		Energy (mol.m^{-3})	
Groundwater				
	C	0.014	C	0.014
	P	1.25×10^{-3}	SO_4^{2-}	7.125
	S	7.156	Fe^{3+}	1.07×10^{-3}
	N	0.032		
Diorite				
	P	115.68	Fe^{2+}	1110.896
			Fe^{3+}	542.26

Table 8. Summary of experiments conducted

Lab Run Number	Groundwater (ml)	Rock (g)	Bacteria	Duration (weeks)
Run 531	20	20	SRB	1
Run 532	20	20	SRB	2
Run 533	20	20	SRB	3
Run 534	20	none	SRB	4
Run 535	20	20	None	1
Run 536	20	20	None	2
Run 537	20	20	None	3
Run 538	20	none	None	4
Run 542	20	20	IRB	1
Run 541	20	20	IRB	2
Run 539	20	20	IRB	3
Run 543	20	none	IRB	4
Run 545	20	20	IRB+SRB	1
Run 544	20	20	IRB+SRB	2
Run 540	20	20	IRB+SRB	3
Run 546	20	none	IRB+SRB	4

Table 9. Sample Preservations

Determinand	Sample volume (ml)	Deionised water volume (ml)	Preservative	Dilution
Fe(II)	1	3.5	0.5ml	1 to 5
S^{2-}	2	8	1% NaOH	1 to 5
NH^{4+}	1	4	1 % H_2SO_4	1 to 5
As,Se	5	5	1 % HCl	1 to 2
Cations	2	8	1 % HNO_3	1 to 5
Anions	3	none	none	none
Bacteria Count	1	none	Glutaraldehyde	none

Table 10. Summary of BGS laboratory batch experiments in Year 1

Lab Run No.	Rock	Bacteria	Duration (weeks)	MPG sample Code
Run 531	YES	SRB	1	D248
Run 532	YES	SRB	2	D249
Run 533	YES	SRB	3	D250
Run 534	NONE	SRB	4	not applicable
Run 535	YES	NONE	1	D251
Run 536	YES	NONE	2	D252
Run 537	YES	NONE	3	D253
Run 538	NONE	NONE	4	not applicable
Run 542	YES	IRB	1	D257
Run 541	YES	IRB	2	D256
Run 539	YES	IRB	3	D254
Run 543	NONE	IRB	4	not applicable
Run 545	YES	IRB + SRB	1	D256
Run 544	YES	IRB + SRB	2	D258
Run 540	YES	IRB + SRB	3	D255
Run 546	NONE	IRB + SRB	4	not applicable

Table 11. Variation in peak intensities (above background) in bulk sample XRD profiles

MPG code	C853	D248	D249	D250	D251	D252	D253	D254	D255	D256	D257	D258	D259
Lab Run No.	-	531	532	533	535	536	537	539	540	541	542	544	545
d - spacing													
10.06 (Mica)	36	80	41	475	46	64	75	421	752	550	790	540	521
7.07 (Chlorite)	120	190	186	152	148	253	143	148	215	161	242	202	157
3.34 (Quartz)	2510	2770	3089	2859	2770	2748	2905	2748	3500	3208	2595	2539	2792
3.24 (Orthoclase)	350	373	465	430	382	541	390	449	530	486	530	491	421
3.19 (Albite)	1070	1148	1359	1312	1105	1398	1204	1278	1495	1343	1374	1374	1229

Table 12a. Variation in peak intensities (above background) in fine fraction XRD profiles

MPG code	C853	D248	D249	D250	D251	D252	D253	D254	D255	D256	D257	D258	D259
Lab Run No.	-	531	532	533	535	536	537	539	540	541	542	544	545
d - spacing													
10.06 (Mica)	786	883	2336	1284	832	583	861	1302	1092	525	451	377	166
7.07 (Chlorite)	372	284	616	314	286	227	304	404	342	192	157	149	74
3.34 (Quartz)	1349	1488	2639	1344	1073	1331	1207	1557	1336	863	769	1101	724
3.24 (Orthoclase)	342	299	637	382	314	320	314	314	322	242	319	337	229
3.19 (Albite)	768	796	1254	789	671	761	780	863	724	594	631	571	476

Table 12b: Peak intensities of fine fraction normalised to quartz (intensity 1349 counts, sample C853 (note: actual values for quartz peak are shown in bold).

MPG code	C853	D248	D249	D250	D251	D252	D253	D254	D255	D256	D257	D258	D259
Hydrothermal Lab Run No.	-	**531**	**532**	**533**	**535**	**536**	**537**	**539**	**540**	**541**	**542**	**544**	**545**
d - spacing													
10.06 (Mica)	786	800.5	1194	1289	1046	590.9	962.3	1128	1103	820.7	791.2	461.9	309.3
7.07 (Chlorite)	372	257.5	314.9	315.2	359.6	230.1	339.8	350	345.3	300.1	275.4	182.6	137.9
3.34 (Quartz)	**1349**	**1488**	**2639**	**1344**	**1073**	**1331**	**1207**	**1557**	**1336**	**863**	**769**	**1101**	**724**
3.24 (Orthoclase)	342	271.1	325.6	383.4	394.8	324.3	350.9	272.1	325.1	378.3	559.6	412.9	426.7
3.19 (Albite)	768	721.6	641	791.9	843.6	771.3	871.8	747.7	731	928.5	1107	699.6	886.9

Table 13. Chemical composition of groundwater samples collected from Äspö borehole KA2858A (September 1997).

Species	Start of collection	End of collection
Field Analyses		
Temp (°C)	14.1	14.2
Eh (mV)	210.0	246.7
pH	8.04	8.25
HCO3 (mg/l)	16	12
Conductivity (µS/cm)	24400	29200
Dissolved O2 (mg/l)	<1	<1
Laboratory Analyses		
pH	6.74	7.16
Ca (mg/l)	3670	4350
Mg (mg/l)	49.7	50.1
Na (mg/l)	2680	2920
K (mg/l)	11.0	12.2
HCO3 (mg/l)	<20	<20
Cl (mg/l)	10309	12405
SO4 (mg/l)	612	664
NO3 (mg/l)	<5.00	<5.00
cation total (meq/l)	305.75	350.82
anion total (meq/l)	304.61	365.03
ionic balance (%)	0.19	-1.99
Br (mg/l)	77.4	94.3
NO2 (mg/l)	<1	<1
HPO4 (mg/l)	0.09	0.12
Total P (mg/l)	<0.10	<0.10
F (mg/l)	1.32	1.29
Total organic carbon (mg/l)	<1.00	1.03
Total inorganic carbon (mg/l)	1.21	1.09
Total S (mg/l)	212	227
Reduced S (µg/l)	13.5	<3.00
NH4 (mg/l)	<0.05	<0.05
Si (mg/l)	4.00	3.81
Ba (mg/l)	0.072	0.088
Sr (mg/l)	56.1	79.9
Mn (mg/l)	0.354	0.369
Total Fe (mg/l)	0.07	0.07
Reduced Fe (mg/l)	0.13	0.14
Al (mg/l)	0.29	0.25
Co (mg/l)	<0.02	<0.02
Ni (mg/l)	<0.02	<0.02
Cu (mg/l)	<0.005	<0.005
Zn (mg/l)	<0.005	<0.005
Cr (mg/l)	<0.01	<0.01
Mo (mg/l)	0.05	0.06
Cd (mg/l)	<0.005	<0.005
Pb (mg/l)	<0.10	<0.10
V (mg/l)	<0.01	<0.01
Li (mg/l)	2.36	2.96
B (mg/l)	1.19	1.10

Table 14. Summary of differences between size fractions of D337 in terms of peak intensities above background (counts/second).

Peak (°2Q)	Mineral phase	Bulk Diorite	Sand fraction	Fines
10.22	Mica	407	214	551
14.50	Chlorite	93	138	94
31.06	Quartz	1768	1723	1891
32.61	Albite	1611	2384	1463
34.39	Calcite	138	73	142

Table 15. Chemical analysis of diorites

	C853	D337	D337		C853	D337	D337
Oxide (wt%)			Sand fraction	element (ppm)			Sand fraction
SiO_2	59.7	60.20	63.40	Sc	10	9	7
TiO_2	0.77	0.78	0.69	V	69	70	52
Al_2O_3	17.6	17.18	18.21	Cr	26	34	15
$Fe_2O_3^t$		4.95	2.92	Co	14	15	9
$Fe_2O_3^*$	2.27	nd	nd	Ni	17	17	9
FeO^*	2.71	nd	nd	Cu	15	8	14
Mn_3O_4	0.11	0.10	0.07	Zn	86	85	129
MgO	2.01	2.02	0.96	As	<1	<2	<2
CaO	3.81	4.15	3.65	Se	<1	<2	<2
Na_2O	4.35	4.95	6.07	Rb	169	124	89
K_2O	3.76	2.89	2.30	Sr	934	897	964
P_2O_5	0.3	0.32	0.11	Y	20	19	20
SrO	nd	0.12	0.13	Zr	253	273	81
BaO	nd	0.13	0.12	Nb	15	15	15
LOI	1.54	2.14	1.57	Pb	18	22	22
				Ba	1786	1081	1024
Total	99	99.97	100.21				

^{t} = total Fe

* = determined by wet chemical methods

Table 16. CIPW norms

Mineral phase	C853	D337	D337
			Sand fraction
Quartz	8.79	9.04	10.4
Orthoclase	22.2	17.1	13.59
Albite	36.8	41.9	51.36
Anorthite	16.9	16.1	15.65
Corundum	0.18		
Diopside		1.91	1.39
Hypersthene	2.03	5.92	2.43
Magnetite	3.28	3.09	1.83
Ilmenite	1.46	1.48	1.31
Apatite	0.7	0.74	0.25
Plagioclase composition	An32	An28	An23

APPENDIX 1. LITHOLOGY OF ÄSPÖ SITE

The background lithological, mineralogical and whole-rock geochemical data are described in detail by Wickman et al. (1988) and are summarised in Tullborg (1995). A summary of the data are given below to provide an useful overview for the interpretation of the BGS laboratory experiments.

1. Äspö Diorite

The modal analysis and chemical composition of representative Äspö Diorite are shown in Appendix 1: Table 1 and Table 2, respectively.

Mineralogy
The Äspö Diorite varies largely from granite, through granodiorite, to quartz monzodiorite, with some lithologies falling within tonalite, quartz diorite and quartz monzonite compositional fields. The rock is porphyritic and contains K-feldspar phenocrysts. Minor amounts of magnetite and pyrite are invariably present but it may show significant variation in the amount of amphibole present. The mineralogy includes (volume %): major plagioclase (45%), K-feldspar (15%), biotite (15%) and quartz (14%); minor epidote (6%), sphene (2%), amphibole (1%) and opaque minerals (magnetite and pyrite) (1%); and accessory apatite (0.5%), muscovite (0.5%). Additionally, calcite, fluorite, prehnite and zircon are present in trace amounts (<0.5%).

Mineral chemistry
To date (up to Tullborg, 1995), no data have been obtained on the chemical composition of separate mineral phases in the Äspö Diorite.

Porosity
The Äspö Diorite has an average porosity of approximately 0.5 0.2 vol.%.

2. Ävrö Granite

The modal analysis and chemical composition of representative Ävrö Granite are shown in Appendix:Table 1 and Table 2, respectively.

Mineralogy
Like the Äspö Diorite, the Ävrö Granite is porphyritic, with K-feldspar phenocrysts. The Ävrö Granite is more siliceous and less calcic than the Äspö Diorite, being dominated by rocks falling within the granite compositional fields. However, it also includes a significant proportion of granodiorite composition rocks. It comprises (volume %): major plagioclase (33%), K-feldspar (29%) and quartz (25%) ; minor biotite (7%) epidote (2.5%), sphene (1.5%) and opaque minerals (magnetite and pyrite) (1%); and accessory apatite (0.5%), muscovite (0.5%). Additionally, amphibole, calcite, fluorite, prehnite and zircon are present in trace amounts (<0.5%).

Mineral chemistry
Some limited electron microprobe analyses are available for biotite and plagioclase (from the fresh host granite) and chlorite and epidote (from altered wallrock samples). These

have been taken from the Large Scale Redox Experiment fracture zone located at c.500 m from the entrance of the Äspö tunnel (Banwart et al., 1992). The mineral compositions are shown in Table 3. The biotite has a Mg/Fe atomic ratio of 1.25 and Fe(II) makes up 85% of the total Fe content (Tullborg, 1995). The plagioclase in the Ävrö granite is typically oligoclase in composition, with Na/Ca approximately 3 (Tullborg, 1995).

Porosity
The Ävrö Granite has an average porosity of approximately 0.4 0.2 vol.%, which is slightly lower than that of the Äspö Diorite.

3. Fine-grained granite

The modal analysis and chemical composition of average fine-grained (<1 mm grain size) granite lithology encountered in the Äspö Hard Rock Laboratory are shown in Appendix 1:Table 1 and Table 2, respectively.

Mineralogy
The rock is more silica-rich, contains less calcium, aluminium, iron and magnesium, and more potassium, than either the Äspö Diorite or Ävrö Granite. It comprises (volume %): major K-feldspar (38%), quartz (31%) and plagioclase (23%); minor muscovite (3%) biotite (2.5%) epidote (1%) and opaque minerals (magnetite and pyrite) (1%); and accessory apatite (0.5%), sphene (0.5%). As in the Äspö Diorite and Ävrö Granite, calcite, fluorite and zircon are present in trace amounts (<0.5%).

Mineral chemistry
To date (up to Tullborg, 1995), no data have been reported on the chemical composition of separate mineral phases in the fine-grained granite.

Porosity
The fine-grained granite has the lowest porosity, with an average of approximately 0.3 - 0.2 vol.%.

4. Altered rocks

Hydrothermal alteration and oxidation of wallrock close to fracture edges are common features in all the granitic rocks at Äspö. The alteration is manifested by the breakdown of biotite and magnetite and the formation of chlorite and hematite secondary minerals. Plagioclase has been altered to an intergrowth of albite, epidote and sericite (referred to as saussuritisation). Alteration zones around fractures and veins vary in width from 5-50 mm. Microscopic grains of pyrite are reported to be more frequent in some samples of the oxidised rocks, in comparison to fresh host rocks (Tullborg, 1995). Tullborg (1995) reports an overall increase in H_2O and loss of CaO in the altered lithologies

Mineral chemistry
Limited chemical data (based on electron microprobe and Fe(II)/Fe(III) analyses for chlorite from the Redox Zone) are summarised in Tullborg (1995). These analyses gave a Mg/Fe ratio of 1.6 and indicate that 80% of the Fe in the chlorite is present as Fe(II).

Electron microprobe analyses for chlorite and epidote from altered wallrock in the Redox Zone at Äspö are also presented in Appendix 1:Table 3.

Porosity
Analyses indicate that there is an overall enhancement of porosity in the altered wallrocks. Porosity values of approximately 0.8 0.2 vol.% are indicated in the wallrock alteration zones compared to 0.2-0.3% in the fresh host rocks. Detailed petrographic examination has revealed that, whereas the porosity in the fresh rocks is largely a homogenous matrix porosity along a network of grain boundaries and intragranular cracks, the porosity in the altered rocks is dominated by porous fissure fillings or open microfractures (cf. Tullborg, 1995 and references therein).

5. Fracture mineralisation and deformation history

The most frequent fracture minerals at Äspö are calcite and chlorite which are widespread throughout the underground facility and drillcores, and particularly in open fractures (Tullborg, 1989; Tullborg et al., 1991). On the basis of petrographic and stable isotope (C, O) studies, it is evident that several generations of calcite are present (Tullborg et al., 1991).

Epidote is also common at Äspö but, with hematite (which is much less common), tends to be concentrated in discrete fracture zones. Petrographic studies (Tullborg, 1989) indicate that hematite and epidote are not contemporaneous but occur in the same fractures due to fracture reactivation. Small amounts of pyrite are a common feature of many veins. Fluorite, quartz, laumontite, muscovite and clay minerals occur sporadically. Quartz is more common in sealed fractures than in open fractures. Rare occurrences of apophyllite and gypsum have also been reported (Tullborg, 1989). Fe-oxyhydroxides are also found, particularly near the surface.

Seven episodes of deformation, associated with the development of foliation, alteration, fracturing and fracture mineralisation, have been recognised in the Äspö region, based on detailed study of borehole material and from observations on the Äspö tunnel (Wikman et al., 1988; Tullborg et al., 1991; Tullborg, 1989; 1995 and references therein). This sequence has been evaluated from detailed examination of cross-cutting field relationships and paragenetic mineral fabrics. The sequence of principal events and fracture mineralisation (Events 1-7) is shown in Appendix 1:Table 4 and summarised below.

Event 1
The first visible deformation produced the E-W to ENE-WSW foliation, which is part of the large-scale regional structural grain. This deformation belongs to the D3 event affecting SW Sweden. The precise age of this event is unknown but pre-dates the intrusion of the Götmar Granite which is dated at 1400 Ma.

Event 2
Event 2 is represented by tectonic deformation which resulted in the formation of E-W trending mylonites mineralised by fine-grained epidote, recrystallised quartz and in some cases, muscovite mineralisation. In part, some of the shearing may be related to the earlier D3 regional event.

Event 3
Event 3 is characterised by fracture mineralisation associated with a second generation of epidote mineralisation. Yellow euhedral crystals of epidote line the walls of these fractures, and often, fluorite fills the centres of these veins and encloses the epidote.. Tullborg (1995) suggests that this mineralisation is related to hydrothermal mineralisation associated with the intrusion of the Götmar Granite to the north of Äspö. The texture of these epidote-fluorite veins suggests that mineralisation occurred under a tensional regime.

Event 4
Event 4 is characterised by veins of euhedral quartz, associated with muscovite, hematite, fluorite and calcite. Spherulitic chlorite is developed as a late-developed phase within these veins. This mineralisation is a frequent feature of the tunnel and drillcores at Äspö. The assemblage indicates high-temperature hydrothermal fluid circulation, and Tullborg (1995) considers it to represent the effects of late-stage circulation of magmatic fluids from the Götmar Granite.

Event 5
Some discrete fractures at Äspö show a mineral paragenesis of prehnite, calcite and hematite-stained laumontite. It has been suggested (Tullborg, 1995) that this mineralisation may correlate with similar mineralisation in central Sweden, dated (Rb-Sr/prehnite) at c.1100 Ma, and interpreted to be related to low temperature burial metamorphism.

Event 6
Later stage fracturing and mineralisation is associated with illite-rich mixed-layer clays and calcite (Event 6). K-Ar ages for the illite mineralisation are between 300-350 Ma (cf. references in Tullborg, 1995). Event 6 is tentatively interpreted to represent fracturing (or fracture reactivation) and mineralisation related to Post-Caledonian deep burial (Tullborg, 1995).

Event 7
Event 7 is the latest episode of fracture mineralisation and alteration recognised at Âspö (Tullborg, 1995). It is dominated by the dissolution and reprecipitation of carbonate minerals, mostly calcite. Pyrite mineralisation also is associated with this mineralisation episode. In the near-surface regions, oxidation of Fe(II) has produced Fe-oxyhydroxides. In addition, low-temperature minerals like kaolinite and smectite may also occur, but in very minor amounts. Stable isotope data (C, O) show that at least part of the calcite mineralisation may be in equilibrium with present-day groundwaters, or with cold (?glacial) recharge waters (Tullborg et al., 1991) and it is considered that Event 7 is related to Recent/Quaternary groundwater circulation (Tullborg et al., 1991; Tullborg, 1995).

Chemical analyses from electron microprobe (major elements) and induced neutron activation analysis (trace elements) of fracture-filling calcite, chlorite, epidote and prehnite have been published from Äspö (Tullborg et al., 1991). The major element data for these minerals are reproduced in Appendix1:Table 5.

Calcite often contains small amounts of reduced Fe(II) and Mn(II). However, reported analyses indicate that calcites from Äspö are fairly pure. Fe(II) contents of Äspö fracture calcites appear to be very low (FeO is generally <0.2 wt%) with a maximum of 0.7 wt% FeO. Mg contents are also low low (MgO=<0.5 wt %). Mn(II) contents appear to be quite variable from <0.1-2.5 wt %.

Fracture chlorites are Fe-rich with up to 27 wt% FeO. They appear to be more variable than wallrock chlorites, containing higher Mg and generally lower Fe and Al than wallrock species (compare Tables 3 and 5). Although 80% of the Fe in the wallrock chlorite of the Redox Zone is present as Fe(II) (Tullborg, 1991), the ratio of Fe(II)/Fe(III) in fracture chlorites has not been determined. However, given the similarity of the electron microprobe data for wallrock chlorite and vein chlorite, it seems likely that the Fe(II)/Fe(III) ratio is also probably broadly similar.

Apart from sulphide minerals (for which there are no chemical data), epidote and prehnite are the only other principal Fe-bearing minerals. Both of these minerals will contain Fe as Fe(III) (Deer et al., 1962). Epidotes are Fe-rich with 11-17 wt% Fe_2O_3, and are similar to epidote seen in altered wallrocks (cf. Table 3). Prehnite is variable in composition from end-member Al-rich prehnite to prehnite containing 10 wt% Fe_2O_3.

Appendix 1:Table 1. Representative modal analyses of principal lithologies from the Äspö Hard Rock Laboratory (data from Tullborg, 1995)

	Äspö Diorite	Ävrö Granite	Fine-grained granite
Mineral Composition (volume %)			
quartz	14	25	31
K-feldspar	15	29	38
plagioclase	45	33	23
biotite	15	7	2.5
muscovite	0.5	0.5	3
epidote	6	2.5	1
amphibole	1	<0.5	0
sphene	2	1.5	0.5
apatite	0.5	0.5	<0.5
opaques	1	1	1
Less frequent minerals include: <0.5% calcite,fluorite,prehnite and zircon			
Porosity	0.5	0.4	0.3
(volume %)	0.2	0.2	0.2

Appendix 1: Table 2. Representative chemical analyses of principal lithologies from the Äspö Hard Rock Laboratory (data from Tullborg, 1995)

	Äspö Diorite	Ävrö Granite	Fine-grained granite
Major Elements (wt %)			
SiO2	61.0	69.0	73.0
Al2O3	17.8	15.2	13.5
CaO	4.1	2.2	1.0
Na2O	4.4	4.0	3.3
K2O	3.2	4.4	5.8
Fe2O3	1.9	2.2	1.7*
FeO	2.7	1.3	-
MgO	2.2	1.0	0.4
MnO	0.09	0.06	0.03
P2O5	0.3	0.1	0.1
TiO2	0.8	0.4	0.3
F	0.2	0.1	0.05
Loss on ignition	1	1	0.5
Trace Elements (ppm)			
Cu	20	20	10
Ni	20	10	7
Zn	70	50	20
Sr	1100	650	400
Ba	1600	1100	900
Rb	120	140	250
Cs	3	2	2
Zr	250	150	(180)
Hf	7.3	3.4	-
Nb	15	-	10
Th	11	8.3	(25)
U	4.5	2.5	(8)
Sc	11	3	-
La	57	35	(70)
Ce	120	69	(150)
Nd	58	25	(60)
Sm	10	3.5	(9.5)
Eu	2.1	0.7	(0.7)
Tb	1.3	-	(1.3)
Yb	2.3	1.2	(3.6)
Lu	0.4	0.2	(0.5)
Y	16	15	35

* = Total Fe

() = Elements showing large variations, 100%

Appendix 1:Table 3. Compositional data (electron microprobe analyses) for host-rock minerals from the Ävrö Granite (data from Banwart et al, 1988). (Concentration in weight %)

	K_2O	Na_2O	CaO	MgO	MnO	FeO	TiO_2	Al_2O_3	SiO_2
Biotites (fresh granite)									
	9.3	0.1	-	12.5	0.6	17.3	1.7	14.9	38.5
	9.4	0.1	-	12.3	0.6	17.7	1.7	15.4	38.2
Chlorite (altered granite wallrock)									
	-	-	0.1	17.1	0.7	22.2	0.04	19.8	27.8
	-	-	0.05	16.8	0.8	23.1	-	19.7	26.8
	-	-	0.3	18.0	0.7	21.7	0.2	17.9	28.9
	-	-	0.2	17.5	0.6	23.0	0.08	17.2	28.7
	-	-	0.1	19.3	0.7	20.6	0.07	19.2	27.8
	-	-	0.05	17.8	0.7	22.5	0.05	19.1	27.5
	-	-	0.4	18.5	0.4	19.5	0.05	18.0	29.5
	-	-	0.3	18.2	0.5	19.7	0.04	18.5	30.6
Epidotes (altered granite wallrock) [Fe_2O_3]									
	-	-	23.4	0.2	0.2	14.5	0.2	22.2	37.2
	-	-	23.2	0.2	0.5	15.6	0.06	21.7	36.9
	-	-	23.5	0.2	0.3	13.8	0.03	23.6	37.1
	-	-	24.0	0.2	0.4	11.6	0.1	24.4	37.1

Appendx 1:Table 4. Sequence of events and fracture mineralisation history (after Tullborg, 1995)

Event	Effect/Mineralisation	Comment
0	Formation of the Äspö granitoids	c. 1800 Ma
1	Regional deformation resulting in E-W to ENE-WSW foliation	D3-event in SW Swedenbetween 1660-1400 Ma
2	Mylonitisation; formation of fine-grained epidote, muscovite and recrystallisation of quartz	Some mylonites probably belong to the last phase (shearing) of D3 above
3	Reactivation of mylonites and formation of idiomorphic epidote and fluorite	Intrusion of the anorogenic Götemar intrusion c.1400 Ma
4	Growth of idiomorphic quartz, muscovite, hematite, fluorite, calcite and spherulitic chlorite	Late-magmatic hydrothermal circulation associated with the Götemar intrusion
5	Prehnite, laumontite, calcite, chlorite and fluorite	Low-temperature burial metamorphism c. 1100 Ma?
6	Illite-dominated mixed-layer clay, calcite chlorite	Low-temperature burial metamorphism and mineralisation associated with burial beneath cover in Sweden
7	Calcite, Fe-oxyhydroxide, pyrite, clay-minerals?	Mineralisation probably associated groundwater circulation

Appendix 1:Table 5. Compositional data (electron microprobe analyses) for selected fracture minerals from Äspö (data from Tullborg et al, 1991). [Concentration in weight %]

	K_2O	Na_2O	CaO	MgO	MnO	FeO	TiO_2	Al_2O_3	SiO_2
Calcites									
	-	-	55.4	0.3	0.3	0.7	-	-	-
	-	-	56.4	0.3	0.04	0.01	-	-	-
	-	-	55.0	0.4	1.3	0.00	-	-	-
	-	-	54.6	0.3	0.8	0.04	-	-	-
	-	-	54.9	0.3	1.2	0.00	-	-	-
	-	-	54.1	0.4	1.2	0.00	-	-	-
	-	-	55.3	0.3	0.4	0.00	-	-	-
	-	-	55.3	0.3	0.4	0.00	-	-	-
	-	-	55.9	0.3	0.1	0.00	-	-	-
	-	-	55.6	0.3	0.06	0.01	-	-	-
	-	-	55.7	0.3	0.02	0.1	-	-	-
	-	-	53.7	0.4	1.4	0.00	-	-	-
	-	-	53.7	0.4	1.7	0.1	-	-	-
	-	-	52.2	0.5	2.5	0.1	-	-	-
	-	-	52.0	0.3	2.5	0.01	-	-	-
Chlorites									
	-	-	0.3	21.2	0.3	17.6	0.03	18.0	29.6
	-	-	0.4	17.4	0.9	22.2	0.02	17.2	27.8
	-	-	0.04	21.0	0.2	16.4	0.00	18.6	30.3
	-	-	0.05	18.8	0.7	20.7	0.03	17.1	29.5
	-	-	0.1	14.4	1.0	27.0	0.00	16.7	28.3
	-	-	0.09	14.4	1.0	27.2	0.02	16.6	28.0
Epidotes					[Fe2O3]				
	-	-	23.4	0.1	0.2	11.4	0.002	24.3	37.9
	-	-	23.5	0.1	0.1	12.4	0.1	23.6	38.4
	-	-	22.7	0.2	0.02	15.1	0.04	22.1	37.5
	-	-	22.7	0.2	0.5	16.3	0.06	20.6	37.6
	-	-	22.9	0.2	0.2	16.6	0.04	20.6	27.6
	-	-	22.8	0.1	0.3	13.9	0.04	22.7	37.8
	-	-	22.8	0.2	0.04	11.8	0.05	24.9	38.2
	-	-	22.8	0.2	0.03	14.0	0.03	23.0	37.7
	-	-	23.1	0.2	0.2	14.3	0.03	22.5	38.0
	-	-	23.3	0.2	0.2	12.7	0.01	23.8	37.6
Prehnites					[Fe2O3]				
	-	-	26.5	0.1	0.07	10.4	0.05	17.3	41.9
	-	-	27.0	0.1	0.04	2.3	0.01	22.7	43.0
	-	-	25.9	0.1	0.00	13.5	0.00	14.6	41.8
	-	-	27.1	0.1	0.03	0.9	0.00	23.9	44.2
	-	-	27.1	0.2	0.00	2.2	0.00	22.5	44.0
	-	-	27.3	0.2	0.05	0.2	0.00	23.7	44.2

APPENDIX 2. MINERALOGICAL OBSERVATIONS

REX Experimental Block Boreholes

1. Methods

1.1. Core logging

The drillcores from boreholes KA2858A and KA2862A were laid out for examination in the Core Examination Room at Äspö Hard Rock Laboratory. All "apparently open" fractures (i.e. all naturally open features and features which had broken as a result of drilling disturbance or subsequent core handling) were examined. Sealed fractures were not studied as they were considered to be of little relevance, since the present study was concerned with evaluating the mineralogy of potentially flowing features. The surface of each discontinuity was examined carefully using a Zeiss binocular microscope to identify the surface mineralogy and to evaluate surface morphology. Simple on-site mineral identification was aided by the use of dilute (10%) hydrochloric acid to test for the presence of calcite. It had also been intended to use chemical stains to refine carbonate mineral identification (modified method after Dickson, 1966). However, this proved unnecessary since the carbonate mineralogy is calcite-dominated.

The observations for each borehole are summarised and tabulated in Appendix 2:Table 1 (KA2858A) and Table 2 (KA2862A). The following information was recorded:

(i) *"Distance along core axis"*
The position of each logged feature in the borehole is defined by reference to the distance of its intersection in the core, from the start of the core (measured in metres). Draft (hand-drawn) fracture logs supplied by SKB were used as a guide to identify fracture location. However, these logs were incomplete, and some minor discrepancies exist between measurements on these logs and BGS measurements. For the most part, BGS measurements were determined sequentially from a known reference point (corresponding to a recognised SKB measurement) in each core stick.

(ii) *"BGS Feature Number"*
Each logged feature was ascribed a unique identifier in each borehole. This is used to define individual features.

(iii) *"Fracture Type"*
On the basis of petrographic (binocular microscope) observations, an assessment was made as to whether the fracture was natural or an artifact of drilling/core handling. The criteria for this distinction are discussed in Section 2 The notation **"v"** (largely veins) is used to define features considered to be natural fractures. This includes features which are naturally open or unsealed, as well as fractures which have opened as a result of reactivation and breakage along pre-existing sealed fractures due to drilling and/or core handling. The notation **"a"** is used to define features which have been induced, purely as

the result of artificial breakage during drilling and/or core handling, and are not breaks along pre-existing features. The notation **"n/a"** stands for not applicable.

Fabric lineation and foliation are not included here as natural discontinuities. It should be noted that many of the drilling-induced fractures have developed along such features.

(iv) *"PFF"*
Each discontinuity feature, which on evaluation of its petrographic characteristics is thought to be a *"Potentially Flowing Feature (PFF)"* is indicated on the summary logs (Appendix 2 Tables 1 and 2). Criteria for the recognition of PFFs are discussed in Section 2. An entry of **"Y"** denotes confident identification of a feature as a PFF; an entry of **"?"** denotes uncertain identity as a PFF, either because of uncertainty in the recognition of late-stage mineralisation attributable to recent groundwater circulation, or because it may not be clear that interconnected porosity is associated with the feature.

(v) *"Surface Mineralogy"*
This column lists all the minerals present in fracture fills or lining potential open fracture porosity that were identified by visual examination. It should be noted that, where relevant, an entry of *wall"* (i.e. host wallrock) denotes that an appreciable proportion of the open fracture surface comprise host rock surfaces. A key to abbreviations used in the Appendices is provided in Appendix 2:Table 3.

(vi) *"Comments"*
This column provides a brief narrative description of the feature. Where appropriate, and if possible, a rough estimate of the proportions of surface-lining components is given. Additional information may include description of surface morphological characteristics (including structural or temporal characteristics - e.g. cross-cutting fabrics, slickensides, polishing and crystal morphology).

1.2. Terminology

Terminology used in this report, with respect to "Flow Zones", "non-flowing zones", "Potentially Flowing Features" and "flowing features", is defined below:

"Flow-Zone"
As used in this report, "Flow Zone" or "FZ" refers to a point at which, or an interval within which, groundwater flow into a borehole (or in the Äspö tunnel) has been identified by production testing (e.g. by flowmeter logging, packer tests), or by direct visual observation (in the case of the Äspö tunnel). For the REX Experimental Block boreholes (KA2858A and KA2862A), information on the locations of groundwater inflows was taken from data reported in the SELECT Report (Winberg, 1996).

"Non-flowing zone"
This refers to an interval in a borehole (or in the Äspö tunnel) within which groundwater flow is not detected or observed. Mineralogical/petrographical examination of core from a "non-flowing zone" may still reveal the presence of one or more potential flowing features.

"Flowing feature"
This refers to a single discontinuity or fracture identified in a borehole or in the Äspö tunnel, from which groundwater flow is detected or observed directly.

"Potentially flowing feature"
A "potentially flowing feature" or "PFF" refers to a fracture or other discontinuity which is considered, on the basis of mineralogical and/or petrographical characteristics alone, to be capable of conducting groundwater flow at the present day, i.e. it has natural, connected porosity at the hand specimen scale. A number of key mineralogical and petrographical criteria are used to identify PFFs during core examination, and are defined in Section 1.3.

1.3 Criteria for the recognition of Potential Flowing Features

In identifying open or conductive features, it is necessary to distinguish clearly those which were open in their natural, undisturbed state (i.e. PFFs), and those fractures which have been opened as a result of drilling and core handling (i.e. drilling breaks). A high proportion of the fractures in the two REX Experimental Block boreholes fall into the later category. These discontinuities are usually mineralised along their margins by hairline films of calcite and chlorite which only weakly bonds the opposing wallrock surfaces. Thus, these represent planes of weakness, many of which have been exploited by fracture reactivation and disturbed during drilling and core handling.

It is difficult to distinguish reliably between drilling breaks and natural fractures unless the fracture surface fabrics are very carefully scrutinised. During this study, fracture surfaces were closely examined under a binocular microscope for evidence of their *in-situ* nature.

A combination of petrographical and mineral paragenetic criteria can be used to define features which possess natural porosity. This methodology has been successfully applied to the recognition of PFFs and the characterisation of Flow Zones at the UK Nirex Site at Sellafield, in northwest England (cf. Milodowski et al., 1995; Nirex 1995). Discontinuities were only considered to be PFFs if one or more of the following criteria were met:

(i) *Intact open fractures:*
The best candidate features for PFFs are those fractures which have an undisturbed "gapped" aperture visible to the unaided eye. Some fractures were observed which possess major open porosity with apertures ranging from 1-3 mm, whilst most others were only very narrow fissures with apertures 1 mm. In most cases, the fractures are also vuggy and commonly mineralised by euhedral late-stage calcite (Fe-sulphide - probably pyrite and/or marcasite).

(ii) *Vuggy porosity:*
Veins possessing obvious vuggy porosity were regarded as PFFs. However, a distinction was drawn between veins containing apparently isolated vugs and veins containing vugs which were interconnected (i.e. creating channels along a discontinuity), at least on the

scale of the core hand specimen. Many PFFs are vuggy on a very fine scale which is only evident from careful microscopic observation (see (v) also).

(iii) *Evidence of mineral dissolution:*
Evidence of mineral dissolution and secondary porosity in veins was taken as being indicative of groundwater movement through the discontinuity. Some apparently unmineralised but open and
intact fissures may be a result of dissolution, and typically have "weathered-looking" fracture surfaces, in contrast to the "fresh-looking" surfaces associated with drilling breaks.

Evidence of calcite dissolution and secondary Fe-oxyhydroxide formation has been reported in association with recent groundwater in higher levels of the Äspö workings and boreholes, and in the Redox Site (Tullborg et al.; 1991; Banwart et al., 1992; Tullborg, 1995).

(iv) *Evidence of recent fluid movement:*
Geochemical interaction between groundwater and the host rock lithology may result in the alteration of host rock minerals and of pre-existing minerals, and the precipitation of new phases in equilibrium with the ambient groundwater environment. A PFF might be expected to exhibit evidence of this alteration or neoformation of minerals. Therefore, the presence of the most recent generation of mineralisation can provide a useful indicator of fractures which have been pathways for most recent fluid movements. The use of mineralogical indicators for recent fluid movements requires an understanding of the history of fracture mineralisation and mineral paragenesis. To this end, a mineral paragenesis and fracture history has been previously established by SKB for the Äspö site (cf. Appendix 1). Work by Tullborg and others has indicated that calcite, fine-grained pyrite and/or secondary Fe-oxyhydroxide mineralisation is associated with relatively recent groundwaters. Evidence for the presence of this late-stage mineralisation was sought in the recognition of PFFs in drillcores from the REX Experimental Block boreholes, and in tunnel walls in the REX area.

(v) *Mineral fabrics:*
Well-developed crystal forms with unoccluded crystal termination typifies much of the late-stage calcite mineralisation on fracture surfaces in the REX boreholes, and is clear evidence of mineral growth into open space. The coarser examples of late calcite mineralisation are obviously vuggy, but most of the late calcite in these boreholes is very fine-grained, and its morphological characteristics and associated porosity are only evident under the microscope. This style of mineralisation typifies thin fissure PFFs. In some cases, the late calcite is accompanied by disseminations and dendritic films of fine-grained iron sulphide (probably pyrite or marcasite).

2. Mineralogical Observations

2.1. REX Experimental Block Boreholes

2.1.1. General

The distinction of genuinely open fractures in cores from these boreholes was difficult. Many "apparently open" fracture surfaces were badly abraded due to rolling and milling of opposing core surfaces during drilling and, consequently, surface morphological information that would aid in feature recognition either lost or damaged. Most of the fracture mineralisation is also very fine grained, and evidence for euhedral crystal forms in surface coatings of calcite and pyrite - which indicates crystal growth into open pore space - was usually visible only on microscopic examination of the surface.

Most of the "apparently open" fractures or joints in the drillcores are artifactal, being fractures induced by drilling or core handling along pre-existing chlorite calcite veins. Some drilling breaks are also manifest along foliation fabrics, or small shears or mylonitic features in the host rock. Pre-existing chlorite-calcite veins are mechanically less coherent than the crystalline host rock and represent planes of weakness in the core. Furthermore, chlorite-mineralised features are commonly slickensided and polished as a result of fault movement, which has caused alignment of fine, platy chlorite crystals parallel to the fracture walls. This, coupled with the well-developed basal cleavage of chlorite, imparts a natural "fissility" to these features. Similarly, the foliation within the host rock comprises well-orientated chloritic components, and similarly tends to represent more fissile material. Mineral grains exposed on the surfaces of these drilling breaks characteristically exhibit rough conchoidal fracture surfaces (e.g. on quartz, sulphides) or mineral cleavage surfaces (e.g. on feldspars, chlorite, calcite).

2.1.2. Potential Flowing Features

Mineralogical characteristics

Evidence for the presence of naturally-open fractures (PFFs) was found in both drillcores. For more discussion on PFFs see West et al (1997). All fractures considered to be PFFs have evidence for vuggy porosity (interconnected on the scale of the core hand specimen) lined with euhedral calcite and/or Fe-sulphide mineralisation. The calcite (and in some cases, sulphide) crystals typically display very fine (sub-millimetre) euhedral form. However, it is apparent from the visual core observations (and from Äspö tunnel walls) that there are at least three generations of calcite present:

(i) At least one earlier generation of anhedral (?recrystallised) calcite intimately associated and intergrown with dark green chlorite;

(ii) Coarser anhedral sparry vein fillings which locally are seen to cross-cut, or reactivate, chlorite veins. These are seen to be brecciated, and may be reactivated by fissures which have surfaces lined by (iii);

(iii) Fine grained euhedral calcite crystals grown into open pore space, or developed as euhedral overgrowths on reactivated surfaces of earlier calcite mineralisation.

Only features with the last generation of calcite (iii) are evidence for genuine in situ porosity. The late-stage calcite possesses sub-equant to stubby c-axis elongated scalenohedral and rhombohedral (short "dog-tooth") crystal forms. This clearly indicates that the crystals grew into open pore space. Furthermore, the morphology of the calcite is consistent with that observed in late-stage calcite mineralisation observed from PFFs associated with present-day brackish to moderately saline groundwater salinities (1000-3000 ppm Cl) in UK Nirex Ltd boreholes at Sellafield (Milodowski et al., 1995; Nirex 1995) - similar to the groundwater salinity encountered in KA2858A and KA2862A (Winberg et al., 1995). Unlike the earlier two calcite generations (i and ii), the delicate euhedral fabrics of the late calcite show no evidence of tectonic disturbance (i.e. brecciation or crushing as a result of fracture reactivation). Although confirmation is required from more detailed petrographic analysis, it appears to be the latest mineralisation feature (other than post-tunnelling Fe-oxyhydroxide films and carbonate/gypsum efflorescences which have actively developed on tunnel walls since construction), and there is evidence to suggest that it posts-dates the last fracture movements. Comparison with the mineral paragenesis previously recorded elsewhere at Äspö (cf. Tullborg, 1995 and Section 3.3), indicates that the late calcite, observed in the REX boreholes during this study, belongs to Event 7 (which is inferred to be related to recent groundwaters). In many fractures, the late-stage calcite crystals coalesce to produce almost continuous film-like coatings. In these cases, the porosity is virtually occluded and the feature may no longer be hydraulically conductive - at least locally on the scale of the drillcore.

The sulphide mineralisation showed no obvious signs of in situ oxidation, although some post-coring oxidation (evident from core surface iron staining) has occurred in some cases. Most of the sulphide appears to be fine grained "brassy-coloured" pyrite (FeS_2), but marcasite (FeS_2) may also be present. Rare chalcopyrite ($CuFeS_2$), and a silvery sulphide mineral tentatively identified as arsenopyrite (FeAsS), were observed on some fracture surfaces. Typically the sulphide grains are disseminated and included within the late calcite. In some fractures, the Fe-sulphide forms very fine dendritic films which patchily coat fractured rock surfaces. The edges of the sulphide dendrites have euhedral crystal faces, but this type of growth morphology indicates the presence of only ultrafine, film-like fissure microporosity (Van Straaten, 1978). Minor to trace amounts of sulphide is associated with some earlier chlorite and calcite veins. Fine-grained Fe sulphide (probably pyrite) is commonly present in trace amounts as disseminations in the matrix of the host granodiorite and granite.

The distribution of mineralisation on most PFF surfaces is non-uniform. Late (Event 7) calcite (Fe sulphide) coatings occur in patches in the "lee" of ridge-like irregularities or asperities in the surface. This implies that the porosity is strongly channelled, rather than forming a continuous film or sheet over the fracture surface. This has major implications for the nature of surfaces exposed to groundwater. In most cases, only very small quantities of calcite and/or pyrite coat the surface of PFFs in KA2858A and KA2862A.

Rough estimates made during logging (Appendix 1 and Appendix 2) indicate that calcite covers less than 10%, and pyrite much less than 1%, of the total wallrock surfaces of typical PFFs, with wallrock phases (host rock minerals and or surfaces of pre-existing vein mineralisation (where earlier veins have been reactivated as PFFs) constituting the bulk of the fracture surface. However, if the channelling is taken into account, then calcite coats up to 100% (typically >50%) and pyrite up to 30% (typically 1-5%) of the total surface of the porous channels, with a considerably lower proportion of exposed wallrock surfaces present.

Distribution of PFFs in Borehole KA2858A

A total of 285 "apparently open"(i.e. naturally open + drilling-induced) fractures were recorded from KA2858A. Only 19 fractures (6.7% of the total) are considered to be PFFs (i.e. they exhibit characteristics that indicate genuine in situ porosity associated with recent (Event 7) mineralisation. Eleven of these PFFs (denoted by "?" entries in Appendix 1) appear to have only very minor evidence of porosity and may, therefore, be virtually sealed in situ or only very weakly conducting. All of the remaining "open" fractures are considered be artifactal drilling-induced breaks, developed either along pre-existing veins, or as fresh breaks through the host rock.

Appendix 2:Figure 1 illustrates the distribution of PFFs relative to the distribution of groundwater flow in KA2858A. Most PFFs are concentrated within the first 10 m of the borehole, with a small group of weak or "uncertain PFFs between 21-22 m and a third group of 2 PFFs between 40-45 m. The only measurable groundwater flow in this borehole occurs between 40-40.7 m (Winberg et al., 1995). This corresponds to the third cluster of 2 PFFs, between 40-45 m, of which only the PFF at 40.17 m has been identified as possessing definitive porosity (Figure 3, Appendix 1). This feature belongs to a well-defined set of sub-parallel fractures within this interval, which are reported to have an orientation of N65W dipping 65% to SW (cf. Winberg et al.,1995). This trend is roughly parallel to the one of the main conductive fracture zones in the area, Zone NW-3.

Two possible reasons why no flow has been detected in association with PFFs recorded between 0-22 m are:

(i) The basic visual examination of the cores suggests that many of the PFFs appear to be almost sealed by calcite mineralisation. Therefore, they may no longer be conducting significant or detectable water flows. This is particularly the case between 5-22 m.

(ii) Fractures between 0-5 m are very close to the wall of the Äspö tunnel. This is likely to have a very significant influence on the flow of groundwater, and will act as a sump, causing drainage away from features close to the tunnel wall. Therefore, the PFF distribution may reflect the original distribution of flows in the REX block, prior to tunnel construction.

Distribution of PFFs in Borehole KA2862A

A total of 86 "apparently open"(i.e. naturally open + drilling-induced) fractures were recorded from KA2858A. 21 fractures (24.4% of the total) are considered to be PFFs (i.e. they exhibit characteristics that indicate genuine in situ porosity associated with recent (Event 7) mineralisation. Eight of these PFFs (denoted by "?" entries in Appendix 2) appear to have only very minor evidence of porosity and may, therefore, be virtually sealed in situ or only very weakly conducting. All of the remaining "open" fractures are considered be artifactal drilling-induced breaks, developed either along pre-existing veins, or as fresh breaks through the host rock.

Appendix 2:Figure 2 illustrates the distribution of PFFs relative to the distribution of groundwater flow in KA2862A. The distribution of flow zones within the borehole coincides very closely with thew distribution of PFFs defined from mineralogical logging of fractures. The major flow occurs between 15-15.98 m (borehole terminal point) where there is a well-defined set of close spaced features. These have a N60-70W tend and very steep dips (between 85% to SE and 85% to NE). This is parallel to the conductive feature identified in borehole KA2858A, and could be considered to be the intersection of KA2862A with the margins of the conductive Fracture Zone NW-3 (Appendix 2:Figure 4).

No detectable flows appear to be associated the small number of PFFs between 0-7 m (appendix 2:Figure 4), probably because of their proximity to the tunnel wall (see discussion on KA2858A).

2.2. Comparison with water-bearing structures in the Äspo tunnel

A number of fractures associated with groundwater seeps were observed within the REX alcove. Representative samples of these were taken during this study for later petrographic analysis. Brief visual examination revealed that a number of these flowing features were associated with the typical fine grained, late calcite mineralisation (often resting on chlorite-mineralised surfaces) that characterises PFFs identified in the REX boreholes. In other cases, the seepages occur along chlorite/clay-mineralised fractures, which have little evidence of in situ porosity from brief examination of their surfaces (by binocular microscope). These surfaces are coated by polished and slickensided chlorite or clay minerals. An earlier, more detailed and systematic study of water-bearing features in the Äspö tunnel (Mazurek et al., 1995) also found a strong association between chlorite-mineralised features and groundwater flow. This is in marked contrast with the mineralogical logging observations from the two REX boreholes, which suggests that calcite Fe sulphide mineralisation is characteristic of present-day conductive features. Tullborg et al. (1991) and Banwart et al. (1992) similarly associate chlorite and/or clay mineralisation with flow zones elsewhere in the Äspö site. These authors also identified oxidative secondary Fe-oxyhydroxide mineralisation in near-surface and higher-level flowing features at Aspö, but this appears to be absent in the REX block.

It seems likely that very many of the flowing fractures in the tunnel walls have dilated as a result of the stress-relief and mechanical disturbance during tunnel construction and may not represent flowing features in the undisturbed system. Our limited observations

indicate much less disturbance and dilation of the fractures in the tunnel wall, and fewer groundwater seeps in areas where the tunnel was constructed by boring machine rather than by using explosive blasting. This tends to support the conclusion that many of the flowing features seen in the tunnel wall are related to mechanical disturbance immediately around the tunnel, rather than natural flowing features. This may explain the difference in the mineralogy of PFFs in the REX boreholes, and that of flowing features seen in the tunnel walls.

2.3. Summary and Conclusions

All "Potentially Flowing Features" (PFFs) have been identified from microscopic (binocular microscope) examination of drillcores from the two REX boreholes, KA2858A and KA2862A. Detailed summaries of the mineralogical data are presented for each borehole in Appendix 2:Table 1 and Table 2, respectively. PFFs are naturally open fractures and have been distinguished from artificial fractures, induced by drilling or core handling (i.e. drilling breaks), on the basis of mineralogical and petrographic criteria. This methodology, adopted from previous flow-zone characterisation studies at the UK Nirex Sellafield site, has been successfully used to define PFFs in the REX boreholes at Äspö. The principal criteria are summarised below:

(i) PFFs exhibit evidence of natural *in situ* porosity. This is evident from the preservation of either:

  (a) vuggy cavities;

  (b) surfaces lined by fracture minerals exhibiting euhedral form - which indicates they grew into open pore space. In contrast, the surfaces of drilling breaks are represented by irregular/conchoidal fracture surfaces through mineral grains or along grain boundaries, or by mineral cleavage surfaces, rather than natural crystal faces.

(ii) PFFs display porosity which is interconnected, at least on the scale of the drillcore intersections, and have been differentiated from veins with isolated vuggy porosity (which are not considered as PFFs).

(iii) PFFs have been recognised on the basis that they contain evidence of the latest paragenetic stage (i.e. Event 7 of Tullborg, 1995) mineralisation which is typified by calcite pyrite. Previous SKB studies (e.g. Tullborg et al., 1991; Tullborg, 1995) suggest that this mineralisation may be contemporaneous with present-day or very recent (i.e. Quaternary) groundwaters. Therefore, the presence of the late-stage calcite pyrite (Event 7) mineralisation clearly indicates that the fractures have been hydraulically active in the relatively recent past, and may therefore, be indicative of present day groundwater flow paths.

The PFFs encountered in the REX boreholes were characterised by the presence of calcite, usually accompanied by minor to trace amounts of pyrite (or sulphide minerals). This mineralisation may rest directly on wallrock (granitic or granodioritic) surfaces, comprising host rock minerals (either fresh granite/granodiorite or hydrothermally altered

- i.e. chloritic/epidotic - variants). Less commonly, it may coat the reactivated surfaces of earlier hydrothermal vein mineralisation - typically chlorite veins - reactivated by later fault movement (polished and slickensided surfaces). This differs from previous studies of flowing features in the tunnel walls at Äspö (and our limited observations on the walls of the REX alcove) which are mineralised dominantly by chlorite. It is considered here that the groundwater inflows through the tunnel walls may be occurring along features which were originally sealed, but have been dilated as a result of stress-relief and mechanical damage during tunnel construction.

Close examination of the PFFs in the REX boreholes indicated that flow is probably strongly channelled along asperities or irregularities in the fracture surface. The distribution of mineralisation on these surfaces suggests that although the total fracture surface area may be dominated by host rock minerals, or reactivated surfaces of old chlorite mineralisation, much of the actual ("wetted") surface in contact with groundwater may be dominated by calcite coated with minor to trace amounts of pyrite. However, more detailed petrographic analysis is required to precisely define the mineralogical characteristics of these surfaces.

It was noted, during the logging of the REX boreholes, that pyrite (or other sulphides) was also present in fine grained disseminations in the matrix of the host rocks in the REX block. This may be significant for the evaluation of microbial interactions in the REX programme, as it will be very susceptible to reaction. Its possible presence in the wallrock surfaces of PFFs as well as in fracture fillings may significantly affect redox buffering, and should be taken into account in the design of laboratory simulations and well as in the interpretation of field data.

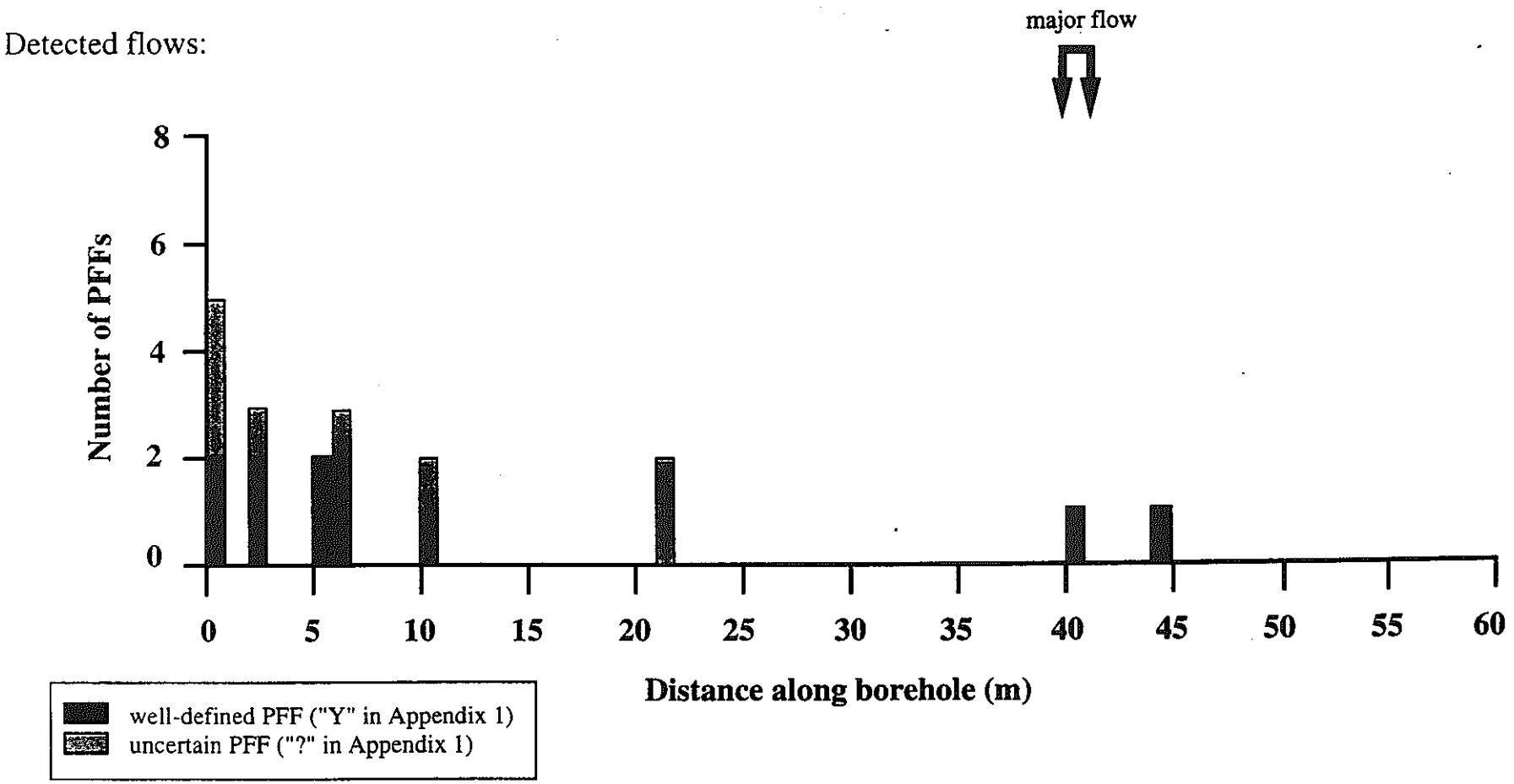

Appendix 2:Figure 1. Distribution of PFFs and flow zones in borehole KA 2858A

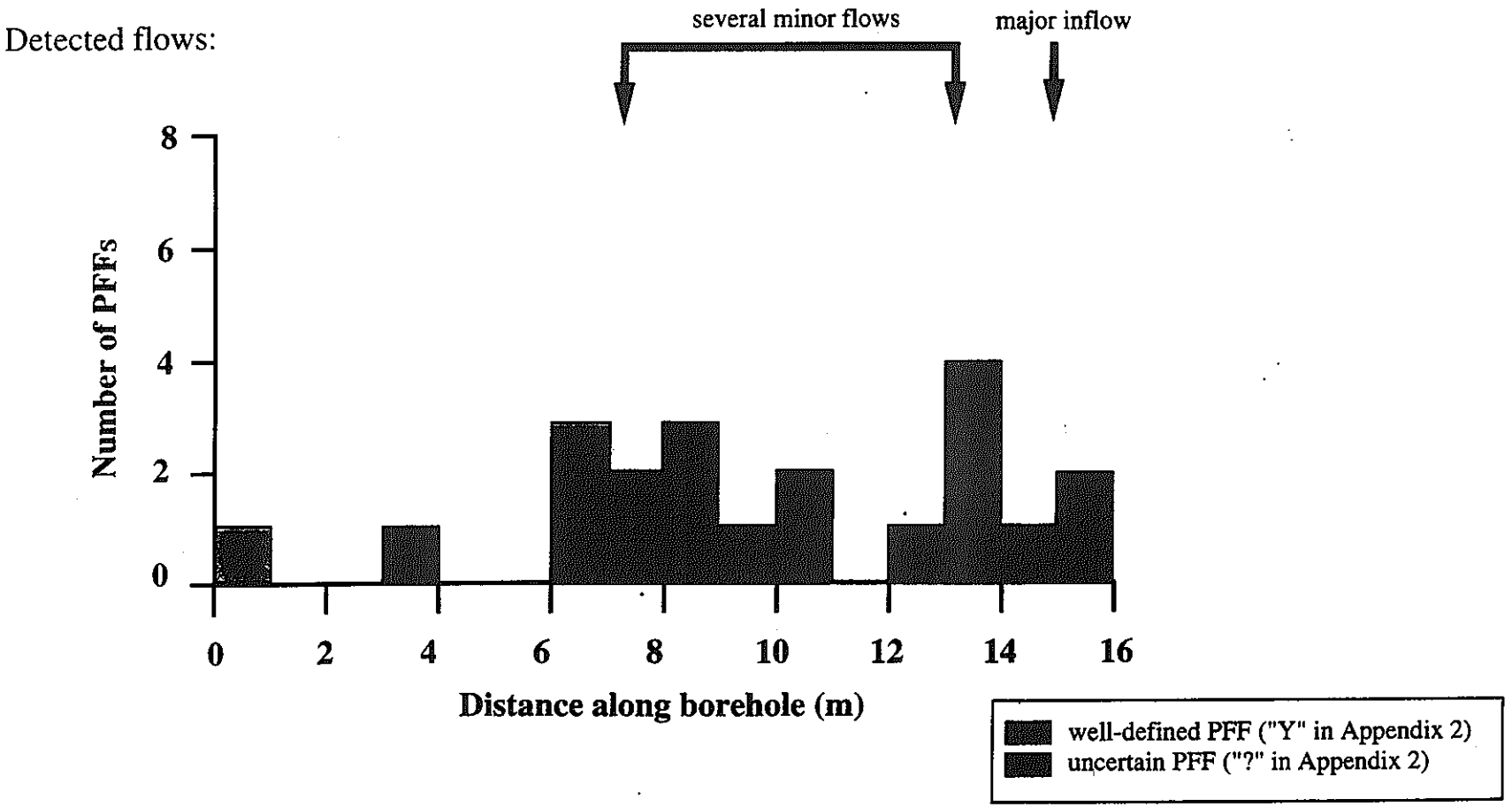

Appendix 2: Figure 2. Distribution of PFFs and flow zones in borehole KA 2862A

Appendix 2 Table 1. Summary mineralogical log of potentially open discontinuities in borehole KA2858A

Distance along core axis (m)	BGS Feature No	Fracture Type	PFF	Surface Mineralogy	Comments
0.00	1	v		?ep, wall	fracture through reactivated pale green ?epidotic film mineralising fresh wallrock marking top of core. Surface polished and slickensided
0.01	2	v	?	cal, wall, Fe-sulp	very fine calcite euhedra, patchy discontinuous coating on mainly fresh wallrock. Traces of euhedral pyrite closely associated with calcite. Very weak PFF, largely drilling break
0.09	3	v	?	cal	traces of euhdral calcite discontinuously coating fresh wallrock. largely drilling break/very weak PFF
0.43	4	v	?	cal, wall	traces of poorly-developed, flattened euhedral calcite resting on fresh wallrock surfaces. possibly only a very weak PFF
0.50	5	v	Y	cal, Fe-sulp, wall	euhedral flattened crystals of calcite resting on slightly "weathered" or abraded wallrock surfaces; trace sulphide in wallrock
0.55	6	a		n/a	drilling break through drilling-induced shatter zone of fresh wallrock
0.63	7	v		cal	rolled surface of drilling induced fracture along incipient hairline calcite vein
0.71	8	v		cal	low-angle drilling break along incipient hairline calcite vein
0.80	9	v	Y	cal, wall	complex: clear, flattened, stubby scalenohedral-subequant euhedra of calcite developed on mainly fresh wallrock surfaces, and on reactivated surfaces of earlier milky calcite vein. Feature parallel to previous steep calcite veins
0.81	10	v		chl	rolled surface of drilling-induced fracture along fine chloritic seam
0.93	11	v		cal, Fe-sulp, wall	drilling break along hairline calcite vein. Minor Fe sulphide present in wallrock

Appendix 2 Table 1. Summary mineralogical log of potentially open discontinuities in borehole KA2858A (continued).

Distance along core axis (m)	BGS Feature No	Fracture Type	PFF	Surface Mineralogy	Comments
1.01	12	v		cal, clay, Fe-sulp, wall	hairline vein of calcite impregnated pale green clay. Traces of Fe sulphide. Drilling break induced along sealed vein in fresh wallrock
1.20	13	a		n/a	drilling break though calcite-impregnated altered wallrock
1.44	14	v		chl, qz, Fe-sulp	drilling break along early chlorite-quartz-pyrite vein. Surfaces reactivated by fault movement, producing slickened and polished surfaces. Traces of Fe sulphide impregnate wallrock
1.58	15	v		cal, chl	drilling break along chloritised shear discontinuity with traces of calcite on surfaces
1.77	16	v		cal	drilling break along hairline calcite vein reactivated with later slickensides along margins
1.85	17	a		n/a	drilling break with rolled core surfaces
2.03	18	a		n/a	drilling break through chloritised wallrock
2.32	19	a		n/a	drilling break
2.61	20	a		n/a	drilling break
2.93	21	v	Y	cal	flattened, euhedral calcite on fresh wallrock. Feldspars are very reddened in host rock. Asperity apertures Š0.5x5mm. "Open" surface = >95% calcite, Š1% pyrite; total fracture surface = 10% calcite <1% pyrite. possibly largely sealed

Appendix 2 Table 1. Summary mineralogical log of potentially open discontinuities in borehole KA2858A (continued).

Distance along core axis (m)	BGS Feature No	Fracture Type	PFF	Surface Mineralogy	Comments
2.94	22	v	Y	cal, Fe-sulp, ?clay	flattened, euhedral calcite on fresh wallrock. Feldspars are very reddened in host rock. Asperity apertures Š0.5x5mm. "Open" surface = >95% calcite, Š1% pyrite; total fracture surface = 10% calcite <1% pyrite. Possibly largely sealed
3.06	23	a		n/a	drilling break cutting steep flourite-chlorite-?epidote vein
3.20	24	v		cal	drilling break along hairline calcite v ein
3.32	25	v	?	cal	discontinuous hairline calcite vein, with fresh wallrock surfaces and fine flattened euhedra of calcite. Probably largely sealed
3.57	26	a		n/a	drilling break through chloritic wallrock
3.63	27	v		cal, ep, chl, qz, cal	drilling break along early calcite-chlorite-?epidote-quartz-silicate vein
3.96	28	a		n/a	drilling break through chloritised wallrock
4.17	29	a		n/a	drilling break along foliated or shear fabric with chloritic surfaces
4.35	30	a		n/a	drilling break along foliated or shear fabric with chloritic surfaces
4.56	31	a		n/a	drilling break along foliated or shear fabric with chloritic surfaces
4.69	32	a		n/a	irregular drilling break through chloritised wallrock
4.75	33	a		n/a	drilling break through chloritised wallrock
4.87	34	a		n/a	drilling break along foliated or shear fabric with chloritic surfaces
4.99	35	a		n/a	drilling break along foliated or shear fabric with chloritic surfaces
n/a	36	n/a		n/a	n/a
5.18	37	a		n/a	drilling break along foliated or shear fabric with chloritic surfaces
5.30	38	a		n/a	drilling break along foliated or shear fabric with chloritic surfaces

Appendix 2 Table 1. Summary mineralogical log of potentially open discontinuities in borehole KA2858A (continued).

Distance along core axis (m)	BGS Feature No	Fracture Type	PFF	Surface Mineralogy	Comments
5.48	39	v	Y	cal, Fe-sulp	fine, clear, subequant to stubby scalenohedra of calcite, + fine Fe sulphide line well-developed porosity. Orientation of PFF is very similar that of features 21 and 22. Calcite covers >99% of open asperity surfaces
5.50	40	v	Y	cal, Fe-sulp	fine, clear, subequant to stubby scalenohedra of calcite, + fine Fe sulphide line well-developed porosity. Orientation of PFF is very similar that of features 21 and 22. Calcite covers >99% of open asperity surfaces
5.51	41	a		n/a	drilling break along epidotic shear fabric in chloritic and epidotic host rock
5.73	42	a		n/a	drilling break through chloritised and silicified granodiorite
5.78	43	a		n/a	drilling break exploiting foliated or sheared fabric of chloritised wallrock
5.83	44	v		chl	drilling break along hairline chloritic feature in chloritised wallrock
5.88	45	v		chl	drilling break along hairline chloritic feature in chloritised wallrock
5.90	46	a		n/a	drilling break
5.90	47	a		n/a	drilling break exploits chloritised fabric
5.91	48	a		n/a	drilling brealk; rolled core surface
6.15	49	v		chl	drilling break exploiting chloritic shear
6.21	50	a		n/a	drilling break
6.36	51	v		qz, hem	hematite-impregnated quartz vein with very fine, isolated vugs
6.37	52	v		qz, hem	hematite impregnated with quartz

Appendix 2 Table 1. Summary mineralogical log of potentially open discontinuities in borehole KA2858A (continued).

Distance along core axis (m)	BGS Feature No	Fracture Type	PFF	Surface Mineralogy	Comments
6.30-6.57				cal	zone of fine stockwork of hairline calcite veins
6.64	53	v		qz, chl	drilling break along reactivated quartz-chlorite mineralised shear
6.67	54	v	Y	cal, Fe-sulp	intact porous vein with clear euhedrally-terminated calcite cross-cutting earlier milky-white calcite vein fill. Gapped with aperture Š0.5mmxŠ20mm. Clearly related to feature 55. "Open surfaces" = 95% calcite, 1-3% pyrite
6.76	55	v	?	cal, Fe-sulp, chl, hem, qz, wall	equant to stubby scalenohedral calcite crystals coalesing to form discontinuous microvuggy film on reactivated surfacec of earlier hematite-silicate vein. Probably largely sealed with surfaces = >95% calcite, 1-3% pyrite
6.82	56	v	?	cal, Fe-sulp, wall, qzt	equant to stubby scalenohedral calcite crystals coalesing to form discontinuous microvuggy film on reactivated surfacec of earlier hematite-silicate vein. Probably largely sealed with surfaces = >95% calcite, 1-3% pyrite
6.95	57	v		n/a	drilling break
7.06	58	a		n/.a	drilling break in sheared, ?silicified host rock
7.14	59	a		n/.a	drilling break in sheared, ?silicified host rock
7.24	60	a		n/.a	drilling break in sheared, ?silicified host rock
7.47	61	a		n/.a	drilling break in sheared, ?silicified host rock
7.50	62	v		cal	
7.59	63	v		cal, Fe-sulp wall	drilling break along hairline vein
7.71	64	a		n/a	drilling break exploiting shear fabric
7.99	65	a		n/a	drilling break through chloritised host rock

Appendix 2 Table 1. Summary mineralogical log of potentially open discontinuities in borehole KA2858A (continued).

Distance along core axis (m)	BGS Feature No	Fracture Type	PFF	Surface Mineralogy	Comments
8.11	66	v		cal	drilling break expoliting early sheared calcite vein. Fe sulphide present in host rock
8.27	67	a		n/a	drilling break through chloritised host rock
8.37	68	v		py, cal	clear (late-type) calcite with fine pyrite, similar to that seen in other PFFs but not obviously developed good crystal form, and therefore possibly now sealed
8.50	69	v		chl	drilling break expoliting sheared hairline chlorite vein
8.59	70	a		n/a	drilling break along chloritic fabric
8.76	71	v		cal	drilling break along incipient hairline calcite vein
8.88	72	a		n/a	drilling break through chloritised wallrock
9.09	73	v		cal, sulp	drilling break along sealed calcite vein with traces of sulphide
9.09	74	a		n/a	drilling break
9.17	75	v		chl	drilling break along chlorite vein
9.21	76	a		n/a	drilling break
9.54	77	a		n/a	drilling break
9.65	78	v		chl-silicates	drilling break partly along early chlorite-silicate vein
9.79	79	a		n/a	drilling break
9.97	80	v		chl, cal	drilling break along early chlorite vein with minor calcite
10.01	81	a		n/a	drilling break
10.13	82	a		n/a	drilling break
10.22	83	a		n/a	drilling break

Appendix 2 Table 1. Summary mineralogical log of potentially open discontinuities in borehole KA2858A (continued).

Distance along core axis (m)	BGS Feature No	Fracture Type	PFF	Surface Mineralogy	Comments
10.37	84	a		n/a	drilling break
10.44	85	v	?	cal, Fe-sulp, wall	chloritised wallrock surfaces with discontinuous coating of flattened fine clear calcite and traces of very fine Fe sulphide, possibly virtually sealed by calcite. Surfaces >80% calcite
10.48	86	v		chl	drilling break along chlorite vein
10.53	87	a		n/a	drilling break
10.58	88	v	?	cal, Fe-sulp, wall	flattened euhedral clear calcite film + traces of Fe sulphide coat reactivated surfaces of earlier fine white calcite veining. probably largely sealed
10.64	89	v		chl	drilling break through chlorite seam
11.01	90	v		chl	drilling break through chlorite seam
11.15	91	v		chl	drilling break through chlorite seam
11.22	92	a		n/a	drilling break
11.37	93	v		chl	drilling break through chlorite seam
11.46	94	v		chl	drilling break through chlorite seam
11.55	95	a		n/a	drilling break through white granodiorite
11.60	96	a		n/a	drilling break through white granodiorite
11.74	97	v		chl	drilling break through chlorite seam
11.84	98	v		chl	drilling break through chlorite seam
11.86	99	v		chl	drilling break through chlorite seam
11.89	100	a		n/a	drilling break through slightly chloritised granodiorite
11.96	101	a		n/a	drilling break through slightly chloritised granodiorite

Appendix 2 Table 1. Summary mineralogical log of potentially open discontinuities in borehole KA2858A (continued).

Distance along core axis (m)	BGS Feature No	Fracture Type	PFF	Surface Mineralogy	Comments
12.01	102	v		chl	drilling break through chlorite seam
12.12	103	v		chl	drilling break through chlorite seam
12.19	104	v		chl	drilling break through chlorite seam
12.34	105	v		chl	drilling break through chlorite seam
12.35	106	v		chl	drilling break through chlorite seam
12.49	107	v		chl	drilling break through chlorite seam
12.54	108	a		n/a	drilling break through fresh granodiorite
12.55	109	a		n/a	drilling break through fresh granodiorite
12.56	110	a		n/a	drilling break through fresh granodiorite
12.57	111	a		n/a	drilling break through fresh granodiorite
12.58	112	a		n/a	drilling break through fresh granodiorite
12.59	113	a		n/a	drilling break through fresh granodiorite
12.60	114	v		chl	drilling break through chlorite seam
12.64	115	v		chl	drilling break through chlorite seam
12.67	116	v		chl	drilling break through chlorite seam
12.72	117	a		n/a	drilling break through fresh granodiorite with core "disking"
12.73	118	a		n/a	drilling break through fresh granodiorite with core "disking"
12.74	119	a		n/a	drilling break through fresh granodiorite with core "disking"
12.75	120	a		n/a	drilling break through fresh granodiorite with core "disking"
12.76	121	a		n/a	drilling break through fresh granodiorite with core "disking"
12.83	122	a		n/a	drilling break through fresh granodiorite with core "disking"
12.84	123	a		n/a	drilling break through fresh granodiorite with core "disking"

Appendix 2 Table 1. Summary mineralogical log of potentially open discontinuities in borehole KA2858A (continued).

Distance along core axis (m)	BGS Feature No	Fracture Type	PFF	Surface Mineralogy	Comments
12.85	124	a		n/a	drilling break through fresh granodiorite with core "disking"
12.96	125	a		n/a	drilling break through fresh granodiorite
13.04	126	a		n/a	drilling break through fresh granodiorite
13.20	127	a		n/a	drilling break through fresh granodiorite
13.39	128	a		n/a	drilling break through fresh granodiorite
13.47	129	a		n/a	drilling break through fresh granodiorite
13.65	130	a		n/a	drilling break through fresh granodiorite
14.06	131	a		n/a	drilling break through fresh granodiorite
14.20	132	a		n/a	drilling break through fresh granodiorite
14.60	132A	a		n/a	drilling break through fresh granodiorite
14.68	133	a		n/a	drilling break through fresh granodiorite
14.86	134	a		n/a	drilling break through fresh granodiorite
15.50	134A	a		n/a	drilling break through fresh granodiorite
15.70	135	a		n/a	drilling break through fresh granodiorite
15.90	136	a		n/a	drilling break through fresh granodiorite
16.06	137	a		n/a	drilling break through fresh granodiorite
16.44	138	a		n/a	drilling break through fresh granodiorite
16.70	139	a		n/a	drilling break through fresh granodiorite
16.84	140	a		n/a	drilling break through fresh granodiorite
16.90	141	a		n/a	drilling break through fresh granodiorite
17.93	142	a		n/a	drilling break through fresh granodiorite
18.65	143	v		chl, cal	drilling break through chlorite-calcite vein

Appendix 2 Table 1. Summary mineralogical log of potentially open discontinuities in borehole KA2858A (continued).

Distance along core axis (m)	BGS Feature No	Fracture Type	PFF	Surface Mineralogy	Comments
19.04	144	a		n/a	drilling break through chloritised granodiorite
19.17	145	a		n/a	drilling break through chloritised granodiorite
19.21	146	v		chl	drilling break through chloritised granodiorite along chlorite veinlet
19.54	147	a		n/a	drilling break through chloritised granodiorite
19.87	148	v		chl	drilling break along chlorite veinlet
20.21	149	a		n/a	drilling break through chloritised granodiorite
20.66	150	a		n/a	drilling break through chloritised granodiorite
21.17	151	v		chl	drilling break along chlorite veinlet
21.38	152	a		n/a	drilling break through chloritised granodiorite
21.38	153	v	?	cal, Fe-sulp, wall	steep fracture with trace of very fine, clear, stubby scalenohedral calcite + trace very fine pyrite on fresh chloritised granodiorite surfaces. probably largely sealed
21.46	154	v	?	cal, Fe-sulph, wall	possibly now sealed
21.51	155	a		n/a	drilling break through chloritised granodiorite
21.51	156	v		wall	incipent fracture, parallel to features 153 & 154
21.63	157	a		n/a	drilling break through chloritised granodiorite
21.76	158	v		cal	drilling break through hairline vein
22.48	159	a		n/a	drilling break through fresh granodioritic wallrock; trace calcite and Fe-sulphide in host rock
22.73	160	a		n/a	drilling break through fresh granodioritic wallrock; trace calcite and Fe-sulphide in host rock

Appendix 2 Table 1. Summary mineralogical log of potentially open discontinuities in borehole KA2858A (continued).

Distance along core axis (m)	BGS Feature No	Fracture Type	PFF	Surface Mineralogy	Comments
22.80	161	a		n/a	drilling break through fresh granodioritic wallrock; trace calcite and Fe-sulphide in host rock
23.05	162	a		n/a	drilling break through fresh granodioritic wallrock; trace calcite and Fe-sulphide in host rock
23.34	163	a		n/a	drilling break through fresh granodioritic wallrock; trace calcite and Fe-sulphide in host rock
23.65	164	a		n/a	drilling break through fresh granodioritic wallrock; trace calcite and Fe-sulphide in host rock
23.74	165	a		n/a	drilling break through fresh, dark granodioritic wallrock
23.88	166	a		n/a	drilling break through fresh, dark granodioritic wallrock
24.01	167	a		n/a	drilling break through chloritised granodioritic wallrock marking facies boundary
24.33	168	v		clay, chl	drilling break along hairline chlorite seam with traces of later ?clay
24.71	169	a		n/a	drilling break through fresh granodiorite wallrock
25.03	170	a		n/a	drilling break through fresh granodiorite wallrock
25.17	171	v		chl	drilling break partly along chlorite seam
25.73	172	v		chl	drilling break partly along chlorite seam
25.87	173	a		n/a	drilling break through fresh granodiorite wallrock
25.94	174	v		cal, chl, ep	traces of very fine, possibly late calcite on reactivated surfaces of earlier chlorite-epidote mineralisation. Drilling break along sealed vein
26.20	175	a		n/a	drilling break through fresh granodiorite wallrock

Appendix 2 Table 1. Summary mineralogical log of potentially open discontinuities in borehole KA2858A (continued).

Distance along core axis (m)	BGS Feature No	Fracture Type	PFF	Surface Mineralogy	Comments
26.31	176	a		n/a	drilling break through fresh granodiorite wallrock
26.46	177	a		n/a	drilling break through fresh granodiorite wallrock
27.03	178	a		n/a	drilling break through fresh granodiorite wallrock
27.14	179	a		n/a	drilling break through fresh granodiorite wallrock
27.91	180	a		n/a	drilling break through fresh granodiorite wallrock
28.22	181	a		n/a	drilling break through fresh granodiorite wallrock
29.09	182	a		n/a	drilling break through fresh granodiorite wallrock
29.27	183	a		n/a	drilling break through fresh granodiorite wallrock
29.39	184	a		n/a	drilling break through fresh granodiorite wallrock
29.49	185	a		n/a	drilling break through fresh granodiorite wallrock
30.47	186	a		n/a	drilling break through fresh granodiorite wallrock
30.56	187	a		n/a	drilling break through partly chloritised granodiorite wallrock, associated with a zone of intact calcite veinlets
30.61	188	v		cal, wall	drilling break along hairline calcite vein
30.72	189	v		cal	drilling break along hairline calcite vein
31.36	190	a		n/a	drilling break through fresh granodiorite wallrock
31.61	191	a		n/a	drilling break through calcite-impregnated granodiorite wallrock
31.81	192	v		chl	drilling break along chlorite seam
31.89	193	v		chl	drilling break along chlorite seam marking top of lithology change
32.24	194	v		chl	drilling break along chlorite seam
32.66	195	a		n/a	drilling break through fresh granodiorite wallrock
32.78	196	a		n/a	drilling break through fresh granodiorite wallrock

Appendix 2 Table 1. Summary mineralogical log of potentially open discontinuities in borehole KA2858A (continued).

Distance along core axis (m)	BGS Feature No	Fracture Type	PFF	Surface Mineralogy	Comments
32.85-33.75		?a		wall	zone of apparently unmineralised, intact, very fine hairline fissures possibly as a result of stress release associated with coring
33.60	197	a		n/a	drilling break through fresh granodiorite wallrock
33.60	198	a		n/a	drilling break through fresh granodiorite wallrock; traces of sulphide disseminated in host rock
33.91	199	a		n/a	drilling break through fresh granodiorite wallrock
34.60	200	v		chl, cal, Fe-sulp	drilling break along reactivated and polished chlorite seam
34.86	201	a		n/a	drilling break through fresh granodiorite wallrock
35.00	202	a		n/a	drilling break through fresh granodiorite wallrock
35.53	203	a		n/a	drilling break through fresh granodiorite wallrock
35.65	204	a		n/a	drilling break through fresh granodiorite wallrock
35.80	205	a		n/a	drilling break through fresh granodiorite wallrock; marks facies change
36.16	206	a		n/a	drilling break through fresh granodiorite wallrock
36.61	207	v		cal	largely drilling break through fresh granodiorite wallrock
36.61	208	v		chl	drilling break through chlorite seam
37.29	209	a		n/a	drilling break through fresh granodiorite wallrock
38.04	210	a		n/a	drilling break through fresh granodiorite wallrock
38.40	211	a		n/a	drilling break through fresh granodiorite wallrock
38.55	212	a		n/a	drilling break through fresh granodiorite wallrock
39.53	213	a		n/a	drilling break through fresh granodiorite wallrock

Appendix 2 Table 1. Summary mineralogical log of potentially open discontinuities in borehole KA2858A (continued).

Distance along core axis (m)	BGS Feature No	Fracture Type	PFF	Surface Mineralogy	Comments
40.17	214	v	Y	cal, Fe-sulp, chl, ?clay, wall	flattened, clear, euhedral late calcite encloses Fe sulphide on wallrock surfaces. Surfaces 10-15% calcite, trace Fe sulphide
40.72	215	a		n/a	drilling break through fresh granodiorite wallrock
41.07	216	a		n/a	drilling break through fresh granodiorite wallrock
41.26	217	v		cal, Fe-sulp	Traces of euhedral Fe sulphide (pyrite) and extremely fine calcite on wallrock surfaces - no good calcite morphology seen and appears to be drdilling break along sealed vein
41.26	218	a		n/a	drilling break through incipient healed joint in fresh granodiorite wallrock
41.61	219	a		n/a	drilling break through fresh granodiorite wallrock
41.80	220	a		n/a	drilling break through fresh granodiorite wallrock
42.59	221	a		n/a	drilling break through fresh granodiorite wallrock
42.98	222	a		n/a	drilling break through fresh granodiorite wallrock
43.23	223	a		n/a	drilling break through fresh granodiorite wallrock
43.60	224	a		n/a	drilling break through fresh granodiorite wallrock
43.85	225	a		n/a	drilling break through fresh granodiorite wallrock
44.03	226	v	?	cal, chl, ?hem, Fe-sulp	microvugs with euhedral calcite in feature with typical orientation (N65W, 70SW); in red-green wallrock; probably sealed or only very weak PFF
44.08	227	a		n/a	drilling break through fresh granodiorite wallrock
44.14	228			chpy, cal	drilling break along fracture with traces of calcite and traces of dendritic chalcopyrite

Appendix 2 Table 1. Summary mineralogical log of potentially open discontinuities in borehole KA2858A (continued).

Distance along core axis (m)	BGS Feature No	Fracture Type	PFF	Surface Mineralogy	Comments
44.39	229	a		n/a	drilling break through fresh granodiorite wallrock
44.42	230	a		n/a	drilling break through fresh granodiorite wallrock
44.57	231	a		n/a	drilling break through fresh granodiorite wallrock
44.87	232	v		cal, Fe-sulp	weak PFF with traces of very fine late calcite and Fe-sulphide
44.89	233	a		n/a	drilling break through fresh granodiorite wallrock
44.93	234	a		n/a	drilling break through fresh granodiorite wallrock
45.20	235	a		n/a	drilling break through fresh granodiorite wallrock
45.30	236	v		chl, ep, ?Fe-sulp	drilling break along early chlorite-epidote seam
46.20	237	v		chl, ep, ?Fe-sulp	drilling break along early chlorite-epidote seam
46.35	238	a		n/a	drilling break through fresh granodiorite wallrock
47.20	239	a		n/a	drilling break through fresh granodiorite wallrock
47.28	240	a		n/a	drilling break through fresh granodiorite wallrock
47.32	241	a		n/a	drilling break through fresh granodiorite wallrock
47.43	242	a		n/a	drilling break through fresh granodiorite wallrock
47.60	243	a		n/a	drilling break through fresh granodiorite wallrock
48.27	244	v		cal, chl, Fe-sulp	drilling break following late calcite (+trace Fe sulphide) mineralisation reactivating early chlorite seam
48.46	245	v		chl, ep, ?Fe-sulp	drilling break along early chlorite-epidote seam
48.51	246	a		n/a	drilling break through fresh granodiorite wallrock
48.60	247	a		n/a	drilling break through fresh granodiorite wallrock
48.85	248	a		n/a	drilling break through fresh granodiorite wallrock
49.04	249	a		n/a	drilling break through fresh granodiorite wallrock

Appendix 2 Table 1. Summary mineralogical log of potentially open discontinuities in borehole KA2858A (continued).

Distance along core axis (m)	BGS Feature No	Fracture Type	PFF	Surface Mineralogy	Comments
49.12	250	a		n/a	drilling break through fresh granodiorite wallrock
49.14	251	a		n/a	drilling break through fresh granodiorite wallrock
49.24	252	a		n/a	drilling break through fresh granodiorite wallrock
49.35	253	a		n/a	drilling break through fresh granodiorite wallrock
49.62	254	a		n/a	drilling break through fresh granodiorite wallrock
50.50	255	a		n/a	drilling break through fresh granodiorite wallrock
50.61	256	a		n/a	drilling break through fresh granodiorite wallrock
50.77	257	a		n/a	drilling break through fresh granodiorite wallrock
51.93	258	a		n/a	drilling break through fresh granodiorite wallrock
53.09	259	a		n/a	drilling break through fresh granodiorite wallrock
53.31	260	a		n/a	drilling break through fresh granodiorite wallrock
53.44	261	a		n/a	drilling break through fresh granodiorite wallrock
53.62	262	a		n/a	drilling break through fresh granodiorite wallrock
53.94	263	a		n/a	drilling break through fresh granodiorite wallrock
54.09	264	a		n/a	drilling break through fresh granodiorite wallrock
54.23	265	a		n/a	drilling break through fresh granodiorite wallrock
54.28	266	a		n/a	drilling break through fresh granodiorite wallrock
55.39	267	a		n/a	drilling break through fresh granodiorite wallrock
55.78	268	v		chl	drilling break along chlorite seam/rock fabric
56.46	269	a		n/a	drilling break through fresh granodiorite wallrock
56.55	270	a		n/a	drilling break through fresh granodiorite wallrock
56.67	271	a		n/a	drilling break through fresh granodiorite wallrock

Appendix 2 Table 1. Summary mineralogical log of potentially open discontinuities in borehole KA2858A (continued).

Distance along core axis (m)	BGS Feature No	Fracture Type	PFF	Surface Mineralogy	Comments
57.60	272	v		cal, wall	drilling break along hairline calcite vein
58.55	273	a		n/a	drilling break through fresh granodiorite wallrock
58.77	274	v		chl	drilling break along chlorite seam/rock fabric; Fe sulphide in wallrock
58.84	275	a		n/a	drilling break through fresh granodiorite wallrock
58.97	276	a		n/a	drilling break through fresh granodiorite wallrock
59.07	277	a		n/a	drilling break through fresh granodiorite wallrock
59.29	278	a		n/a	drilling break through fresh granodiorite wallrock
59.33	279	v		hem, chl, ?clay, ?dol	drilling break along sealed vein, possibly containing hematitised dolomite
59.40	280	a		n/a	drilling break through fresh granodiorite wallrock
59.50	281	a		n/a	drilling break through fresh granodiorite wallrock
59.54	282	a		n/a	drilling break through fresh granodiorite wallrock
59.62	283	a		n/a	drilling break through fresh granodiorite wallrock

Appendix 2: Table 2. Summary mineralogical log of potentially open discontinuities in borehole KA2862A

Distance along core axis (m)	BGS Feature No	Fracture Type	PFF	Surface Mineralogy	Comments
0.00	1	a		n/a	rolled core surface
0.17	2	a		n/a	rolled core surface
0.29	3	v	?	cal, Fe-sulp, ?chl	very thin (<0.2mm) discontinuous film of mineralisation on fresh wallrock surfaces; Fe-sulphide appears to have partly oxidised to Fe oxyhydroxides post-drilling
1.14	4	v		cal, chl, Fe-sulp, wall	discontinuous very thin (<0.2mm) coating of calcite on reactivatated (sheared chlorite) mineralised surfaces of granodiorite; exposed surface exposed is 89% chlorite,10% calcite, 1% Fe-sulphide (probably pyrite)
1.36	5	v		chl, wall	reactivated early chlorite vein with polished and slickensided chloritic surfaces
1.36	6	v		Fe-sulp, cal, wall	drilling break along hairline vein; probably largely sealed except for isolated calcite-lined microvugs; some vugs carry fine euhedral Fe-sulphide
1.91	7	v		cal, chl, Fe-sulp	thin (<0.2mm) film of calcite on sheared chlorite surfaces, with traces of Fe-sulphide; granodiorite wallrock is epidotised; calcite probably relatively recent by probably seals fracture. 89% chlorite, 10% calcite, <1% pyrite
1.98	8	v		cal, Fe-sulp, wall	drilling break along thin, discontinuous film of clear calcite coat stepped, fresh fracture surface of wallrock; wallrock contains traces of fine fresh pyrite cubes
2.51	9	v		cal	drilling break along thin calcite vein

Appendix 2: Table 2. Summary mineralogical log of potentially open discontinuities in borehole KA2862A (continued)

Distance along core axis (m)	BGS Feature No	Fracture Type	PFF	Surface Mineralogy	Comments
2.94	10	v		chl, cal	drilling break along reactivated thin chlorite vein with traces of calcite; slickensided and polished surfaces
3.17	11	a		n/a	drilling break
3.79	12	v		cal, Fe-sulp	traces of very fine calcite and Fe-sulphide on largely fresh wallrock surfaces; no evidence of openess
3.93	13	v	Y	cal, Fe-sulp, wall	Euhedral calcite on open pore surfaces. Overall surface is >90% fresh granodiorite and <10% calcite. However, calcite distribution indicates channelled flow in asperities with surfaces >99% calcite, 1% pyrite, <1% wallrock
4.06	14	v		wall, ep, Fe-sulp, cal, ?arsenpyr	fresh wallrock surfaces with minor epidote, fresh Fe-sulphide, traces of calcite and possible traces of arsenopyrite. Mineralisation similar to feature 13 but apparently drilling break along sealed vein
4.29	15	a		n/a	drilling break
4.41	16	v		cal	probable sealed hairline vein disturbed by drilling; fresh wallrock with scattered microvugs in wallrock matrix
4.59	17	v		cal	drilling break along very thin, discontinuous hairline calcite vein; mainly wallrock surfaces
4.90	18	v		chl, Fe-sulp, ?zeol, myl	drilling break along thin healed mylonitic seam containing chlorite and traces of pyrite and possible zeolite
5.23	19	v		cal, Fe-sulp, wall	drilling break along original vein; irregular broken surfaces
5.41	20	a		n/a	drilling break
5.70	21	a		n/a	rolled core surfaces
5.78	22	a		n/a	drilling break through ? pegmatite vein containing pyrite

Appendix 2: Table 2. Summary mineralogical log of potentially open discontinuities in borehole KA2862A (continued

Distance along core axis (m)	BGS Feature No	Fracture Type	PFF	Surface Mineralogy	Comments
5.88	23	a		n/a	drilling break through old shear-zone; fresh wallrock
6.50	24	v	?	cal, wall	fresh wallrock surfaces to fracture with traces of very fine calcite; morphology and porosity attributes unclear
6.65	25	v		cal, Fe-sulp, wall	reactivated hairline vein comprising mainly fresh wallrock surfaces with minor calcite and traces of Fe sulphide (pyrite); probably sealed
6.82	26	v		wall, cal	mainly fresh wallrock with traces of calcite forming patchy coating
6.87	27	v	Y	cal, Fe-sulp	microvuggy calcite vein with stubby (Š0.5mm) clear, scalenohedral calcite on reactivated margin of silicate vein. Scattered and dendritic pyrite (<0.1mm) in fissured wallrock feldspar. >95% wallrock, 1-5% calcite, Š1% pyrite
6.90	28	v	?	cal, Fe-sulp, wall, ?ep	discontinuous vein containing traces of calcite, Fe-sulphide and traces of earlier ? epidote. Probably sealed or only very weak PFF
7.10	29	a		n/a	drilling break
7.25	30	v	Y	cal, Fe-sulp, wall	clear, fine equant to stubby scalenohedral calcite enclosing euhedral pyrite. Overall surface Š10% calcite, 80% wallrock, <1% pyrite. Distribution indicates channelled flow in pod-like asperities Š3mm wide with surfaces 95-99% calcite, 1-5% pyrite
7.27	31	v	?	Fe-sulp, cal, wall	fresh dendritic Fe-sulphide, intimately associated with, and ?post-dating very minor calcite. Most fracture surfaces comprise wallrock. Probably largely sealed or only weak PFF
7.37	32	a		n/a	drilling break
7.61	33	a		n/a	drilling break

Appendix 2: Table 2. Summary mineralogical log of potentially open discontinuities in borehole KA2862A (continued

Distance along core axis (m)	BGS Feature No	Fracture Type	PFF	Surface Mineralogy	Comments
7.68	34	v		cal, Fe-sulp, wall	reactivated fracture along major calcite vein filling and wallrock, probably drilling induced. Major calcite, trace scattered Fe sulphide
6.50-7.51		v		ep-qz	altered and reddened zone associated with many finely-anastomosing, sealed, thin epidote-silicate veins. The zone is sharply defined at the top but grades into background host rock at base
7.78	35	v		cal, Fe-sulp, wall	
8.09	36	v		cal, wall	
8.70	37	a		n/a	drilling break
8.80	38	v	Y	cal, Fe-sulp, wall	thin patchy coating of flattened, scalenohedral calcite and dendritic pyrite film with euhedral edges. . Overall surface 10-15% calcite, 1-5% pyrite, up 89% wallrock. Channelled porosity in asperities up to 10x0.05m; surfaces 70-95% calcite, 5-30% pyrite.
8.85	39	v	Y	cal, wall	rolled fracture surface due to drilling but evidence of porosity in thin discontinuous vein of calcite with flattened euhedral crystals; surface Š40% calcite, 60% fresh wallrock
8.88	40	v	Y	cal, Fe-sulp	porous fracture, calcite with flattened crystal forms and traces of pyrite. Surfaces 70% calcite, Š30% wallrock, trace pyrite
9.03	41	v		cal, clay	fracture through very thin clay film, impregnated by calcite, resting on wallrock surfaces
9.04	42	v		cal, ?clay, wall	
9.23	43	v		cal, wall	discontinuous v.thin vein with calcite resting on fresh wallrock surfaces. Probably sealed in situ but now opened by drilling

Appendix 2: Table 2. Summary mineralogical log of potentially open discontinuities in borehole KA2862A (continued

Distance along core axis (m)	BGS Feature No	Fracture Type	PFF	Surface Mineralogy	Comments
9.44	44	a		n/a	drilling break
9.51	45	v		cal, Fe-sulp, other	fracture through major calcite vein with trace Fe-sulphide and other unidentified metallic mineral mineral
9.75	46	v	?	cal	thin film of calcite; 50% of surface is wallrock
9.83	47	a		n/a	drilling break
10.00	48	v	Y	cal, Fe-sulp, wall	reactivated earlier ?chlorite vein; v. fine, flattened stubby scalenohedral-subequant, calcite crystals (Š10%) and dendritic, fine, pyrite (<1%) on chloritised and reddened wallrock (90%). Channel asperities with >60% calcite, >5% pyrite
10.17	49	a		n/a	drilling break marking top of zone of shearing with many c.1mm epidotic shear planes. Top of reddened host rock zone
10.28	50	v		cal, chl, Fe-sulp, hem, other	break along sheared and slickensided chlorite vein which has been reactivated by later calcite vein. Traces of Fe sulphide and an unidentified silvery metallic mineral
10.38	51	a		n/a	drilling break partially through earlier epidotic shear feature
10.60	52	v		cal, chl, wall	conjugate to 53. Trace of calcite along mainly sheared and chloritised wallrock
10.60	53	v	?	cal, wall	conjugate feature to 53. Possible but unclear euhedral faces to patchy calcite coating on wallrock
10.69	54	v		cal, wall	trace of calcite veining in chloritised wallrock
10.75	55	a		n/a	drilling break through chloritised wallrock
10.81	56	a		n/a	drilling break

Appendix 2: Table 2. Summary mineralogical log of potentially open discontinuities in borehole KA2862A (continued

Distance along core axis (m)	BGS Feature No	Fracture Type	PFF	Surface Mineralogy	Comments
10.86	57	v		chl, cal	trace of calcite along channelled surfaces in reactivated earlier chlorite vein. Probably sealed in situ but disturbed by drilling
10.92	58	v		chl	polished chlorite surfaces
11.06	59	v		cal, chl	trace of calcite veining on chloritised wallrock surfaces, probably sealed in situ
11.77	60	v		cal, chl, feld, hem, ?ep or preh	hematised feldspar in wallrock surfaces, possible prehnite or epidote veining
11.97	61	a		n/a	drilling break
12.06	62	v		qz	drilling break along old quartz/silicate vein
12.12	63	v		qz	drilling break along old quartz/silicate vein
12.33	64	v		cal, chl, wall, hem	reddened feldspar (hematrised) in wallrock, slickened and polished chloritic fracture surfaces. Marks top of zone of highly altered and sheared wallrock impregnated by calcite
12.50	65	a		n/a	drilling break
12.65	66	v	?	cal, wall	fine euhedral calcite coats surface of asperities (S0.2x2mm wide) in fracture dominated by wallrock surfaces. Largely sealed by calcite in situ. Weak PFF only
12.83	67	v		cal, chl, wall	
13.00	68	v		cal, hem, wall	hematised feldspar in wallrock, mainly wallrock surfaces
13.11	69	v		cal, wall	mainly wallrock surfaces with minor calcite veining, sheared appearance

Appendix 2: Table 2. Summary mineralogical log of potentially open discontinuities in borehole KA2862A (continued

Distance along core axis (m)	BGS Feature No	Fracture Type	PFF	Surface Mineralogy	Comments
13.41	70	v		cal, wall	mainly wallrock surfaces, minor calcite + traces of unidentified silvery metallic mineral (possibly arsenopyrite). No clear evidence of euhedral calcite development to indicate open pore space, probably drilling induced break along sealerd vein
13.55	71	v	Y	cal, chl, wall	flattened euhedral calcite crystals developed on reactivated chlorite fracture surfaces. Porosity in channel-like asperities (1x1mm max.) with 100% calcite surfaces
13.74	72	v	?	cal, Fe-sulp	patches of dendritic pyrite or marcasite with traces of calcite developed on fracture surfaces dominated by wallrock (>99%). Weak PFF
13.86	73	v	Y	cal, wall	abundant, coalesced, very fine scalenohedral ("dog-tooth") calcite and traces of pyrite in vuggy asperities (Š0.1mm). Open surfaces 50-100% calcite. Granulated or tectonised (sheared) granodiorite wallrock is probably not exposed in asperities. Weak PFF
13.96	74	v	Y	cal, sulp wall	abundant, very fine euhedral "dog-tooth" scalenohedral calcite. Minor fresh wallrock exposed. Calcite forms a film like coating up to 100% of surfaces of asperities (0.2x2mm), trace sulphide in zone of PFFs
14.12	75	v	Y	cal, wall	minor euhedral calcite developed on surfaces dominated by fresh wallrock. Extremely thin fissure PFF
14.35	76	a		n/a	drilling break
14.81	77	v		brec, hem, cal	drlling break through calcite vein breccia. Sheared green wallrock
14.87	78	v		hem, cal	drilling break partly along sealed hematite-calcite vein
15.36	79	a		n/a	drilling break

Appendix 2: Table 2. Summary mineralogical log of potentially open discontinuities in borehole KA2862A (continued

Distance along core axis (m)	BGS Feature No	Fracture Type	PFF	Surface Mineralogy	Comments
15.57	80	v		cal, wall	drlling break along probably sealed old calcite vein. surfaces mainly wallrock
15.73	81	v	Y	cal, sulp, wall	Definite PFF with fine, equant to stubby, clear, scalenohedral calcite. V rare Fe sulphide in vein but present as trace impregnation in wallrock. Overall surface 5-10% calcite but surface of channel asperities (Š0.5x1mm) up to 50% of surface is calcite
15.81	82	v		cal, wall	trace hairline calcite vein in chloritised wallrock
15.85	83	a		n/a	drlling break through strong foliated fabric of chloritised wallrock
15.90	84	v	Y	cal, ep, chl, py	early hairline epidote-chlorite vein, reactivated by later calcite vein with trace pyrite. Calcite forms thin film but develops some euhedral faces into open pore space. Definite PFF
15.92	85	a		n/a	drilling break
15.98	86	v		chl, wall	

Appendix 2: Table 3. Key to abbreviations used

a	=	artificial fracture or drilling-induced fracture (cf. Fracture Type column)
arsenpyr	=	arsenopyrite
brec	=	fault breccia or brecciated host rock fragments
calc	=	calcite
chl	=	chlorite
chpy	=	chalcopyrite
clay	=	clay mineral
dol	=	dolomite
ep	=	epidote
Fe-sulp	=	iron sulphides (undefined: e.g. includes; pyrite, chalcopyrite, marcasite)
hem	=	hematite or fine-grained, red Fe oxides
myl	=	mylonite
other	=	unidentified mineral(s)
preh	=	prehnite
py	=	pyrite
qz	=	quartz
wall	=	wallrock
zeol	=	zeolite
?	=	denotes uncertain identity

APPENDIX 3: Summary field data for groundwater geochemistry and bulk groundwater samples taken from the REX area, ?sp` tunnel.

Site/sample:	**Borehole KA2858A**	**Comments**
Date:		12 April 1996
Time:		1700hrs (analytical measurements)
Bulk Sample Collection		one x 20 litre sample collected anaerobically under oxygen-free nitrogen in stainless steel vessel.Sample collection started 1350hrs finished 1605hrs. Flow very slow. Borehole flushed by flowing for 20minutes before sampling. Significant CO2 outgassing in groundwater on discharge from borehole was noted
Analytical samples:	**Type**	**Preservation details**
	(i) Cations	Filtered 0.45Fm (Nylon Acrodisc); acidified with 3mls conc HNO_3 in 60ml total volume.
	(ii) Anions	Filtered 0.45 (Nylon Acrodisc), unpreserved
	(iii) Trace cations	Filtered 0.45Fm (Nylon Acrodisc); acidified with 3mls conc HCl in 60ml total volume.
	(iv) As	Filtered 0.45Fm (Nylon Acrodisc); acidified with 6mls conc H_2SO_4 in 125ml total volume.
	(v) Sulphide	Unfiltered. Preserved with 2 pellets NaOH
Field Analyses:	**Test**	**Value/Comments**
	(i) Eh	+159.5 mV (corrected for T) measured in flowing system through flow-through cell slowly drifting down continuously after 20 mins
	(ii) pH	7.79 very slowly drifting to 8.01 after 20 mins
	(iii) T	12.5EC (stable)
	(iv) K	28.7 mS/cm (stable)
	(v) dissolved O_2	<0.05 mg/l [CheMets field colorimetric test Kit]
	(vi) bicarbonate	(a) 11.78 mg/l (determined 20 minutes after collection) (b) 12.40 (determined 72 hours after collection). Determined by titration with dilute HCl and bromocresol indicator using SKB on-site autotitration equipment.

Site/sample:	**Borehole KA2862A**	**Comments**
Date:		12 April 1996
Time:		1345 hrs (analytical measurements)
Bulk Sample Collection		one x 20lites sample collected anaerobically under oxygen-free nitrogen in stainless steel vessel. Sample collection started 1130hrs finished 1150hrs. Good flow from borehole. Borehole flushed by flowing for 20 minutes before sampling. Significant CO2outgassing in groundwater on discharge from borehole was noted
Analytical samples:	**Type**	**Preservation details**
	(i) Cations	Filtered 0.45Fm (Nylon Acrodisc); acidified with 3mls conc HNO_3 in 60ml total volume.
	(ii) Anions	Filtered 0.45 (Nylon Acrodisc), unpreserved
	(iii) Trace cations	Filtered 0.45Fm (Nylon Acrodisc); acidified with 3mls conc HCl in 60ml total volume.
	(iv) As	Filtered 0.45Fm (Nylon Acrodisc); acidified with 6mls conc H_2SO_4 in 125ml total volume.
	(v) Sulphide	Unfiltered. Preserved with 2 pellets NaOH
Field Analyses:	**Test**	**Value/Comments**
	(i) Eh	+146 mV (corrected for T) measured in flowing system through flow-through cell slowly drifting from +170 to +146 over 20 mins
	(ii) pH	7.41 very slowly drifting to 7.90 after 20 mins
	(iii) T	12.6EC (stable)
	(iv) K	33.5 mS/cm (stable)
	(v) dissolved O_2	<0.05 mg/l [CheMets field colorimetric test kit)
	(vi) bicarbonate	(a) 15.19 mg/l (determined 20 minutes after collection) (b) 14.88 (determined 72 hours after collection). Determined by titration with dilute HCl and bromocresol indicator using SKB on-site autotitration equipment.

Site/sample:	**Borehole KA2880A**	**Comments** Monitoring borehole located 18 m down-tunnel from REX borehole KA2862A, within REX Block area Significant CO2 outgassing in groundwater on discharge from borehole was noted
Date:		12 April 1996
Time:		1730 hrs (analytical measurements)
Bulk Sample Collection		none
Analytical samples:	**Type**	**Preservation details**
	(i) Cations	Filtered 0.45Fm (Nylon Acrodisc); acidified with 3mls conc HNO_3 in 60ml total volume.
	(ii) Anions	Filtered 0.45 (Nylon Acrodisc), unpreserved
	(iii) Trace cations	Filtered 0.45Fm (Nylon Acrodisc); acidified with 3mls conc HCl in 60ml total volume.
	(iv) As	Filtered 0.45Fm (Nylon Acrodisc); acidified with 6mls conc H_2SO_4 in 125ml total volume.
	(v) Sulphide	Uniltered. Preserved with 2 pellets NaOH
Field Analyses:	**Test**	**Value/Comments**
	(i) Eh	+152 mV (corrected for T) measured in open collecting vessel system (not through flow-through cell) slowly drifting (unstable)
	(ii) pH	7.04 (stable)
	(iii) T	12.1EC (stable)
	(iv) K	25.3 mS/cm (stable)
	(v) dissolved O_2	<0.05 mg/l [CheMets field colorimetric test kit)
	(vi) bicarbonate	(a) 27.60 mg/l (determined 20 minutes after collection) (b) 33.49 (determined 72 hours after collection). Determined by titration with dilute HCl and bromocresol indicator using SKB on-site autotitration equipment.

Appendix 3: Table 1. Summary of analytical data for groundwater geochemistry and bulk groundwater samples taken from the REX area, Äspö tunnel.

Sample	Conductivity FS/cm	pH	Ca mg/l	Mg mg/l	Na mg/l	K mg/l	HCO_3 mg/l	Cl mg/l	SO_4 mg/l	NO_3 mg/l
BH 2880 A	>20000	7.24	3582	46.7	2600	14.0	25	11080	589	<2.00
KA2862 A	>20000	6.99	4130	32.7	3270	15.3	<20	14400	755	<2.00
KA 2858 A	>20000	7.26	4270	46.7	2900	11.5	<20	12300	684	<2.00
Sample	**Br mg/l**	**NO_2 mg/l**	**HPO_4 mg/l**	**S_2O_3 mg/l**	**F mg/l**	**TOC mg/l**	**TIC mg/l**	**Total P mg/l**	**Total S mg/l**	**NH_4 mg/l**
BH 2880 A	72.6	0.43	0.11	<2.00	1.21	2.26	5.09	<0.10	191	0.08
KA2862 A	112	<0.40	0.15	<2.00	1.27	<1.00	1.46	<0.10	250	0.30
KA 2858 A	88.4	<0.40	0.12	<2.00	1.43	<1.00	1.26	<0.10	229	<0.10
Sample	**Si mg/l**	**Ba mg/l**	**Sr mg/l**	**Mn mg/l**	**Total Fe mg/l**	**Reduced Fe mg/l**	**Al mg/l**	**Li mg/l**	**B mg/l**	
BH 2880 A	4.35	0.101	55.7	0.416	0.67	0.85	1.86	2.60	1.00	
KA2862 A	4.21	0.098	65.4	0.270	0.08	0.09	2.54	3.92	0.99	
KA 2858 A	4.61	0.088	68.4	0.324	0.06	0.07	2.12	3.02	1.12	

Appendix 4: Table 1. LAMPS-ICP-MS data

(All values in mg/kg. Concentrations in italics are below that detection limit value (ppm)

	Sample Name	Phase (PJH)	Magnesium	Aluminium	Calcium	Iron	Strontium	Barium	Thorium	Uranium
			Mg 24	Al 27	Ca 44	Fe 57	Sr 88	Ba 138	Th 232	U 238
Bulk	C853AP1A	Plagioclase	2910	150000	*134740*	*118068*	784	699	*71*	*16*
	C853AP1B	Plagioclase	7264	150000	*37543*	*32819*	679	2105	*20*	*5*
	C853AP1C	Plagioclase	3659	150000	*31496*	*27469*	637	1205	*17*	*4*
	C853AP1D	Plagioclase	8476	150000	21811	27875	714	543	*9*	*2*
	C853AP1E	K-feldspar	3668	150000	*20515*	*17771*	1326	555	*11*	*3*
	C853AP1F	K-feldspar	4508	150000	26826	18931	1305	2979	*9*	*2*
	C853AP1G	K-feldspar	21204	150000	*18071*	*54172*	1611	2767	*10*	*2*
	C853AP1H	K-feldspar	18492	150000	*24826*	*21369*	1493	2996	*14*	*3*
	C853AP1I	K-feldspar	23339	150000	28492	53909	528	9172	*15*	*3*
	C853AP1J	K-feldspar	46717	150000	*25208*	104426	361	4601	*14*	*3*
	C853AP1K	K-feldspar	17388	150000	31740	29702	669	1726	*13*	*3*
	C853AP1L	K-feldspar	16815	150000	17431	43859	788	3381	*6*	*1*
	C853AP1M	Chlorite	204049	150000	*20406*	326330	*2*	*4*	*13*	*3*
	C853AP1N	Chlorite	185204	150000	*11893*	332635	*1*	*6*	*7*	*2*
	C853AP1O	Chlorite	204138	150000	*8697*	338629	*1*	*8*	*5*	*0*
	C853AP1P	Chlorite	212606	150000	*15916*	390751	*2*	*8*	*10*	*2*
	C853AP1Q	Plagioclase	6192	150000	55611	15264	1004	1792	*4*	*1*
	C853AP1R	Plagioclase	2056	150000	15673	6456	385	845	*4*	*1*
	C853AP1S	K-feldspar	29015	150000	26637	38962	838	1140	*11*	*2*
	C853AP1T	K-feldspar	5128	150000	29919	11234	714	2526	*5*	*1*

Appendix 4: Table 1. LAMPS-ICP-MS data (continued)

(All values in mg/kg. Concentrations in italics are below that detection limit value (ppm)

	Sample Name	Phase (PJH)	Magnesium	Aluminium	Calcium	Iron	Strontium	Barium	Thorium	Uranium
			Mg 24	Al 27	Ca 44	Fe 57	Sr 88	Ba 138	Th 232	U 238
PFF	C851AP1A	Calcite	2889	1082	400000	3947	78	59	0.5	0.1
	C851AP1B	Calcite	885	289	400000	2174	132	17	0.6	0.2
	C851AP1C	Calcite	39096	20892	400000	73850	591	51	[illegible]	1.3
	C851AP1D	Calcite	451	226	400000	3020	55	15	0.6	0.4
	C851AP1E	Calcite	396	191	400000	2880	85	13	0.5	0.2
	C851AP1F	Calcite	720	110	400000	2770	70	25	0.8	1.2
	C851AP1G	Calcite	304	153	400000	2067	83	7	0.6	0.7
	C851AP1H	Chlorite	241816	150000	13132	350756	188	54	2	6
	C851AP1I	Chlorite	208224	150000	9568	271720	141	13	5	3
	C851AP1J	Chlorite	213276	150000	10326	271166	136	19	4	4
	C851AP1K	Calcite	946.7	1270	400000	1783.1	145.2	931	[illegible]	0.3
	C851AP1L	Calcite	1177	1015	400000	2481.7	85.7	[illegible]	3.4	0.3
	C851AP1M	Chlorite	192123	150000	9490	234911	142	40	3	3
	C851AP1N	Chlorite	222131	150000	8636	275244	143	25	4	3
	C851AP1O	Epidote	13408	150000	57017	45321	1566	1056	31	9
	C851AP1P	Epidote	224751	150000	23892	391485	162	172	8	7
	C851AP1Q	Epidote	56528	150000	1252709	227145	8193	663	154	258
	C851AP1R	Epidote	23951	150000	174548	137421	7468	349	7	19
	C851AP1S	Epidote	185271	150000	682981	272931	4073	167	41	53
	C851AP1T	Epidote	4340	150000	160816	213804	13510	86	30	228
	C851AP1U	Epidote	11344	150000	167258	231271	16604	1864	24557	559
	C851AP1V	Epidote	7090	150000	208507	189226	15492	1984	18732	463

Appendix 4: Table 1. LAMPS-ICP-MS data (continued)
(All values in mg/kg. Concentrations in italics are below that detection limit value (ppm)

	Sample Name	Phase (PJH)	Magnesium	Aluminium	Calcium	Iron	Strontium	Barium	Thorium	Uranium
			Mg 24	Al 27	Ca 44	Fe 57	Sr 88	Ba 138	Th 232	U 238
PFF	C851AP1W	Epidote	146785	150000	1874157	680789	1409	554	2655	592
	C851AP1X	Epidote	53760	150000	820387	141274	3661	790	1254	273
	C851AP1Y	Chlorite	251546	150000	9336	222533	5	2	6	1
	C851AP1Z	Chlorite	141280	150000	8035	207693	2	2	3	1
	C851AP1AA	Epidote/Calcite	47	215	400000	5301	144	5	7	0
	C851AP1AB	Epidote/Calcite	136	197	400000	2252	8	8	1	0

APPENDIX 5

A. Growth Media Compositions

Iron Citrate medium for enrichment of IRB

0.01g	Peptone
2.5g	$NaHCO_3$
1.5g	NH_4Cl
0.6g	NaH_2PO_4
0.1g	NaCl
0.1g	$MgCl_2.6H_2O$
0.005g	$MnCl_2.4H_2O$
0.001g	$Mn_2MoO_4.2H_2O$
1.195g	Iron citrate (energy source)
6.897g	Sodium lactate (electron donor)
1000ml	Distilled water

Postgates B medium for SRB

0.5g	KH_2PO_4
1.0g	NH_4Cl
1.0g	$CaSO_4$
2.0g	$MgSO_4.7H_2O$
0.5g	$FeSO_4.7H_2O$
3.45ml	Sodium lactate
1.0g	Yeast extract
0.1g	Ascorbic acid
0.1ml	Thioglycollic acid
1000ml	Distilled water

Ajusted pH to 7.0 using sodium hydroxide

B. Microscopy reagents

Glutaraldehyde fixative

0.1M Cacodylate buffer: Dissolve 8 g of Cacodylic acid (BDH) in 500 ml of distilled water and adjust to pH 7.4. Filter sterilise through a 0.45 Fm Millipore filter.

0.5 % Glutaraldehyde fixative in cacodylate buffer: Dilute a 25 % glutaraldehyde solution (BDH) with cacodylate buffer. Store in the dark at 4°C.

Phosphate buffers

Potassium phosphate dibasic solution: Dissolve 4.35 g K_2HPO_4 (BDH) in 500 ml distilled water and sterilise. Store in the dark at 4/C.

Potassium phosphate monobasic solution: Dissolve 3.4 g KH_2PO_4 (BDH) in 500 ml distilled water and sterilise. Store in the dark at 4°C.

Acridine Orange Stain

Prepare a potassium phosphate buffer by combining 42 ml of potassium phosphate dibasic solution and 8 ml of potassium phosphate monobasic solution. Adjust pH to 7.5 with further monobasic solution. Add 5 mg of acridine orange (BDH, Microscopical stains). Filter sterilise with a 0.45 Fm Millipore filter. If stored in the dark at 4/C this solution will keep for 5 days.

Appendix 6: Table 1. Laboratory Run Sample analysis (continued)

(concentrations in mol/l)

Sample Code	Bugs	Rock	Ba	Sr	Mn	Total Fe	Reduced Fe	Oxidised Fe	Al	Co	Ni	Cu	Zn	Cr	Mo	Cd	Pb	V	Li	B	As ICP-AES	As AFS	Total Se
KA 2858 A	Starting Fluid	-	6.4E-7	7.8E-4	5.9E-6	1.1E-6	1.3E-6	<2.0E-7	7.9E-5	<3.4E-7	<1.7E-6	<7.9E-8	<7.6E-8	<1.9E-7	5.2E-7	<4.4E-8	<4.8E-7	<2.0E-7	4.3E-4	1.0E-4	<1.3E-6	0.0E+0	<3.8E-9
Run 531	SRB	Yes	2.1E-6	6.7E-4	2.9E-5	3.8E-5	6.3E-5	<2.5E-5	5.1E-5	<1.7E-6	<8.6E-6	<4.0E-7	1.9E-6	<9.7E-7	<1.1E-6	<2.2E-7	<2.4E-6	<9.9E-7	3.4E-4	1.0E-4	n/a	n/a	<1.0E-8
Run 532	SRB	Yes	2.4E-6	8.2E-4	3.9E-5	1.7E-4	2.3E-4	<5.8E-5	5.1E-5	<1.7E-6	<8.6E-6	7.8E-7	<1.5E-6	<9.7E-7	<1.1E-6	<2.2E-7	<2.4E-6	<9.9E-7	4.3E-4	1.3E-4	n/a	n/a	n/a
Run 533	SRB	Yes	1.9E-6	6.7E-4	3.2E-5	1.3E-4	1.7E-4	<4.8E-5	5.2E-5	<1.7E-6	<8.6E-6	4.2E-7	<1.5E-6	<9.7E-7	<1.1E-6	<2.2E-7	<2.4E-6	<9.9E-7	3.4E-4	1.1E-4	n/a	n/a	n/a
Run 534	SRB	No	8.6E-7	7.9E-4	7.0E-6	1.7E-4	2.2E-4	<5.5E-5	5.5E-5	<1.7E-6	<8.6E-6	4.5E-7	<1.5E-6	<9.7E-7	<1.1E-6	<2.2E-7	<2.4E-6	<9.9E-7	4.6E-4	1.1E-4	<6.7E-6	4.9E-8	<2.5E-9
Run 535	-	Yes	2.5E-6	8.5E-4	3.3E-5	5.1E-6	6.8E-6	<1.7E-6	5.2E-5	<1.7E-6	<8.6E-6	<4.0E-7	<1.5E-6	<9.7E-7	<1.1E-6	<2.2E-7	<2.4E-6	<9.9E-7	4.4E-4	1.3E-4	n/a	n/a	<1.0E-8
Run 536	-	Yes	2.2E-6	8.1E-4	3.7E-5	1.1E-5	1.4E-5	<3.3E-6	4.6E-5	<1.7E-6	<8.6E-6	6.8E-7	<1.5E-6	<9.7E-7	<1.1E-6	<2.2E-7	<2.4E-6	<9.9E-7	4.1E-4	1.3E-4	n/a	n/a	n/a
Run 537	-	Yes	2.1E-6	8.2E-4	3.7E-5	1.2E-5	1.8E-5	<5.1E-6	5.1E-5	<1.7E-6	<8.6E-6	<4.0E-7	<1.5E-6	<9.7E-7	<1.1E-6	<2.2E-7	<2.4E-6	<9.9E-7	4.0E-4	1.3E-4	n/a	n/a	n/a
Run 538	-	No	8.1E-7	7.9E-4	6.8E-6	1.8E-6	2.4E-6	<5.8E-7	5.2E-5	<1.7E-6	<8.6E-6	5.0E-6	8.4E-6	<9.7E-7	<1.1E-6	<2.2E-7	<2.4E-6	<9.9E-7	4.5E-4	1.2E-4	<6.7E-6	<1.3E-8	<2.5E-9
Run 542	IRB	Yes	2.4E-6	7.7E-4	3.0E-5	5.2E-6	7.9E-6	<2.7E-6	6.5E-5	<3.4E-6	<1.7E-5	<7.9E-7	<3.1E-6	<1.9E-6	<2.1E-6	<4.5E-7	<4.9E-6	<2.0E-6	3.9E-4	1.2E-4	n/a	n/a	n/a
Run 541	IRB	Yes	2.2E-6	7.9E-4	3.3E-5	8.0E-6	1.6E-5	<8.1E-6	4.1E-5	<1.7E-6	<8.6E-6	<4.0E-7	<1.5E-6	<9.7E-7	<1.1E-6	<2.2E-7	<2.4E-6	<9.9E-7	4.1E-4	1.2E-4	<6.7E-6	n/a	n/a
Run 539	IRB	Yes	2.3E-6	9.0E-4	3.9E-5	9.4E-6	1.0E-5	<1.1E-6	4.9E-5	<1.7E-6	<8.6E-6	<4.0E-7	<1.5E-6	<9.7E-7	<1.1E-6	<2.2E-7	<2.4E-6	<9.9E-7	4.5E-4	1.4E-4	n/a	n/a	n/a
Run 543	IRB	No	9.7E-7	8.6E-4	8.0E-6	4.8E-6	8.1E-6	<3.3E-6	6.3E-5	<1.7E-6	<8.5E-6	1.3E-6	4.8E-6	<9.6E-7	<1.0E-6	<4.4E-7	<2.4E-6	<9.8E-7	4.6E-4	1.2E-4	n/a	n/a	n/a
Run 545	IRB + SRB	Yes	2.6E-6	8.0E-4	3.5E-5	1.1E-4	1.3E-4	<2.8E-5	3.8E-5	<1.7E-6	<8.6E-6	6.0E-7	<1.5E-6	<9.7E-7	<1.1E-6	<2.2E-7	<2.4E-6	<9.9E-7	4.3E-4	1.2E-4	<6.7E-6	n/a	n/a
Run 544	IRB + SRB	Yes	2.4E-6	6.2E-4	2.7E-5	6.0E-5	8.1E-5	<2.1E-5	3.9E-5	<1.7E-6	<8.6E-6	5.9E-7	<1.5E-6	<9.7E-7	<1.1E-6	<2.2E-7	<2.4E-6	<9.9E-7	3.2E-4	9.9E-5	1.8E-4	n/a	n/a
Run 540	IRB + SRB	Yes	3.4E-6	8.2E-4	3.5E-5	1.1E-4	1.5E-4	<4.1E-5	5.4E-5	<1.7E-6	<8.6E-6	<4.0E-7	<1.5E-6	<9.7E-7	<1.1E-6	<2.2E-7	<2.4E-6	<9.9E-7	4.1E-4	1.3E-4	<6.7E-6	n/a	n/a
Run 546	IRB + SRB	No	1.0E-6	8.7E-4	8.0E-6	4.2E-4	4.8E-4	<5.9E-5	5.2E-5	<1.7E-7	<8.5E-6	<7.9E-7	4.9E-6	<9.6E-7	<1.0E-6	<4.4E-7	<2.4E-6	<9.8E-7	4.7E-4	1.2E-4	n/a	n/a	n/a

Appendix 6: Table 1. Laboratory Run Sample analysis (concentrations in mol/l)

Sample Code	Bugs	Rock	pH	Ca	Mg	Na	K	HCO3	Cl	SO4	NO3	Br	NO2	HPO4	S2O3	F	TOC	TIC	Total P	Total S	Reduced S	NH4	Si
KA 2858 A	Starting Fluid	-	7.0E+0	1.1E-1	1.9E-3	1.3E-1	2.9E-4	<3.3E-4	3.5E-1	7.1E-3	<3.2E-5	1.1E-3	<8.7E-6	1.3E-6	<1.8E-5	7.5E-5	<8.3E-5	1.0E-4	<3.2E-6	7.1E-3	<1.5E-7	<5.5E-6	1.6E-4
Run 531	SRB	Yes	6.6E+0	9.7E-2	2.9E-3	1.2E-1	2.8E-3	4.2E-3	3.7E-1	6.8E-3	<3.2E-5	1.3E-3	<1.3E-5	<1.0E-5	<1.8E-5	4.3E-5	<1.7E-3	4.1E-3	<1.6E-5	6.2E-3	<4.9E-7	2.7E-5	2.6E-4
Run 532	SRB	Yes	6.4E+0	1.2E-1	3.8E-3	1.4E-1	3.4E-3	4.7E-3	3.7E-1	6.5E-3	<3.2E-5	1.3E-3	<1.3E-5	<1.0E-5	<1.8E-5	4.8E-5	<1.7E-3	4.5E-3	1.6E-5	6.8E-3	2.4E-6	1.0E-5	3.7E-4
Run 533	SRB	Yes	6.3E+0	9.6E-2	3.1E-3	1.2E-1	2.7E-3	4.1E-3	3.6E-1	6.7E-3	<3.2E-5	1.3E-3	<1.3E-5	<5.2E-6	<1.8E-5	4.9E-5	9.3E-4	3.7E-3	1.8E-5	5.9E-3	1.6E-6	8.3E-6	2.9E-4
Run 534	SRB	No	5.7E+0	1.1E-1	2.2E-3	1.4E-1	3.8E-4	8.0E-4	3.7E-1	6.8E-3	<3.2E-5	1.3E-3	<1.3E-5	<1.0E-5	<1.8E-5	7.8E-5	<1.7E-3	<1.7E-3	<1.6E-5	7.0E-3	1.2E-6	3.3E-5	1.4E-4
Run 535	-	Yes	6.6E+0	1.2E-1	3.5E-3	1.5E-1	3.4E-3	3.6E-3	3.9E-1	7.2E-3	<3.2E-5	1.3E-3	<1.3E-5	<1.0E-5	<1.8E-5	4.1E-5	<1.7E-3	3.6E-3	<1.6E-5	8.0E-3	<4.9E-7	6.1E-6	3.1E-4
Run 536	-	Yes	6.4E+0	1.2E-1	3.6E-3	1.4E-1	3.4E-3	4.2E-3	3.7E-1	7.2E-3	<3.2E-5	1.3E-3	<1.3E-5	<1.0E-5	<1.8E-5	5.3E-5	<1.7E-3	5.3E-3	<1.6E-5	7.7E-3	<4.9E-7	1.6E-5	3.2E-4
Run 537	-	Yes	6.3E+0	1.1E-1	3.6E-3	1.4E-1	3.4E-3	4.0E-3	3.6E-1	7.1E-3	<3.2E-5	1.3E-3	<1.3E-5	<1.0E-5	<1.8E-5	5.9E-5	1.8E-3	3.8E-3	<1.6E-5	7.7E-3	<4.9E-7	2.0E-5	3.1E-4
Run 538	-	No	5.4E+0	1.1E-1	2.2E-3	1.4E-1	3.6E-4	<6.6E-4	3.6E-1	6.9E-3	<3.2E-5	1.3E-3	<1.3E-5	<1.0E-5	<1.8E-5	6.8E-5	<1.7E-3	<1.7E-3	<1.6E-5	6.9E-3	<4.9E-7	3.0E-5	1.4E-4
Run 542	IRB	Yes	6.4E+0	1.1E-1	3.2E-3	1.4E-1	2.9E-3	3.7E-3	3.6E-1	7.3E-3	<3.2E-5	1.3E-3	<1.3E-5	<5.2E-6	<1.8E-5	4.2E-5	9.9E-4	3.5E-3	<3.2E-5	7.3E-3	<4.9E-7	2.1E-5	2.9E-4
Run 541	IRB	Yes	6.4E+0	1.1E-1	3.4E-3	1.4E-1	3.3E-3	3.9E-3	3.5E-1	7.3E-3	<3.2E-5	1.3E-3	<1.3E-5	<1.0E-5	<1.8E-5	6.5E-5	<1.7E-3	4.1E-3	<1.6E-5	7.4E-3	<4.9E-7	6.9E-5	2.9E-4
Run 539	IRB	Yes	6.3E+0	1.3E-1	3.9E-3	1.6E-1	3.7E-3	4.4E-3	3.5E-1	7.3E-3	<3.2E-5	1.3E-3	<1.3E-5	<5.2E-6	<1.8E-5	4.7E-5	1.0E-3	4.2E-3	<1.6E-5	8.4E-3	<4.9E-7	<2.8E-5	3.3E-4
Run 543	IRB	No	5.3E+0	1.2E-1	2.3E-3	1.4E-1	3.1E-4	<6.6E-4	3.6E-1	7.2E-3	<3.2E-5	1.2E-3	<8.7E-6	<1.0E-5	<1.8E-5	3.2E-5	2.8E-3	<8.3E-4	<3.2E-5	7.3E-3	<9.1E-6	5.5E-5	1.8E-4
Run 545	IRB + SRB	Yes	6.4E+0	1.1E-1	3.5E-3	1.4E-1	3.4E-3	4.2E-3	3.4E-1	6.9E-3	<3.2E-5	1.3E-3	<1.3E-5	<1.0E-5	<1.8E-5	3.7E-5	<1.7E-3	4.0E-3	<1.6E-5	7.3E-3	3.3E-6	<2.8E-5	3.3E-4
Run 544	IRB + SRB	Yes	6.4E+0	8.6E-2	3.2E-3	1.1E-1	2.9E-3	4.5E-3	3.0E-1	5.0E-3	<3.2E-5	1.0E-3	<1.3E-5	<5.2E-6	<1.8E-5	4.1E-5	2.3E-3	4.8E-3	<1.6E-5	5.0E-3	1.1E-5	<2.8E-5	3.4E-4
Run 540	IRB + SRB	Yes	6.4E+0	1.2E-1	3.7E-3	1.5E-1	3.2E-3	4.5E-3	3.6E-1	5.8E-3	<3.2E-5	1.3E-3	<1.3E-5	<1.0E-5	<1.8E-5	5.2E-5	<1.7E-3	5.3E-3	<1.6E-5	6.3E-3	6.5E-6	<2.8E-5	4.0E-4
Run 546	IRB + SRB	No	5.8E+0	1.2E-1	2.5E-3	1.5E-1	3.2E-4	<6.6E-4	3.7E-1	7.4E-3	<3.2E-5	1.2E-3	<8.7E-6	1.4E-5	<1.8E-5	3.7E-6	1.8E-3	<4.2E-4	3.3E-4	7.3E-3	<9.1E-6	1.2E-4	1.7E-4

Appendix 7: Table 1. Results of total counts of bacteria using epifluorescence microscopy

Run Number	Initial number of bacteria per ml of groundwater	Standard error	Number of bacteria after incubation period	Standard error
531	157,000	24,100	45,500	2,830
532	157,000	24,100	18,060	946
533	157,000	24,100	19,600	966
534	157,000	24,100	None detected	
542	316,100	41,700	None detected	
541	316,100	41,700	396,200	80,860
539	1,288,000	61,340	133,500	3,690
543	1,060,000	34,800	628,300	6,510
545	1,075,000	61,600	1,209,000	98,200
544	1,075,000	61,600	357,400	34,600
540	1,574,700	110,700	None detected	
546	2,040,000	67,500	1,742,000	33,700

TASK 2. GEOCHEMICAL PROFILE THROUGH TSUKIYOSHI FAULT ZONE

2a. Stress-sensitivity of the hydraulic properties of a clay-bearing fault gouge from the Tsukiyoshi Fault, Tono Mine, Central Japan

2b. Geochemical profile through the Tsukiyoshi fault zone: Pore-water Characterisation

PNC Representatives:	**H. Yoshida, K. Hama, K. Aoki**
Project Manager:	**M. Sen and J. West**
Hydraulic properties studies:	**J Harrington, S Horseman**
Pore water characterisation:	**S. Reeder, M. Cave, P. Blackwell, J. Trick, J. Wragg and S. Burden**
Adminstration, QA Procedures and Report Preparation:	**S.Baker, P. Coombs,C. Cole, R. U. Leader, J. Mackrill**
Financial administration:	**L. Riley**

1. INTRODUCTION

Tono Mine is located about 350 km south-west of Tokyo and is the site of Japan's most extensive uranium deposits. The geology consists of Tertiary sedimentary rocks overly a Cretaceous granitic basin. The Tsukiyoshi Fault cuts through this sequence. As part of its hydrogeological studies, PNC is evaluating the impact of the Tsukiyoshi Fault on groundwater flow in the Tertiary sediments.

Hydrogeochemical data obtained from pore-waters in the sandstone on either side of the clay gouge and within the clay gouge material itself should provide information about groundwater flow across the low permeability barrier formed by the gouge. However, the acquisition of accurate data from low permeability media and in fresh groundwater conditions present special challenges. This study provides an important opportunity to develop techniques for extracting and chemically and isotopically characterising pore-water from the low permeability clay gouge and from the surrounding higher permeability conglomerate and sandstone rocks.

The Tsukiyoshi Fault research studies carried out by the BGS are aimed at understanding the potential role of a fault in controlling groundwater flow patterns and geochemical conditions, and at developing methods of investigation. The programme of work considers two aspects: (i) hydrochemical characterisation of clay pore-waters from the fault zone and surrounding lithology ; and (ii) characterisation of the hydraulic properties of the fault gouge.

2. SCOPE OF WORK

The scope of work described in this report was to conduct a series of laboratory experiments to provide information on the hydrochemical properties of the Tsukiyoshi Fault clay gouge and surrounding sandstone and conglomerates.

Cores are preserved under anaerobic conditions immediately following collection to prevent oxidation and loss of moisture. Extraction of pore-water from the clay gouge material is performed using mechanical squeezing techniques. For the higher permeability formations on either side, pore-waters are attempted principally by centrifugation. Aqueous leaching is used to obtain residual solutes data for samples from which pore-water cannot be extracted.

The pore waters and aqueous leachates are chemically characterised for pH, alkalinity, Ca, Mg, Na, K, Cl, SO_4, NO_3, NO_2, Br, F, TOC, TIC, Si, Ba, Sr, Mn, Fe, Al, Li and B. Isotopic characterisation of stable $\delta^{18}O$ and $\delta^{2}H$ isotopes is also carried out. The cation exchange capacity (CEC) of the clay gouge material has also been determined.

Isotopic characterisation of sulphur and strontium isotopes, ^{36}Cl and tritium have not been carried out because of the limited volume of fluid obtained by the extraction methods.

3. COLLECTION AND PRESERVATION OF DRILLCORE

Sampling of the fault zone was carried out in July 1997 in the North Extension Drift of Tono Mine, approximately 160 m below surface. A 116 mm diameter borehole was drilled at an angle of 5 degrees below horizontal to a total length of 29.96m. The sample was cored using a triple-tube core barrel fitted with a split sample tube and a diamond bit. The hole was water-flushed using local river water dosed with uranine (fluorescence) tracer.

On collection, a representative number of samples were preserved by sealing in double aluminised plastic bags after flushing with nitrogen gas. Friable core and material likely to puncture the aluminium were wrapped in cling film prior to preservation. The remaining core was stored, unpreserved, in core boxes. The core preservation was carried out under the supervision of a BGS chemist, Mr S Reeder.

Several of the preserved core samples were selected for testing, and shipped to the United Kingdom in wooden core boxes. On receipt at the BGS, the samples were maintained in cold storage at less than 4°C prior to testing. A list of the samples provided, and the subsequent testing methods applied, is given in Table 1. Samples of the make-up water used for flushing the borehole and return fluids collected during drilling were also collected and sent to the BGS for analysis. A list of these samples is given in Table 2.

4. PORE-WATER EXTRACTION METHODS

4.1 Pore-Water Extraction by Mechanical Squeezing

4.1.1 The Theory of Pore-Water Extraction by Mechanical Squeezing

The extraction of pore-water from rocks and soils by squeezing is analogous to the natural process of consolidation, caused by the deposition of sediments during geologic time. The technique has been applied mainly to unconsolidated marine silts and clays. A heavy duty squeezer was developed by the British Geological Survey from the designs of a number of Soviet workers, notably Kriukov (1947), and is capable of applying pressures up to 70 MPa (Manheim, 1966). Brightman *et al.* (1985) reviewed the extraction of pore-water by squeezing and described the early work of the BGS. A more detailed description of the technique and its application to a wide range of samples is given by Entwisle and Reeder (1993).

The squeezing process involves the expulsion of pore-water from the mudrocks being compressed. The mudrocks consist of solid particles, or the mineral phase, and the spaces, or voids, which in a saturated rock are filled with water.

When the squeezing stress is applied to a saturated mudrock its volume decreases by three main processes: compression of the solid grains; compression of the pore-water between the grains and escape of water from the voids. In most circumstances the compression of the solid phase and water phase is negligible (one exception is peat)

and most of the change in volume is due to the escape of pore-water by primary consolidation. The increasing stress, which is normally added incrementally at regular intervals, results in reduction of pore size, hence reducing permeability, and the extraction of pore-water.

Mechanical squeezing has been used previously to extract pore-water under anaerobic and aerobic conditions from the target Opalinus clay formation from the Mount Terri tunnel site in Switzerland (Gautschi *et al.*, 1992; Cave *et al.*, 1996). More recently, the BGS has undertaken work for the French nuclear waste agency (ANDRA) in which successful anaerobic squeezing of clay material from the Mol facility in Belgium has allowed chemical analysis and isotopic characterisation of sulphate-sulphur and oxygen to be carried out. The BGS has also successfully carried out mechanical squeezing of very low moisture content clays from ANDRA investigation sites in France. A particularly relevant recent investigation is that undertaken at Down Ampney, southern England. Here pore-water data were used to develop a model for geologically recent groundwater flow in a faulted mudrock (Metcalfe *et al.* 1996).

4.1.2 The Squeezing Apparatus and Test Procedure

The squeezing apparatus utilises available technology based on pumps producing a maximum output stress of 70 MPa. A diagram of the cell body is given in Figure 1.

The metal parts of the cell are made of Type 316 stainless steel, which was selected because of its resistance to corrosion and high tensile strength. The sample chamber is 75 mm in diameter and has a height of about 100 mm. The cell temperature is controlled by a heater/chiller which is capable of maintaining the temperature between -10°C and 50°C.

The samples for squeezing are prepared in a soil lathe using a large knife to remove the outer annulus of the core. The trimmed cylinder is weighed and placed into the body of the cell. In cases where the core is friable and falls apart, samples are trimmed and then placed into the body of the cell as separate pieces. A separate sub-sample is also taken for moisture content determination. This is carried out by measuring the loss in mass after heating between 100 to 200g of sample at a temperature of 105-110°C for approximately 24 hours.

A small stress of about 1 to 3 MPa is applied initially to remove most of the inert gas from the cell and allow the sample to bed in. The temperature control is switched on and the system is left to equilibrate at the selected temperature of about 10°C. The syringe tap and filter assembly is pushed into the top of the pore-water collection pipe and a labelled syringe of known weight inserted into the top syringe tap. The temperature of the cell is measured with a thermometer probe and when it is within ±2°C of the required test temperature the stress is increased to start pore-water extraction. The stepped increase in stress during testing is dependent on the material tested and volume of water required. A particular stress may be maintained for a few hours or for several days depending on the rate of pore-water flow.

When the maximum volume of pore-water has been obtained, the syringe is removed, a syringe tap placed over the end of the syringe to isolate the sample from the atmosphere, and the weight of extracted sample determined.

The PNC studies were carried out under 'anaerobic' conditions using a squeezing cell housed in a specially designed chamber with a nitrogen atmosphere containing between 10 to 100 mg l^{-1} oxygen. All core preparation, pore-water extraction and pore-water preservation is carried out in this low oxygen environment.

4.1.3 Contamination and Artifacts of Squeezing

Contamination of pore-water may possibly arise from the metal of the cell, the seals, the filters or the plastic syringes and syringe taps.

There is no indication of contamination of the pore-water by corrosion of the metal of the cell. The values of nickel, an important constituent of the metal used in the construction of the cell are less than the analytical detection level of 0.02 mg l^{-1}. The use of iron as an indicator of corrosion is more complex as its natural abundance in pore-waters may fluctuate considerably. Tests over a number of years have, however, frequently resulted in total iron contents less than the analytical detection level (0.01 mg l^{-1}), indicating that corrosion of the cell is not a problem. High levels of iron may be observed if pore-waters become acidic owing to pyrite oxidation (Bath *et al.*, 1989), but this was not observed in the samples tested in this study.

It is also considered unlikely that the seals, filters and plastic syringe apparatus contribute any significant levels of contamination for any of the species determined.

4.2 Pore-Water Extraction by Immiscible Liquid Displacement Centrifugation

4.2.1 Discussion of the Extraction Process

The principle of the centrifugation method, including a discussion of fractionation, contamination and the degree to which the extracted water represents *in-situ* pore-water is discussed by Edmunds and Bath (1976) and Kinniburgh and Miles (1983). A direct comparison of analyses of pore-waters extracted by this technique, those obtained by squeezing, and those of actual groundwater samples (Entwisle *et al.*, 1989) also confirms the centrifugation method as a technique for obtaining reliable data for natural pore-water compositions.

4.2.2 Extraction Method

Core material is crushed to approximately pea-sized fragments then preserved by taking 110±1g in a centrifuge bucket and adding approximately 200g of the heavy liquid displacent (1,1,2-trichloro-1,2,2-trifluoroethane, trade name Arklone). Each sample is prepared in triplicate. Immediately prior to extraction, the sample bottles are balanced, by the addition of extra Arklone, such that all bottles are within 2 g and opposing bottles in the centrifuge head are in agreement to within ±0.1g. The samples

are then centrifuged for a period of 30 minutes at 13,000 rpm. Any pore-water displaced is collected from the upper layer using a Pasteur pipette.

4.3 Dispersive Leaching of Residual Solutes

4.3.1 Core Sample Preparation

The core sample is firstly trimmed, using a mechanical core splitter, in order to remove the edges and outer 1-2 cm annulus, which are discarded. The sample section is broken into suitably sized fragments (<1 cm diameter) using a mechanical jaw crusher. The jaws, blades and surrounding areas of test apparatus are thoroughly cleaned with distilled water, followed by acetone, and dried before crushing each sample. The crushed sample is dried for 12 hours at 40°C in a fan assisted oven before being separated and collected through a 180 μm sieve (nylon mesh held in a plastic frame) to ensure that particles finer than this are not milled. The retained coarser material is transferred to a tungsten carbide Tema™ disc mill and processed for short periods of no more than 30 s before collecting through a 350 μm sieve, repeating this process until all of the sample had been milled to less than 350μm. This material is then mixed with the initial <180 μm fraction and stored in preparation for aqueous leaching. At all stages of preparation it is ensured that the milling apparatus is thoroughly cleaned with distilled water and acetone then dried.

4.3.2 Discussion of the Dispersive Leaching Process

The simple aqueous leach used provides quantitative data for conservative tracers, but only semi-quantitative or qualitative data for other solutes (Spears, 1976; Couture *et al.*, 1983; Couture and Seitz, 1986). The concentrations of the latter are modified by water-rock interactions and oxidation during the experimental procedure (Entwisle *et al.*, 1989). Entwisle and his co-workers discuss how these interactions, including accelerated oxidation of labile minerals such as pyrite and dissolution of carbonate and sulphate minerals, may enhance, and in some cases deplete, solute concentrations in a highly variable manner.

Fontanive *et al.* (1993) and Baeyens and Bradbury (1994) have shown that aqueous leaching of clay material at a series of different rock to water ratios can be used to estimate pore-water compositions.

4.3.3 Abstraction Method

For constant ratio leach tests, 5g ± 0.1 g of milled samples, as described in Section 4.3.1, are accurately weighed into a centrifuge tube and 30 ml ± 0.1 ml of deionised water added. The sample is then shaken under constant conditions for a period of about 24 hours at room temperature. The supernatant leachate is centrifuged for a period of 15 minutes at 13,500 rpm, filtered through a 0.45 μm filter (containing no surfactants) and preserved for chemical analysis.

An estimate of the original interstitial water concentration (the equivalent concentration) may be calculated using the original sample moisture contents:

$$\text{Equivalent Conc. (mg/l)} = \frac{\text{Extract Concentration (mg/l) x Weight Water Added (g) x 100}}{\text{Original Sample Moisture Content (\%) x Weight of Sample Used (g)}}$$

This equivalent concentration is not representative of 'true' interstitial water compositions, with the possible exception of conservative species, without further reconstruction of the data by multivariate statistical analysis.

4.4 Determination of Moisture Content

Moisture contents are determined on all test samples prepared for aqueous leaching and on pore-water extraction samples for which leaching tests were not being conducted. The tests involve accurately determining the weight of a minimum mass of 50 g of sample before and after heating for a minimum of 12 hours. For samples prepared for aqueous leaching, the samples are heated at 40°C, and for those subjected to squeezing, a temperature of 105°C to 110°C is used. The moisture content is calculated with respect to dry weight as:

$$\text{Moisture Content (\%)} = \frac{\text{Wet Weight (g) - Dry Weight (g)}}{\text{Dry Weight (g)}} \times 100\%$$

5. ANALYTICAL TECHNIQUES

5.1 Determination of pH and Total Alkalinity by Titration

5.1.1 Instrumentation

The instrumentation used is a Radiometer VIT90 Video Titrator Controller module with an ABU93 autoburette and a SAM90 sample station. Sample pH is determined using Radiometer pHG200 glass pH and REF200 reference electrodes.

5.1.2 Theory

'Total alkalinity' may be defined as the amount of sulphuric acid required to titrate the sample to the equivalence point of bicarbonate at approximately pH 4.5, expressed as the equivalent mg/l of bicarbonate (HCO_3). It is actually a measure of the acid neutralising capacity of the sample but, as this is dominated in groundwaters by the carbonic acid equilibria system, the expression of total alkalinity in terms of bicarbonate is common practice. In reality, total alkalinity is a measure of the hydroxide, carbonate (x2) and bicarbonate contents, as well as any contribution from other anions that take part in hydrolysis, e.g. organic bases, silicates, borates, sulphides and phosphates.

5.1.3 Analytical Method

Total alkalinity and pH were determined on all samples as soon as possible after collection and with minimal contact with the atmosphere. The pH electrode is calibrated using Whatman high resolution pH 7 and 10 buffers. Two ml of sample was titrated to pH 2.5 with 0.01M sulphuric acid, and the amount of acid added to the bicarbonate equivalence point at approximately pH 4.5 automatically calculated and used to determine the bicarbonate concentration. An independent check standard is analysed after not more than 10 samples and at the end of the run to check for any drift.

5.1.4 Data Quality

The inflection point for samples which gave clearly defined end-points, was in the range pH 4.3 to 5.0. However, the determination of total alkalinity is complicated by the presence of species other than bicarbonate and carbonate (e.g. organic bases, silicates, borates, sulphides or phosphates) that buffer the titration causing higher than expected results. It is difficult to calculate the total buffering capacity to the neutralisation point because, in most cases, the end point is poorly defined. In cases where the total inorganic carbon content was very low, it was often found that a total alkalinity could not be determined because of the ill defined end point.

5.2 Determination of Major Cations and Trace Elements by Inductively Coupled Plasma-Atomic Emission Spectrometry (ICP-AES)

5.2.1 Instrumentation

The ICP-spectrometer used in this work is a Perkin-Elmer Plasma II sequential scanning system with twin 1m vacuum monochromators. Monochromator A has a 3600 line/mm grating and wavelength range of 160-400 nm and the second (B) has a 1800 line/mm grating and wavelength range of 160-800 nm. The monochromator gratings, plasma power, plasma gas flows, plasma viewing height, 50-position auto-sampler and nebuliser peristaltic pump are all under computer control.

5.2.2 Theory

The nebulised sample is swept into the central channel of the inductively coupled plasma in a stream of argon carrier gas. On introduction to the plasma, the sample undergoes desolvation, evaporation, atomisation/ionisation and excitation. The atoms or ions decay from their excited state through radiative energy transitions, emitting light of specific energies (or wavelengths). The light emission from the plasma is separated into its component wavelengths by a monochromator, and a photomultiplier tube at the exit slit of the monochromator quantifies the light intensity at specific wavelengths. The intensity of the light emitted at the characteristic wavelength for a particular element is proportional to the amount of the element in the sample being sprayed into the plasma. The instrument is calibrated against standards containing known amounts of the elements to be analysed.

5.2.3 Analytical Method

Major cations (Ca, Mg, Na, K), trace cations (Ba, Sr, Mn, Fe, Al, Li) and B and Si were determined directly by ICP-AES. Analysis is carried out on approximately 10 ml of sample acidified to 1% v/v with respect to Aristar HNO_3. The instrument is standardised after not more than 10 samples and quality control checks were run every 20 samples. The control standards were always analysed at the end of the run to check for drift. Reported measurements are based on the average of three replicate analyses.

5.2.4 Data Quality

All species preserved by acidification were considered to be stable over an appreciable length of time and certainly within the delay between sampling and analysis. Wavelengths and conditions of analysis were optimised to ensure that interference effects are minimised for all elements; samples with complex matrices are diluted prior to analysis. The accuracy of the major cation (and anion) determinations can be determined by considering the ionic charge balances.

5.3 Determination of Major and Trace Anions by Ion Chromatography

5.3.1 Instrumentation

The ion chromatography system used for the anion analysis is a Dionex 2000i fitted with an auto sampler. An integral conductivity detection module and an additional on-line Philips PU4110 UV/VIS detector are used for analyte detection. The data were processed using a Dionex advanced computer interface and AI-450 data capture and manipulation software loaded onto a Dell personal computer

5.3.2 Theory

When a solvent containing dissolved anions is passed through a column of anion exchange resin, the progress of the anions through the column are retarded with respect to the solvent. Different anions are retained by different degrees according to their size and charge. The conductivities of the separated anions eluted from the column are detected as transient peaks and quantification may be achieved by comparing the peak area or peak height of the samples to those of known standards. For measurements to be accurate, the high background conductivity of the eluent is removed using chemical suppression. This relies on the exchange of sodium and hydrogen ions across a membrane to convert the sodium carbonate and sodium bicarbonate eluent to weakly conducting carbonic acid, and the weakly conducting anionic salts of the sample to more conductive anionic acids.

5.3.3 Analytical Method

Major and trace anions (Cl^-, SO_4^{2-}, NO_3^-, NO_2^-, and Br^-) are determined using approximately 1 ml of unpreserved sample by ion chromatography. The instrument is calibrated at the start of the run and recalibrated after not more than 33 samples.

Quality control check samples were analysed with each calibration and bracket the analytical samples. The analysis follows a pre-programmed schedule and the data are collected by the software with peaks identified by retention time. Quantitation is performed by comparing peak areas against a quadratic calibration curve based on the peak areas of standards over an appropriate concentration range. All raw data are stored on the computer's hard drive and can, if required, be re-integrated, for example using different standards.

The method is limited by the number of exchange sites available within the column. With the injection loop and column used in this study, solutions with total anion concentrations of up to 500mg/l can be analysed; above this the column becomes overloaded, causing poor peak shapes, variable retention times and thus unreliable results. To overcome this problem, more concentrated solutions are diluted. Dilution is also used to bring the analyte concentration within the concentration range covered by the standards and to reduce sample viscosity.

5.3.4 Data Quality

Most anions are stable in solution for an appreciable length of time and certainly within the delay between sampling and analysis. Nitrate and nitrite may, however, be modified by microbial activity and for this reason samples are analysed by ion chromatography as soon as possible after collection.

5.4 Determination of Fluoride by Ion Selective Electrode

5.4.1 Instrumentation

The analysis is carried out using an Orion Model 94-09 fluoride ion selective electrode with an Orion Model 90-01 single junction reference electrode connected to an Orion Model SA 720 pH/ISE meter.

5.4.2 Theory

The fluoride ion selective electrode is constructed from a calcium fluoride sensing element bonded to an epoxy body. When the sensing element is in contact with a solution containing fluoride an electrode potential develops across the sensing element. The measured potential corresponding to the level of fluoride ion in solution is described by the Nernst equation:

$$E = E_0 + S \log(A)$$

where:

E = measured electrode potential
E_0 = reference potential (a constant)
A = activity of fluoride ion in solution
S = electrode slope (~ -57 mV per decade)

A, the fluoride activity or 'effective concentration', is related to the free concentration, C_f by the activity coefficient, g:

$A = g\ C_f$

Ionic activity coefficients are variable and largely depend on total ionic strength, where total ionic strength is defined as:

$0.5\ S\ (C_iZ_i)^2$

where:

C_i = concentration of ion i
Z_i = charge of ion i

If the background ionic strength is maintained high and constant relative to the sensed concentration, the activity coefficient becomes constant and is directly proportional to the concentration.

The Nernst equation can then be written:

$E\text{-}E_0 = S \log + S \log C_f$

where E_0, S and g are all constants.

The electrode potential relative to the standard reference potential can be plotted against the log of concentration giving a straight line calibration.

Total Ionic Strength Adjustment Buffer (TISAB) is added to all fluoride standard and samples to maintain a high and constant ionic strength relative to the variable concentrations of fluoride. The TISAB also contains a buffer to maintain the pH at about 5.0-5.5 to prevent interferences by complexation of fluoride by hydrogen ions or hydroxide ions at extremes of pH, and a complexing agent (CDTA) to preferentially complex interfering metal ions, particularly iron and aluminium.

5.4.3 Analytical Method

Samples and standards are equilibrated to the same temperature and mixed at a 1:1 ratio with the TISAB buffer. Measurements are made while the samples and standards are being stirred by a magnetic stirrer. The fluoride electrode is calibrated with a series of standards from 0.01 to 100 mg l^{-1} fluoride. The electrode response for samples and QC check standards run at regular intervals is then measured. A calibration curve of log fluoride concentration versus electrode response is plotted, from which values for the samples are determined.

5.4.4 Data Quality

The major source of interference for this analysis is complexation of the fluoride ion which prevents interaction between free fluoride and the electrode and causes a low

result. As discussed in Section 3.5.2, the TISAB is designed to buffer the effects of high and low pH and the CDTA is used to complex preferentially interfering ions such as aluminium and iron. The TISAB should work effectively for levels of Al and Fe up to about 10 mg l^{-1}, above this level low readings may be obtained which become progressively worse as the level of interferent increases.

5.5 Determination of Total Organic and Inorganic Carbon

5.5.1 Instrumentation

Measurements are made on a Shimadzu TOC-5000 total organic carbon analyser fitted with an ASI-5000 autosampler.

5.5.2 Theory

In the measurement of total carbon, pure air carrier gas (containing no CO_2) flows at 150 ml min^{-1} through the Total Carbon (TC) combustion tube, which is packed with Pt-coated alumina catalyst maintained at 680°C by an electrically heated furnace. When the sample enters the TC combustion tube, all of the carbon is oxidised to carbon dioxide and swept out of the tube by the carrier gas into a non-dispersive infrared (NDIR) detector which measures the carbon dioxide concentration by energy absorption. The output analogue signal of the NDIR detector is displayed as a response peak. The area of the peak is proportional to the total carbon concentration. The total carbon in a sample can be determined from the calibration curve prepared using standard solutions containing known amounts of organic and inorganic carbon. The total carbon is the sum of the TOC and the TIC.

In the measurement of inorganic carbon, the sample is injected into the Inorganic Carbon reaction vessel which has carrier gas bubbling through a phosphoric acid reaction solution. The IC reacts with the acid to form carbon dioxide which is detected by the NDIR detector. The inorganic carbon content is the sum of the aqueous carbon dioxide, carbonate and bicarbonate present in solution.

5.5.3 Analytical Method

The instrument is calibrated at 10, 30 and 100mgl^{-1} using separate organic and inorganic carbon standards. Mixed quality control standards containing 5, 25 and 50mgl^{-1} organic and inorganic carbon are analysed every 10 samples. Approximately 5 ml of unpreserved sample is used for each analysis. Samples exceeding the top calibration standard are automatically re-injected at a smaller volume to bring them into the calibration range.

5.5.4 Data Quality

TOC and TIC are stable for short periods of time if the sample is stored at <4°C although every effort was made to analyse the samples as soon as possible after collection. The method is essentially interference free as long as the IC or OC is 100% converted to CO_2 during the two different oxidation procedures. This has been

thoroughly investigated by the instrument manufacturer and is also verified by the external check standards that are run.

5.6 Determination of Stable Oxygen and Hydrogen Isotopes

5.6.1 Instrumentation

The isotopic ratios are determined with a VG-Isogas 602E dual-inlet twin analyser gas source mass spectrometer dedicated to stable isotope ratio measurements on approximately 5 ml of sample. The mass spectrometer is equipped with a 24-position inlet manifold with computer controlled valves, which enables continuous unsupervised analysis of a batch of 24 samples/standards. Data are collected on an on-line HP85 microcomputer.

5.6.2 Theory

The purpose of this analysis is to measure the ratios of the stable oxygen and hydrogen isotopes, $^{18}O/^{16}O$ and $^{2}H/^{1}H$, making up the water sample. The measurement is carried out by mass spectrometry on carbon dioxide and hydrogen gases, for O and H respectively, which are prepared from the original water sample. The methods of preparation are crucial to eliminate any possibility of random isotopic fractionation; this is assured by quantitative transfers of O and H within the preparation procedures. The measurements of $^{18}O/^{16}O$ and $^{2}H/^{1}H$ are carried out on a special mass spectrometer which has a double collector arrangement for the two nuclides in each case (e.g. masses 46 and 44 in the case of ^{18}O and ^{16}O) and also a dual inlet system to permit the rapid switching between the sample gas and a standard gas having calibrated $^{18}O/^{16}O$ or $^{2}H/^{1}H$ ratios. Thus the design of the instrument and the mode of operation reduces considerably the effects of instrumental variability on the precision of isotope ratio measurements. The precision of $^{18}O/^{16}O$ and $^{2}H/^{1}H$ measurements is thus very high when measured as deviation from ratios of a standard. The standard against which all environmental water samples are measured is the international SMOW (Standard Mean Ocean Water) standard, with a further standard being the SLAP (Standard Light Antarctic Precipitation) which ensures precision in the scale (the SMOW-SLAP scale) quoted from different laboratories.

5.6.3 Analytical Method

The VG-Isogas 602E dual-inlet twin analyser gas source mass spectrometer is a Siamese instrument, which means that it has two analysers - one for hydrogen, and one for all the other gases. The general operating principles are the same whichever head is in use. Sample and reference gases are separately admitted via a double inlet system through a balanced capillary leak to a changeover valve and on to the ion source or to waste. While one gas is being measured the other is bled to waste, each gas being regularly alternated by automatic operation of this changeover valve. The major and minor isotope ion beams produced at the ion source are focused and passed along a tube through a 90° bend of radius 60 mm between the poles of a magnet. The resulting deflections cause a separation of the two beams which are individually detected and amplified. The signals are fed into the ratio integrator unit which ratios

the minor signal over the major for each gas alternately, giving both printout and digital readout.

5.6.4 Data Quality

Analysis is generally completed within two months of the receipt of the samples, although samples are stored under conditions such that the delay has no affect on the data quality.

The absolute accuracy is determined by the inclusion in each batch of samples analysed, a working standard water (the WTW standard); this in turn has been calibrated against the SMOW-SLAP standards).

The overall method precision (2s) achieved is estimated to be better than ±4‰ $\delta^{2}H$ or ±0.2‰ $\delta^{18}O$, retrospectively based on the repeated determination of an independent QC standard.

5.7 Determination of Cation Exchange Capacity (CEC)

Cation exchange capacity is determined on the milled core (as described for aqueous leaching). The technique is based on the compulsive exchange between an aqueous solution of magnesium sulphate and a barium soil as described by Bascomb (1964). The cation exchange sites on the sample are saturated with barium, supplied as barium chloride solution, and excess reagent is removed by washing. Magnesium sulphate solution is added and the displace barium removed as insoluble barium sulphate; the excess magnesium is determined by titrating with EDTA.

6. RESULTS

The extraction protocol originally envisaged was: (i) pore water from one or at most two samples of clay material from the fault would be extracted by squeezing; (ii) pore-water from the surrounding sandstones and conglomerates would be extracted by displacement centrifugation; (iii) variable ratio aqueous leaching would be carried out on the clay material for comparison with extracted pore-waters.

More clayey material of suitable composition for squeezing was obtained then was originally envisaged. Therefore, three samples were tested by squeezing and each successfully yielded pore-water. Details of the samples tested and the geotechnical squeezing conditions are given in Table 3.

Sufficient pore-water was obtained to analyse all three sample for the full suite of chemical constituents. It was possible to determine stable oxygen and hydrogen isotopes on two of the samples. Insufficient volume of sample was obtained to enable the determination of strontium or sulphur isotopes, ^{36}Cl or tritium. Chemical data for the extracted pore-waters is presented in Table 4.

Eight samples of sandstones and conglomerates were tested by centrifugation but, surprisingly, failed to yield pore-water. The inability of the samples to yield pore-water resulted from the lower than expected porosity. Because of the failure of the centrifugation technique, the only method available to characterise the non-clayey material was aqueous leaching. Six samples were therefore tested using a constant ratio method. One sample was tested in duplicate.

The seven leachate samples were re-tested and re-analysed because of problems with the analytical charge balances. The data have been reported separately because of the interesting variations arising from the filtration of fine suspended matter. All uncorrected aqueous leachate data are reported in Table 5. The data after subsequent correction, using the formula given in Section 4.3.3 to give an equivalent concentration, are reported in Table 6. It should be noted that the data are not representative of in-situ pore water compositions, except possibly for the conservative species (e.g. Cl), because of water-rock interactions occuring during the leaching process.

Three core samples were tested for cation exchange capacity (CEC) according to the method described in Section 5.7. Data are presented in Table 7.

Because of problems with the drilling fluid tracer experienced on-site, it was necessary to obtain data on the drilling fluid returns of relevance to the extracted pore-waters. A total of 13 drilling fluid samples have been analysed for the basic inorganic chemistry. Details of the samples tested are given in Table 2 and the chemical data are presented in Table 8.

7. DISCUSSION

The chemical composition data obtained from mechanically squeezed pore-waters, aqueous leachates of core material and the drilling fluids are made up from a mixture of residual solutes from the pore-water, rock dissolution products and drilling fluid residues. As this study is aimed at obtaining the chemical composition of the pore-water, it is necessary to correct for these contamination effects.

The addition of a chemical tracer to the drilling fluid and its measurement in the groundwater samples is the normal method for calculating the contamination in pore-waters collected during a drilling programme. In this study, however, quantitative data on the amount of drilling fluid in the pore-waters was not available as the choice of a drilling fluid tracer was not compatible with the formation under test.

In order to allow some interpretation of the data to be carried out it was necessary to use a different method to calculate pore-water/groundwater compositions from the available data. Cave and Reeder (1996) have suggested that chemometric data processing can be used to calculate pore-water compositions from aqueous leachate data and contaminated pore-water data. An improved method for chemometric resolution of geochemical mixtures has recently been described by Cave and Wragg (1997). By combining the data from the pore-waters, aqueous leachates of core

material and the drilling fluids (Tables 4, 5 and 8) and using the mixture resolution method of Cave and Wragg (1977), an attempt has been made to identify and quantify the *in-situ* pore-water composition. It must be noted, however, that this type of data processing usually requires at least 50 to100 data points to arrive at a stable solution but that there are only 32 data points in this study. Some caution in interpretation of the results should therefore be exercised.

The data processing technique has identified eight separate components within the data set, the chemical compositions for which are given in Figure 2. The relative quantities of each component in each sample type are given in Figure 3 (black squares are squeezed pore-waters, dark grey squares are drilling fluids and pale grey squares are drilling fluids). The total dissolved solids content of each component for the leachates calculated back to the pore-water compositions (filled circles) and the squeezed pore-waters (filled triangles) are shown as borehole distance profiles in Figure 4.

In identifying which of the eight components are derived from pore-water residual solutes, the following criteria are relevant:

1. The chemical composition of any pore-water component must be compatible with known groundwater compositions in the area (Figure 2);

2. Is likely to have a relatively high contribution to the squeezed pore-water data (Figure 3);

3. Any pore-water component is likely to have similar total dissolved solids content in both the pore-water samples and the leachate sample (Figure 4).

Using these criteria, each of the eight component identified by the mixture resolution procedure may be considered in turn.

Component 1 is occurs in all sample types (Figure 3) and consists of bicarbonate and TOC (Figure 2). The source of this component is not entirely clear but it possibly reflects sample contamination.

Component 2 occurs mainly in the leachate samples (Figure 3) which suggests that this is a rock dissolution component.

Component 3 occurs mainly in one of the pore-waters and in the two drilling fluid make up waters (Figure 3) and is possibly a drilling fluid component.

Component 4 mainly occurs in the drilling fluid samples (Figure 3) and probably arises from the drilling fluid.

Component 5 is dominant in the squeezed pore-waters and to a much lesser extent in the drilling fluids and leachates (Figure 3). The total dissolved solids in the reconstructed leachate data are in relatively close agreement with the pore-water data (Figure 4). The chemical composition of this component (Figure 2) is reasonably

typical of pore-water. This suggests that this component may be derived from the pore-water.

Component 6 occurs mostly in the drilling fluids and aqueous leachates (Figure 3) and has a chemical composition consisting mainly of Ca and bicarbonate, suggesting that this component is derived from dissolution of calcite.

Component 7 has its highest abundance in the leachate samples (Figure 3) and is probably a rock water interaction component.

Component 8 occurs mainly in the squeezed pore-waters but also in the drilling fluids and leachates (Figure 3). The total dissolved solids in the reconstructed leachate data is in relatively close agreement with the pore-water data (Figure 4). This suggests that this component may also derived from pore-water.

If it is assumed that components 5 and 8 are derived from pore-waters, then the profiles given in Figure 4 suggest that a Na - HCO_3 - F water dominates on the tunnel side of the fault gouge and a Na - SO_4 water dominates on the other side of the gouge. This interpretation, however, should be treated with caution as the chemometric model may not be particularly rugged because of the relatively small data set used.

8. ACKNOWLEDGEMENTS

The authors would like to thank Mr M A Allen and the staff of the British Geological Survey Sample Preparation and Testing Facility for their assistance in the preparation of core material for the leaching studies.

9. REFERENCES

Baeyens B and Bradbury M H. 1994. Physico chemical characterisation and calculated in situ pore-water chemistries for a low permeability Pafris marl sample from Wellenburg. Paul Scherrer Institut Technical Report 94-19.

Bascomb C L. 1964. Rapid method for the determination of cation exchange capacity of calcareous and non-calcareous soils. *Journal of the Science of Food and Agriculture*, **15**, 821-823.

Bath A H, Ross C A M, Entwisle D C, Cave M R, Fry M B, Green K A and Reeder S. 1989. Hydrochemistry of pore-waters from London Clay, Lower London Tertiaries and Chalk at the Bradwell site, Essex. Nirex Safety Studies Research Report NSS/R170.

Brightman M A, Bath A H, Cave M R and Darling W G. 1985. Pore fluids from the argillaceous rocks of the Harwell region. British Geological Technical Report FLPU 85-6.

Cave M R, Reeder S, Entwisle D C, Blackwell P A, Trick J K, Wragg J and Vickers B P. 1996. Chemical Characterisation of Squeezed Pore-waters and Aqueous Leachates from Opalinus Marl Core Material from the Mount Terri Tunnel, Switzerland. British Geological Survey Technical Report WI/96/12C.

Cave M R and Reeder S. 1996. Reconstruction of In-Situ Pore-Water Compositions Obtained by Aqueous Leaching of Drill Core: An Evaluation Using Multivariate Statistical Deconvolution. *Analyst*, **120**, 1341-1351.

Cave M R and Wragg J. 1997. Measurement of Trace Element Distributions in Soils and Sediments Using Sequential Leach Data and a Non-specific Extraction System with Chemometric Data Processing. *Analyst*, **122**, 1211-11221.

Couture R A, Seitz M G and Steindler M J. 1983. Sampling of brine cores of Pre-Cambrian Granite from Northern Illinois. *Journal of Geophysical Research*, **88**, 7331-7334.

Couture R A and Seitz M G. 1986. Movement of fossil pore fluids in Granite Basement, Illinois. *Geology*, **14**, 831-834.

Edmunds W M and Bath A H. 1976. Centrifuge extraction and chemical analysis of interstitial waters. *Environmental Science and Technology*, **10**, 467-472.

Entwisle D C, Reeder S, Bath A H and Ross C A M. 1989. Techniques for the characterisation of solutes in drillcore from mudrocks. British Geological Survey Technical Report WE/89/29.

Entwisle D C and Reeder S. 1993. New apparatus for pore fluid extraction from mudrocks. In: Manning D C, Hall P L and Hughes C R (Eds) Geochemistry of Clay-

Pore Fluid Interactions. The Mineralogical Society Series Volume 4, Chapman and Hall, London. pp 365-388.

Fontanive A, Gragnani R, Mignuzzi C. and Spat G. 1993. Chemical compositions of pore-waters in Italian Plio-Pleistocene clayey formations. In: Manning D C, Hall P L and Hughes C R (Eds) Geochemistry of Clay-Pore Fluid Interactions. The Mineralogical Society Series Volume 4, Chapman and Hall, London. pp 389-410.

Gautschi A, Ross C A M and Scholtis A. 1992. Pore-water - groundwater relationships in Jurassic shales and limestones of northern Switzerland. In: Manning D C, Hall P L and Hughes C R (Eds) Geochemistry of Clay-Pore Fluid Interactions. The Mineralogical Society Series Volume 4, Chapman and Hall, London. pp 412-422.

Kinniburgh and Miles D L. 1983. Extraction and chemical analysis of interstitial water from soils and rocks. *Environmental Science and Technology*, **17**, 6, 362-368.

Kriukov P A. 1947. Methods of contracting soil solutions in modern methods for physiochemical studies of soils. V2, pp3-15, Moscow.

Manheim F T. 1966. A hydraulic squeezer for obtaining interstitial water from consolidated and unconsolidated sediments. United States Geological Survey, Professional Papers 550-556, USGS, Washington, pp 256-261.

Metcalfe R, Cave M R, Reeder S, Green K A and Entwisle D C. 1996. Fault-controlled Groundwater Flow in Mudrocks at Down Ampney, UK: Geochemical evidence. Fluid Flow Through Faults and Fractures in Argillaceous Formation; A joint NEA/EC Workshop, Berne, Switzerland, 10-12 June.

Spears D A. 1976. Information on groundwater composition obtained from a laboratory study of sediment-water interaction. *Quarterly Journal of Engineering Geology*, **9**, 25-36.

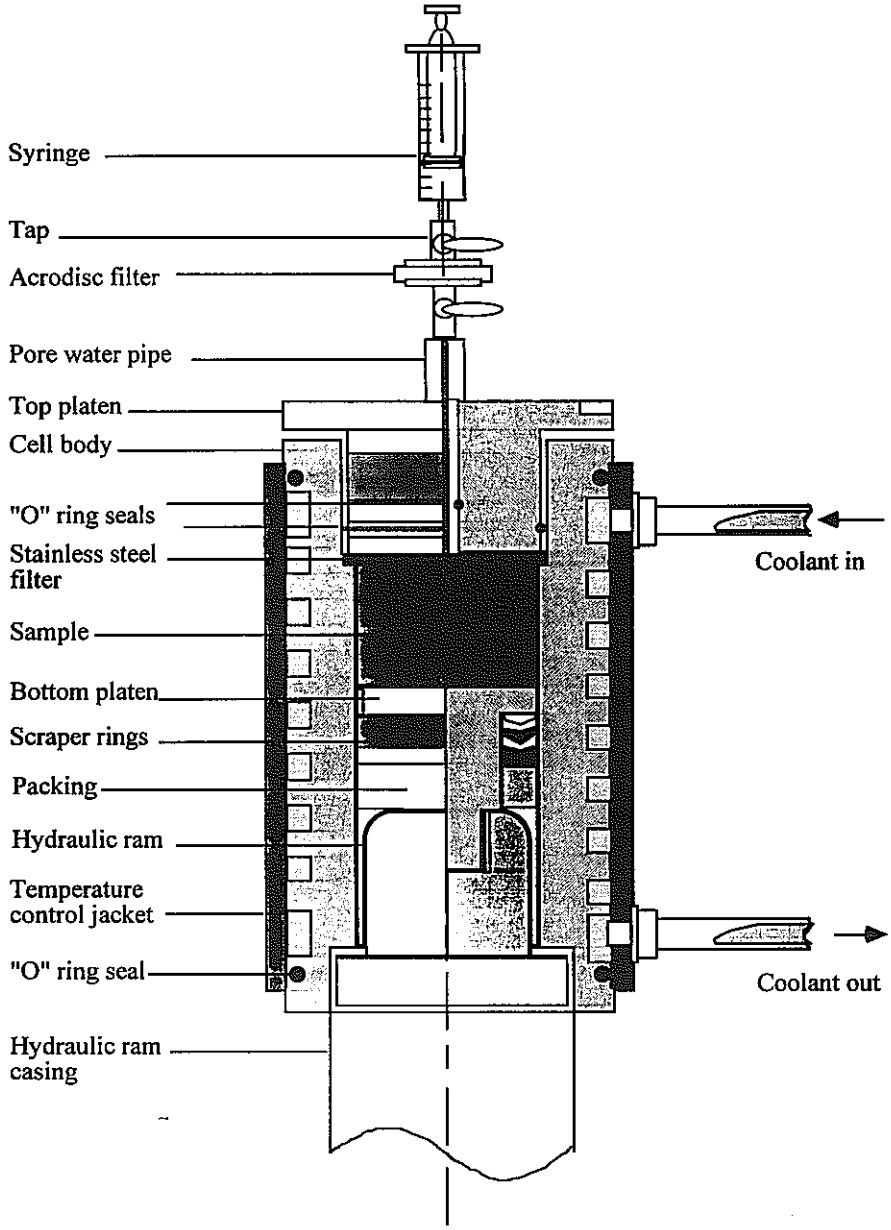

Figure 1. Schematic Diagram of the Squeezing Cell Body

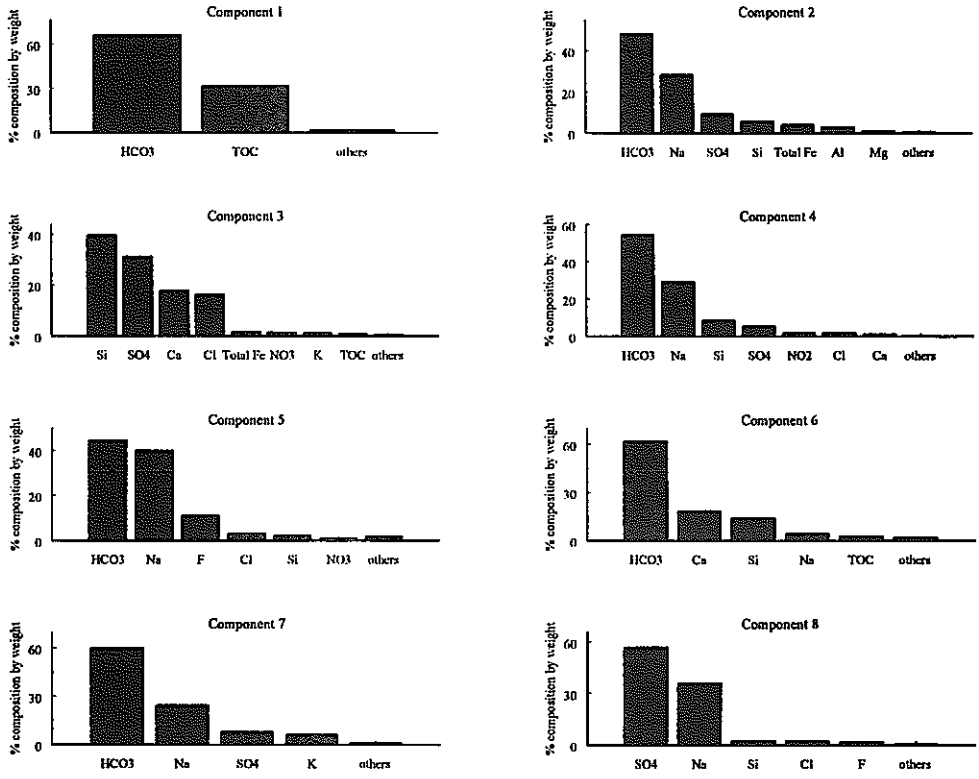

Figure 2. Chemical compositions of resolved components

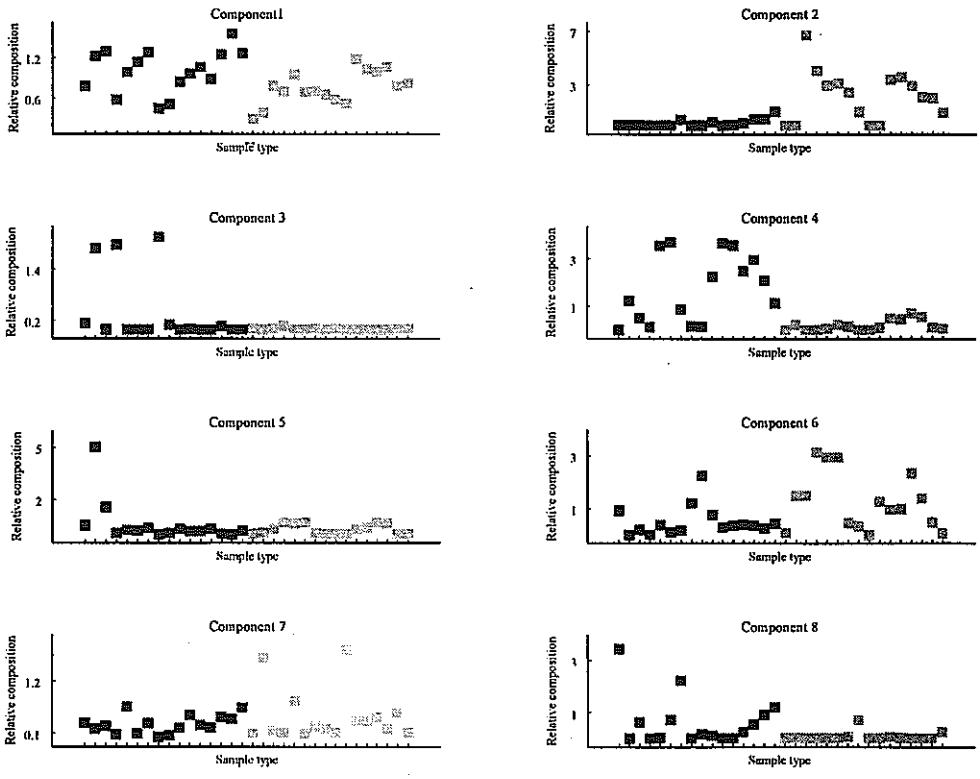

Figure 3. Relative contributions of each component to sample type

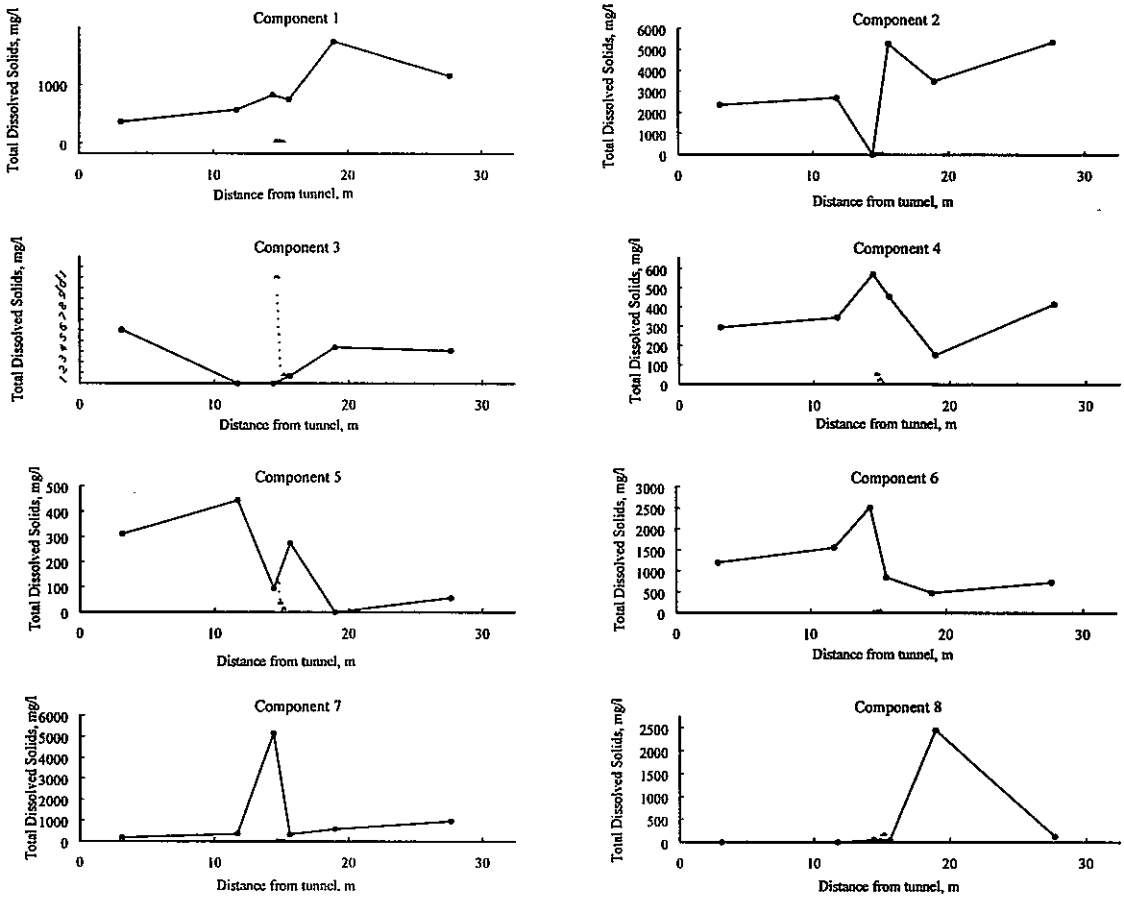

Figure 4. Total dissolved solids profiles for each resolved component

Table 1. Summary of Core Samples Provided and Test Methods

Sample Code	Test
3.00-3.25	Aqueous Leaching
11.19-11.41	Not Tested
11.41-11.59	Not Tested
11.59-11.90	Aqueous Leaching
13.85-14.25	Not Tested
14.25-14.60	Aqueous Leaching
14.60-14.79	Squeezing/Cation Exchange Capacity
14.79-15.04	Squeezing/Cation Exchange Capacity
15.04-15.30	Squeezing/Cation Exchange Capacity
15.30-15.50	Not Tested
15.50-15.74	Aqueous Leaching
17.62-17.86	Not Tested
18.83-19.10	Aqueous Leaching
27.55-27.85	Aqueous Leaching

Table 2. Summary of Drilling Fluid Samples

Sample Code	Date/Time Collected	Sample Type	Test
7	01/07/1997 15:00	return water	Not analysed
8	01/07/1997 15:50	tank 1	Not analysed
11		make up 3	Analysed
12		make up 4	Analysed
13	02/07/1997 11:05	tank 1	Not analysed
14	02/07/1997 11:05	tank 2	Not analysed
15	02/07/1997 11:05	return water	Analysed
16	02/07/1997 13:30	return water	Not analysed
17	02/07/1997 15:30	tank 1	Not analysed
18	03/07/1997 09:15	return water	Not analysed
19	03/07/1997 10:15	return water	Analysed
20	03/07/1997 13:20	return water	Analysed
21	03/07/1997 14:45	return water	Analysed
22	04/07/1997 10:00	return water	Analysed
23	04/07/1997 10:35	return water	Analysed
24	04/07/1997 13:25	return water	Analysed
25	07/07/1997 10:40	tank 1	Not analysed
26	07/07/1997 10:40	tank 2	Not analysed
27	07/07/1997 10:55	return water	Analysed
29	07/07/1997 13:40	return water	Not analysed
30	07/07/1997 14:45	return water	Analysed
31	08/07/1997 09:27	return water	Not analysed
32	08/07/1997 10:50	return water	Analysed
33	08/07/1997 13:40	return water	Not analysed
35	09/07/1997 09:40	return water	Not analysed
37	09/07/1997 11:00	return water	Analysed

Table 3. Geophysical Data for Samples Extracted by Mechanical Squeezing

Sample code	Pore fluid extracted (g)	Moisture content %		Max Stress (Mpa)	Time (Hrs)		Moisture content %
		Initial	Final		Increment	Total	
14.60-14.79	18.78	16.99	12.37	2	16:47	16:47	18.66
				5	25:13	42:00	
				10	22:48	64:48	
				20	72:02	156:50	
				30	24:48	181:38	
14.79-15.04	27.12	37.25	27.20	2	0:22	0:22	38.84
				5	15:32	15:54	
				10	25:13	41:07	
				20	22:48	63:55	
				40	24:42	88:37	
15.04-15.30	9.06	23.35	14.16	5	15:22	15:22	23.79
				10	6:55	22:17	
				20	18:18	40:35	
				30	22:50	63:25	
				45	72:15	155:40	
				60	6:30	162:10	

14.60-14.79 Firm, pale green, slickensided clay/rock particles with white streaks. Fault gauge.
14.79-15.04 Dark grey, mudstone with white veins, slickedsided fault zone material.
15.04-15.30 Dark grey, mudstone with white veins.

Table 4. Pore-Water Chemistry Data for Samples Extracted by Mechanical Squeezing

		Sample Code		
		14.60-14.79	**14.79-15.04**	**15.04-15.30**
pH		8.14	7.96	7.47
Ca	mg/l	0.76	0.25	1.44
Mg	mg/l	0.32	0.29	0.58
Na	mg/l	49.9	31.9	62.9
K	mg/l	<1.00	<1.00	<1.67
HCO_3	mg/l	79.0	48.3	30.6
Cl	mg/l	6.33	2.62	3.67
SO_4	mg/l	7.42	10.4	97.5
NO_3	mg/l	1.84	0.67	<0.20
Br	mg/l	<0.06	<0.03	<0.06
NO_2	mg/l	1.24	0.40	0.19
F	mg/l	12.0	5.09	4.26
TOC	mg/l	9.03	9.10	6.35
TIC	mg/l	13.4	8.59	6.43
Si	mg/l	6.87	6.07	5.80
Ba	mg/l	0.086	<0.002	<0.003
Sr	mg/l	0.016	0.008	0.022
Mn	mg/l	<0.002	<0.002	<0.003
Total Fe	mg/l	<0.02	<0.02	<0.03
Al	mg/l	0.23	0.12	0.16
Li	mg/l	<0.04	<0.04	<0.06
B	mg/l	1.03	0.56	0.50
δ^2H	‰ wrt SMOW	-56	-59	n/s
$\delta^{18}O$	‰ wrt SMOW	-8.9	-9.1	n/s
Balance	%	-1.17	2.39	0.19

Table 5a.Uncorrected Aqueous Leachate Data

Sample Code	Weight sample (g)	Weight water (g)	pH	Ca (mg/l)	Mg (mg/l)	Na (mg/l)	K (mg/l)	HCO_3 (mg/l)	Cl (mg/l)	SO_4 (mg/l)
DI water blank	0.0000	30.0431	5.85	0.31	<0.10	<0.10	<0.50	<20	0.17	<0.10
3.00-3.25	5.0087	30.0080	10.0	11.8	2.25	41.3	<2.00	115	0.48	1.11
11.59-11.90a	4.9979	30.0298	9.35	11.5	1.75	39.7	<4.00	108	0.25	1.68
11.59-11.90b	4.9984	30.0088	9.14	11.7	1.70	39.4	<1.00	104	0.29	1.57
14.25-14.60	5.0105	30.0675	7.87	5.56	<0.10	19.9	3.36	64	0.57	4.42
15.50-15.74	5.0028	30.0672	9.03	6.83	3.60	53.8	<1.00	123	0.59	18.7
18.83-19.10	5.0005	30.0325	7.89	1.90	0.50	23.6	<1.00	<40	0.83	23.3
27.55-27.85	5.0027	30.0855	8.06	2.94	0.90	24.5	<1.00	56	1.05	7.53
DI water blank	0.0000	36.0218	5.01	<0.05	<0.10	<0.10	<0.50	<20	0.16	<0.10
3.00-3.25	6.0158	36.1053	10.4	8.32	1.50	49.6	1.29	133	0.54	1.16
11.59-11.90	6.0063	36.0422	9.34	5.65	1.10	35.1	0.75	103	0.38	1.65
14.25-14.60	6.0080	36.1166	7.94	4.81	0.10	14.7	3.82	56	0.62	3.55
15.50-15.74a	6.0214	36.1661	9.10	4.69	1.60	48.4	0.68	132	0.47	19.3
15.50-15.74b	6.0048	35.9972	9.14	4.74	1.70	47.9	0.64	134	0.39	19.3
18.83-19.10	6.0262	36.1884	7.56	0.99	0.40	12.1	<0.50	24	0.70	10.8
27.55-27.85	6.0095	36.0145	7.89	2.70	0.80	21.4	1.04	58	0.90	6.35

Sample Code	Weight sample (g)	Weight water (g)	NO_3 (mg/l)	Br (mg/l)	NO_2 (mg/l)	F (mg/l)	TOC (mg/l)	TIC (mg/l)	Si (mg/l)	Ba (mg/l)
DI water blank	0.0000	30.0431	0.10	<0.03	<0.02	<0.05	2.12	<0.50	<0.02	<0.001
3.00-3.25	5.0087	30.0080	0.34	<0.03	0.11	1.66	6.57	9.42	20.4	0.003
11.59-11.90a	4.9979	30.0298	0.42	<0.03	0.14	1.46	8.20	16.1	16.1	0.002
11.59-11.90b	4.9984	30.0088	0.34	<0.03	0.12	1.47	6.50	16.1	16.3	0.003
14.25-14.60	5.0105	30.0675	0.11	<0.03	0.07	0.19	3.40	11.5	4.98	0.004
15.50-15.74	5.0028	30.0672	0.23	<0.03	0.11	0.75	5.96	21.0	11.1	<0.001
18.83-19.10	5.0005	30.0325	0.10	<0.03	0.08	0.27	4.96	5.61	4.32	0.001
27.55-27.85	5.0027	30.0855	0.17	<0.03	0.08	0.28	4.79	10.2	5.38	0.001
DI water blank	0.0000	36.0218	<0.10	<0.03	<0.02	<0.05	3.99	1.58	<0.02	<0.001
3.00-3.25	6.0158	36.1053	0.25	<0.03	0.02	1.75	8.27	11.4	24.9	<0.001
11.59-11.90	6.0063	36.0422	0.35	<0.03	0.06	1.55	8.48	15.0	13.1	0.001
14.25-14.60	6.0080	36.1166	<0.10	<0.03	0.02	0.21	4.29	10.0	4.65	0.004
15.50-15.74a	6.0214	36.1661	0.19	<0.03	0.02	0.83	8.49	20.4	7.14	<0.001
15.50-15.74b	6.0048	35.9972	0.15	<0.03	<0.02	0.91	7.42	20.5	6.86	<0.001
18.83-19.10	6.0262	36.1884	<0.10	<0.03	0.02	0.29	5.53	5.32	3.97	<0.001
27.55-27.85	6.0095	36.0145	0.10	<0.03	0.03	0.34	5.34	9.83	5.46	<0.001

NB: Aqueous leachates prepared and analysed twice because of analytical anomalies. Data are not necessarily representative of *in-situ* pore-water compositions. Samples marked a and b are duplicate determinations. See text for further details.

Table 5b. Uncorrected Aqueous Leachate Data (continued)

Sample Code	Weight sample (g)	Weight water (g)	Sr (mg/l)	Mn (mg/l)	Tot Fe (mg/l)	Al (mg/l)	Li (mg/l)	B (mg/l)	Balance (%)
DI water blank	0.0000	30.0431	0.002	0.003	<0.01	<0.02	<0.005	<0.05	42.24
3.00-3.25	5.0087	30.0080	0.021	0.107	3.43	5.39	<0.005	0.49	25.09
11.59-11.90a	4.9979	30.0298	0.018	0.064	2.51	4.26	<0.005	0.42	23.42
11.59-11.90b	4.9984	30.0088	0.018	0.063	2.50	4.25	<0.010	0.41	24.77
14.25-14.60	5.0105	30.0675	0.009	0.003	0.09	0.16	0.016	0.08	3.33
15.50-15.74	5.0028	30.0672	0.011	0.156	9.98	5.73	0.012	0.24	25.45
18.83-19.10	5.0005	30.0325	0.004	0.029	1.46	1.22	0.010	0.05	44.84
27.55-27.85	5.0027	30.0855	0.003	0.068	3.84	2.14	0.017	0.07	21.52
DI water blank	0.0000	36.0218	<0.001	<0.001	<0.01	<0.02	<0.005	<0.05	-100.00
3.00-3.25	6.0158	36.1053	0.016	0.061	2.33	3.78	<0.005	0.44	17.35
11.59-11.90	6.0063	36.0422	0.009	0.032	1.55	2.80	<0.005	0.32	12.01
14.25-14.60	6.0080	36.1166	0.008	0.002	0.12	0.16	0.009	0.06	-0.77
15.50-15.74a	6.0214	36.1661	0.006	0.067	4.25	2.89	0.009	0.19	7.30
15.50-15.74b	6.0048	35.9972	0.006	0.072	4.58	3.01	0.011	0.18	7.03
18.83-19.10	6.0262	36.1884	0.002	0.022	1.15	1.14	0.008	<0.05	10.23
27.55-27.85	6.0095	36.0145	0.003	0.056	3.08	1.93	0.014	0.05	15.36

NB: Aqueous leachates prepared and analysed twice because of analytical anomalies. Data are not necessarily representative of *in-situ* pore-water compositions. Samples marked a and b are duplicate determinations. See text for further details.

Table 6a. Corrected Aqueous Leachate Data

Sample Code	Weight sample (g)	Weight water (g)	Moisture content (%)	MC temp (°C)	Ca (mg/l)	Mg (mg/l)	Na (mg/l)	K (mg/l)	HCO_3 (mg/l)	Cl (mg/l)	SO_4 (mg/l)
3.00-3.25	5.0087	30.0080	5.45	110	210	55.1	2602	<110	<4412	91.9	2565
11.59-11.90a	4.9979	30.0298	7.01	40	476	<8.56	1706	287	5501	48.7	378
11.59-11.90b	4.9984	30.0088	17.12	40	240	126	1887	<35.1	4323	20.8	655
14.25-14.60	5.0105	30.0675	29.45	110	239	45.8	840	<40.7	2331	9.76	22.6
15.50-15.74	5.0028	30.0672	20.05	40	345	52.4	1189	<120	3232	7.41	50.5
18.83-19.10	5.0005	30.0325	20.05	40	349	50.9	1181	<29.9	3126	8.70	47.0
27.55-27.85	5.0027	30.0855	8.23	40	215	65.8	1791	<73.1	4082	77.1	551
3.00-3.25	6.0158	36.1053	29.45	110	170	30.6	1011	26.3	2701	11.1	23.6
11.59-11.90	6.0063	36.0422	20.05	40	169	32.9	1050	22.4	3076	11.4	49.5
14.25-14.60	6.0080	36.1166	7.01	40	412	8.57	1260	327	4834	52.8	304
15.50-15.74a	6.0214	36.1661	17.12	40	165	56.1	1698	23.9	4634	16.3	677
15.50-15.74b	6.0048	35.9972	17.12	40	166	59.5	1677	22.4	4693	13.6	675
18.83-19.10	6.0262	36.1884	5.45	110	109	44.1	1334	<55.1	2625	76.9	1194
27.55-27.85	6.0095	36.0145	8.23	40	197	58.3	1559	75.8	4241	65.5	463

Sample Code	Weight sample (g)	Weight water (g)	Moisture content (%)	MC temp (°C)	NO_3 (mg/l)	Br (mg/l)	NO_2 (mg/l)	F (mg/l)	TOC (mg/l)	TIC (mg/l)	Si (mg/l)
3.00-3.25	5.0087	30.0080	5.45	110	11.5	<3.31	8.60	29.4	547	619	476
11.59-11.90a	4.9979	30.0298	7.01	40	9.24	<2.57	6.41	16.1	291	984	426
11.59-11.90b	4.9984	30.0088	17.12	40	8.08	<1.05	4.02	26.4	209	738	389
14.25-14.60	5.0105	30.0675	29.45	110	6.96	<0.61	2.16	33.8	134	192	414
15.50-15.74	5.0028	30.0672	20.05	40	12.6	<0.90	4.28	43.8	246	482	482
18.83-19.10	5.0005	30.0325	20.05	40	10.2	<0.90	3.67	43.9	194	482	488
27.55-27.85	5.0027	30.0855	8.23	40	12.7	<2.19	5.58	20.5	350	746	393
3.00-3.25	6.0158	36.1053	29.45	110	5.02	<0.61	0.45	35.6	169	233	506
11.59-11.90	6.0063	36.0422	20.05	40	10.6	<0.90	1.65	46.3	254	447	393
14.25-14.60	6.0080	36.1166	7.01	40	<8.57	<2.57	1.94	17.6	368	861	399
15.50-15.74a	6.0214	36.1661	17.12	40	6.83	<1.05	0.80	29.3	298	716	250
15.50-15.74b	6.0048	35.9972	17.12	40	5.18	<1.05	<0.70	31.7	260	718	240
18.83-19.10	6.0262	36.1884	5.45	110	<11.0	<3.31	2.55	31.8	610	587	438
27.55-27.85	6.0095	36.0145	8.23	40	7.61	<2.19	1.90	24.8	389	716	398

NB: Aqueous leachates prepared and analysed twice because of analytical anomalies. Data are not necessarily representative of *in-situ* pore-water compositions. Samples marked a and b are duplicate determinations. See text for further details.

Table 6b. Corrected Aqueous Leachate Data (continued)

Sample Code	Weight sample (g)	Weight water (g)	Moisture content (%)	MC temp (°C)	Ba (mg/l)	Sr (mg/l)	Mn (mg/l)	Total Fe (mg/l)	Al (mg/l)	Li (mg/l)	B (mg/l)
3.00-3.25	5.0087	30.0080	5.45	110	0.110	0.441	3.20	161	135	1.10	5.96
11.59-11.90a	4.9979	30.0298	7.01	40	0.342	0.770	0.26	7.44	13.7	1.37	6.93
11.59-11.90b	4.9984	30.0088	17.12	40	<0.04	0.386	5.48	350	201	0.42	8.56
14.25-14.60	5.0105	30.0675	29.45	110	0.061	0.427	2.18	69.9	110	<0.10	10.1
15.50-15.74	5.0028	30.0672	20.05	40	0.060	0.539	1.92	75.2	128	<0.15	12.4
18.83-19.10	5.0005	30.0325	20.05	40	0.090	0.539	1.89	74.9	127	<0.30	12.2
27.55-27.85	5.0027	30.0855	8.23	40	0.073	0.219	4.97	281	156	1.24	5.34
3.00-3.25	6.0158	36.1053	29.45	110	<0.02	0.326	1.23	47.5	77.0	<0.10	8.95
11.59-11.90	6.0063	36.0422	20.05	40	0.030	0.269	0.96	46.3	83.8	<0.15	9.70
14.25-14.60	6.0080	36.1166	7.01	40	0.343	0.686	0.17	10.0	13.7	0.77	5.14
15.50-15.74a	6.0214	36.1661	17.12	40	<0.04	0.210	2.35	149	101	0.32	6.49
15.50-15.74b	6.0048	35.9972	17.12	40	<0.04	0.210	2.52	160	105	0.39	6.13
18.83-19.10	6.0262	36.1884	5.45	110	<0.11	0.221	2.43	127	126	0.88	<5.51
27.55-27.85	6.0095	36.0145	8.23	40	<0.07	0.219	4.08	224	141	1.02	3.64

NB: Aqueous leachates prepared and analysed twice because of analytical anomalies. Data are not necessarily representative of *in-situ* pore-water compositions. Samples marked a and b are duplicate determinations. See text for further details.

Table 7. Cation Exchange Capacity (CEC) Data for Core Samples

Sample Code	Cation Exchange Capacity
	meq/100g
14.60-14.79	32.2
14.79-15.04	53.4
15.04-15.30	49.5

Table 8. Chemical Analysis of Drilling Fluid Samples

Sample Code	Date/Time Collected	Sample Type	pH	Ca (mg/l)	Mg (mg/l)	Na (mg/l)	K (mg/l)	HCO_3 (mg/l)	Cl (mg/l)	SO_4 (mg/l)	NO_3 (mg/l)
11		make up 3	7.07	1.32	<0.10	0.22	0.59	<20	1.95	1.79	0.39
12		make up 4	7.40	6.89	<0.10	<0.02	<0.50	24	1.40	1.93	0.29
15	02/07/97 11:05	return	7.48	8.83	<0.10	2.85	<0.50	34	1.24	2.40	0.28
19	03/07/97 10:15	return	10.1	3.54	<0.10	36.8	<0.50	86	2.13	6.85	0.48
20	03/07/97 13:20	return	10.2	2.85	<0.10	43.8	1.22	106	3.33	9.92	0.37
21	03/07/97 14:45	return	10.5	2.97	<0.10	42.8	1.24	107	2.58	7.33	0.57
22	04/07/97 10:00	return	10.3	2.61	<0.10	42.0	0.93	105	2.17	9.37	0.33
23	04/07/97 10:35	return	10.2	2.70	<0.10	43.6	0.92	86	1.85	12.2	<0.20
24	04/07/97 13:25	return	10.1	2.39	<0.10	49.4	<0.50	86	3.76	29.6	0.28
27	07/07/97 10:55	return	10.1	2.95	<0.10	42.9	1.05	88	3.81	19.2	0.22
30	07/07/97 14:45	return	10.0	2.58	<0.10	44.1	1.00	83	2.93	29.0	<0.20
32	08/07/97 10:50	return	9.85	2.98	<0.10	46.0	1.15	87	3.78	33.1	<0.20
37	09/07/97 11:00	return	9.06	2.37	<0.10	58.8	0.90	68	4.19	63.1	0.23

Sample Code	Date/Time Collected	Sample Type	Br (mg/l)	NO_2 (mg/l)	F (mg/l)	TOC (mg/l)	TIC (mg/l)	Si (mg/l)	Ba (mg/l)	Sr (mg/l)	Mn (mg/l)
11		make up 3	<0.03	0.04	0.05	3.85	2.25	5.78	0.070	0.012	<0.001
12		make up 4	<0.03	0.52	0.10	3.90	4.51	6.02	0.086	0.020	<0.001
15	02/07/97 11:05	return	<0.03	0.04	0.11	4.81	8.26	6.12	0.004	0.015	<0.001
19	03/07/97 10:15	return	<0.03	1.50	0.56	6.10	14.0	10.6	<0.001	0.006	<0.001
20	03/07/97 13:20	return	<0.06	2.71	0.75	6.56	14.8	11.9	<0.001	0.004	<0.001
21	03/07/97 14:45	return	<0.06	3.16	0.88	6.72	6.52	13.1	<0.001	0.004	<0.001
22	04/07/97 10:00	return	<0.06	2.89	0.92	7.16	13.4	12.6	<0.001	0.004	0.002
23	04/07/97 10:35	return	<0.06	1.85	1.11	6.23	7.70	11.2	<0.001	0.004	0.006
24	04/07/97 13:25	return	<0.06	2.98	1.26	7.31	11.5	11.5	<0.001	0.004	0.010
27	07/07/97 10:55	return	<0.06	2.17	1.46	8.19	11.1	14.0	<0.001	0.005	0.025
30	07/07/97 14:45	return	<0.06	1.51	1.54	10.3	6.86	11.8	<0.001	0.005	0.025
32	08/07/97 10:50	return	<0.06	0.59	1.53	8.85	14.3	10.4	0.002	0.005	0.032
37	09/07/97 11:00	return	<0.06	0.43	1.75	9.16	11.2	6.55	<0.001	0.005	0.017

Sample Code	Date/Time Collected	Sample Type	Tot Fe (mg/l)	Al (mg/l)	Li (mg/l)	B (mg/l)	$\_^{2}H$ ‰ wrt SMOW	$\_^{18}O$ ‰ wrt SMOW	Balance (%)
11		make up 3	<0.01	<0.02	<0.005	<0.05	-51	-8.6	-5.22
12		make up 4	<0.01	<0.02	<0.005	<0.05	n/a	n/a	-17.20
15	02/07/97 11:05	return	<0.01	<0.02	<0.005	<0.05	n/a	n/a	-6.62
19	03/07/97 10:15	return	0.13	0.41	<0.005	0.15	n/a	n/a	4.32
20	03/07/97 13:20	return	0.10	0.44	<0.005	0.23	n/a	n/a	-0.25
21	03/07/97 14:45	return	0.14	0.52	<0.005	0.25	n/a	n/a	0.11
22	04/07/97 10:00	return	0.17	0.54	<0.005	0.25	n/a	n/a	-0.99
23	04/07/97 10:35	return	0.31	0.69	<0.005	0.30	n/a	n/a	8.50
24	04/07/97 13:25	return	0.45	0.90	<0.005	0.34	n/a	n/a	2.55
27	07/07/97 10:55	return	0.91	1.26	<0.005	<0.05	n/a	n/a	3.61
30	07/07/97 14:45	return	0.94	1.29	<0.006	<0.05	n/a	n/a	2.35
32	08/07/97 10:50	return	1.35	1.09	<0.005	<0.05	n/a	n/a	1.18
37	09/07/97 11:00	return	0.62	0.84	<0.005	0.39	n/a	n/a	3.14

1. INTRODUCTION

1.1 Scope of work

As part of its hydrogeological studies, PNC is evaluating the impact of the Tsukiyoshi Fault on groundwater flow in the Tertiary sediments. The construction of a new shaft provided an opportunity to study draw-down effects. A series of boreholes were instrumented with multiple piezometers allowing transient hydraulic heads to be monitored during shaft excavation. Comparison of head responses on either side of the fault allowed inferences to be made on the hydraulic properties of the fault (Koide et al., 1998).

In the No. 2 Measurement Drift, the hanging wall of the fault (upthrow side) comprises the conglomerate of the Toki Lignite-bearing Formation and the footwall (downthrow side) comprises the tuffaceous sandstone of the Akeyo Formation. The fault zone consists of gouge material with two clay-bearing layers around 2-3 cm thick, separated by a 10-20 cm thick layer of unconsolidated fine sandy material.

The scope of the work described in the report was to conduct a series of laboratory experiments on a single specimen of clay-bearing fault gouge to provide information on hydraulic properties and the sensitivity of these properties to isotropic confining stress (i.e. the spherical component of the stress tensor). The specimen was prepared so that the direction of flow was perpendicular to the strike of the fault and roughly horizontal. The tests therefore relate to the transverse hydraulic conductivity of the fault zone.

Controlled flow-rate experiments were performed at three levels of isotropic confining stress with a fixed backpressure. Hydraulic conductivities were calculated from steady-state pressure gradients and from analysis of the pressure transients. Transient analysis also yielded values for specific storage.

1.2 Description of test material

Sampling of the fault gouge material was undertaken in July 1997. A 116 mm diameter sub-horizontal borehole was drilled using a Koken OE-8 rotary drilling machine at a location in the North Extension Drift of Tono Mine, approximately 160 metres below surface. The borehole was inclined at an angle of 5 degrees below horizontal and the total length was 29.96 m. The sample was obtained using a triple-tube core barrel fitted with a split sample tube and a diamond bit. The hole was water-flushed using local river water. In total, 15 cm of clay-bearing fault gouge material was recovered. This was substantially more than the reported exposure in No. 2 Measurement Drift. The sample was trimmed to length, then vacuum sealed in double aluminised plastic bags which were flushed with nitrogen prior to sealing. The sample was carefully packed in a wooden transit box and shipped to the United Kingdom.

On receipt, the sample was examined by a geologist. Photographs and sketches were prepared. The sample comprised a crumbly and poorly-cohesive matrix of olive-

green/grey gouge material with particles ranging from clay-size through to sand-size (i.e. poorly-sorted in sedimementological terms), containing conspicuous white crystals of a soft, friable and altered mineral, possibly calcite (Figure 1). Data supplied by PNC show the green colour is due to the presence of the clay mineral chlorite. The sample had a strongly-sheared fabric and was cut by numerous shiny shear surfaces (slickensides) with a grey-brown colouration suggestive of chemical alteration. These so-called listric surfaces appeared to be regions of clay mineral re-orientation with the basal surfaces of clay platelets lying in the plane of shear deformation. This mineral alignment was apparent even at the fine scale, with platy clay minerals draped around inclusions forming "Augen-like" structures.

2 EXPERIMENTAL DETAILS

The BGS controlled flow rate permeameter (Figure 2) consists of five main components: (1) a sample assembly, (2) a 40 MPa-rated pressure vessel and associated confining pressure system, (3) a fluid injection system, (4) a backpressure system and (5) a microcomputer-based data acquisition system. The sample is subject to an isotropic confining stress.

2.1 Pressure vessel and sample assembly

The pressure vessel, shown in Figure 3, comprises a cylindrical Autoclave Engineers bolted single-closure reactor vessel, made from 316 stainless steel. The specimen is 4.90 cm in diameter with a length of 2.54 cm. It is sandwiched between two end-caps, each with a 316 sintered stainless steel porous disc, and jacketed in heat-shrink Teflon to exclude confining fluid and provide a flexible pressure seal.

2.2 Injection, backpressure and confining pressure circuits

The ingoing volumetric flow rate and backpressure are controlled using a pair of ISCO-100, Series D, syringe pumps operated from a single digital control unit. A pressure transducer monitors outgoing pressure to provide a feedback signal to the microprocessor when each pump is set to constant pressure mode. Piston motion then gives a direct measure of the net volumetric flow out of each pump. The pumps can also be set to constant volumetric pumping rate, whereby the piston is advanced at a constant velocity. Confining pressure is maintained using compressed nitrogen.

2.3 Instrumentation and data acquisition

The ISCO pump controller has an RS232 serial port which allows volume, flow rate and pressure data to be transmitted to an equivalent port on a 32-bit personal computer.
A programme written in QBASIC prompts the pump controller to transmit data to the computer at pre-set time intervals. Acquisition rate was one scan per 30 minutes.

2.4 Calibration

Both ISCO syringe pumps were pressure calibrated using a Druck PTX610 transmitter. Steps of 1.0 MPa in pressure were applied, with increments and decrements to quantify hysteresis. Using a spreadsheet, least-squares regression fits were calculated and the parameters used to correct the raw data.

2.5 Sample preparation

The sample was manufactured in the normal manner using a former with a sharpened leading edge. Excess material was trimmed away using a scalpel. The upper and lower surfaces were finished-off using a scraping action with a flat-bladed knife, leaving the end-surfaces flat and parallel. Purite-saturated[1] sintered discs were placed on each face of the specimen, the end-caps were positioned, and the resulting assembly jacketed in Teflon heat-shrink tube. The jacket was shrunk to size using a hot air gun. Two hose clamps were tightened onto copper shims to compress the Teflon on to the end-caps, resulting in a leak-tight seal. Tubing connections were then made to the vessel end-closure (Figure 3).

2.6 Basic physical properties

Table 1 shows the basic physical properties of the test sample based on pre-test measurements of water content[2] and an assumed specific gravity for the mineral solids. The prepared specimen was found to be slightly desaturated under atmospheric conditions (degree of saturation = 86.8%).

Previous work has shown that it is very important to correct the degree of saturation and other dependent properties for the effect of applying the confining stress to the material. Assuming ideal gas behaviour and no dissolution of gas in porewater, the relationship between the void ratio of a compressible clay-like material and the saturation S_w^{at} under atmospheric conditions and the void ratio of the same material under confinement e^{tc}, can be estimated using

$$e^{tc} = e^{at}\left(S_w^{at}\right) + e^{at}\left(1 - S_w^{at}\right)R_p \qquad (1)$$

where R_p is the ratio of atmospheric pressure (0.1 MPa) to the air pressure in the sample when subjected to confinement. This ratio is likely to be around 0.03 for the lowest value of confining stress used in these experiments. The degree of saturation of the confined specimen becomes

$$S_r^{tc} = \frac{wG_s}{e^{at}\left(S_w^{at}\right) + e^{at}\left(1 - S_w^{at}\right)R_p} \qquad (2)$$

[1] Purite is a commercial name for double-distilled water.
[2] Water content was determined by oven drying at 105°C for a period in excess of 24 hours.

where w is the gravimetric water content and G_s is the average specific gravity of the mineral solids. Under experimental conditions, void ratio falls to around 0.414 and the degree of saturation rises very close to unity (Table 2). Any residual gas left within the specimen probably enters solution, a process assisted by the use of vacuum de-aired Purite.

2.7 Stress conditions for testing

Taking the vertical total stress gradient in the region of Tono Mine as 0.022 $MPa.m^{-1}$, the undisturbed vertical stress in the fault zone at 160 m below surface is 3.5 MPa. Assuming the hydrostatic pressure of water at this depth to be around 1.5 MPa, the vertical effective stress on the fault gouge would be 2 MPa. The test programme was scheduled to include controlled flow rate (CFR) stages at an effective stress close to 2 MPa.

2.8 Experimental history

Table 3 shows the experimental history. During an equilibrium (EQ) stage the specimen is backpressured with Purite on both faces (i.e. zero hydraulic gradient). The purpose of this stage is to allow excess pore pressures to dissipate. A controlled flow rate (CFR) stage is used to evaluate hydraulic conductivity and specific storage and involves the injection of Purite into the specimen at volumetric flow rates shown in Table 3.

3 DATA REDUCTION

Data were transferred to a spreadsheet for processing and plotting. Hydraulic transients were very well-defined and largely free of experimental noise.

The one-dimensional equation of flow is

$$S_s \frac{\partial h}{\partial t} = K \frac{\partial^2 h}{\partial x^2} \qquad (3)$$

where S_s (m^{-1}) is the specific storage, K ($m.s^{-1}$) is the hydraulic conductivity, h (m) is the hydraulic head and x (m) is distance in the flow direction. This equation must be solved subject to the boundary conditions

$$q = \frac{Q}{A_s} = -K \left. \frac{\partial h}{\partial x} \right|_{x=0} \qquad (4)$$

and

$$h = 0 \text{ at } x = L_s \qquad (5)$$

where q ($m.s^{-1}$) is the Darcy velocity, Q ($m^3.s^{-1}$) is the volumetric flow rate, A_s (m^2) and L_s (m) are the cross-sectional area and length of the specimen, respectively. Hydraulic head is related to the pore pressure, P (Pa), by

$$h = \frac{P}{\rho_w g} \qquad (6)$$

where r_w ($kg.m^{-3}$) is the density of water and g (= 9.81 $m.s^{-2}$) is the acceleration due to gravity.

The head at x = 0 as a function of time was obtained by numerically inverting the Laplace Transform solution given in Appendix 1. Five parameters are required to define the solution. Three are experimentally determined: Q, A_s, and L_s. The remaining two are the material properties that the test is designed to determine (i.e. K and S_s). In order to estimate the values of these parameters, a general nonlinear least squares fitting routine was used to minimise the differences between the calculated curves and the measured head data.

Hydraulic conductivity was also calculated from the head gradient at steady-state enabling the two values to be compared.

Permeability, k (m^2), was calculated from hydraulic conductivity using the relationship

$$k = \frac{K\eta_w}{\rho_w g} \qquad (7)$$

where η_w (Pa.s) is the viscosity of water.
Volumetric strains and instantaneous values of void ratio were obtained from the difference between the volume pumped in and the volume pumped out of the specimen. No correction was applied for compression of the pump barrel, piston, seals and liquid phase.

4 RESULTS

Figure 4 shows a typical consolidation curve for an equilibrium (EQ) stage. The cumulative flow out of the specimen is plotted against the square root of time in the usual manner. Figures 5 to 19 show the hydraulic transients following changes in flow rate for the controlled flow rate (CFR) stages. The least square fits to the data are shown in red and clearly provide a very good representation of the transient responses. Summarised results are presented in Table 4. Overall, the experiments were highly successful and provide a very consistent data set for this gouge material.

4.1 Adequacy of Darcy's Law

For each level of confining stress, the hydraulic conductivity values are fairly constant over the ranger of flow rates. This is evidence for the general validity of Darcy's Law for this material. However, close inspection of the data reveals a degree of flow-rate sensitivity accompanied by some hysteresis. This can be partially explained by the dependence of hydraulic conductivity on effective stress (Section 4.4). As flow rate increases, the average pore pressure in the test specimen also increases. Under a fixed confining stress, an increase in pore pressure signifies a decrease in effective stress. This decrease in effective stress causes the small change in hydraulic conductivity, leading to the apparent flow-rate sensitivity of this parameter.

4.2 Comparison between methods of obtaining hydraulic conductivity

At a confining stress of 3.5 MPa the average hydraulic conductivity from analysis of steady-state pressure gradients is 1.84×10^{-12} m.s^{-1}. The equivalent value from analysis of the pressure transients is 2.09×10^{-12} m.s^{-1}.

At a confining stress of 7.5 MPa the average hydraulic conductivity from analysis of steady-state pressure gradients is 1.79×10^{-13} m.s^{-1}. The equivalent value from analysis of the pressure transients is 2.06×10^{-13} m.s^{-1}.

At a confining stress of 13.5 MPa the average hydraulic conductivity from analysis of steady-state pressure gradients is 7.9×10^{-14} m.s^{-1}. The equivalent value from analysis of the pressure transients is 8.4×10^{-14} m.s^{-1}.

Apparently, the hydraulic conductivity from steady-state pressure gradients is always a little smaller (87 to 94%) than the value derived by analysis of the transient response. Inspection of Table 4 shows that hydraulic conductivity from transient analysis is more sensitive to flow rate (and effective stress) than hydraulic conductivity from steady-state pressure gradients. Theses differences are reflected in the averages.

4.3 Volume changes during testing

The void ratio, e, of the gouge material is defined as the ratio of the volume of voids to the total volume of the sample. It is related to porosity, n, by

$$n = \frac{e}{1+e} \qquad (8)$$

Figure 20 shows the standard soil mechanics plot of void ratio against the logarithm of effective stress. The blue curve represents the behaviour of the sample when the confining stress is increased and backpressure held constant. In soil mechanics terms, this curve is known as the rebound-reconsolidation line (RRL). It is sensibly linear in the log-linear parameter space, and can be represented by the expression

$$e = e_o - \kappa \ln\left(\frac{\sigma'}{\sigma_0'}\right) \quad (9)$$

where -κ is the slope of the RRL, s' is the effective stress acting on the specimen, e_o is the void ratio intercept at an effective stress s_0' = 1.0 MPa (Schofield and Wroth, 1968). For effective stresses in the range 2 to 6 MPa, κ = 0.036 and e_o = 0.4385. For effective stresses in the range 6 to 12 MPa, κ increases to 0.044.

The data shown in red represent the volumetric behaviour of the specimen during the CFR test stages. For effective stresses greater than 4 MPa, the volumetric behaviour for an increasing history of flow rate corresponds fairly closely with the RRL. This provides good confirmation that the fault gouge is overconsolidated (Atkinson and Bransby, 1978). For a decreasing history of flow rate, the path in e-ln(s') space is less steep than the RRL. For effective stresses around 2 MPa, both paths are less steep than the RRL.

4.4 Sensitivity of hydraulic conductivity to stress

Figure 21 is a plot of hydraulic conductivity against average effective stress. Extrapolation gives a value of around 1 $x10^{-11}$ $m.s^{-1}$ at zero effective stress. Based on this trend, hydraulic conductivity changes most rapidly between zero and 5.0 MPa. Beyond 5.0 MPa hydraulic conductivity becomes less sensitive to changes in effective stress. One possible interpretation is that the fault gouge is clay matrix-supported at stress less than 5.0 MPa and is framework-supported at higher stresses. However, the measured increase in κ with stress is not consistent with this hypothesis.

4.5 Sensitivity of specific storage to stress

According to Horseman et al. (1996, p173), the drained bulk modulus, B, of an overconsolidated clay can be expressed as a function of void ratio and effective stress as follows

$$B = \frac{(1+e)\sigma'}{\kappa} \quad (10)$$

The specific storage of the material is given by

$$S_s = \rho_w g\left[\frac{1}{B} + \frac{n}{B_w}\right] \quad (11)$$

where n is the porosity and B_w (= 2.2 GPa) is the bulk modulus of water. Combining (8), (10) and (11) gives the relationship:

$$S_s = \frac{\rho_w g}{1+e}\left[\frac{\kappa}{\sigma'} + \frac{e}{B_w}\right] \quad (12)$$

Specific storage therefore depends on two variables, the current void ratio and the effective stress. Figure 22 shows experimentally-determined values for specific storage, together with this theoretical relationship (assuming κ = 0.036). The theoretical curve is less satisfactory at low values of effective stress. This can be explained by the discrepancy between the slopes of the paths in e-ln(s') space during CFR testing at low effective stress and the slope of the RRL (Figure 20).

5 CONCLUSIONS

The experiments were highly successful and have provided a very consistent data set for this clay-bearing gouge material from the Tsukiyoshi Fault.

Given the crumbly and poorly-cohesive matrix of this material, the presence of significant amounts of sand-sized material, and the occurrence of shear-induced features (e.g. slickenslides), the fault gouge has exceptionally low hydraulic conductivity.

The specimen was prepared so that the direction of flow was perpendicular to the strike of the fault and roughly horizontal (i.e. the tests relate to the transverse hydraulic conductivity of the fault zone).

At confining stresses of 3.5, 7.5 and 13.5 MPa the average hydraulic conductivities based on analysis of steady-state pressure gradients were 1.84 $x10^{-12}$ $m.s^{-1}$, 1.79 $x10^{-13}$ $m.s^{-1}$ and 7.9 $x10^{-14}$ $m.s^{-1}$. The equivalent values from analysis of the pressure transients were 2.09 $x10^{-12}$ $m.s^{-1}$, 2.06 $x10^{-13}$ $m.s^{-1}$ and 8.4 $x10^{-14}$ $m.s^{-1}$. Hydraulic conductivity is strongly-dependent on the spherical component of the effective stress tensor. Beyond 5 MPa, hydraulic conductivity becomes less sensitive to effective stress. One possible interpretation is that the fault gouge is clay matrix-supported at low stress and framework-supported at high stress. In other words, the coarser particles may lock together at high stress, sheltering the fine-grained component from the full effect of the applied stress.

The hydraulic conductivity from steady-state pressure gradients is always a little smaller (87 to 94%) than the value derived by analysis of the transient response. For each level of confining stress, the hydraulic conductivity values are fairly constant over the range of flow rates. This is evidence for the general validity of Darcy's Law for this material. However, close inspection of the data reveals a degree of flow-rate sensitivity accompanied by some hysteresis. This can be partly explained by the dependence of hydraulic conductivity on effective stress.

Based on these experiments, the transverse hydraulic conductivity of the clay-bearing fault gouge at a the sampling depth of 160 m in the North Extension Drift is around

2×10^{-12} $m.s^{-1}$ (i.e. roughly equivalent to the hydraulic conductivity to the Boom Clay at the depth interval of the Hades URL in Belgium). Extrapolation of the experimental data suggests that hydraulic conductivity increases at shallower depths, with a value of around 1×10^{-11} $m.s^{-1}$ at the surface. Although it is not possible to comment on the effects of scale and heterogeneity, it would appear that the clay-bearing component of the fault gouge has much lower hydraulic conductivity than the surrounding country rocks.

A plot of void ratio against the logarithm of effective stress is sensibly linear showing that the fault gouge exhibits normal soil-like behaviour. There is strong evidence that the locus in e-ln(s') space corresponds to the rebound-reconsolidation line (RRL) of theoretical soil mechanics. The slope of this line, $-\kappa$, has a value of around 0.036, increasing to 0.044 at effective stresses greater than 6 MPa.

These observations show that Tsukiyoshi Fault gouge behaves as an overconsolidated material (Atkinson and Bransby, 1978). In effect, the current effective stress on this material is substantially less than the effective stress during faulting. The material is therefore in a much denser state of packing than one would anticipate from current effective stress. The combined effects of prior consolidation under high spherical effective stress and high deviatoric (shear) stress may explain the very low hydraulic conductivity of this material.

Estimates for the recent burial history of the formation indicate that around 600 m of overburden have been removed by erosion. Since the fault gouge is overconsolidated, it indicates that faulting occurred prior to geological exhumation. This estimate for geological uplift (600 m) is in line with the geotechnical data which indicates that the fault gouge is still overconsolidated and on the same RRL at a stress equivalent to a depth of burial of 550 m ($\approx$12 MPa).

For effective stresses greater than 4 MPa, the volumetric behaviour for an increasing history of flow rate corresponds fairly closely with the RRL. Specific storage can be written in terms of the drained bulk modulus of the material and the bulk modulus of water. Since the drained bulk modulus depends on the slope of the RRL, it is possible to predict specific storage from soil mechanics parameters. The derived theoretical relationship is in reasonable agreement with experimental data for effective stresses greater than 4 MPa, but is inadequate in the low stress regime.

At the sampling depth in the North Extension Drift, the specific storage of the clay-bearing fault gouge is around 7.5×10^{-5} m^{-1}. Specific storage increases at shallower depths.

6 RECOMMENDATIONS

Given that laboratory experiments are now proven to provide very useful results, we strongly recommend that more samples be tested in this way to provide information on spatial variability and possible anisotropy of hydraulic properties. The study has focused on the role of the spherical component of the stress tensor additional work

might also be performed on deviatoric (shear) component. We recommend that all test samples are analysed for mineralogy, fabric (SEM studies), specific surface and particle and pore size distributions. Furthermore, all cores from the Tsukiyoshi Fault should be logged by a competent structural geologist with the aim of recording all features linked to fault movement. As a final recommendation, we suggest that gas breakthrough pressures and gas permeabilities be measured to assist in generic studies of repository gas migration.

REFERENCES

Atkinson, J.H. and P.L. Bransby (1978). The Mechanics of Soils: An Introduction to Critical State Soil Mechanics. McGraw-Hill, New York.

Horseman, S.T., J.J.W. Higgo, J. Alexander and J.F. Harrington (1996). Water, gas and solute movement through argillaceous media. A report prepared for the OECD/NEA Working Group on Measurement and Physical Understanding of Groundwater Flow Through Argillaceous Media ("Clay Club"), prepared by Fluid Processes Group, British Geological Survey, Nottingham, UK, Rept CC-96/1, OECD Paris, 290pp.

Koide, K., M. Yamane and K. Kobayashi (1998). Heterogeneity of hydraulic conductivity of a fault in sedimentary sequences at the Tono Mine, Central Japan. In: Proceedings of a joint NEA/EC Workshop on Fluid Flow through Faults and Fractures in Argillaceous Formations, Berne, Switzerland, 10-12 June 1996, 189-198.

Schofield, A. and P.W. Wroth (1968). Critical State Soil Mechanics, McGraw-Hill, London.

Talbot, A. (1979). The accurate numerical inversion of Laplace Transforms. J. Inst. Math. Applications, (23), 97.

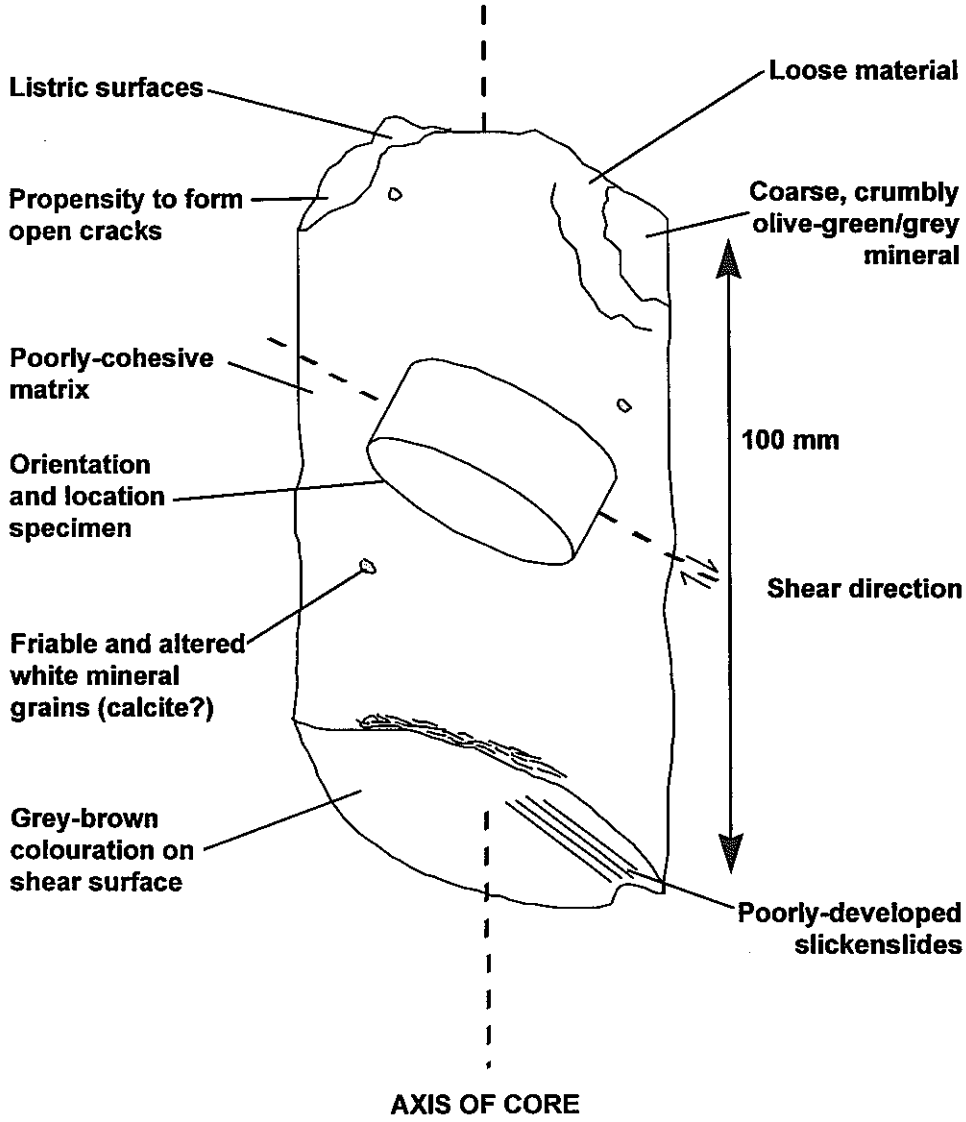

Figure 1. Sketch of sample showing location of test specimen.

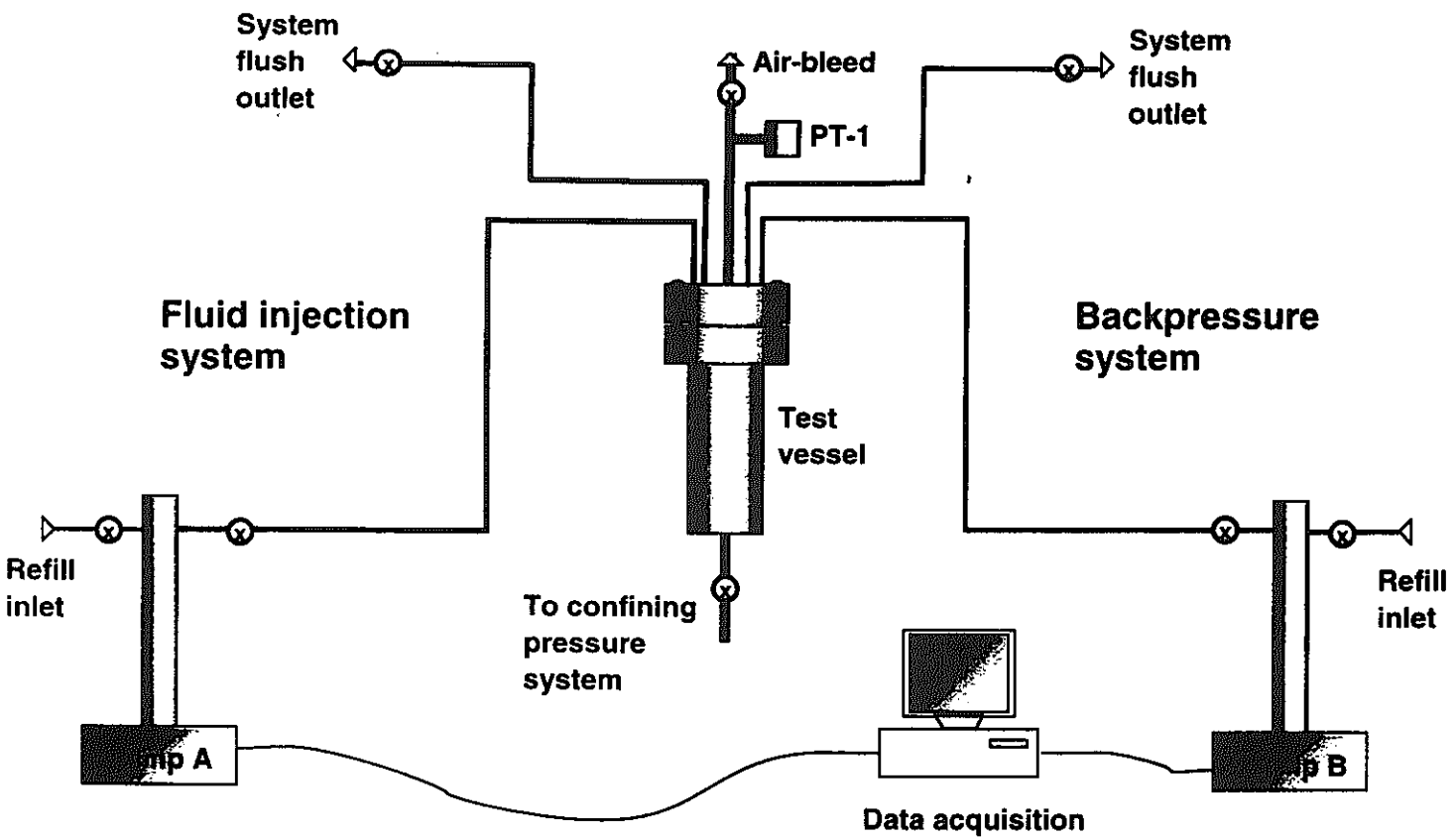

Figure 2. Schematic of test apparatus.

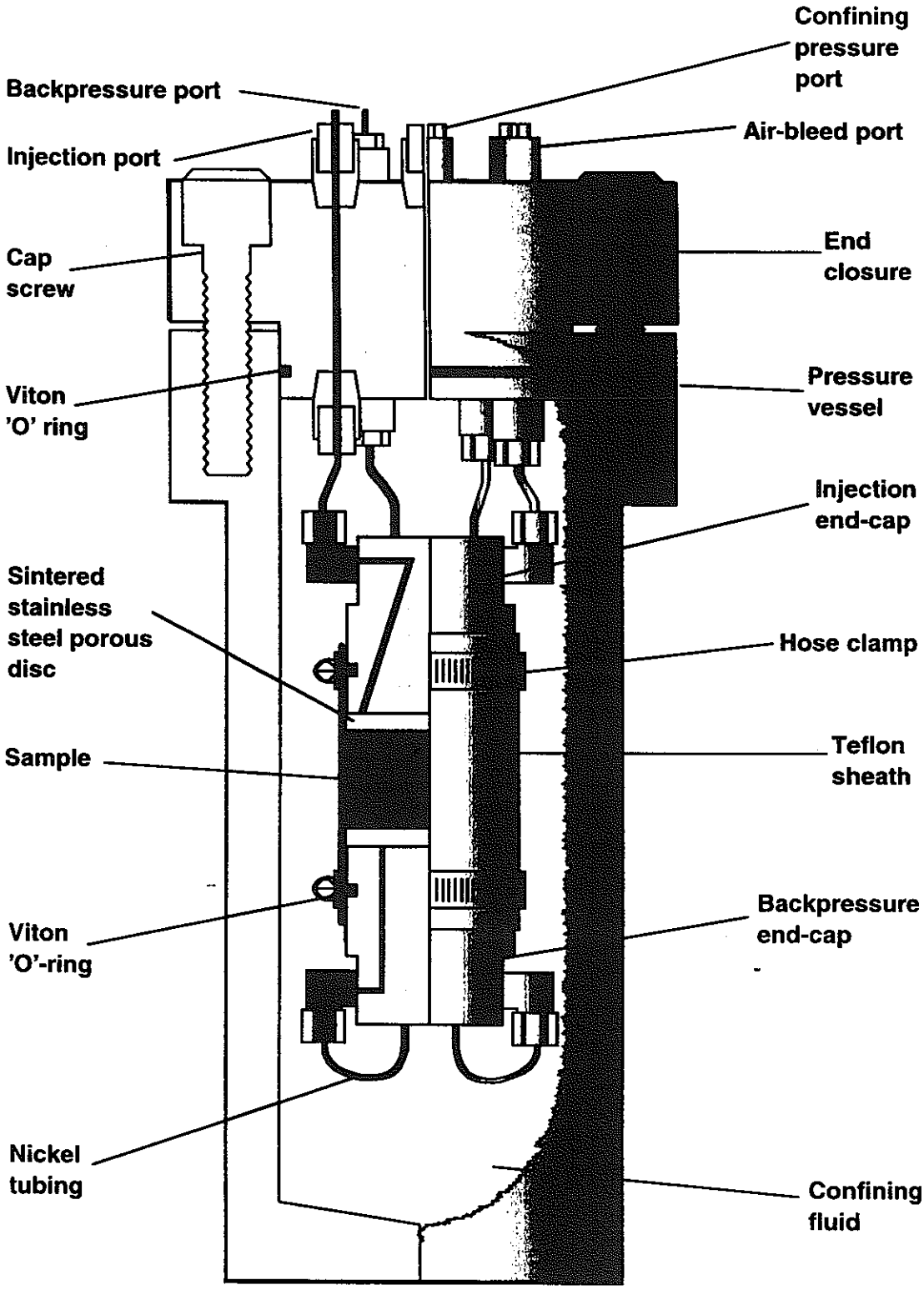

Figure 3. Schematic of pressure vessel and sample assembly.

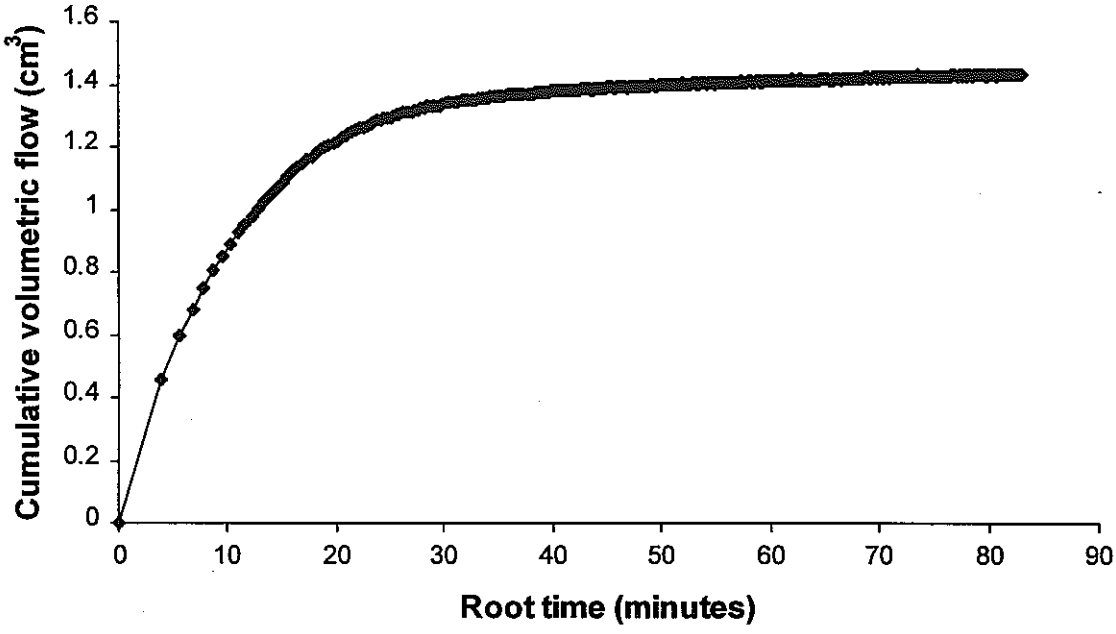

Figure 4 Typical consolidation curve (EQ - stage 8)

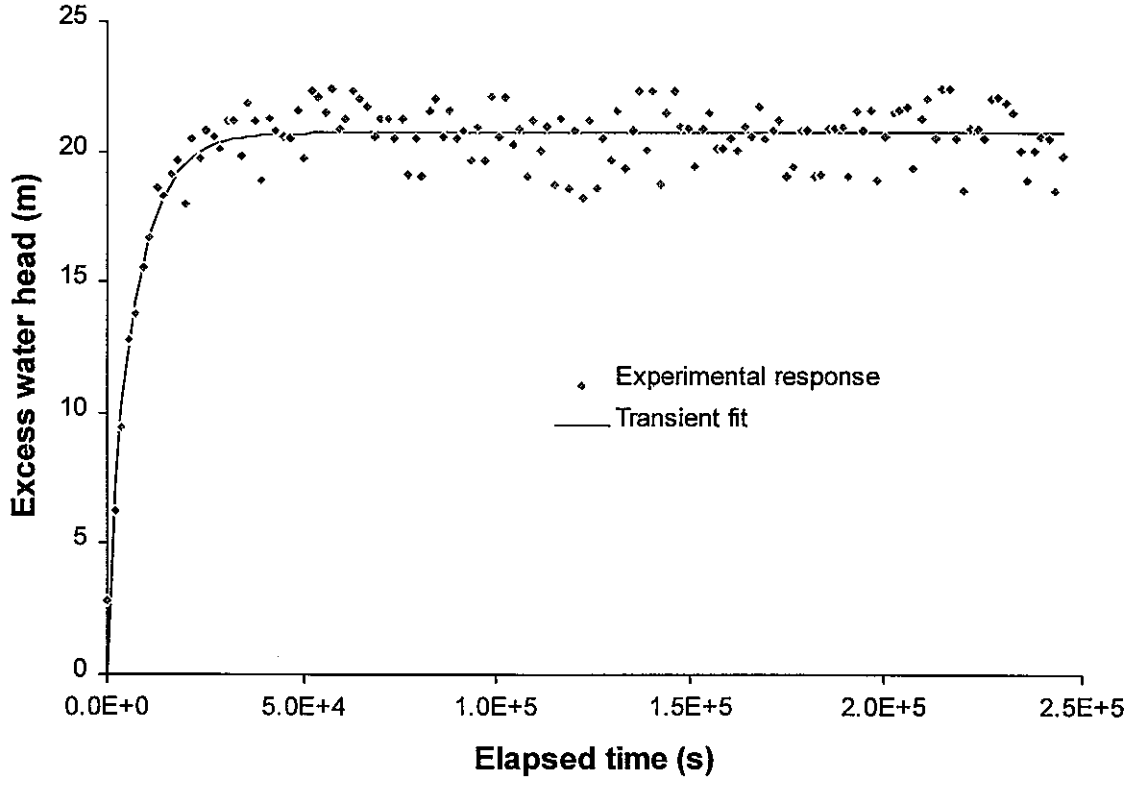

Figure 5. Transient analysis of excess water head (stage 2)

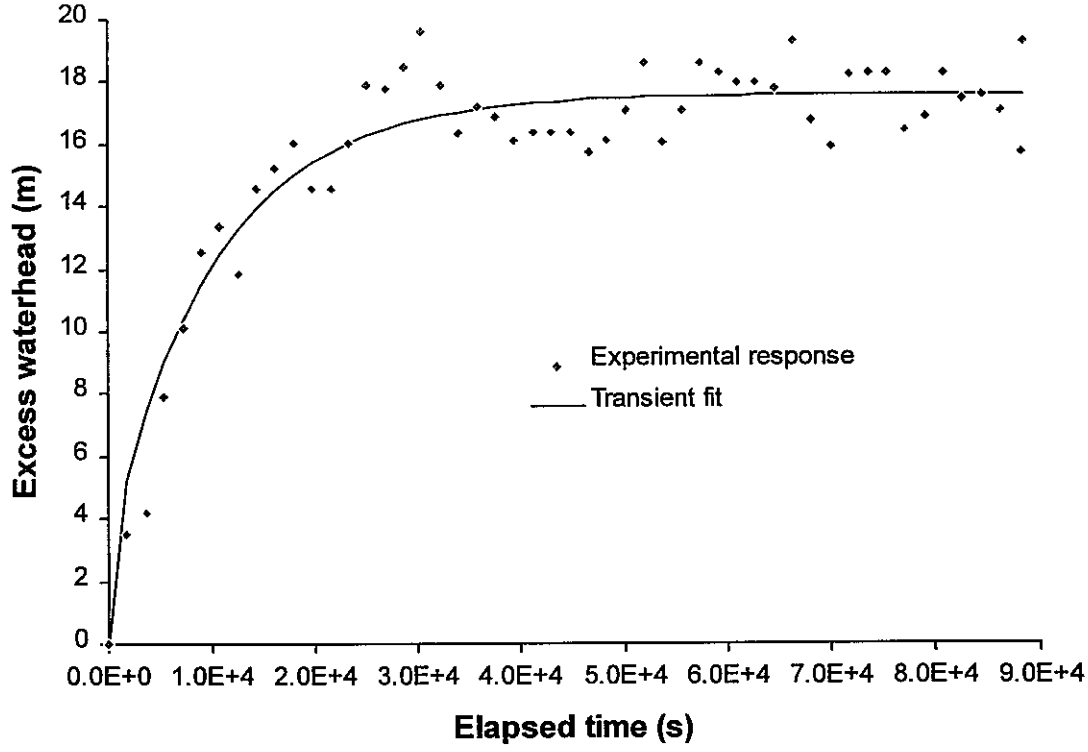

Figure 6. Transient analysis of excess water head (stage 3)

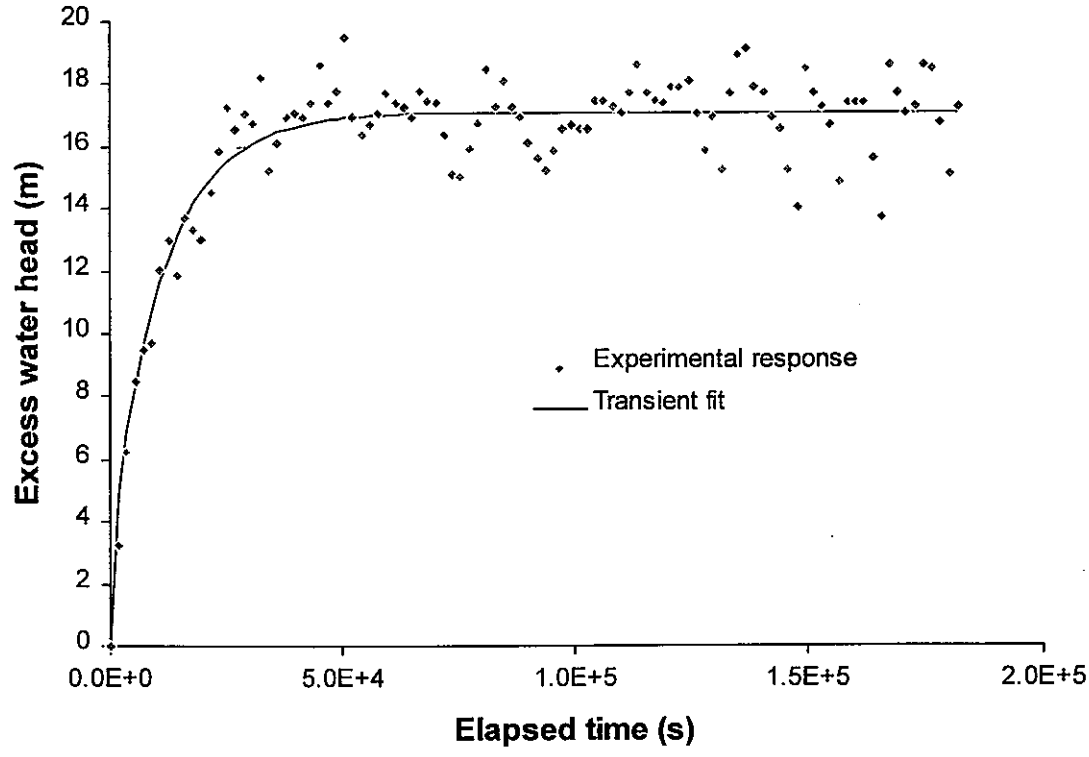

Figure 7. Transient analysis of excess water head (stage 4)

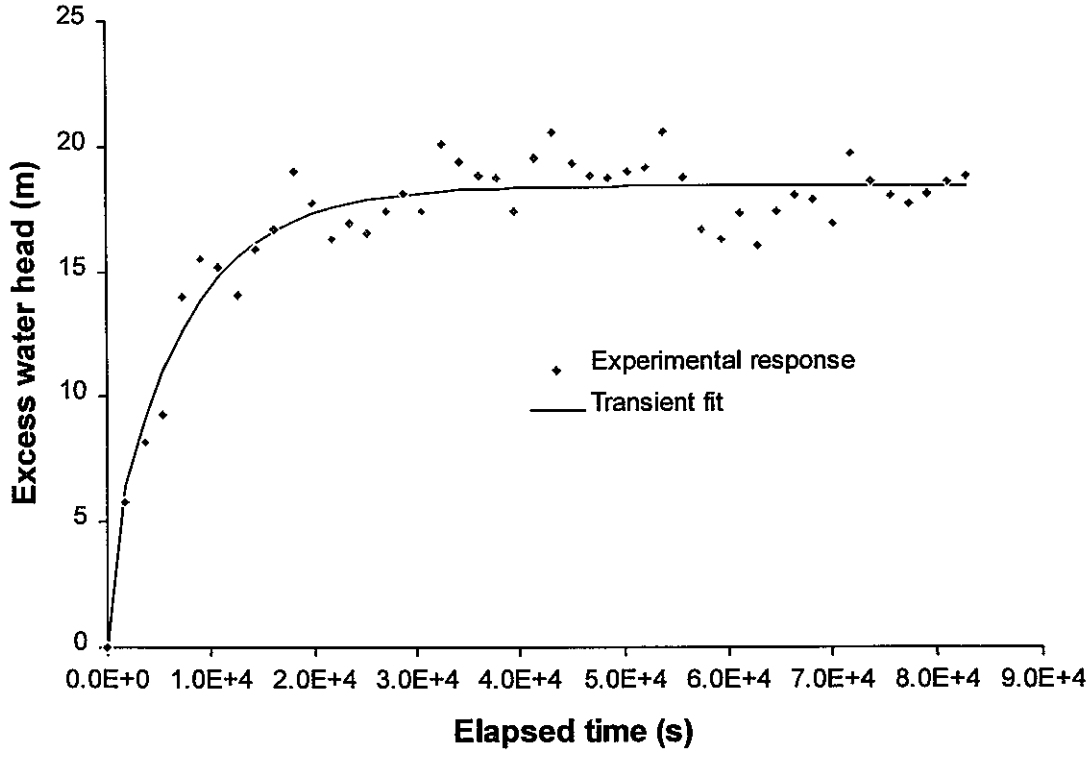

Figure 8. Transient analysis of excess water head (stage 5)

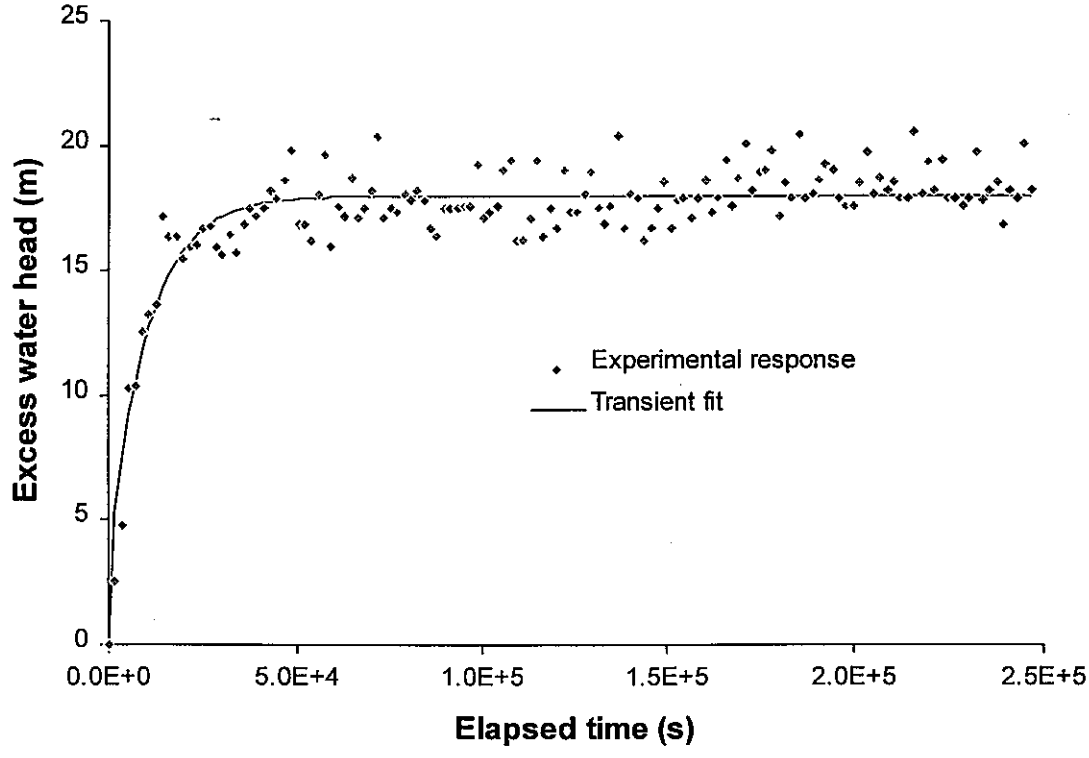

Figure 9. Transient analysis of excess water head (stage 6)

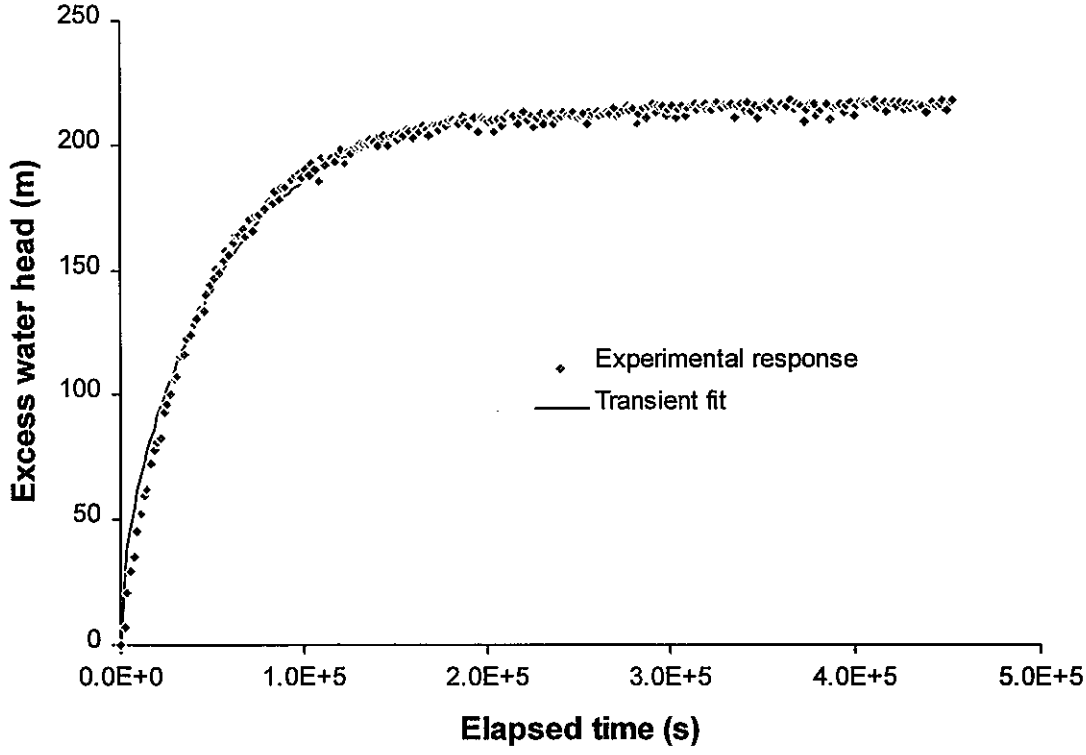

Figure 10. Transient analysis of excess water head (stage 9)

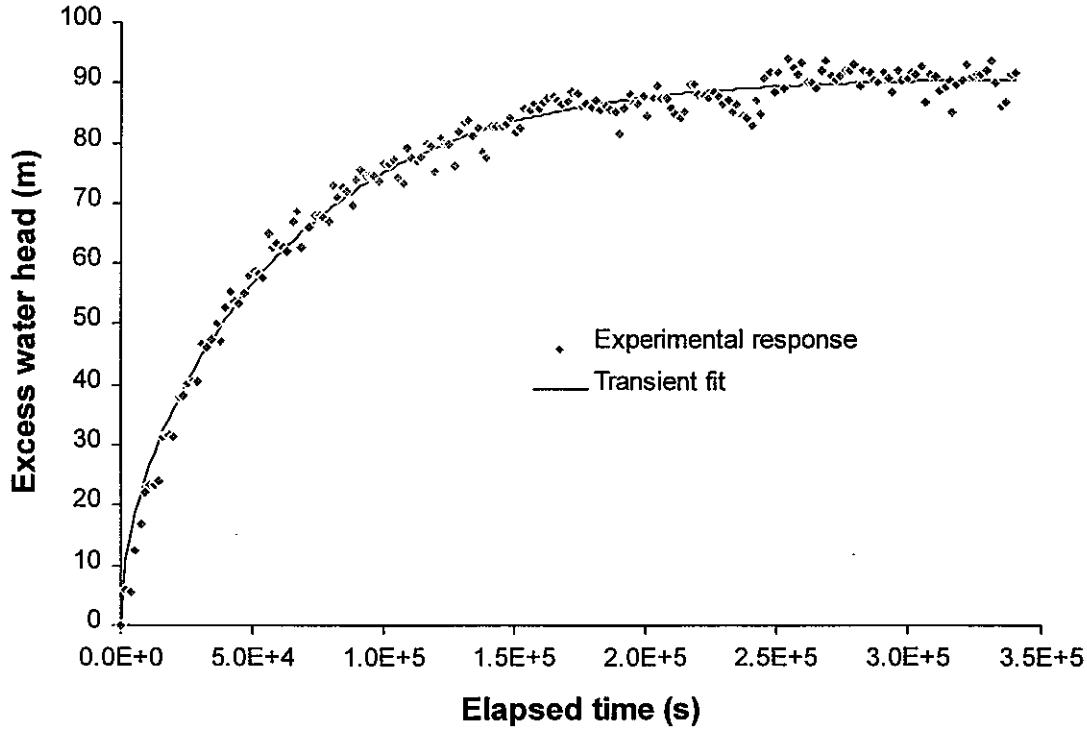

Figure 11. Transient analysis of excess water head (stage 10)

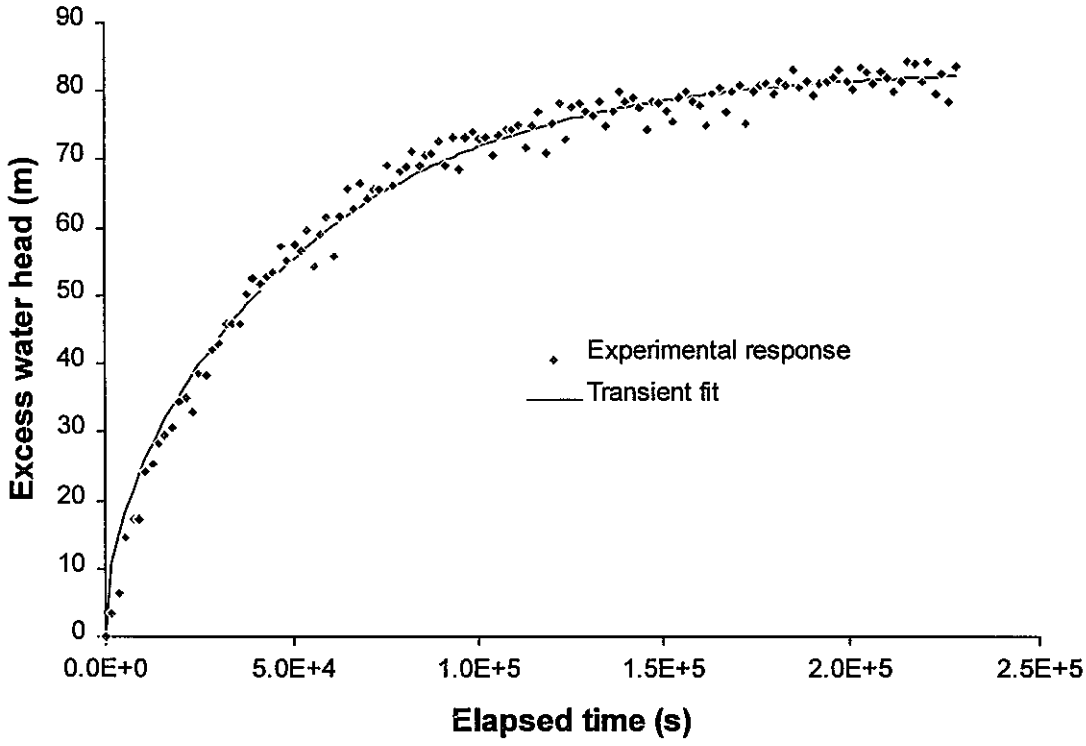

Figure 12. Transient analysis of excess water head (stage 11)

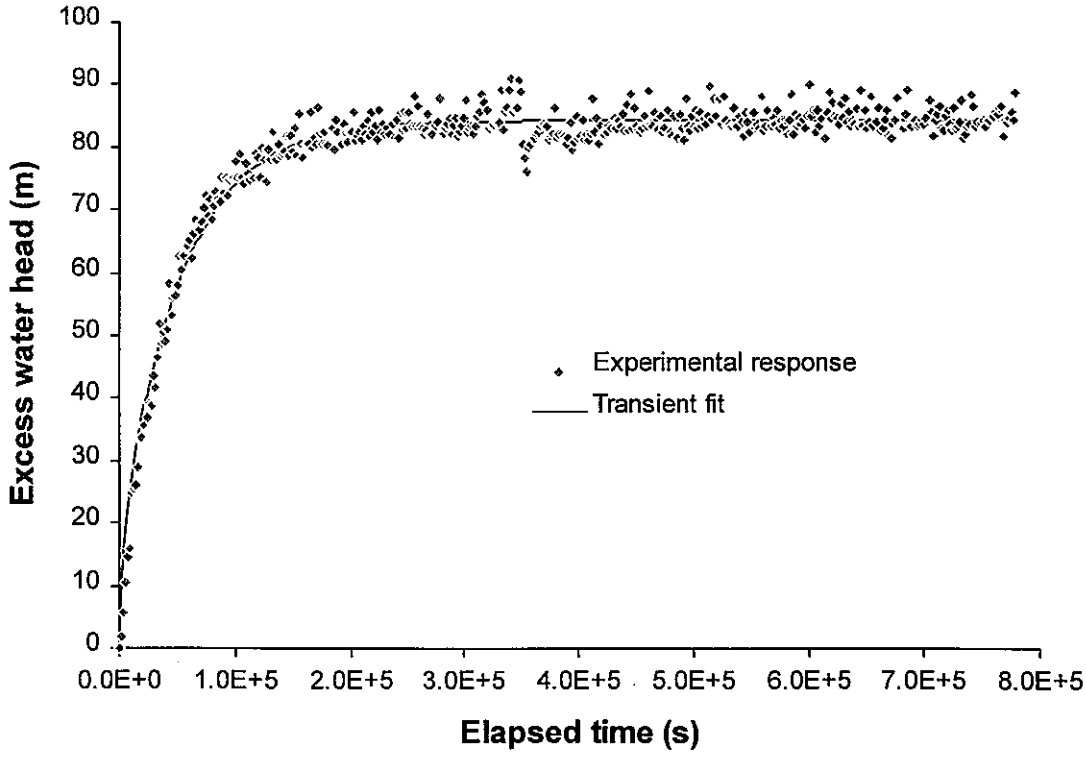

Figure 13. Transient analysis of excess water head (stage 12)

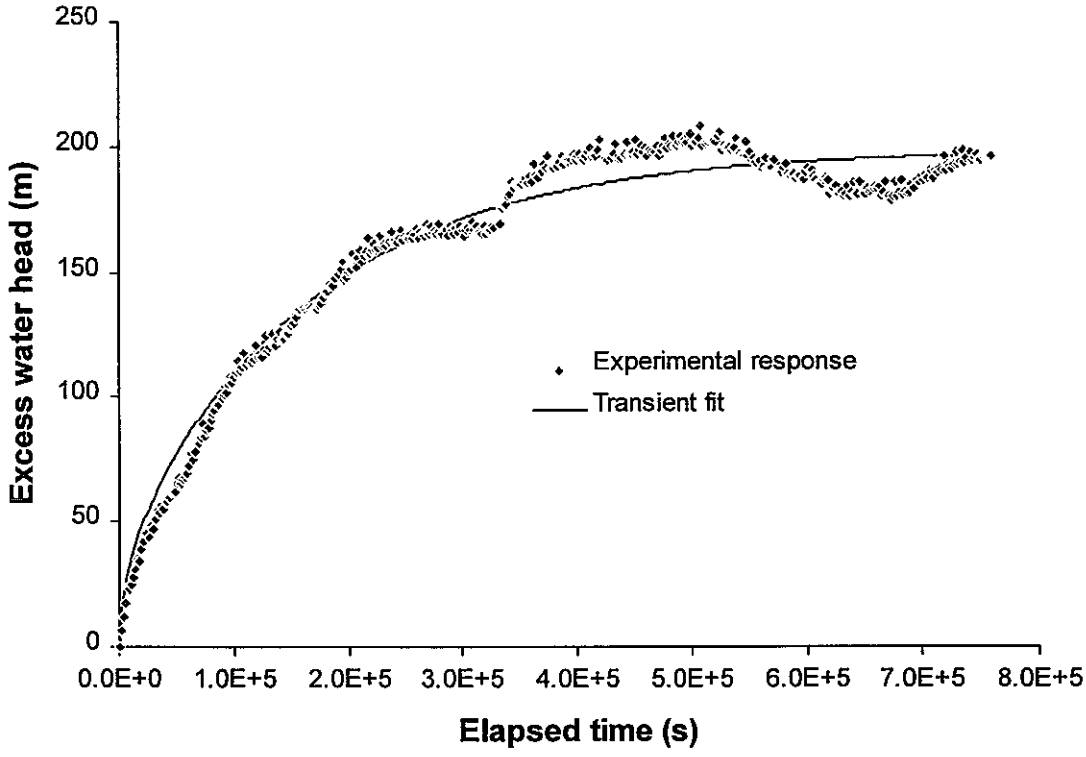

Figure 14. Transient analysis of excess water head (stage 13)

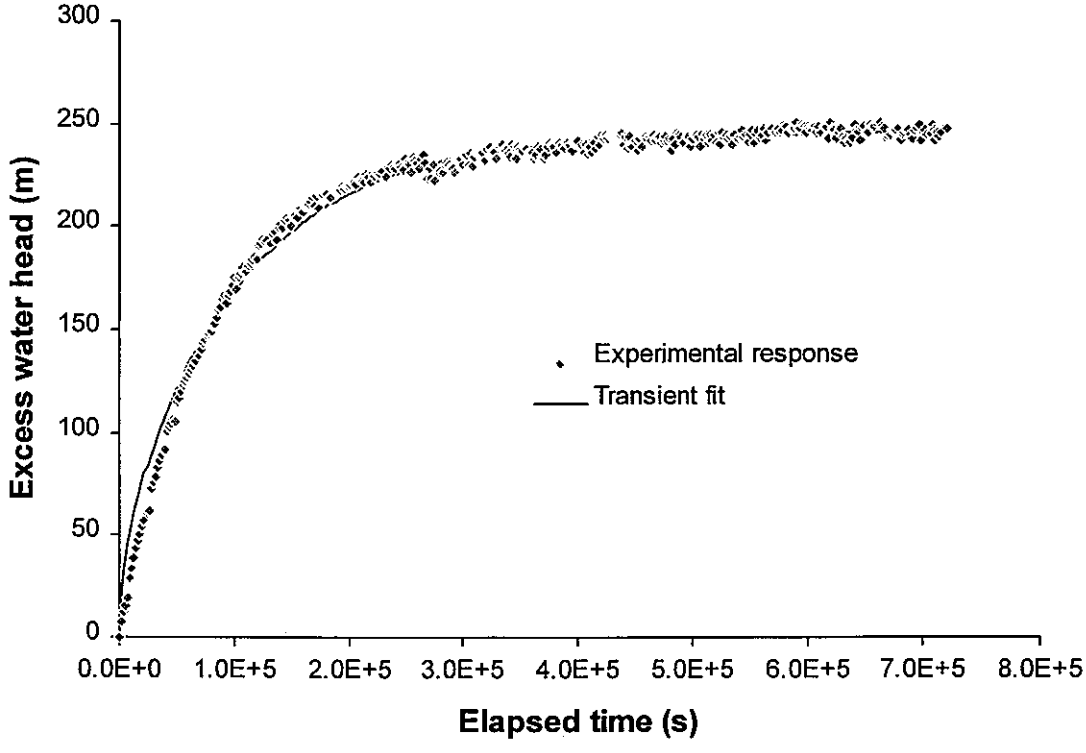

Figure 15. Transient analysis of excess water head (stage 16)

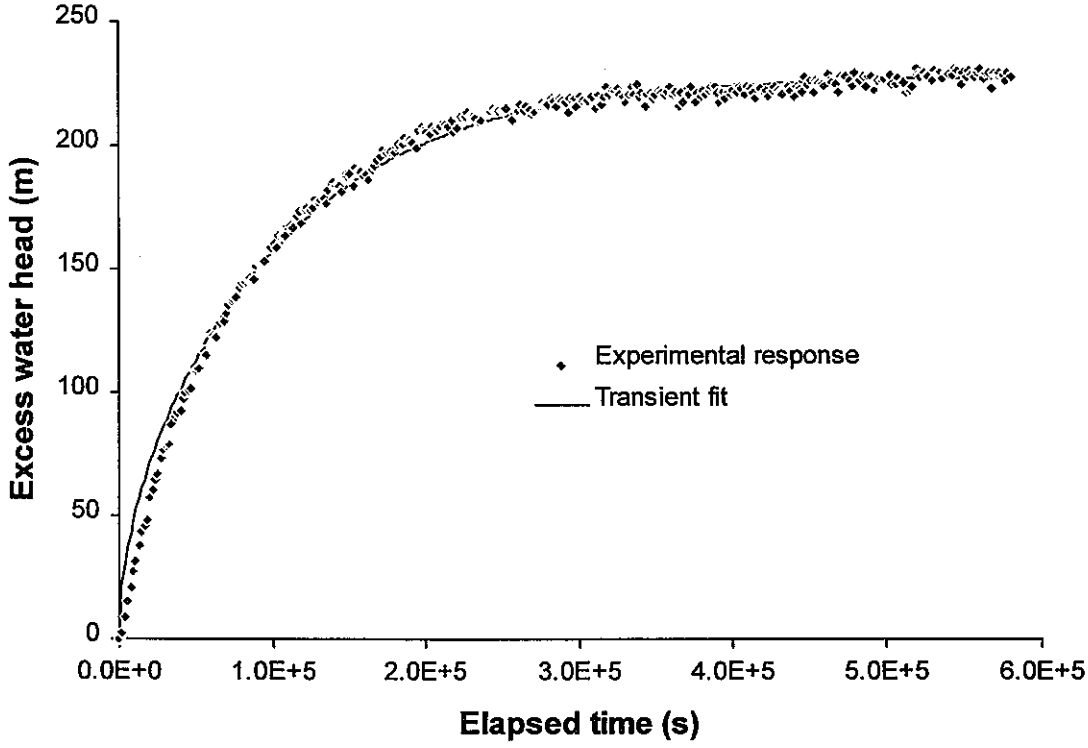

Figure 16. Transient analysis of excess water head (stage 17)

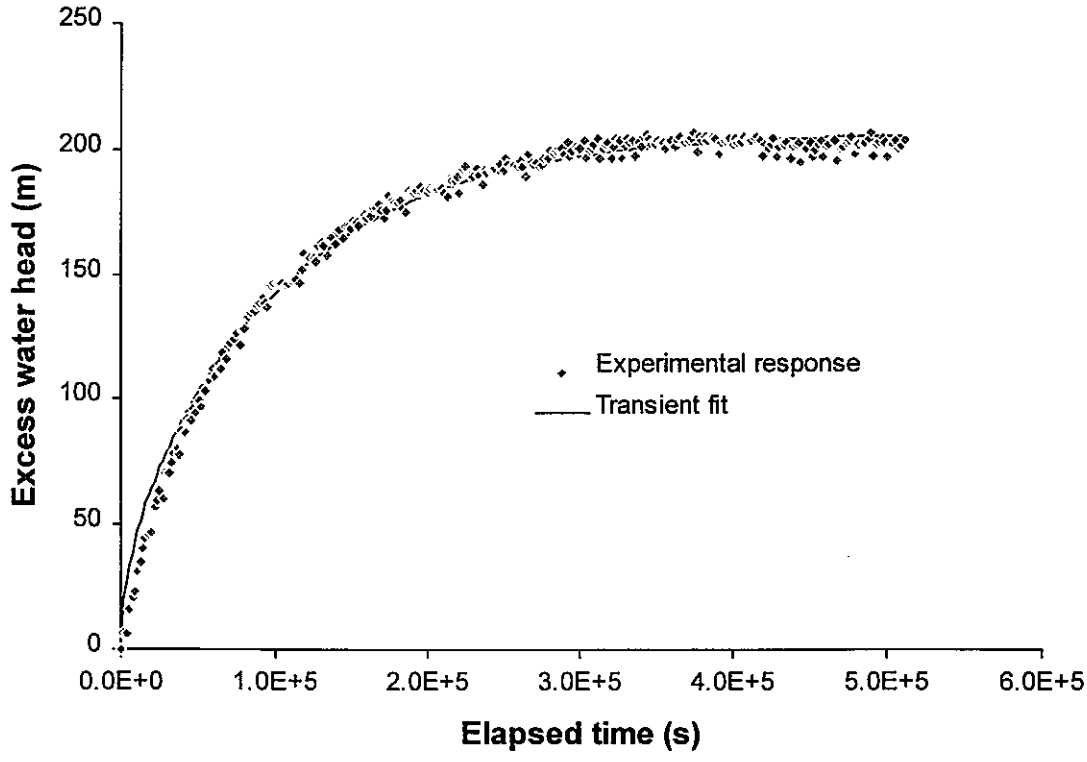

Figure 17. Transient analysis of excess water head (stage 18)

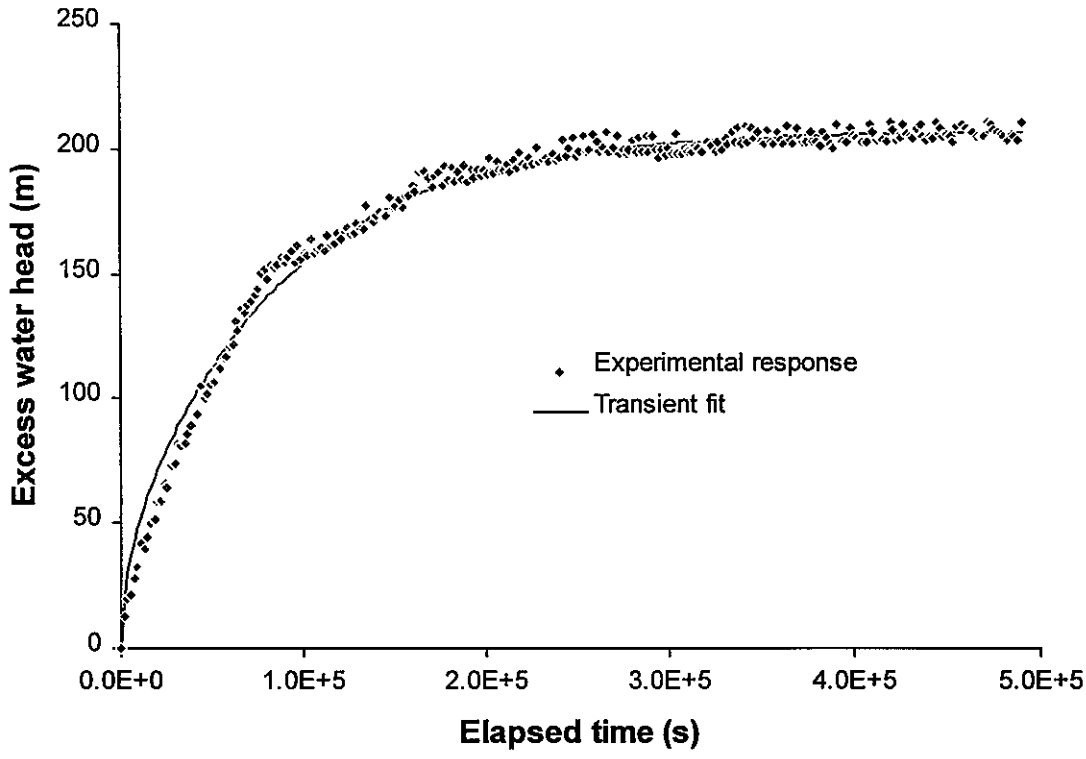

Figure 18. Transient analysis of excess water head (stage 19)

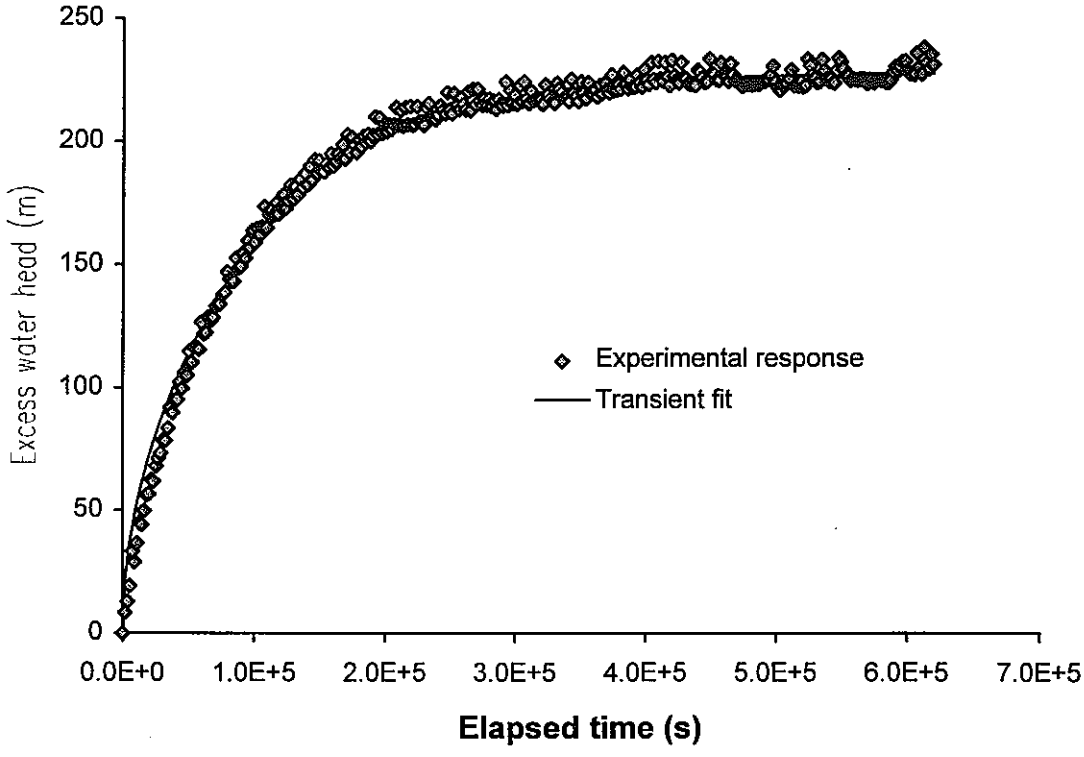

Figure 19. Transient analysis of excess water head (stage 20)

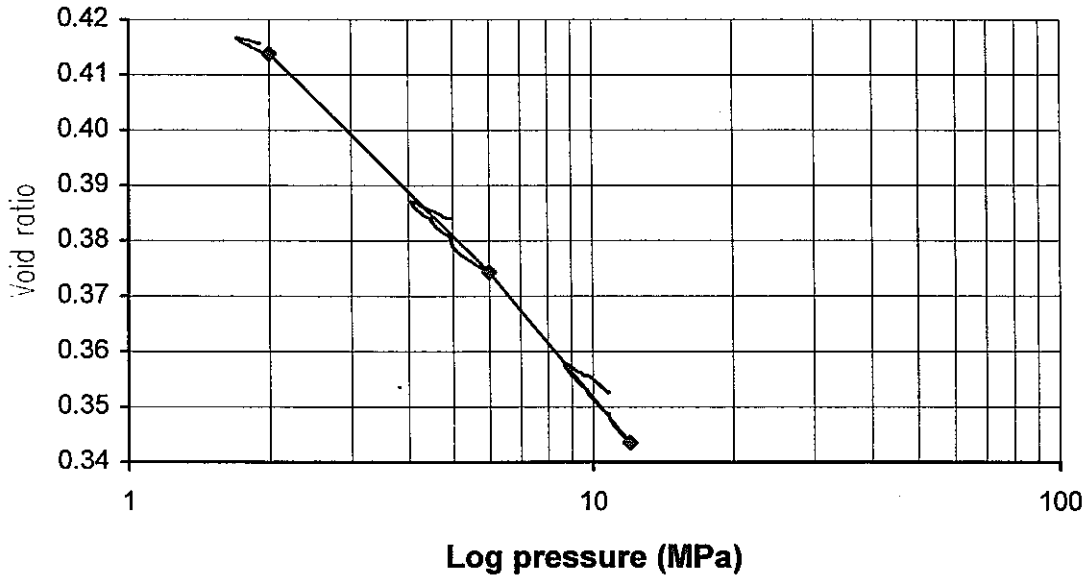

Figure 20. Void ratio against log effective stress for TFA-1

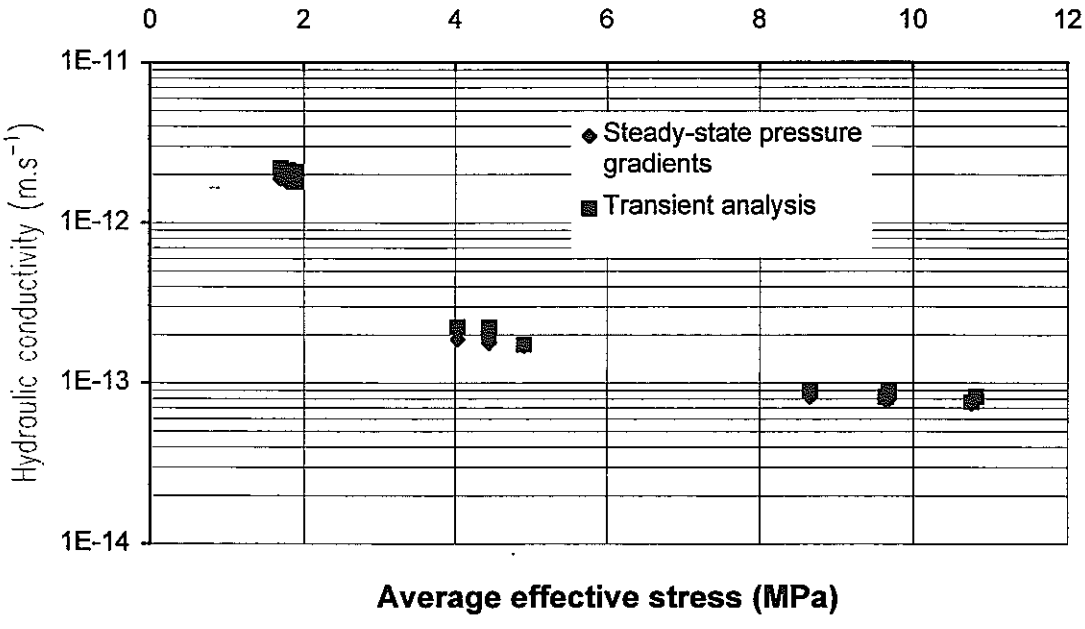

Figure 21. Hydraulic conductivity against average effective stress

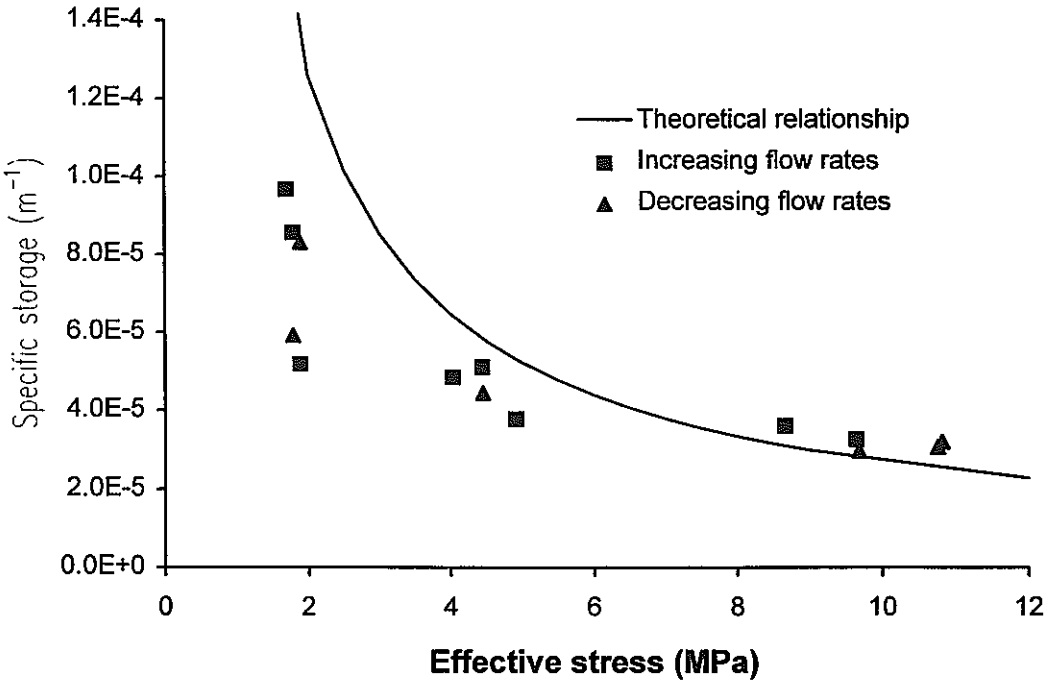

Figure 22. Specific storage against average effective stress

Plate 1. Sample TFA-1 after removal from the aluminised plastic wrapping.

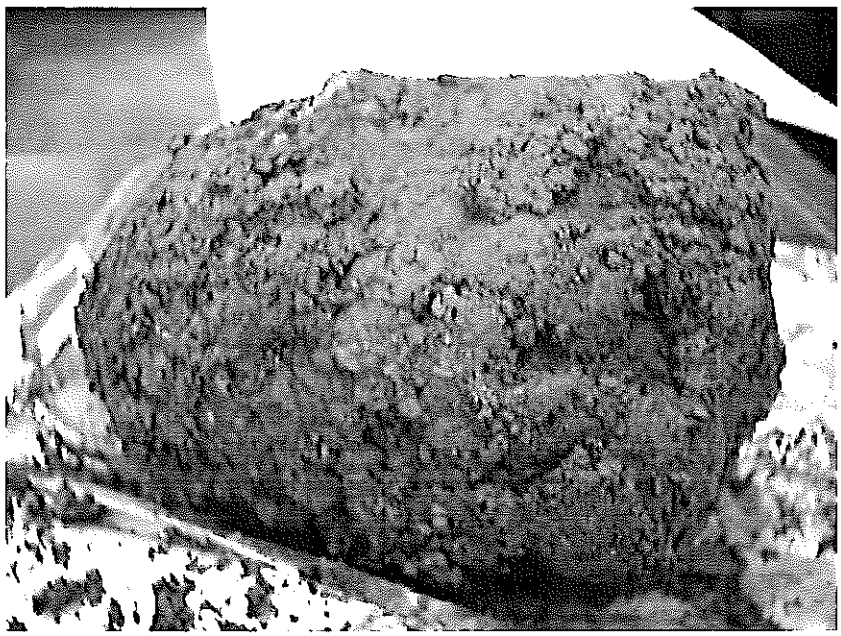

Plate 2. Sample TFA-1 showing the crumbly, poorly-cohesive nature of the gouge material. The olive-green/grey colouration is due to the presence of the clay mineral chlorite

Sample number	Sampling interval (m)	Water content (wt-%)	Bulk density ($Mg.m^{-3}$)	Dry density ($Mg.m^{-3}$)	Void ratio	Porosity	Degree of saturation
TFA-1	14.60-14.79	15.3	2.10	1.82	0.475	0.32	0.868

Table 1. Basic physical properties of the test specimen from pre-test measurements of water content assuming an average specific gravity for the mineral phases of 2.69 $Mg.m^{-3}$. The sampling interval is relative to driller's datum.

Sample number	Sampling interval (m)	Water content (wt-%)	Bulk density ($Mg.m^{-3}$)	Dry density ($Mg.m^{-3}$)	Void ratio	Porosity	Degree of saturation
TFA-1	14.60-14.79	15.3	2.19	1.90	0.414	0.29	0.996

Table 2. Basic physical properties of the test sample corrected for the effects of confining pressure on degree of saturation using Equations (1) and (2).

Stage No.	Type	Flow rate ($mL.hr^{-1}$)	Confining pressure (MPa)	Back-pressure (MPa)	Effective stress (MPa)
1	EQ	-	3.50	1.51	1.99
2	CFR	10	3.50	1.51	-
3	CFR	20	3.50	1.51	-
4	CFR	30	3.50	1.51	-
5	CFR	20	3.50	1.51	-
6	CFR	10	3.50	1.51	-
7	EQ	-	3.50	1.51	1.99
8	EQ	-	7.50	1.51	5.99
9	CFR	10	7.50	1.51	-
10	CFR	15	7.50	1.51	-
11	CFR	20	7.50	1.51	-
12	CFR	15	7.50	1.51	-
13	CFR	10	7.50	1.51	-
14	EQ	-	7.50	1.51	5.99
15	EQ	-	13.50	1.51	11.99
16	CFR	5	13.50	1.51	-
17	CFR	10	13.50	1.51	-
18	CFR	15	13.50	1.51	-
19	CFR	10	13.50	1.51	-
20	CFR	5	13.50	1.51	-
21	EQ	-	13.50	1.51	11.99

Table 3. Summary of experimental history showing stage numbers, type of stage (EQ = equilibration, and CFR = conntrolled flow rate), flow rate, confining pressure (MPa), backpressure (MPa) and effective stress (MPa).

Stage No.	Average effective stress (MPa)	From steady-state pressure		From transient analysis		Specific storage S_s / 10^{5} (m^{-1})
		Hydraulic conductivity K / 10^{12} ($m.s^{-1}$)	Permeability k / 10^{19} (m^2)	Hydraulic conductivity K / 10^{12} ($m.s^{-1}$)	Permeability k / 10^{19} (m^2)	
Isotropic confining stress = 3.5 MPa						
2	1.89	1.81	1.85	1.80	1.84	5.19
3	1.79	1.85	1.89	2.12	2.17	8.57
4	1.70	1.88	1.92	2.19	2.34	9.68
5	1.78	1.80	1.83	2.02	2.06	5.93
6	1.89	1.84	1.88	2.08	2.13	8.32
AVERAGE		**1.84**	**1.88**	**2.04**	**2.09**	**7.54**
Isotropic confining stress = 7.5 MPa						
9	4.91	0.171	0.174	0.173	0.177	3.78
10	4.44	0.178	0.182	0.206	0.210	5.12
11	4.03	0.187	0.191	0.224	0.229	4.86
12	4.45	0.179	0.183	0.222	0.227	4.46
13*	5.37	0.298	0.304	0.094	0.096	6.08
AVERAGE		**0.179**	**0.182**	**0.206**	**0.211**	**4.56**
Isotropic confining stress = 13.5 MPa						
16	10.76	0.075	0.076	0.076	0.078	3.08
17	9.65	0.078	0.080	0.082	0.084	3.27
18	8.66	0.083	0.084	0.090	0.092	3.61
19	9.69	0.080	0.081	0.090	0.092	2.98
20	10.82	0.078	0.080	0.082	0.084	3.21
AVERAGE		**0.079**	**0.080**	**0.084**	**0.086**	**3.23**

Table 4. Hydraulic properties of clay-bearing gouge material from the Tsukiyoshi Fault, showing stage number, average effective stress, hydraulic conductivity and permeability (based on controlled flow rate tests), transient hydraulic conductivity, permeability and specific storage (based on analysis of the transient pore pressure responses). Test stage indicated by * is considered unrepresentative and values are omitted from the averages.

APPENDIX 1

Calculation of hydraulic parameters from flow transients

Consider a specimen of length L_s and cross-sectional area A_s with hydraulic head initially everywhere at zero. A fluid flow of Q is initiated at t = 0 into the specimen at the end x = 0 and the response of the hydraulic head at x = 0 is sought as a function of time.

The equation of one-dimensional flow is given by

$$S_s \frac{\partial h}{\partial t} = K \frac{\partial^2 h}{\partial x^2} \qquad \text{(A-1)}$$

where S_s is the specific storage, K is the hydraulic conductivity, and h is the hydraulic head. This equation must be solved subject to the boundary conditions

$$q = \frac{Q}{A_s} = -K \left. \frac{\partial h}{\partial x} \right|_{x=0} \qquad \text{(A-2)}$$

and

$$h = 0 \text{ at } x = L_s \qquad \text{(A-3)}$$

To obtain the solution to (A-1), we take its Laplace Transform

$$pS_s \bar{h} = K \frac{\partial^2 \bar{h}}{\partial x^2} \qquad \text{(A-4)}$$

where p is the transform parameter and $\bar{h}$ is the Laplace Transform of the head. The solution to this may be written as

$$\bar{h}(x) = Ae^{(\lambda x)} + Be^{(-\lambda x)} \qquad \text{(A-5)}$$

where A and B are constants to be determined from the boundary conditions and

$$\lambda = \sqrt{\frac{pS_s}{K}} \qquad \text{(A-6)}$$

From the boundary condition in (A-3), we have

$$Ae^{(\lambda L)} + Be^{(-\lambda L)} = 0 \qquad \text{(A-7)}$$

Taking the Laplace Transform of (A-2), we have

$$A\lambda - B\lambda = -\left(\frac{q}{K}\right)\frac{1}{p} \qquad \text{(A-8)}$$

Substituting using (A-7) and re-arranging, we have

$$A = -\left(\frac{q}{K\lambda}\right)\frac{1}{p}\frac{e^{(-\lambda L)}}{\left(e^{(\lambda L)} + e^{(-\lambda L)}\right)} \qquad \text{(A-9)}$$

and

$$B = \left(\frac{q}{K\lambda}\right)\frac{1}{p}\frac{e^{(\lambda L)}}{\left(e^{(\lambda L)} + e^{(-\lambda L)}\right)} \qquad \text{(A-10)}$$

Thus we may write the Laplace Transform of the head at x = 0 as

$$\bar{h}(x=0) = \frac{q}{Kp\lambda}\tanh\left(\lambda L_s\right) \qquad \text{(A-11)}$$

The head at x = 0 as a function of time is obtained by numerically inverting the Laplace Transform solution given in Equation A-11 using the method of Talbot (1979). Five parameters are required to define the solution. Three are experimentally determined: Q, A_s and L_s. The remaining two are the material properties that the test is designed to determine (i.e. K and S_s). In order to estimate the values of these parameters, a general nonlinear least squares fitting routine was used to minimise the differences between the calculated curves and the measured head data.

TASK 3. PRESENTATION OF YEAR ONE RESULTS AT TWO INTERNATIONAL CONFERENCES

PNC Representatives:	**H. Yoshida, K. Aoki**
Project Manager:	**J. M. West**
Authors of papers:	**As specified on papers**
Adminstration, QA Procedures:	**S. Baker, C. Cole, P Coombs, R. U. Leader, J. Mackrill**
Financial administration:	**L. Riley**

Two conferences were attended to present work from Year 1:

1. MRS Symposium on the Scientific Basis of Nuclear Waste Disposal (28 September 1997 to 3 October 1997), Davos, Switzerland.
K. Bateman, J. M. West, K. Aoki, H. Yoshida, P. Coombs, M. Gillespie, P. Henney, S. Reeder and A. E. Milodowski. Laboratory examination of microbial effects upon redox in a geological disposal site for radioactive waste.
Materials Research Society - Symposium Proceedings. Volume 506 (1998).

2. Migration '97 (26 - 31 October 1997) at Sendai, Japan.
Steven J. Baker, Julia M. West, Richard Metcalfe, David J. Noy, H. Yoshida and K. Aoki. A biogeochemical assessment of the Tono site, Japan. Journal of Contaminant Hydrology (*in press*)

Both papers were presented as posters and copies of the poster have been sent to the Tono Geoscience Centre. The papers form the rest of this section.

LABORATORY EXAMINATION OF MICROBIAL EFFECTS UPON REDOX IN A GEOLOGICAL DISPOSAL SITE FOR RADIOACTIVE WASTE.

K. BATEMAN[1], J. WEST[1], K. AOKI[2], H. YOSHIDA[2], P. COOMBS[1], M. R. GILLESPIE[1], P. HENNEY[1], S. REEDER[1] and A. E. MILODOWSKI[1]

[1]British Geological Survey, Keyworth, Nottingham, NG12 5GG, UK.

[2]Power Reactor and Nuclear Fuel Development Corporation of Japan

ABSTRACT

The laboratory experiments described here, were aimed at examining the interaction of microbes with mineralogical surfaces involved with groundwater flow. These experiments were designed to study simple systems and were aimed at identifying relevant reactions both chemical and biological. They contained groundwater with either sulphate reducing bacteria (SRB), iron reducing bacteria (IRB) or a mixture of both, together with control experiments without bacteria. The results of the chemical analyses of fluid phases showed evidence for dissolution of primary minerals. Microbial analysis showed both SRB and IRB appeared to be active albeit for a limited period due to exhaustion of nutrient and energy supplies. SRB seem to have a greater effect on groundwater chemistry than IRB with sulphide being produced. However, when the two types of bacteria are mixed together, the IRB appear to dominate the system. Further work is underway to give detailed mineralogical analysis of the solids in order to better understand the influence of microbial interaction on the redox reactions.

INTRODUCTION

The Power Reactor and Nuclear Fuel Development Corporation (PNC) of Japan is currently undertaking a joint research programme with the Swedish Nuclear Fuel and Waste Management Company (SKB). This programme will investigate the capability of a near-repository host rock to consume dissolved oxygen in groundwater remaining in the backfill and near-field rock following the operational phase of a nuclear waste repository. It is planned to carry out these investigations *in situ* in a single hydraulically-conductive fracture within SKBs underground research facility at the Ä spö Hard Rock Laboratory, Sweden. The project objectives are described by Banwart [1] which gives details of The Redox Experiment in detailed Scale (REX) to be conducted at Ä spö . The laboratory experiments described here, were aimed at simulating the conditions within the REX Experimental Block to examine the interaction of microbes with mineralogical surfaces involved with groundwater flow. The mineralogical nature of the fracture surfaces and subsequent changes to those

surfaces will be important with regard to radionuclide sorption and retardation, and also with respect to buffering groundwater redox through rock-water interaction. The mineralogy of the surfaces will also be important with respect to microbial interaction in terms of redox reactions mediated by microbial activity, and in providing substrates for microbes.

EXPERIMENTS

A series of batch experiments were conducted to study rock-water interactions. These experiments were designed to study simple systems and were aimed at identifying relevant reactions both chemical and biological. They were essentially pilot studies to aid in the development of microbial and analytical geochemical procedures, as well as gathering basic data on rock-water interactions relevant to the Aspo site. The experiments were conducted in reactors, constructed of PEEK. The experiments conducted were of either 1, 2, or 3 weeks duration, at a temperature of 30° C. All reaction vessels were sterilized by autoclaving prior to assembly, and contained 20g of crushed Å spö Diorite and 20 ml of Å spö groundwater. Analysis of the Åspö Diorite showed it to be composed of major quartz, with minor albite, mica, orthoclase, calcite and trace amounts of chlorite and possibly titanite and magnetite.

The experiments were assembled in an anaerobic chamber ($H_2/CO_2/N_2$ atmosphere) and contained either sulphate reducing bacteria (SRB, *Desulfovibrio asponium*), Iron reducing bacteria (IRB, *Shewanella putrefaciens*) or a mixture of both SRB and IRB, together with control experiments without any bacteria. Both SRB and IRB have been highlighted as being of particular significance in Åspö geochemistry [2] The implications of both iron and sulphate reduction are discussed in detail in an earlier study [1]. The bacteria were cultured in appropriate enrichment media before being added to the reaction vessels in the predetermined numbers.

On termination of the experiments the reactors were opened in an anaerobic chamber and samples of the fluids and solids removed for analysis. The fluids were characterised both chemically (major anions and cations; trace elements; redox sensitive species) and microbially (epifluorescence microscopy [3] before and after the experimental runs.

DISCUSSION

The results of the chemical analyses of fluid phases from the batch systems showed evidence for dissolution of primary minerals. Many of the redox sensitive species ($NH_4/NO_3/NO_2$, As^{III}/As^{V}, Se^{IV}/Se^{VI}) were found to be below the detection limits of analytical methods used. Total sulphur remains

fairly constant (within experimental and analytical errors) in all the experiments. In the experiments involving SRB there is a small amount of reduced sulphur observed which suggests that the SRB were 'active' in these experiments, although the concentrations of HS^- detected were small. No reduced sulphur was observed in the other experiments. There appears to be little dissolution of any iron phases present in the rock used in the experiments. When SRB are present the concentrations of iron (both total iron and reduced iron) increases from that of the starting fluid. The source of this iron is not clear, but may be determined by mineralogical analysis of the solids recovered from experiments, which is yet to be completed.

Both SRB and IRB appeared to be able to grow in the batch systems albeit for a limited period due to exhaustion of nutrient and energy supplies. SRB seem to have a greater effect on groundwater chemistry than IRB with sulphide being produced. IRB appear to have no effect on groundwater chemistry in these experiments. However, when the two types of bacteria are mixed together, the IRB appear to dominate the system but the significance of this on the system cannot be interpreted without mineralogical information from an analysis of the solid components of the batch experiments. Further work is underway to give detailed mineralogical analysis of the solids in order to better understand the influence of microbial interaction on the redox reactions.

ACKNOWLEDGEMENTS

We gratefully acknowledge the funding from PNC for this work. SKB are acknowledged for providing access and facilities during this work. Grateful thanks to the Department of General and Marine Microbiology, Goteborg University for their help in selecting and obtaining the bacterial isolates; and to Dr Peter Wikberg (SKB), Dr Ignasi Puigdomenech (Studsvik Eco and Safety AB) and Dr Steven Banwart (University of Bradford) for their support and technical advice. This extended abstract is published with the permission of the Director of the British Geological Survey.

REFERENCES

1 S Banwart (Ed). SKB Technical Report 95-26. Stockholm 1995.

2 K Pedersen, and F Karlsson. SKB Technical Report 95-10. Stockholm. 1995.

3 J. E. Hobbie, R. J. Daley, and S. Jasper. Applied and Environmental Microbiology, 33, (5), p1225 (1977).

A BIOGEOCHEMICAL ASSESSMENT OF THE TONO SITE, JAPAN.

STEVEN J. BAKER [A,*], JULIA M. WEST [A], RICHARD METCALFE [A], DAVID J. NOY [A],H. YOSHIDA [B] AND K. AOKI [C].

[a] Fluid Processes and Waste Management Group, British Geological Survey, Keyworth, Nottingham, NG12 5GG, UK. E-mail: s.j.baker@bgs.ac.uk, Fax: 0044-115-9363261. [b] Power Reactor and Nuclear Fuel Development Corporation, Tono Geoscience Center, 959-31 Sonodo, Jorinji, Izumi, Tokishi, Gifu, 509-51, Japan. Fax: 0081-572-550180. [c] Power Reactor and Nuclear Fuel Development Corporation, Kamaishi Site Office, 1-80 Kassi, Kamaishi, Iwate, 026, Japan. Fax: 0081-193-592227. *Corresponding author.

ABSTRACT

When designing investigations of microbial populations in the subsurface, it is extremely valuable to undertake scoping calculations to estimate the likely microbial abundancies and evaluate the effects of contamination during sampling.

A biogeochemical assessment of the groundwater and lithologies of the Tono mine Japan, has been made using the BGS/NAGRA computer code BGSE (Bacterial Growth in Subsurface Environments). This code enables an assessment to be made of the maximum microbial growth rates that may be achieved in ideal circumstances, based on availability of nutrients and energy calculated from mineralogical and groundwater analyses. The effect of drilling fluid/groundwater mixing on biomass was assessed using a hypothetical drilling fluid composition. The results of modelling the mixing between groundwater and drilling fluid shows that the addition of only small concentrations of drilling fluid (< 1% (*v/v*)) to the groundwater gives rise to significant microbial growth rates for the systems studied. Maximum growth rates were observed at ratios of 50:50 (*v/v*) (groundwater: drilling fluid) for the Akeyo and Toki lower groundwaters, and ratios of 90:10 (*v/v*) (groundwater: drilling fluid) for the Toki upper and Granite groundwaters. At low ratios of drilling fluid (<1% (*v/v*)) the limiting factor in each system was the availability of an energy source. This reflects the fact that the system is approaching pristine conditions. However, there was sufficient energy to permit a significant growth rate to be observed.

INTRODUCTION

The geochemistry of natural groundwaters, particularly at depths of more than a few tens of meters, is usually interpreted with little or no consideration of microbial processes, whether caused by indigenous microbial populations, or by populations

introduced during perturbing processes such as borehole drilling. However, these microbial effects can be profound, as demonstrated at the Aspö hard rock laboratory in Sweden (Pedersen and Karlsson, 1995). During a redox experiment at this site, unexpected groundwater redox stability was encountered. This could only be explained by the dissolution and reduction of solid phase Fe(III) oxy-hydroxides to aqueous Fe(II) by iron-reducing bacteria using organic carbon as the electron donor (Banwart *et al*, 1994). The bacteria appeared to be maintaining an anoxic environment. The implications of this are wide reaching, but are particularly important in connection with performance assessments for repositories of radioactive wastes, since the migration of many radionuclides is redox-sensitive. Redox conditions are also a control on the integrity of waste forms. In the Swedish disposal concept, for example, there could be inhibited corrosion of the copper canisters, used to contain wastes, during the operational phase of a repository due to the maintenance of reducing conditions by microbially mediated processes.

For these reasons, it is important to estimate microbial numbers and growth rates in groundwater systems. The Power Reactor and Nuclear Fuel Development Corporation of Japan (PNC), has been developing techniques to evaluate microbiological effects within *in-situ* groundwaters around the Tono Mine (located 350 km west of Tokyo). The Tono mine is the largest uranium ore reserve in Japan. The uranium deposits lie within Tertiary carbonaceous sandstone and fluidstone units which overlie a Cretaceous granitic basement. Studies are being undertaken to understand: 1) the hydrogeological, geochemical and mechanical properties of the rock mass; 2) the geochemical properties of the groundwater; 3) the radionuclide migration processes. These studies will provide the basis for a generic feasibility study of the geological disposal of radioactive wastes in Japan. Much effort has been directed towards obtaining data from the mine and also in conducting *in-situ* experiments.

This paper describes a generic microbial model BGSE (Bacterial Growth in Subsurface Environments) and details the results of a pilot study whose specific objectives were to: 1) To assess the capability of the Tono mine groundwaters to support a microbial biomass; 2) To determine the maximum biomass in the varying groundwater compositions, in the Tono mine and determine controls on indigenous microbial growth; 3) To provide a detailed assessment of natural baseline microbiological numbers, in a number of rock formations in the Tono mine; 4) To evaluate the likely influence of drilling perturbations on indigenous microbial populations, and the subsequent effect on the groundwater geochemistry.

THE MODEL

The BGS (British Geological Survey) and NAGRA (National co-operative for the disposal of radioactive waste, Switzerland) developed model (BGSE), a development of the earlier British Geological Survey developed model MGSE (Microbial Growth in Subsurface Environments), was used in this study. The general conceptual approach adopted in BGSE was first developed in Grogan and McKinley (1990), and enables an assessment of the maximum microbial growth rates based on the availability of nutrients and energy, calculated from existing mineralogical and groundwater analyses. Emphasis is placed on elements which are major microbial

nutrient sources (carbon, nitrogen. sulphur and phosphorus); and on species which can act as electron donors and acceptors for energy generation (organic carbon, oxygen, nitrate, FeOOH and sulphate).

It is assumed in the model that reactions and microbial growth take place within a mixing cell into which nutrients and oxidising/reducing agents can flow together with the ground water. Additionally, the mixing cell may contain a solid phase with leachable components which can also supply nutrients, oxidising agents, and reducing agents. In order to conduct the calculations, it is assumed that the nutrients form a completely separate system from the energy system (defined to consist of oxidising and reducing agents). A diagrammatic representation of the model is shown in Figure 1.

The calculations are divided into an initial yield stage, defined by the initial composition of the groundwater in the mixing cell, which is followed by a series of steps defined by the times at which one or more components of the solid phase become exhausted. Each of these calculation steps is comprised of two parts. Firstly, the potential yield of microbes is determined by the supply of nutrients in the system. Secondly, the energy supply from all permissible redox reactions amongst the oxidising and reducing agents provides an alternative estimate of the potential microbe yield. The overall potential yield at a given time step is assumed to be determined by the smaller of the two estimates.

Microbial energy requirements are taken to be 45 $KJ.g^{-1}$ microbe (dry weight) as growth energy, a maintenance energy of 45 $KJ.g^{-1}$ microbe (dry weight) and a minimum utilisable energy of 15 $KJ.g^{-1}$ microbe (dry weight) (Thauer and Morris, 1984; Thauer *et al.*, 1977).

MICROBIOLOGICAL BASE CASE

The initial modelling concentrated on the uncontaminated pristine *in-situ* groundwater system that exists currently. This modelling scenario is referred to as the 'base case' against which, the impact of invasive procedures such as borehole drilling could be compared.

The fluid components of the system were derived from analysis of each rock formation. It is recognised that these data will not be truly representative of the natural baseline chemical conditions prior to the development of the Tono mine because of biased sampling, contamination from the atmosphere, drilling fluids and drilling equipment, and degassing of the fluids. However, the reported concentrations of microbiologically significant constituents were considered adequate for the purposes of the scoping calculations described here. The composition of the inflowing fluids were the same as the initial composition of the fluid within the mixing cell as the groundwater was assumed to be chemically undisturbed. Concentrations for the groundwaters from the four formations considered (Akeyo, Toki Upper, Toki Lower and Granite) for the systems are given in Table 1. No interaction between the bulk rock and the inflowing groundwater was considered i.e. the hydrogeochemical system was assumed to be at equilibrium.

THE INFLUENCE OF DRILLING FLUID ON THE BASE MICROBIOLOGY

The Tono mine has been extensively used for a number of in-situ experiments (Sato *et al*, 1995) and has been characterised using borehole arrays. During the drilling operations, fresh water was used to prevent geochemical and biological contamination. However, in some cases, drilling fluid containing organic polymers was circulated through the borehole to assist in the drilling process. The purpose of these fluids was to keep the drill bit cool, ensure borehole stability and to provide a pressure head to prevent blow-out, if a gas pocket was encountered. Often the fluids were at greater than the formation pressure and thus could be forced into the rock, either along open fractures or via matrix porosity. The fluids will have disturbed the local geochemical environment in the bulk rock and could also have provided additional nutrient and energy sources for microbial growth.

The conceptual model used for these simulations is of a borehole intersecting a flowing feature, through which drilling fluid flows (Figure 2). As the drilling fluid migrates away from the borehole it will become increasingly diluted by groundwater. Five different simulations for each of the four ground waters were run, in order to simulate the effect of mixing the drilling fluid and groundwater. These were: 100% drilling fluid; 50:50 *(v/v)* (groundwater/drilling fluid); 90:10% *(v/v)* (groundwater/drilling fluid); 99:1 *(v/v)* (groundwater/drilling fluid); 99.9:0.1 *(v/v)* (groundwater/drilling fluid).

For this study, since the precise composition of the drilling fluid was not known a generic 'drilling fluid' was used in the model. This was comprised of a mix of the organic polymer xanthan gum, (a known ingredient of drilling fluids), surface water and formation water. The most important data were the concentrations of the redox sensitive components: i.e. dissolved oxygen content, NO_3^-, NO_2^-, HPO_4^-, Fe^{2+}, and organic material content, these are listed in Table 2. Xanthan gum is used to control the viscosity and density of the drilling fluid, and it was assumed to be a potential source of carbon, which could be utilised as a nutrient as well as a reducing agent. The structure of the xanthan polymer (Figure 3) is, in many ways, similar to cellulose consisting of repeated pentasaccharide units. Two components of the polymer are likely to be prone to microbial attack: the acetyl side groups, and the carboxyl groups. The complex nature of the polymer, and the presence of non-fermented sugar and other impurities, makes detailed modelling difficult without further detailed investigation. However, for this study, only use of the <HCOO> groups were considered, three of which are present in each repeating polymer unit (Figure 3.). This simplification will give an underestimation of the amount of carbon. However, it will serve as a useful bounding condition.

RESULTS

Where the assumption is made that the system is at equilibrium, BGSE modelling of the reported geochemical data from the Tono mine site, gives no biomass production for each of the four rock systems studied. The growth was constrained, in each case, by the availability of energy sources. Even when aerobic groundwaters were simulated, by mixing with meteoric recharge water, there was insufficient energy to allow growth to occur.

The composition of the drilling fluid used for the current study is given in Table 2 and shows that there is no sulphur present and therefore, on its own, the drilling fluid cannot support microbial growth. Thus, in the drilling fluid the lack of nutrient availability prevents microbial growth. However, since the groundwaters contain significant amounts of sulphur in the form of SO_4^{2-}, when the drilling fluid mixes with groundwater, microbial growth is possible. The results of the modelling for the mixing of groundwater with drilling fluid (Figure 4.) show that the addition of only a small concentration of drilling fluid (< 1% (*v/v*)) to the groundwater gives rise to significant microbial growth rates for the systems studied. Maximum growth rates are observed at ratios of 50:50 (*v/v*) (groundwater/drilling fluid) for the Akeyo and Toki lower groundwaters, and ratios of 90:10 (*v/v*) (groundwater/drilling fluid) for the Toki upper and Granite groundwaters. At these drilling fluid concentrations the limiting factor in each case was the availability of nitrogen. The similarity in the calculated growth rates for Akeyo and Toki lower groundwaters, when mixed with drilling fluid, was due to the almost identical chemical composition of these groundwater (Table 1). The higher growth rates predicted with Toki upper and granite groundwaters, when mixed with drilling fluid, were due to elevated concentrations of nitrate and nitrite respectively, when compared with the Akeyo and Toki lower groundwaters (Table 1).

At low ratios of drilling fluid (<1% (*v/v*)) the limiting factor in each system was the availability of an energy source. This reflects the fact that the system is approaching 'base case' conditions. However, there was sufficient energy source available to permit a significant microbial growth rate to be calculated. This is important as such low levels of contamination may not be detected by, for example, the use of chemical tracers in drilling fluids. Any chemical constituent of drilling fluids used as an index of contamination in sampled waters may be present at levels indistinguishable from those of groundwater in samples with <1% drilling fluid contamination. Analyses for aqueous constituents may not detect *variations* in the concentrations of nutrients and energy sources until well after microbially significant degrees of mixing between drilling fluids and groundwaters have occurred. Only variation in organic carbon concentrations are likely to be detected when the drilling fluid comprises <1% of a mixture. In practise, at such low degrees of mixing, the nutrients and energy sources considered here, can not be determined accurately. Consequently a groundwater sample containing only 0.1% (*v/v*) drilling fluid contamination, and showing enhanced microbial growth as a result, may not be readily distinguishable from uncontaminated groundwater. An important corollary of this is that the use of biological tracers may allow much lower concentrations of drilling fluid contamination to be determined than can be detected utilising conventional elemental tracers. A further important point is that analytical data for certain key microbial nutrients and energy sources are often not acquired during investigations of groundwaters. In particular, there are relatively few published data for P, while most studies of groundwater chemistry do not determine data for Fe(II) and Fe(III), or sulphide. This partly reflects the technical difficulty of obtaining high quality data for these constituents, particularly in deep groundwaters (> a few tens of metres). Thus, basic published data are lacking with which to evaluate the importance and variability of microbial growth in the deep sub-surface.

CONCLUSIONS

The scoping study described in this paper has highlighted the importance of borehole drilling as a potential stimulant of microbial growth in the subsurface. The approach outlined demonstrates how the magnitude of this effect can be estimated and compared with likely natural *in-situ* microbial growth.

The 'base case' modelled for each of the four rock formations (Akeyo, Toki upper, Toki lower and Granite), yielded no new biomass as there were insufficient energy sources.

The modelling of mixtures of drilling fluid and groundwaters have shown the potential significance of the organic polymer-based fluids in stimulating microbial growth in subsurface environments. The modelling reported here indicates that microbial growth can occur in the presence of less than 1% (*v/v*) drilling fluid mixed with groundwater.

The theoretical calculations here have highlighted the importance of acquiring high quality analytical data for concentrations of nutrients and energy sources in groundwaters. Higher quality data than are acquired normally in groundwater investigations are needed particularly for sulphide, P, Fe(II) and Fe(III).

The importance of calculated growth rates on the concentrations of analysed solutes in the groundwaters must also be considered. Potential microbial growth may cause perturbations in the dissolved constituents that are comparable to, or greater than, the uncertainties in determining *in-situ* groundwater solute concentrations. The modelling performed in the present study was aimed primarily at estimating the limiting, maximum microbial growth rates, rather than changes in groundwater compositions. More data would be required to predict any changes in solute chemistry over varying periods of time.

ACKNOWLEDGEMENTS

We gratefully acknowledge the funding from PNC for this work. We acknowledge the support of the British Geological Survey and NAGRA for the development of the code BGSE. The paper is published by permission of the Director of the British Geological Survey (Natural Environmental Research Council).

References

Banwart, S. A., Gustafsson, E., Laaksoharju, M., Nilsson, A-C., Tullborg, E-L. and Wallin, B. 1994. Large scale intrusion of shallow water into granite aquifer. Water Resources Research, 30, 1747-1763.

Grogan, H. A. and McKinley, I. G. 1990. An approach to microbiological modelling: application to the near field of a Swiss low/intermediate-level waste repository. NAGRA technical report, 89-06.

Pedersen, K. and Karlsson, F. 1995. Investigations of subterranean microorganisms: their importance for performance assessment of radioactive waste disposal. SKB Technical Report, 95-10.

Kang, K. S. and Pettit, D. J. 1993. Industrial Gums, 3rd edition, Academic Press.

Sato, T., Suigihara, K. and Matsui, H. 1995. Geoscientific studies at the Tono mine and the Kamaishi mine in Japan.

Thauer, R. K., Kungermann, K. and Decker, K. 1977. Energy conservation in chemotrophic anaerobic bacteria. Biological Reviews, 41, 100-180.

Thauer, R. K. and Morris, I. G. 1984. Metabolism of chemolithotrophic anaerobes_ Old views and new aspects. In: The microbe Part II Prokaryotes and Eukaryotes (Eds D. P. Kelly, N. G. Carr) Cambridge University Press. pp. 123-168.

Table 1. Composition of the four groundwaters used in the BGSE simulations (mol m^{-3}). Akeyo, Tuffaceous Medium Sandstone; Borehole, Toki upper, Tuffaceous Fluidstone; Toki lower, Lignite bearing Tuffaceous Fluidstone.

	Akeyo	Toki (up)	Toki (low)	Granite
Nutrients				
C	1.90	3.08	1.90	1.90
N	$7.57x10^{-4}$	$1.89x10^{-3}$	$7.57x10^{-4}$	$1.19x10^{-3}$
P	$1.36x10^{-2}$	$8.21x10^{-3}$	$1.36x10^{-2}$	$1.68x10^{-3}$
S	$4.27x10^{-1}$	$5.31x10^{-1}$	$4.27x10^{-1}$	$8.54x10^{-1}$
Oxidising Agents				
O_2	0	0	0	0
SO_4^{2-}	$4.27x10^{-1}$	$5.31x10^{-1}$	$4.27x10^{-1}$	$8.54x10^{-1}$
NO_3^-	$3.23x10^{-4}$	$1.45x10^{-3}$	$3.23x10^{-4}$	$3.23x10^{-4}$
NO_2^-	$4.35x10^{-4}$	$4.35x10^{-4}$	$4.35x10^{-4}$	$8.70x10^{-4}$
HCO_3^-	1.74	2.97	1.74	1.95
CO_3^-	$1.67x10^{-1}$	$1.17x10^{-1}$	$1.67x10^{-1}$	0
Fe^{3+}	$3.57x10^{-4}$	$3.57x10^{-4}$	$3.57X10^{-4}$	$3.57x10^{-4}$
Reducing Agents				
Fe^{2+}	$3.57x10^{-4}$	$3.57x10^{-4}$	$3.57x10^{-4}$	$3.57x10^{-4}$
<HCOO>	0	0	0	0
pH	7.79	8.08	9.0	7.8

Table 2. Representative composition of drilling fluid used for the BGSE modelling (values in mol.m^{-3}). *Xanthan component only used.

pH	9.87
NO_3^-	$3.23x10^{-4}$
NO_2^-	$5.43x10^{-4}$
HPO_4^-	$1.17x10^{-2}$
Fe^{2+}	$9.67x10^{-3}$
O_2	$2.77x10^{-1}$
<HCOO>	9.18
Nutrient C	107.1*
Nutrient N	$8.66x10^{-4}$
Nutrient P	$1.17x10^{-2}$
Nutrient S	0

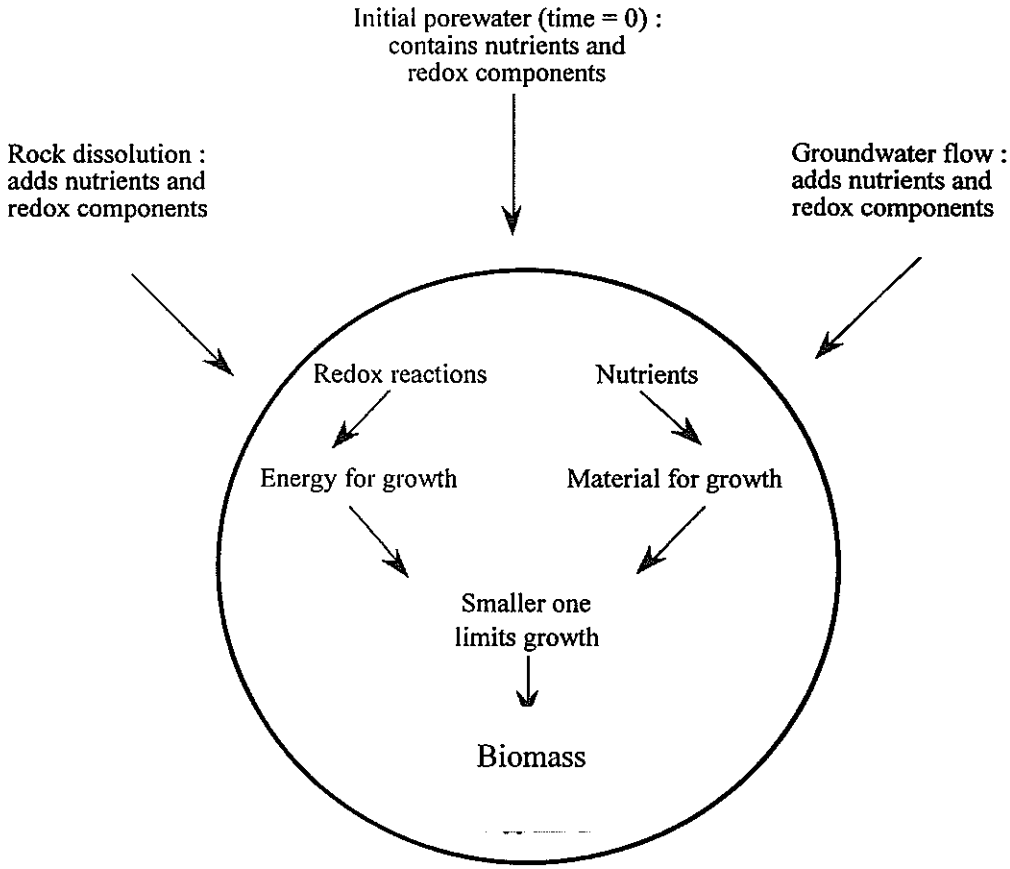

Figure 1. Diagrammatic representation of the BGSE computer model.

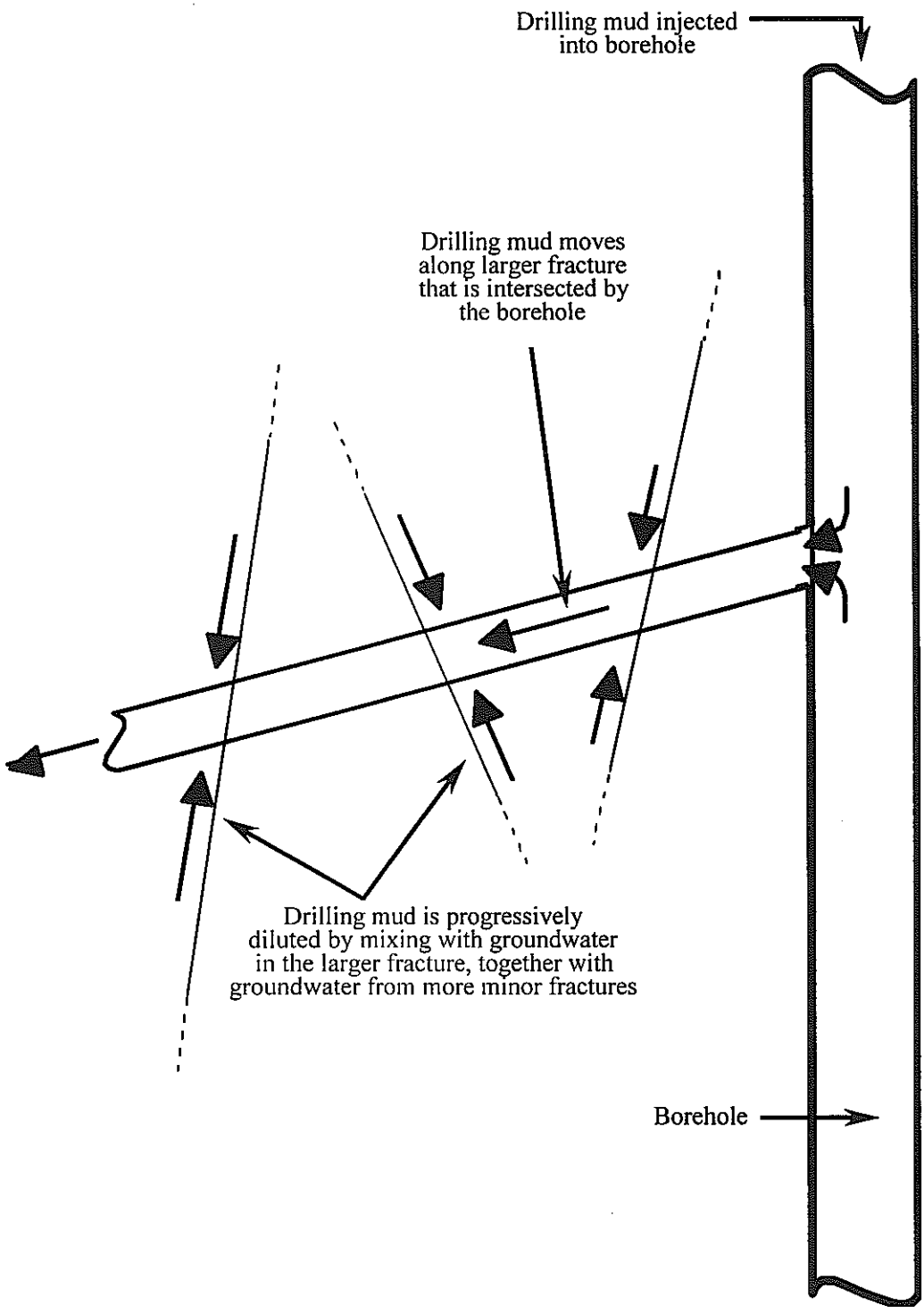

Figure 2. Conceptual model used during BGSE simulations, where drilling fluid mixes with local ground water.

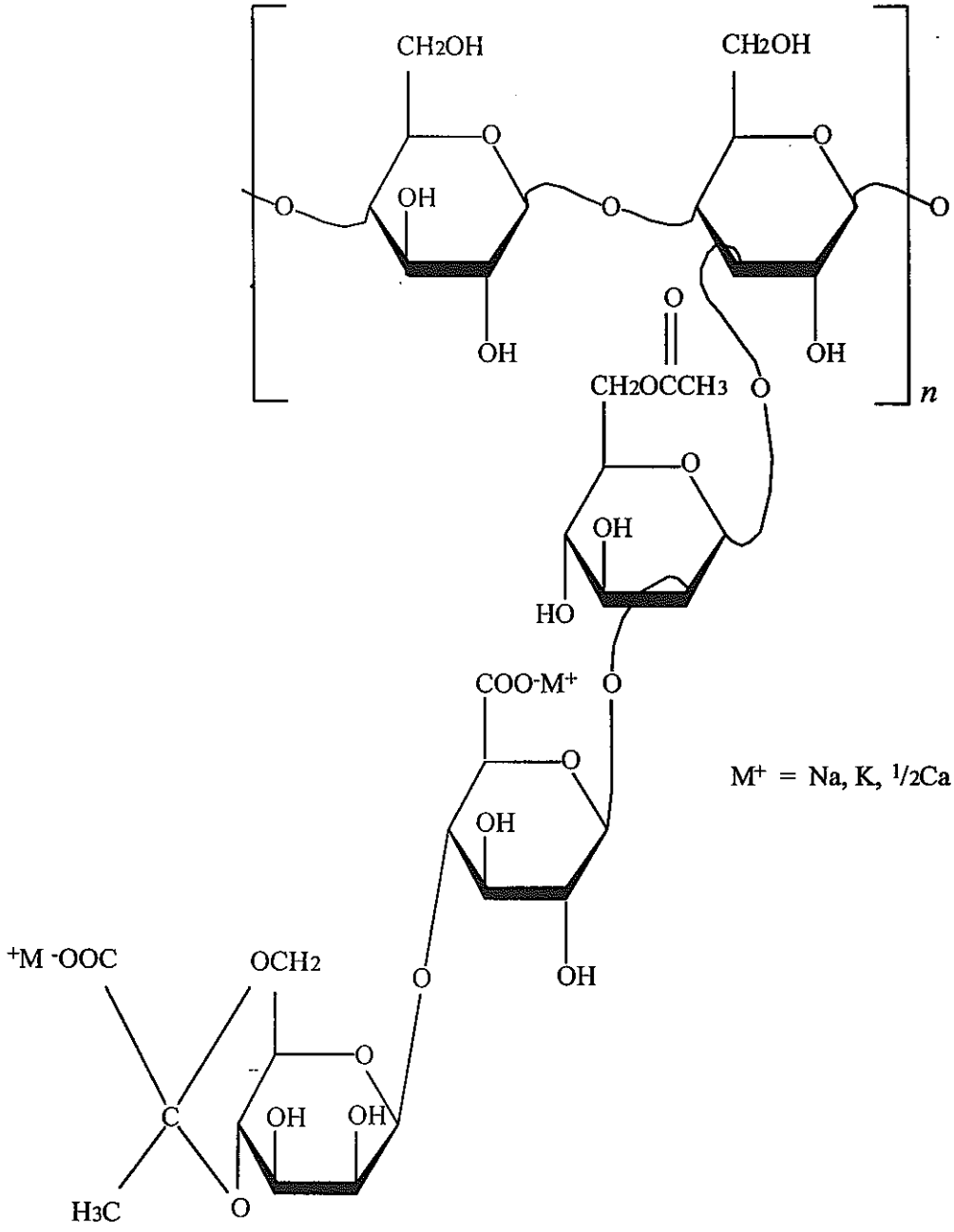

Figure 3. Xanthan polymer structure (Kang and Pettitt, 1993).

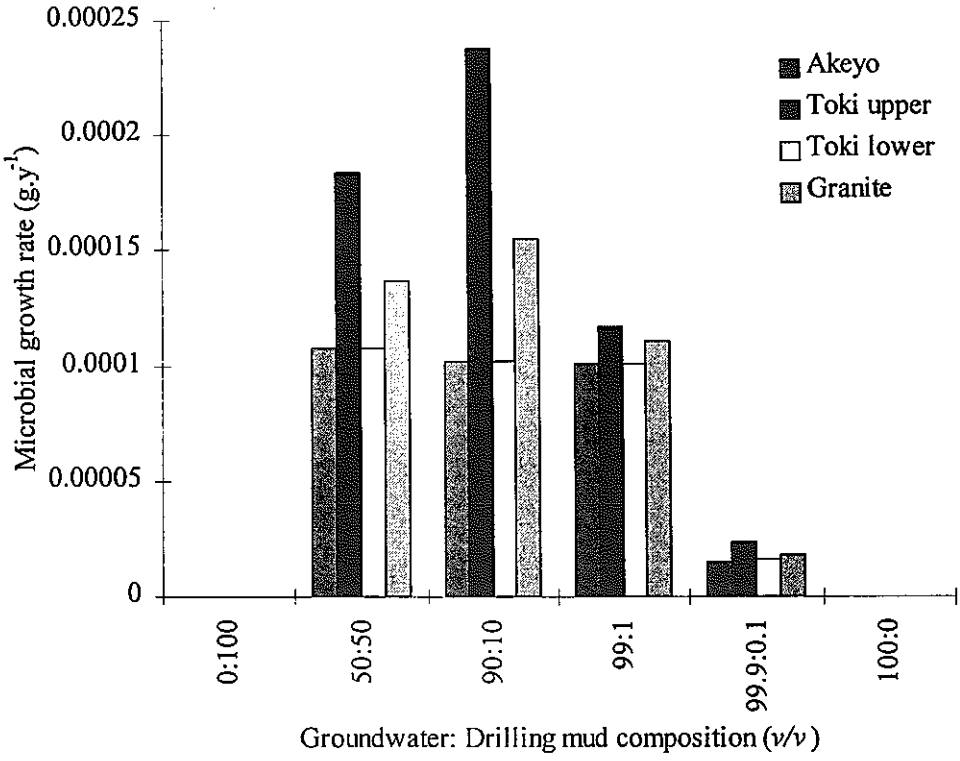

Figure 4. Predicted microbial growth rates as a function of groundwater: drilling fluid ratio for the four rock formations.

BRITISH GEOLOGICAL SURVEY

BRITISH GEOLOGICAL SURVEY
KEYWORTH
NOTTINGHAM, NG12 5GG
UNITED KINGDOM

TEL (0115) 9363100
FAX (0115) 9363261

DOCUMENT TITLE AND AUTHOR LIST

A THREE TASK PROJECT
TASK 1. Laboratory work to examine microbial effects on redox.
TASK 2. Geochemical profile through Tsukiyoshi Fault Zone.
TASK 3. Presentation of Year One Results at two international conferences

CLIENTS:	CLIENT REPORT #
PNC Japan	
	BGS REPORT # WE/98/11C
	CLIENT CONTRACT REF
	BGS PROJECT CODE E83PJ009
	CLASSIFICATION Commercial-in-confidence

ISSUE NUMBER	STATUS	PREPARED BY:	CHECKED BY:	APPROVED BY:	DATE
2.0	A	[signature]	I A Moore	Julia M West	11.6.98

Form RA1 v.3, May 1992